MECHANICAL BEHAVIOUR OF SELF-PIERCING RIVETED ALUMINIUM JOINTS

LI HAN

A thesis in partial fulfillment of the requirements of the University of Hertfordshire for the degree of Doctor of Philosophy

The programme of research was carried out in the department of Aerospace, Automotive and Design Engineering, University of Hertfordshire in collaboration with Alcan International Limited and Textron Fastening Systems

November 2003

ABSTRACT

The introduction of alternative materials and in particular aluminium alloys, for vehicle body applications has impelled the development of new joining techniques. Traditional joining methods such as spot-welding and arc-welding are being challenged. Self-piercing riveting has attracted considerable interest by the automotive industry and has been used as an alternative to spot-welding in vehicle body assembly. However, self-piercing riveting is a relatively new joining method and as such it is not well understood. The aim of this project was therefore to develop an understanding of the mechanical behaviour of self-piercing riveted joints. The effects of paint-baking, shelf-life, pre-straining and surface condition of the sheet material on the joint quality and behaviour were therefore examined. Aluminium alloy sheet materials, 5754 and AA6111, were used in this investigation.

The project began with a metallographic inspection of cross-sections of samples that were joined under different conditions in order to examine the effect of process variables on the joint quality. This part of the investigation led to the identification of suitable setting parameters that produced joints which, by metallographic inspection, were of good quality. It was also observed that some process variables, such as sheet thickness combination, rivet and die design and setting force, affected the joint quality and therefore needed to be taken into consideration in the choice of the processing parameters.

Subsequent work focused on mechanical testing. Lap shear, T-peel, pull-out and fatigue tests were carried out in order to examine the mechanical behaviour and to analyse the failure mechanisms of the joints. The work showed that the strength, the thickness and the surface condition of the riveted sheets affected the strength and the failure mechanisms of the joints. The joint strength was also observed to be dependent on the rivet and anvil design as well as the setting force. In addition, the joint strength and behaviour differed as the specimen geometry thus emphasising the need for a test standard for self-piercing

riveted joints. Paint baking led to a marginal and insignificant reduction in the static strength, whilst resulting in a reduction in the fatigue strength of the joints as a consequence of recovery of the 5754 alloy and the removal of the wax-based surface lubricant. The effect of 3%, 5% and 10% pre-straining of the 5754 sheet on the quality and performance of the self-piercing riveted joints was also examined. It was established that it was possible to produce joints of good quality, higher strength and superior fatigue performance by using the same setting parameters as for joints without additional pre-straining. An investigation of the effect of the shelf-life of AA6111 indicated that this only had a minor and insignificant effect on the joint quality and behaviour. It was therefore deduced that the quality and performance of joints would not be compromised even after an AA6111 self-life of 21 months. The effect of the interfacial characteristics on the joint quality and behaviour was examined by placing a PTFE layer at the interface between the riveted sheets. It was observed that the PTFE insert significantly reduced the joint strength and changed the failure mechanism.

Three distinct failure modes, referred to as rivet pull-out, rivet fracture and sheet material failure, were observed during this investigation. All shear tested samples failed by rivet pull-out. The same failure mechanism was the only one observed for the pull-out tests. The failure mechanism for the peel test depended on the thickness of the rivet sheet. For joints with a (1mm+2mm)/(0.9mm+2mm) combination, fracture of the thinner sheet material dominated the failure mechanism, whilst for joints with a (2mm+2mm) combination, rivet pull-out was the only failure system. Rivet fracture and sheet material failure were also observed during fatigue testing.

Examination of samples following fatigue testing led to the observation of fretting which had not been reported by previous investigators working with self-piercing rivets. Fretting had an important effect on the fatigue strength and fatigue failure mechanisms. Inspection of fatigue fractured samples which were tested at maximum applied loads ranging from 50% to 85% of the ultimate shear load of the joints exhibited fretting scars at three different interfaces. Flange-face fretting was observed to take place at one side of the interface between the two riveted sheets and led to the formation of mainly Al_2O_3 debris. Pin-bore fretting was observed to occur between the rivet shank and the aluminium alloy sheet and led to debris containing oxides of aluminium and iron together with the oxides of

zinc and tin from the wear of the corrosion protective coating of the rivet. Both types of fretting were affected by the applied load and the surface condition of the riveted sheets. Further examination indicated that fretting contributed to the initiation and propagation of fatigue cracks. The failure modes during fatigue testing were affected by the fretting behaviour and were dependent on the applied load and the interfacial conditions. A PTFE layer introduced a very low coefficient of friction leading to a significantly reduction in the amount of fretting. However, this was accompanied with a change in the load transfer mechanism resulting in rivet fracture and a shorter fatigue life. The paint-baking process led to the removal of the wax-based surface lubricant and fretting cracks therefore initiated at an earlier stage of the fatigue test. In addition, fretting also led to a significant work-hardening of the riveted sheets. It was observed that there was an increase in microhardness at the regions immediately below the fretting area from the riveted sheets. The depth of the work-hardened area below the fretting interface after different periods of fretting represented the depth of damage as a result of fretting fatigue. It was therefore further indicated that fretting played an important role in the fatigue behaviour and would probably affect the crash behaviour of the joints.

The effect of secondary bending, an inherent feature of lap joints, was examined and analysed using strain gauge measurements. It was established that secondary bending contributed to the failure mechanism and led to a significant reduction in the fatigue strength of such joints. Using the experimental data an analysis has been carried out to predict the fatigue strength in the absence of secondary bending.

ACKNOWLEDGEMENTS

I would like to acknowledge the guidance and support received from my supervisors, Dr Andreas Chrysanthou, Dr Yong Kang Chen and Dr Jim O'Sullivan. Special gratitude is expressed to Dr Andreas Chrysanthou for the daily discussions of the work, for the careful reading of the thesis chapter by chapter from the early stages of its production and for patiently discussing with me many of the academic concerns as well as grammatical problems.

Thanks also go to those at Alcan International Limited who co- funded the project and deserve a special mention. These are Dr Dubravko Nardini, Mr Douglas Boomer and Mr Colin Scott who ensured the supply of material and offered their support throughout the project. Thanks are also expressed to Mr Dean Homewood of Textron Fastening Systems in Canada for the preparation of all the specimens.

Thanks are also extended to the Department of Aerospace, Automotive and Engineering Design, University of Hertfordshire for the financial support and in particular the Head of Department, Professor Peter Bullen. I also express my thanks to the technical officers, Mr Peter Thompson, Mr Dave Smith and Mr Bill Liley who offered their help during the experimental work.

Sincere thanks must go to my honest husband and my lovely daughter for their understanding and for giving me the drive and motivation to complete the project. Finally, I would like to express my gratitude to my parents and my brothers for their constant support.

CONTENTS

List of Figures

List of Tables

CHAPTER ONE

1. INTRODUCTION

Today's automotive industry is a challenging business, which is required not only to respond to environmental concerns about greenhouse gases and fuel economy, but also to meet customer expectations. Therefore, the next generation of vehicles must achieve fewer emissions, higher fuel efficiency and better performance. According to Polmear [1], fuel consumption can be reduced by 5.5% for each 10% reduction in vehicle weight. Moreover, for every kilogram saved in vehicle weight, a reduction of 20kg of CO_2 emissions can be achieved for a vehicle covering 170,000km. The need for weight reduction has led to the growing application of lightweight materials, such as aluminium and polymer composites.

The use of aluminium alloys offers a vehicle of lower weight and may lead to better fuel economy and fewer emissions, whilst the performance, comfort and safety are not compromised. Aluminium alloys have the advantage of high corrosion resistance, good formability and crashworthiness. In addition, the outstanding recyclability of aluminium alloys also poses a considerable attraction to manufacturers. Therefore, there are significant benefits in using aluminium alloys, particularly in the car body. However, the use of aluminium requires not only a different approach in car design, but also a new manufacturing technology including new joining methods. This has therefore triggered many investigations into new joining techniques for aluminium alloys.

1.1 Conventional Joining Methods for Aluminium Alloys

1.1.1 Spot-Welding

Spot-welding and arc-welding are the most popular conventional joining techniques in the automotive industry. Spot-welding has been the principal joining process for decades in steel vehicle body structures. However, the quality of spot-welds for aluminium alloys may be poor. In addition, there are other concerns due to the short electrode life and the requirement of a higher manufacturing capital.

Aluminium easily reacts with oxygen in the atmosphere and forms an oxide film on the metal surface giving protection to the metal from corrosion. However, according to Patrick et al. [2], the substantially higher melting point of this oxide film requires significantly higher resistance heating to break it down in order to allow weld formation to take place. Coupled with the high electrical and thermal conductivity of aluminium alloys, nearly three times the current and two times the electrode force are required for welding bare aluminium compared with welding bare steel. Consequently, the electrode life for aluminium alloy spot-welding is 2.5 to 5 times lower, compared with the electrode life for the spot-welding of mild steel. However, the welding time for aluminium alloys is only a quarter to half the time that is required to weld the same thickness of steel, due to the lower melting temperature. In addition, more accurate control of the welding parameters is required compared with steel, due to the effect of the surface oxide and surface roughness as well as the very narrow plastic range of aluminium. Auhl et al. [3] reported that these critical variables led to poor welds that could occur at random and at any time. It is obvious that the shorter electrode life requires more investment in the electrode. Apart from this, the different requirements on current and electrode force make the equipment which is used in the automotive production lines for steel spot-welding unlikely to be used for aluminium alloys. The investment in the development of new equipment for spot-welding aluminium alloys is considerable. Therefore, employing the technique for aluminium is likely to be more expensive. These factors have impelled manufacturers to look for alternative joining techniques.

1.1.2 Arc-welding

Metal Inert Gas (MIG) and Tungsten Inert Gas (TIG) are the two main processes of arc-welding used by industry. In automotive manufacture, the process has been well-automated and has significant advantages in steel structure fabrication. However, the process requirements for welding aluminium are extremely difficult.

The high thermal conductivity of aluminium requires an intensive and localized heat source, while its relatively large coefficient of thermal expansion demands a high welding speed to minimize the distortion. Polmear [1], Gingell et al. [4] and Barnes et al. [5] reported that the surface oxide film, which has a high melting point, needed to be removed or it might become entrapped and form inclusions in the weld bead. In addition, low hydrogen content was required due to the high solubility of this gas in molten aluminium, otherwise, weld porosity occurred after solidification. Furthermore, the environmental issues related to oxide fumes, arc-eye and the requirement of intensive energy, presented difficulties for arc-welding of aluminium alloys. Additional costs were thought to be inevitable to improve the process and protect the human operator from the hazardous environment. Therefore, to employ the process for aluminium, further development is necessary in order to minimise the disadvantages and facilitate the application of the process in service.

There is growing interest in other joining techniques for aluminium due to the notable disadvantages of the conventional joining methods. Many studies have examined the suitability of other joining methods and explored new joining techniques. As a result, relatively new joining techniques have been developed, as outlined in the next section.

1.2 Relatively New Joining Techniques for Aluminium Alloys

Laser welding, friction stir welding and mechanical fastening as well as adhesive bonding are the relatively new joining methods that are considered as candidates for joining aluminium in the automotive fabrication and assembly.

1.2.1 Laser Welding

Two main types of lasers can be considered for sheet metal joining. They are CO_2 lasers and Nd: YAG lasers. According to Jones [6], laser welding offered many advantages for joining sheet materials, such as a lower overall heat input, which resulted in very little thermal distortion, a higher welding speed and a smaller heat affected zone. Barnes et al. [5] also reported that the potential for automation and the inherent flexibility of the system made laser welding more attractive. However, high surface reflectivity, high thermal conductivity, and for some alloys, low melting point constituents, low viscosity in the liquid phase and the presence of the surface oxide layer, are the main difficulties encountered by laser welding process for aluminium. Therefore, Jones et al [7] suggested that a high power density and a high welding speed are necessary to avoid limited penetration depths, an irregular shape and a rough appearance. Apart from these, the relative expense of capital equipment and the consumable items, such as the shielding gas, must be taken into account. In addition, according to Barnes et al. [5], the risks of accidental injury whilst the laser is in operation and damage to the eye, which can result from exposure to some laser beams, also need to be considered. Further work on real aluminium components is necessary in order to assess the performance of laser-welded assemblies in service.

1.2.2 Friction Stir Welding

Friction stir welding (FSW) was invented at The Welding Institute (TWI) in 1991. It is a solid phase process and particularly suitable for joining lightweight sheet materials, such as aluminium, copper, lead and plastics to produce straight-line welds. According to Kallee et

al. [8], Waldron et al. [9], the process has a number of advantages including low cost, low power demand, good appearance of the weld bead, no emission of fumes and radiation. In addition, as a solid-phase weld, many of the problems associated with liquid-phase welding aluminium alloys are avoided. The surface oxide layer can be effectively broken and dispersed throughout the weld due to the weld action. However, as a relatively new joining method, FSW limitations still remain. Besides a relatively slow process rate, Kallee et al. [10] also reported that two components being joined need to be clamped rigidly onto a backing bar due to the high pressure involved in the process in order to avoid the two pieces being forced apart, whilst a hole left at the end of each run has to be filled. In addition, according to Powell et al. [11], for some aluminium alloys, post-weld heat-treatment is required to optimise the properties in the joint area and this is not a practical solution for many applications, Therefore, further development is necessary.

1.2.3 Adhesive Bonding

Adhesive technology can be an alternative method for joining aluminium alloys. Compared with other joining techniques, such as welding and mechanical fastening, adhesive bonding can reduce stress concentrations and is more flexible and versatile, in addition to its ability to seal joints against moisture. Furthermore, according to Tavakoli [12], the process can save weight, reduce cost and is capable of joining dissimilar materials. However, the adhesive joints are inherently weak in peel and vehicle design would need to take account of this, particularly with regard to crashworthiness. Additionally, the long-term durability of adhesive joints and the effects of weathering and eventual water ingress are not clearly understood. Furthermore, the environmental issue in connection with adhesive dispensing is also a significant area of concern. Therefore, Barnes et al. [13] have reported that adhesive bonding is less competitive in the domain of joining techniques for the automotive industry.

1.2.4 Self-piercing Riveting and Clinching

Self-piercing riveting and clinching are relatively new mechanical fastening techniques with considerable potential for use in the automotive industry.

Self-piercing riveting is a point joining process and, unlike conventional riveting, does not require a pre-drilled hole. The process cycle is illustrated in Fig.1.1.

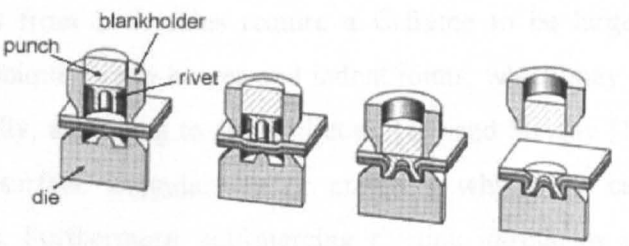

Figure 1.1 Schematic representation of the self-piercing riveting process

The sheets to be joined are clamped between a blank-holder and an upset die. A semi-tubular rivet is fed under the punch through a feeding system. The punch is then driven down by a setting force which is produced from a hydraulic or electrical power system. As the setting force increases, the rivet is forced to pierce the upper sheet and flare into the bottom sheet under the effect of the upset anvil. The punch is then lifted and a joint with a mechanical interlock is formed. A button is left on the underside of the bottom sheet due to the effect of the upset die. The joint can be set flush in one side if a countersunk rivet is used. Oval head rivets can also be used if non-flush on both sides is acceptable. Ideally, the rivet tail should not break through the bottom sheet. Clinching, as an offshoot of self-piercing riveting, is a similar operation, but without a rivet.

Both self-piercing riveting and clinching offer several benefits to assemblers. The process of no pre-drilled hole not only saves labour and time, but also avoids the problem of alignment encountered by conventional riveting. Moreover, the processes can join a wide range of materials, combinations of similar or dissimilar materials and multi-layered sheets with an equivalent speed of operation. In comparison with spot-welding, the process is safe and environmentally friendly due to a lower energy requirement, low noise emission and

no fumes or heat radiation. In addition, the process is simple and can be easily automated. Furthermore, the equipment has a long tool-life, and therefore the capital and operating costs are relatively low. Riches et al [14] and Barnes et al [13] have reported that compared with clinching, self-piercing riveting has a better load-bearing ability, and therefore, can be used in load-bearing situations, while clinching is suitable for areas of lower loading.

In spite of these advantages, there are still a number of barriers to widespread exploitation of these techniques. It was reported by Westgate et al. [15] that the high setting force and the need for access from both sides require a C-frame to be large and stiff enough. Moreover, both techniques leave bulges and indent joints, which may not be aesthetically desirable. Additionally, according to Howard et al. [16] and Sunday [17], corrosion could occur due to the surface irregularities or crevices, which are caused by the cold deformation process. Furthermore, self-piercing riveting introduces a consumable rivet, which adds weight to the process. For aluminium alloys, steel rivets are used and this may cause galvanic corrosion in the joint.

According to Patrick et al. [18], the self-piercing riveting process is extremely robust, simple and cost-effective even with the rivet consumable cost, The difficulties posed by the surface oxide in welding aluminium and the high capital investment as well as the high running cost make welding less competitive in the domain of joining aluminium. Martukanitz et al. [19], Matsumoto et al. [20] and Larsson et al. [21] reported that laser welding can be used to join steel components. Whether it can be successfully used for aluminium alloys in practice is still under investigation. Besides the requirement of a backing bar and the fade-out problem, friction stir welding can only be applied as straight line welds on a sheet. Therefore, with its advantages, mechanical fastening is likely to be a competitive joining method in the near future. As a result, the development of mechanical fastening and in particular self-piercing riveting has been accelerated.

1.3 Development of Self-piercing Riveting

Self-piercing riveting is considered to be an alternative to spot-welding. Therefore, the process reliability, the possibility for mass production as well as the mechanical performance of self-piercing riveted joints including static and dynamic strength characteristics and the failure mechanisms must be evaluated and compared with alternative methods.

King [22] conducted a detailed study of the process, in which a four-step setting force-displacement curve was used to identify the measurable process parameters affecting the quality of the joint. Based on this study, a process quality monitoring system was successfully developed and computerised thus enabling 100% inspection as well as partial control of the fastening quality. The automated process quality monitoring system for self-piercing riveting, "FASTRIV", provides the possibility of further development of the process. In addition, according to Lapensee [23] and Westgate et al. [15], the innovation of modern equipment including robot-mounted equipment and a lightweight long reach C-frame riveting gun with an adequate stiffness also facilitates the development of the process and makes it more reliable. The development has not only solved the problem of the reach limitation, but also provided the possibility of using self-piercing riveting in a high volume automated assembly.

As the process developed, most research studies focused on the comparison of the mechanical behaviour of self-piercing riveted joints with spot-welded joints. Lapensee [23] reported that compared with spot-welding, the static strength of self-piercing riveting was higher in the case of aluminium to aluminium and lower in the case of steel to steel. However, Razmjoo et al. [24] indicated that the static strength of self-piercing riveted joints was lower than that of spot-welded joints for both steel to steel and aluminium to aluminium joints. It was also observed that the static strength of spot-welded joints was at least 60% higher in steel specimens and 30% higher in aluminium specimens compared with self-piercing riveted joints for identical combinations. Olivier [25] conducted an investigation on the static properties of a self-piercing riveted joint and a spot-welded joint in steel sheet and indicated that the static strength of spot-welded joints was higher than that of self-piercing riveted joints, Additionally, both Riches [14] and Westgate [26]

predicted that a high static strength could be achieved for self-piercing riveted joints through a suitable rivet and anvil design. The fatigue strength of self-piercing riveted joints in a number of materials, which are favoured by the automotive industry, was reported to be superior to spot-welded joints, by Razmjoo [24], Krause et al [27], Sunday [17], Booth et al. [28].

In addition to the measurement of the static and fatigue strength, research studies also reported a variety of failure modes. King [22] has summarised six types of failure mode, which occurred during static testing. The failure mode, which occurred during fatigue testing of self–piercing riveted aluminium sheets, was described as an eyebrow crack by Krause et al [27]. Westgate and Razmjoo [26] reported that different failure modes occurred in steel specimens and aluminium specimens. The most recent research that was carried out by Fu and Mallick [29, 30] at the University of Michaen indicated that fracture of the pierced sheet was the only failure system during fatigue testing. Despite the description of the failure mode in the literature, the failure mechanism for a self-piercing riveted joint still remains uncertain.

1.4 Further Development

The substantial advantages that can be gained from self-piercing riveting make the process more attractive than the welding process. Coupled with the development of the process, self-piercing riveting is beginning to be incorporated into the manufacturing procedures for low weight vehicles. Audi's A8, the first generation of Aluminium Space Frame vehicle first adopted this joining technique in its assembly. According to Mackenzie [31], following positive experience with the A8, the use of self-piercing rivets was increased by 40% to a total of 1800 in the Audi A2, mainly to join sheet metal and extruded sections, At Jaguar, the first aluminium car, the XJ350, employed 3300 rivets in its assembly. In addition to the application in car-body assembly, self-piercing rivets have also been used in truck assembly. According to Sibley [32] and Bonde et al. [33], Volvo used 42 self-piercing rivets to improve the fatigue strength of the FH12 cab. However, the application is still at an early stage and as a relatively new joining technique, further development is necessary.

Despite the limitations mentioned above, no agreed standard for testing self-piercing riveted joints exists. The specimen geometry and testing methodology need to be standardised, in order to relate test performance to in-service performance. All tests performed in previous studies followed the existing standard either for spot-welding, [Westgate [26]], or for blind riveting, [King [22]], in which most of the specimen geometry was a single lap joint. Such lap joints are simple to fabricate. However, the inherent eccentricity that results in deformation and referred to as secondary bending, as shown in Fig.1.2, creates additional axial stresses in the lap joint. These stresses are restricted to a small area, where cross-sectional discontinuities occur. Secondary bending is an inherent feature of a single lap joint and affects the mechanical behaviour of a conventional riveted single lap joint. Kulak at al. [34] reported that secondary bending played a dominant role in the fatigue behaviour of a conventional riveted lap joint, whilst not significantly affecting the ultimate strength of such joints. Hartman [35] investigated the effects of secondary bending on the fatigue strength of 2024-T3 Alclad conventional riveted joints and reported that the symmetric butt-joint was definitely superior to the lap-joint and the single-strap butt-joint. Schűtz et al [36] have performed a detailed investigation on the effect of secondary bending on the fatigue strength of conventional riveted joints. Single-shear specimens with secondary bending and double-shear specimens without secondary bending were produced by keeping all other factors including the type of fastener the same. The test results revealed that double-shear specimens had higher fatigue strength than single-shear samples. However, the effect of secondary bending on the mechanical behaviour of a self-piercing riveted joint has only been investigated by Razmjoo and Westgate [24], who carried out a study by using so called "H" section specimens to eliminate the effect of secondary bending. The results indicated that the fatigue strength of the single-point lap joints was 30% to 50% lower than that of the "H" specimens for both steel to steel and aluminium to aluminium joints. However, Carr et al [37] pointed out that the "H" section geometry was not a suitable geometry for the selection of joining system, since the accuracy of the machining and manufacture of the sample, together with the alignment of the specimen could greatly affect the test results. Therefore the effect of secondary bending on the behaviour of a self-piercing riveted single lap joint needs to be examined.

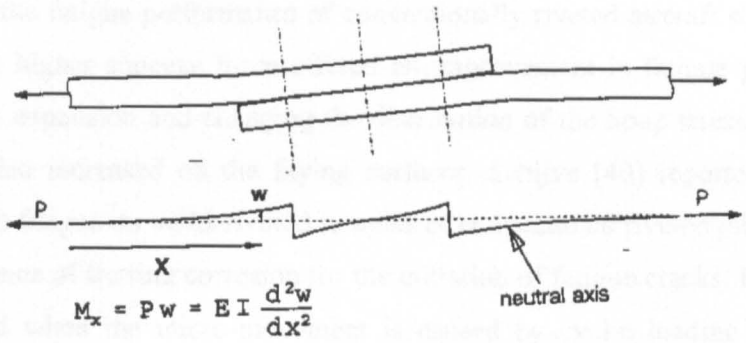

Figure 1.2 Schematic of secondary bending

In addition, the mechanical behaviour of self-piercing riveted joint is still not fully understood. Very little or no data are available in the public domain even though some applications have taken place in the automotive sector. It is evident that some materials can be joined by such means and excellent performance can be achieved. However, for individual materials, whether such a joint can achieve good performance still needs to be investigated. The mechanical behaviour of such a joint is strongly dependent on the materials being joined. Furthermore, it has been known that the change of material properties affects the performance of such a joint. However, the effect of the change of the material properties during vehicle production on the behaviour of such joints still remains uncertain. Additionally, in the automotive industry, the most important single factor to be considered for the application of such joints is the effect of cyclic loading in service.

Conventional riveting, in contrast to self-piercing riveting, has been a major joining method in the aircraft industry for a long time and the failure mechanisms are well documented. Fretting, as a kind of wear and corrosion phenomenon, which occurs between two contacting components when subjected to an oscillatory load and micro-slip was observed to take place in conventional riveted joints. For example, Iyer et al. [38] investigated the effect of fretting on fatigue and corrosive wear deterioration of a conventional riveted lap joint. A 3-D finite element model was developed and used to analyse the deformation of a riveted lap joint and the factors that can lead to fretting damage. According to the study, serious fretting occurred at the interface between two riveted sheets, when the rivet tilted and pressed its head with a large force against the panel at the edge of the hole. Szolwinski et al. [39] examined the influence of the process

parameters on the fatigue performance of conventionally riveted aircraft structures. It was revealed that a higher squeeze force offered an improvement in fatigue performance by increasing hole expansion and changing the distribution of the hoop stress, whilst fretting damage was also increased on the faying surfaces. Schijve [40] reported Multiple-Site Damage (MSD) fatigue on multi-riveted samples of conventional riveted joints and pointed out the importance of fretting corrosion for the initiation of fatigue cracks. Fretting fatigue, which occurred when the micro-movement is caused by cyclic loading on one of the contact members, has been shown to play an important role in the initiation of fatigue cracks and MSD fatigue in conventional riveted joints.

Self-piercing riveting is very different from conventional riveting and there is no reason to expect the two to behave in the same manner. Very few previous investigations have examined the fatigue behaviour of self-piercing riveted joints and none of these has reported fretting to occur. There is therefore a need to examine the fatigue behaviour and failure mechanisms of self-piercing riveted joints.

1.5 Research Objectives

The project aimed to underpin the fundamentals of the mechanical behaviour of 5754 and 6111 aluminium alloys joined by self-piercing rivets in a variety of joint combinations. The heat-treatment and work-hardening processes which take place during vehicle assembly were taken into account. The mechanical behaviour of self-piercing riveted joints was investigated in terms of strength characteristics and failure mechanisms. Some of the work was carried out in the context of requirements from the automotive industry. Alloys 5754 and 6111 are the materials that are of interest to the automotive industry and in fact have been used in the Jaguar XJ350 model. Paint-baking and pre-straining were involved in the manufacturing process and therefore their effect on joint quality and behaviour were of specific interest. In addition, due to industrial requirements, the effect of the shelf-life of the material was also investigated.

The project was split into the following objectives:

1. The investigation of cross-sectional deformation characteristics of riveted joints in order to establish the setting conditions for good-quality joints.
2. The investigation of the strength characteristics of riveted joints by performing static and dynamic testing.
3. The examination of the influential factors such as sheet thickness, alloy heat-treatment and work-hardening on the joint quality and behaviour.
4. The investigation of the failure mechanisms of self-piercing riveted joints and in particular of the fatigue failure mechanisms.
5. The examination of the distribution of secondary bending in riveted joints in order to clarify the influence of secondary bending on the mechanical behaviour.

The project has been performed in collaboration with Alcan International Limited and Textron Fastening Systems. Alcan has supplied the aluminium alloy sheet material whilst Textron Fastening Systems have manufactured all the specimens that were tested.

CHAPTER TWO

2. EXPERIMENTAL PROCEDURE

2.1 Test specimens for Fastener Evaluation

The most important requirement of any standard specimen is that it should be representative of the structural feature which it is to be simulated. Alcan International Limited has classified joint types with respect to the joint angle in an actual vehicle. The results of this classification are shown in Fig.2.1. It is evident that the lap-shear joint, which has a 0° angle, represents almost 50% of the total joint length in this vehicle. Therefore there is a good case for studying such a joint type. In addition, self-pierce riveting is being considered as an alternative to spot-welding and therefore for comparison, it is better to follow the test standard for spot-welding. The latest test standard for spot-welding by the International Organisation for Standardisation (ISO) is titled "Methods for the fatigue testing of spot-welded joints" [41], in which the basic specimen geometry of specimens is a single lap joint. Therefore a single lap joint was chosen as the basic geometry for this study.

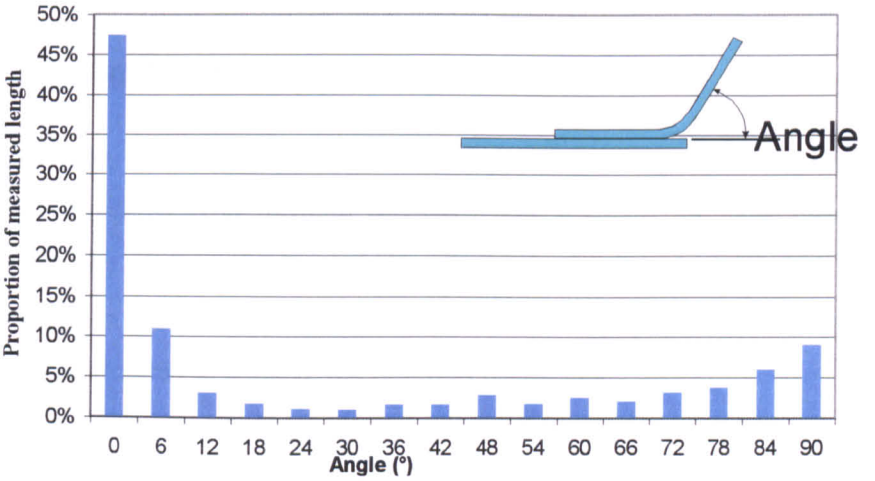

Figure 2.1: Joint angle distribution (0° is lap, 90° is T)

2.2 Objectives of the Experimental Approach

The objectives of the experimental work can be summarised as follows:

1. To produce self-piercing riveted joints for sheet material of various conditions, including different surface conditions, pre-straining levels, thickness and thickness combination as well as shelf-life by using an identical rivet and anvil design.
2. To investigate the cross-sectional characteristics of the self-piercing riveted joints, relating to rivet and sheet material deformation during setting, in order to establish the effect of the variations mentioned above on joint quality.
3. To determine the strength characteristics of the self-piercing riveted joints by performing lap shear, peel, pull-out and fatigue tests.
4. To examine the deformation characteristics and the failure mechanisms of the self-piercing riveted joints from the tests by means of light microscopy, Scanning Electron Microscopy (SEM) and Energy Dispersive System (EDS) analysis.
5. To investigate the influence of Secondary Bending (SB) by using strain gauges to measure the strain level on the sheet material.

2.3 Setting Parameter of Self-piercing Riveted Joints

2.3.1 Self-piercing Rivets

A semi-tubular type is the basic form of a self-piercing rivet, which is made of wire material by a multi-blow cold forming process. The material for rivet manufacture is limited by its ability to be cold formed, but it can be hardened up to 550 Vickers. A standard specification BS EN 10263 of wire material is used for the formation of the rivets, which are then heat-treated to achieve the required properties.

Fig.2.2 shows a self-piercing rivet with a countersunk head. The proportions of the head diameter, poke diameter and poke depth are dependent on the rivet shank diameter.

Shank Diameter: The two most common rivet diameters of 4.8mm and 3.9mm were used in this study. Table 2.1 presents the head diameter, poke diameter, poke depth and the tolerance range for a given rivet shank diameter.

Shank Length: The length of the rivet shank is selected based on the thickness of the material to be joined. As the joint thickness increases the rivet length also has to increase in proportion. However, the rivet shank must not break through the lower sheet because of the requirement of good visual quality. In this study, three typical rivet lengths were selected based on the experience of Textron Fastening Systems and confirmed by metallographic investigation of fastening sections.

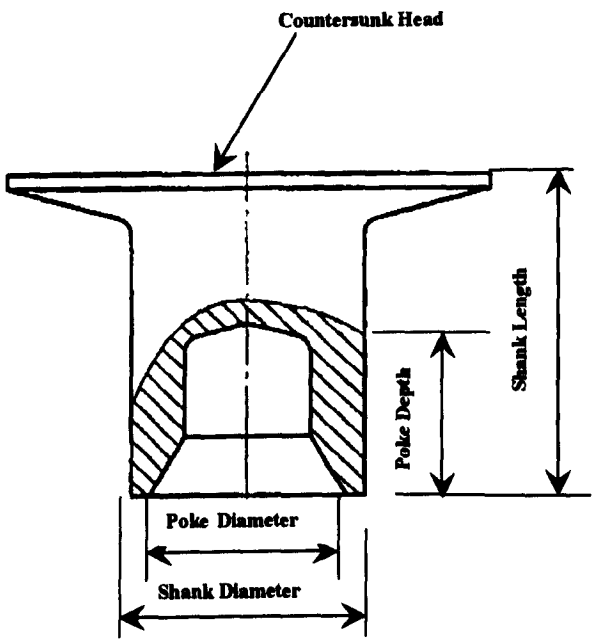

Figure 2.2 Self-piercing Rivet

Rivet Head: A standard countersunk head has been used throughout, as seen in Fig.2.2. The diameters of the head are also listed in Table 2.1.

Surface Coating: The external surface of the rivet was protected by a coating to prevent galvanic corrosion. Four kinds of alternative rivet coatings are available currently in Textron Fastening Systems, named Mechanical Zinc, Mechanical Zinc/Tin, Silver Almac and Delta Seal coating. A silver Almac coating, which contains tin and zinc, was chosen for this project.

Table 2-1 Rivet Geometrical Data (All dimensions: mm)

Shank Diameter	Shank Length	Head Diameter	Poke Diameter	Poke Depth	Hardness (H_V)	Rivet Code
$4.8_{-0.15}$	$6.5^{\pm 0.15}$	$8.7_{-0.3}$	$3.8^{\pm 0.1}$	$4.0^{+0.2}$	380/420	23-0282
$4.8_{-0.15}$	$7.0^{\pm 0.15}$	$8.7_{-0.3}$	$3.9^{\pm 0.1}$	$4.6^{+0.2}$	450/500	23-5233
$3.9_{-0.1}$	$6.0^{\pm 0.15}$	$8.1_{-0.3}$	$3.3^{\pm 0.1}$	$3.5^{+0.2}$	450/500	FSC3960002Z11
$3.9_{-0.1}$	$5.0^{\pm 0.15}$	$8.1_{-0.3}$	$3.3^{\pm 0.1}$	$3.0^{+0.2}$	450/500	FSC3950001Z11
$3.2_{-0.1}$	$3.0^{\pm 0.15}$	$6.5_{-0.3}$	$2.8^{\pm 0.1}$	$2.0^{+0.2}$	400/450	FSC3230001Z11

2.3.2 Sheet Materials

Depending upon the application, aluminium alloys for car-body sheet applications must have a strength comparable to steel, adequate formability, they must be dent and corrosion resistant, and must have good surface appearance. Therefore, alloys of 5xxx series and 6xxx series have been favoured for use by the automotive industry.

Standard tensile tests were performed on the two sheet materials used in the investigation in order to obtain their mechanical properties. The specimen geometry is shown in Fig. 2.3.

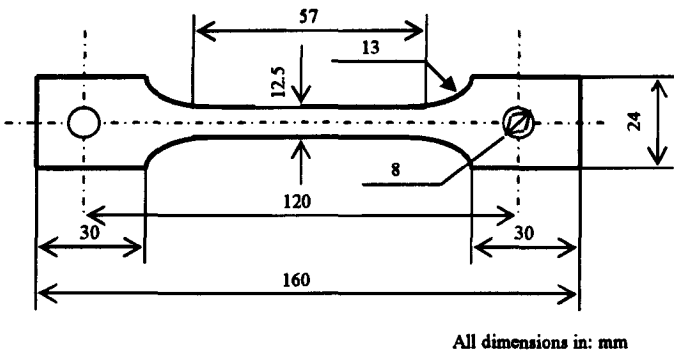

Figure 2.3 Specimen geometry for tensile test of sheet material

2.3.2.1 NG5754

Wrought NG5754 aluminium alloy sheets of 1mm and 2mm thickness were used in this study. The NG5754 alloy sheets were pre-treated with a chromate free film. The sheet was also coated with a wax-based surface lubricant whose concentration was below 1%.

2.3.2.2 HS5754

The HS5754 aluminium alloy sheets were the same as the NG5754 alloy sheets except that the HS5754 sheets were not coated by the wax-based surface lubricant. Only 2mm thick HS5754 sheets were tested.

The mechanical properties and the nominal alloy composition of the NG5754 and the HS5754 aluminium alloy sheets are listed in Table. 2.2.

Table 2-2 Compositions and Mechanical Properties of 5754

MECHANICAL PROPERTIES					
Young's Modulus (GPa)	Tensile strength (MPa)		Elongation	Hardness (H_V)	
70	250		25%	68	
NOMINAL COMPOSITIONS					
Si	Fe	Cu	Mn	Mg	Al
0-0.40	0-0.40	0-0.10	0-0.50	2.60-3.60	Balance

2.3.2.3 Pre-strained NG5754

Strain-hardening occurs during most working and forming operations. Therefore, the pre-strained NG5754 sheets were tested in order to simulate the forming process during car-body assembly.

The pre-strained NG5754 alloy sheets were obtained from the NG5754 sheets by pre-straining to different levels at a crosshead speed 15mm/min. Three pre-straining levels were achieved and tested. The load versus extension curves obtained during pre-straining are presented in Figs. 2.4-2.6.

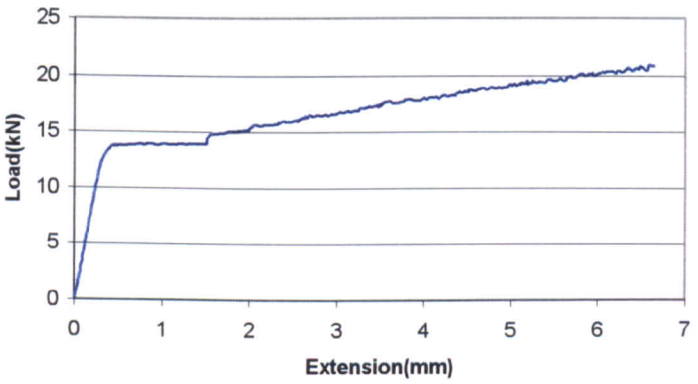

Figure 2.4 Load vs. Extension for 3% Pre-straining of NG5754

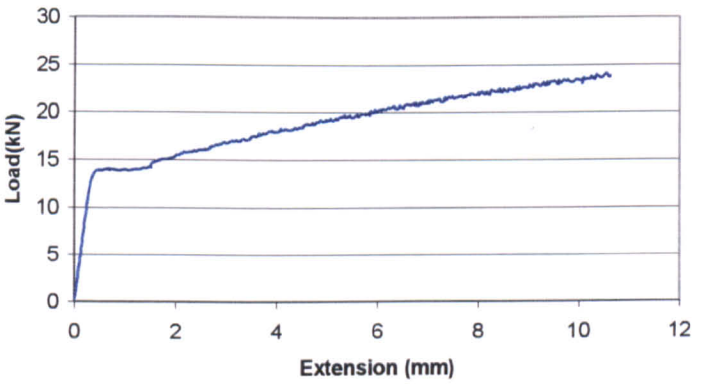

Figure 2.5 Load vs. Extension for 5% Pre-straining of NG5754

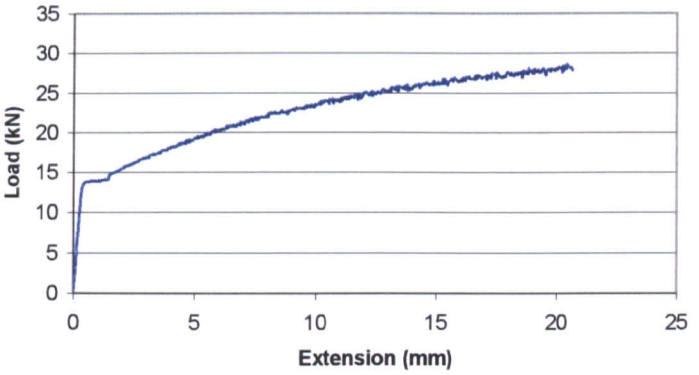

Figure 2.6 Load vs. Extension for 10% Pre-straining of NG5754

The composition of the pre-strained 5754 aluminium alloy sheet is the same as NG5754 and HS5754, but the mechanical properties had changed as a result of pre-straining and are shown in Table 2.3.

Table 2-3 Mechanical Properties of Nominal 5754

MECHANICAL PROPERTIES			
Pre-strain level	Tensile strength (MPa)	Elongation (%)	Hardness (H_V)
3%	254	20	73
5%	261	18	77
10%	276	16	86

2.3.2.4 AA6111

The heat-treatable aluminium alloy AA6111 sheet was in wrought form and initially in the T4 condition. The material was riveted after a shelf-life of various period of time. During the shelf-life period, the material was expected to undergo natural ageing. Two thicknesses of 0.9mm and 2mm were used for the AA6111 alloy sheets. The chemical composition and the mechanical properties of the AA6111 alloy sheet are shown in Table 2.4.

Table 2-4 Composition and Mechanical Properties of AA6111

MECHANICAL PROPERTIES					
Young's Modulus (GPa)	Tensile strength (MPa)	Elongation	Hardness (H_V)		
70	308	26%	93		
NOMINAL COMPOSITIONS					
Si	Fe	Cu	Mn	Mg	Al
0.20-1.70	0.70	0.90	0.80	0.10-1.40	Balance

2.3.3 Anvil Tooling

The purpose of the anvil is to provide a shaped cavity to accommodate the extent of deformation and to cause the rivet shank to flare during joint formation. The anvil shape affects both the piercing force and the flaring in the rivet shank and therefore, the joint strength. Four different anvil profiles are available at Textron Fastening Systems. The selection of the anvil profile is dependent on the rivet dimensions and the material specifications. Therefore, a specific anvil design should be adopted for each different fastening application. In this investigation, the selection of the anvil profile was accompanied with a corresponding different rivet design in order to make the test results comparable.

2.3.4 Setting Force

A relatively high setting force is required by a self-piercing rivet to deform and compress the sheet material until the rivet is set fully down. A rivet with a flat countersunk head normally requires a higher setting force than a rivet with an oval head in order to flush with the top sheet. The value of the setting force depends on the material specification, material hardness and thickness as well as the rivet and anvil design. Therefore different setting force values were selected.

2.3.5 Fastening Conditions

For the purpose of this investigation, all fastenings were created between two sheets of material only, as this is seen as the most common application in auto-body assembly. Different codes were introduced to identify the fastening conditions. An explanation of the fastening codes is summarised below:

FS: refers to fastening, N5: refers to NG5754, H5: refers to HS5754, A6: refers to AA6111, P5: refers to Pre-strained NG5754 and the accompanying number refers to the percentage amount of pre-straining.

2.3.5.1 FSN5 Series

The NG5754 alloy sheets were jointed in pairs to create the FSN5 series of fastenings. The fastenings identified by '*' were exposed to a paint-bake cycle (PB) at 180°C for 30 minutes after joining but prior to testing. The geometry of the FSN56 fastening was smaller than the other samples and will be described later.

Table 2.5 shows the fastening conditions of the FSN5 series of fastenings.

Table 2-5 Fastening Conditions for FSN5 Series

Fastening Code	Rivet Code	Sheet Material Thickness (mm)		Anvil Code	Setting Pressure (bar)	Note
		Upper sheet	Lower sheet			
FSN51	23-5233	2	2	64015	240	
FSN51*	23-5233	2	2	64015	240	PB
FSN52	FSC3960002Z11	2	2	64220	120	
FSN53	FSC3950002Z11	1	2	64220	100	
FSN53*	FSC3950002Z11	1	2	64220	100	PB
FSN54	FSC3950002Z11	2	1	64220	100	
FSN55	FSC3230001Z11	1	1	SK46527/15	60	
FSN56	23-5233	2	2	64015	240	Small

2.3.5.2 FSH5 Series

The FSH5 series of fastenings was prepared from the HS5754 alloy sheets only. A PTFE tape was inserted at the interface between the two riveted sheets before the riveting process to form the FSH52 fastening. The PTFE tape had a 1.9mm width and a 0.2mm thickness.

The fastening conditions of the FSH5 series are shown in Table 2.6.

Table 2-6 Fastening Conditions for FSH5 Series

Fastening Code	Rivet Code	Sheet Material Thickness (mm)		Anvil Code	Setting Pressure (bar)	Note
		Upper sheet	Lower sheet			
FSH51	23-5233	2	2	64015	240	
FSH52	23-5233	2	2	64015	240	PTFE

2.3.5.3 FSP5 Series

The pre-strained NG5754 alloy sheets with three pre-straining levels were joined in pairs. The fastening conditions for the pre-strained NG5754 sheets were the same as the FSN51 fastening, which was made from the NG5754 with 0% pre-straining in order to make the test results comparable. The FSP50 and the FSP50* fastenings were the same as the FSN51 and the FSN51* fastenings respectively. Half of the fastenings were exposed to a paint-bake cycle indicated by a "*" in the fastening code, while the others were not.

Table 2.7 lists the fastening conditions for the pre-strained NG5754 sheet.

Table 2-7 Fastening Conditions for FSP5 Series

Fastening Code	Rivet Code	Sheet Material Nominal Thickness (mm)		Anvil Code	Setting Pressure (bar)	Note
		Upper sheet	Lower sheet			
FSP50	23-5233	2	2	64015	240	0% pre-straining
FSP53	23-5233	2	2	64015	240	3% pre-straining
FSP55	23-5233	2	2	64015	240	5% pre-straining
FSP510	23-5233	2	2	64015	240	10% pre-straining
FSP50*	23-5233	2	2	64015	240	0% pre-straining & PB
FSP53*	23-5233	2	2	64015	240	3% pre-straining & PB
FSP55*	23-5233	2	2	64015	240	5% pre-straining & PB
FSP510*	23-5233	2	2	64015	240	10% pre-straining &PB

2.3.5.4 FSA6 Series

The AA6111 alloy sheets with two thickness values at a different shelf-life time were combined with the NG5754 sheets in 2mm gauge to make the FSA6 series of fastenings. The shelf-life of AA6111 for automotive applications is 6 months. It was originally planned to examine the effect of 0-month, 3-month and 6-month shelf-life of AA6111 on the joint quality and behaviour. However, material that was 19 months old was sent for use by mistake and this was not discovered until the latter stages of the project. Although a new batch of AA6111 was received, no fresh material was available and re-solutionising could not be performed on time. Therefore the shelf-life of AA6111 was extended to a 21-month period. The riveted samples that were produced were from different batches of AA6111.

The AA6111 sheets in 0.9mm gauge were riveted and tested after a shelf-life of 3, 5 and 8 months. The 2mm thick AA6111 sheets were riveted and tested after a shelf-life of 5, 19 and 21 months. Most of the FSA6 fastenings was exposed to a paint-bake cycle indicated by a "*" in the fastening code. The fastening conditions for the FSA6 series of fastenings are listed in Table 2.8.

Table 2-8 Fastening Conditions for AA6111 to NG5754

Fastening Code	Rivet Code	Sheet Material Thickness (mm)		Anvil Code	Setting Pressure (bar)	Note
		Upper sheet (AA6111)	Lower sheet (NG5754)			
FSA61*	23-5233	2	2	64015	240	5 months shelf-life
FSA62	23-5233	2	2	64015	240	19 months shelf-life
FSA62*	23-5233	2	2	64015	240	19 months shelf-life
FSA63*	23-5233	2	2	64015	240	21 months shelf-life
FSA64*	FSC3950002Z11	0.9	2	64220	100	3 months shelf-life
FSA65*	FSC3950002Z11	0.9	2	64220	100	5 months shelf-life
FSA66*	FSC3950002Z11	0.9	2	64220	100	8 months shelf-life

2.4 Test Conditions of Self-piercing Riveted Joints

Typical lap-shear, T-peel and fatigue tests were carried out to examine the potential failure modes and to allow comparison of the behaviour of joints prepare under various fastening conditions. To determine the effect of the rivet geometry characteristics, such as rivet flare, on the joint strength, the pull-out test was developed in this study. The basic geometry of the samples referred to the proposed ISO standard "Method for the fatigue testing of spot welded joint" [41].

2.4.1 Shear Test

The geometry of a single-riveted lap joint specimen for the shear test is illustrated in Fig.2.7. For each fastening condition, at least 4 samples were tested. The ultimate shear load was recorded to determine the shear strength of the joints and the load levels for the fatigue test. The failure mode was also assessed in order to establish the failure mechanisms of a self-piercing riveted joint. For comparison purposes, the geometry of the FSN56 fastening was different from the other samples and is shown in Fig.2.8.

The shear test was performed using an Avery Denison Testing Machine with a load capacity of 50kN. The test speed was 10mm/min as specified by Alcan.

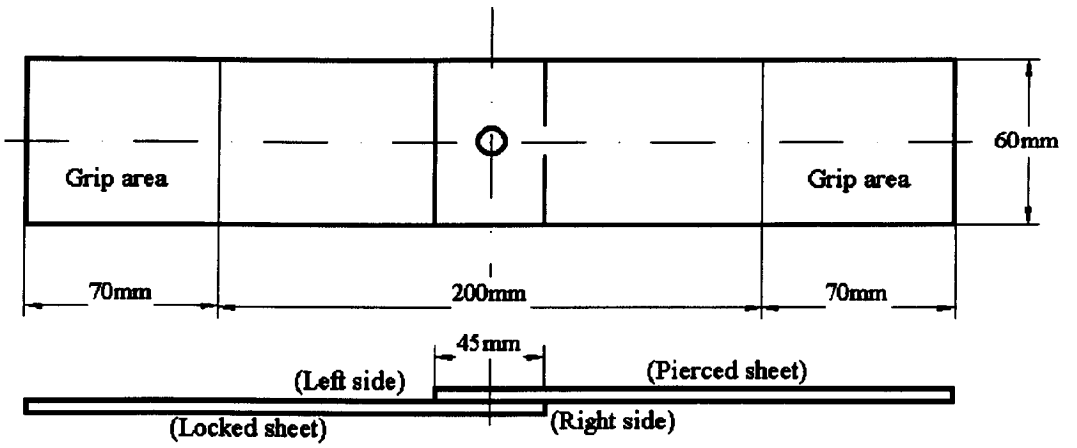

Figure 2.7 Specimen Geometry for the Shear and the Fatigue tests

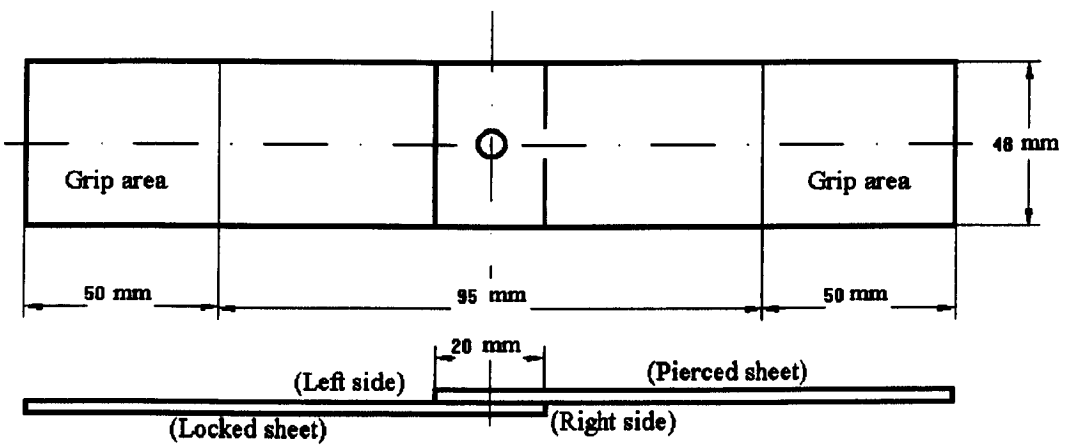

Figure 2.8 Specimen Geometry for the FSN56 fastening

2.4.2 Peel Test

A specimen for the peel test is shown diagrammatically in Fig.2.9. Four samples were tested for each fastening condition in order to obtain the joint peel strength and assess the failure mode of the joints.

An Avery Denison Testing Machine with a load capacity 50kN was used to carry out the peel test. The test speed was about 10mm/min as specified by Alcan.

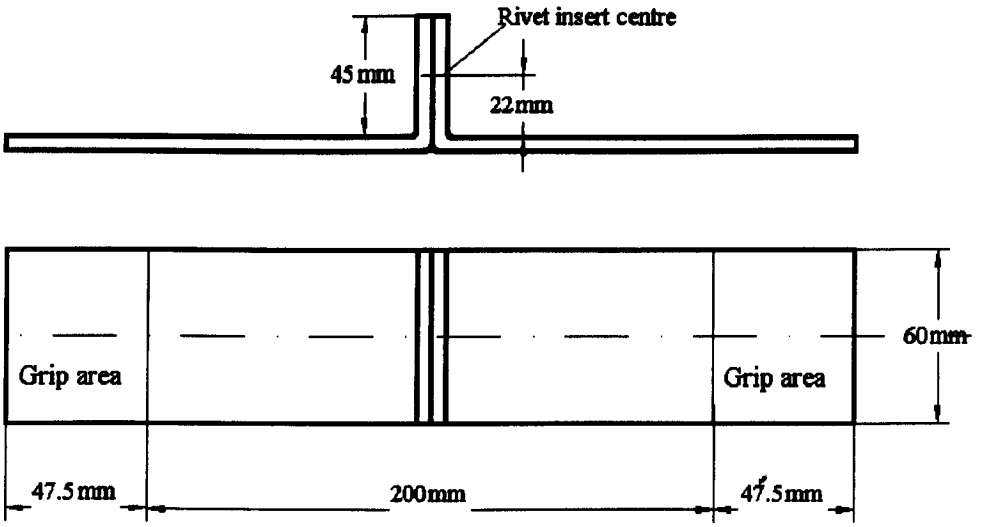

Figure 2.9 Specimen Geometry for the Peel test

2.4.3 Pull-out Test

There are no current published standards for the pull-out test. Two important factors were considered in the design of such a test. Firstly, to avoid the effect of bending on the joint, both the upper and bottom sheets had to be bent to a symmetrical U shape before being joined. Therefore, a special tool was designed to bend the sheets being joined to a U shape, as shown in Fig.2.10. Secondly, in order to effectively avoid buckling of the sheet during the pull-out test, two fixtures were also designed to fasten the U shape sheets. The presence of the two fixtures led to uniform loading during the test.

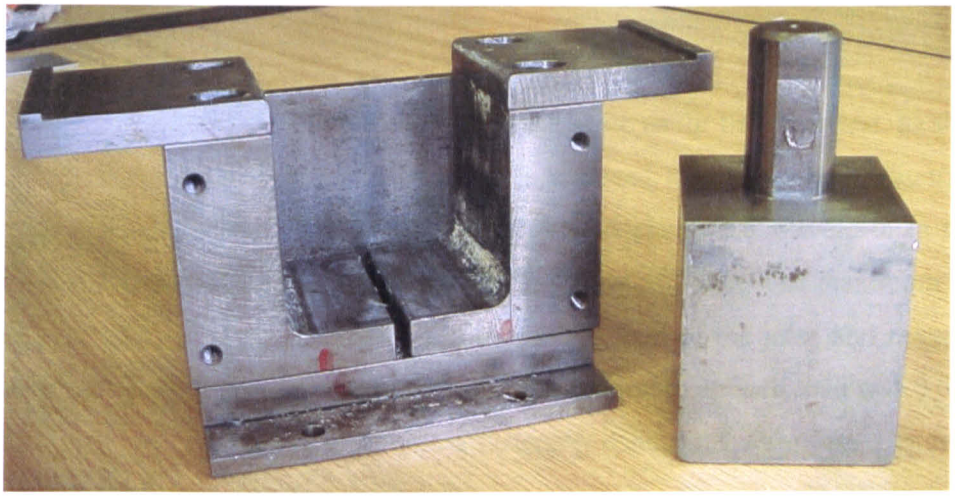

Figure 2.10 Tool for bending sheet to U shape

The pull-out test was performed on a Hounsfield Tensometer tensile test machine at a test speed of 10mm/min.

The geometry of a single riveted joint specimen for the pull-out test with two fixtures is shown in Fig.2.11.

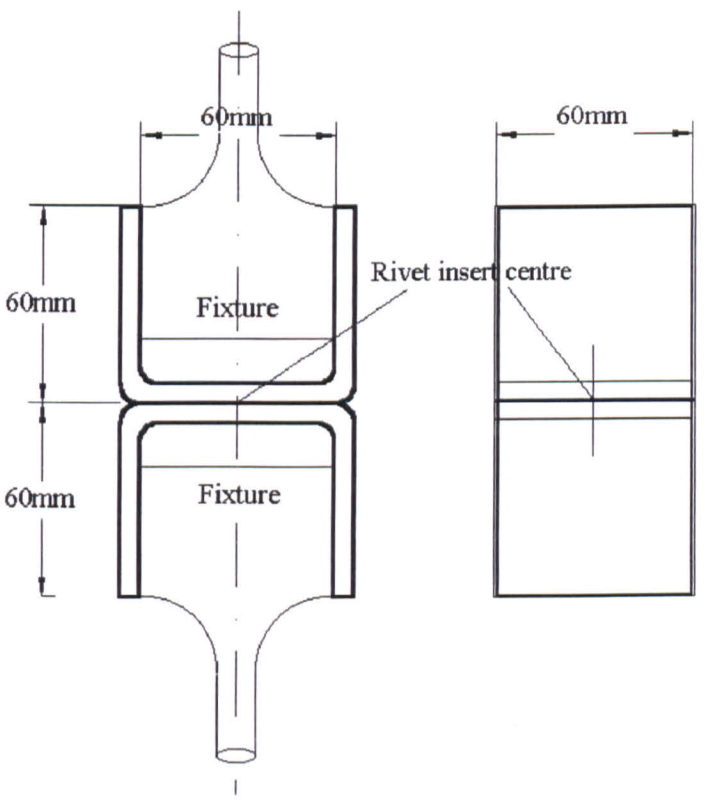

Figure 2.11 Specimen geometry for the pull-out test

2.4.4 Fatigue Test

The specimen geometry for the fatigue tests was the same as for the shear test, as shown in Figs.2.7, 2.8. The fatigue tests were performed in a closed-loop servo-hydraulic universal fatigue test machine with a load capacity of 200kN. A sinusoidal waveform in tension-tension was chosen as the applied load with a frequency of 20Hz. The maximum applied loads were calculated from the average ultimate shear load of the joint and ranged from 85% to 50% of the average ultimate shear load. The minimum applied load was 0.5kN due to the limitation of the test machine. Some fastening conditions were tested at five load levels, while others were at three load levels.

At least 2 samples were tested at each load level for each fastening condition. In order to perform statistical analysis 21 samples were tested at each fastening condition. Some tests were manually stopped after a fixed number of cycles and the samples were disassembled and examined microscopically.

2.5 Metallographic Investigation of Self-piercing Riveted Joints

Metallographic investigation was carried out to examine the deformation and failure characteristics of the joints. Light microscopy and Scanning Electron Microscopy (SEM) were employed for the investigation. In order to assess the effect of the setting parameters on the quality of the joints, metallographic investigation was performed on a limited number of samples in cross-section. The characteristics that represent a good quality joint include the following:

1. Flushness of the rivet head.
2. Symmetrical and properly flared rivet shank.
3. No significant gaps between the riveted sheets and between the rivet and the sheets.
4. No breakthrough.
5. No cracks in the rivet or the sheet materials.

The influence of certain setting parameters on the cross-sectional deformation characteristics was established by comparing the various fastening conditions investigated.

Metallographic investigation was also performed on a number of samples after fatigue failure. Some samples that had not failed after fatigue testing were also examined in order to examine the deformation characteristics of the joints.

CHAPTER THREE

3. EXPERIMENTAL RESULTS

3.1 FSN5 Series

The FSN5 series of fastenings was created for joining NG5754 alloy sheet together with thickness combinations of (1mm+2mm), (2mm+2mm), (2mm+1mm) and (1mm+1mm). Four types of rivet and anvil combinations were selected for this series of fastenings. The FSN51 and the FSN52 fastenings had a (2mm+2mm) combination, but the rivet and anvil design were different in each case. The only difference between the FSN51 and the FSN56 fastenings was the specimen size, as shown in Figs.2.6 and 2.7. The FSN53 fastening had a (1mm+2mm) thickness combination with a corresponding reduction in rivet length compared with the FSN52 fastening. Therefore, any difference between the two fastenings would be referred to as a variation in thickness. The FSN51* and FSN53* fastenings were produced using identical fastening conditions as the FSN51 and FSN53 fastenings. The FAN51* and FSN53* samples were exposed to a paint-bake cycle for 30 minutes at 180°C prior to testing.

3.1.1 Cross-sectional Examination

Cross-sectional examination was performed on all the FSN5 series of fastenings in order to examine the effect of the setting parameters on the joint quality. The aim of this was to optimise the setting parameters. Two FSN51 fastenings were initially prepared under different setting parameters, as listed in Table 3.1. A cross-section of the $FSN51_a$ fastening is shown in Fig.3.1 (a). It was observed that there was a gap between the two riveted sheets and the rivet shank did not flare symmetrically. Fig.3.1 (b) shows a cross-section of the FSN51 fastening. It was evident that the longer rivet shank, compared with the $FSN51_a$ fastening, did not break through the lower sheet and the rivet flared symmetrically, while no gap developed between the two riveted sheets. The results suggested that the quality of the FSN51 fastening was satisfactory and better than that of the $FSN51_a$ fastening. The setting parameters for the FSN51 fastening were thus optimised and the setting parameters for the rest of fastenings were therefore selected based on this selection.

Table 3-1 Setting parameters for $FSN51_a$ and FSN51 fastenings

Fastening Code	Rivet Code	Sheet Material Thickness (mm)		Anvil Code	Setting Pressure (bar)
		Upper sheet	Lower sheet		
$FSN51_a$	23-0282	2	2	P634	120
FSN51	23-5233	2	2	64015	240

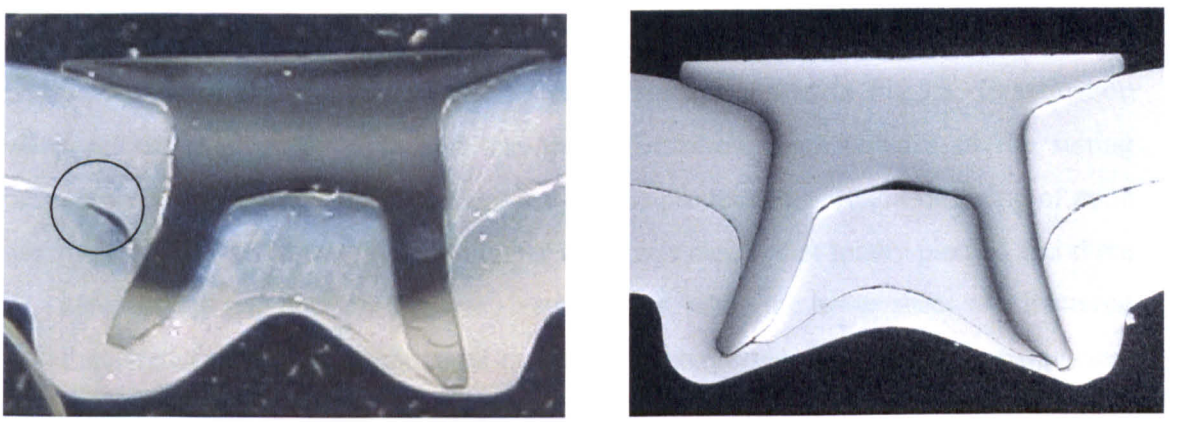

(a) **(b)**

Figure 3.1 (a) cross-section of $FSN51_a$, (b) cross-section of the FSN51

Fig.3.2 (a) shows a cross-section of the FSN52 fastening. It was apparent that the deformation characteristics of the fastening were not as good as for the FSN51 fastening. The rivet shank was slightly shorter leading to insufficient piercing of the upper sheet and flaring into the lower sheet. For comparison, the FSN52 fastening underwent mechanical tests even though the setting parameters for this fastening were not optimised as for the FSN51 fastening. A cross-section of the FSN55 fastening with a (1mm+1mm) combination is shown in Fig.3.2 (b). The joint quality is acceptable although there was a small gap between the two riveted sheets. This was probably caused by the low volume of the 1mm locked sheet over the cavity of the anvil profile.

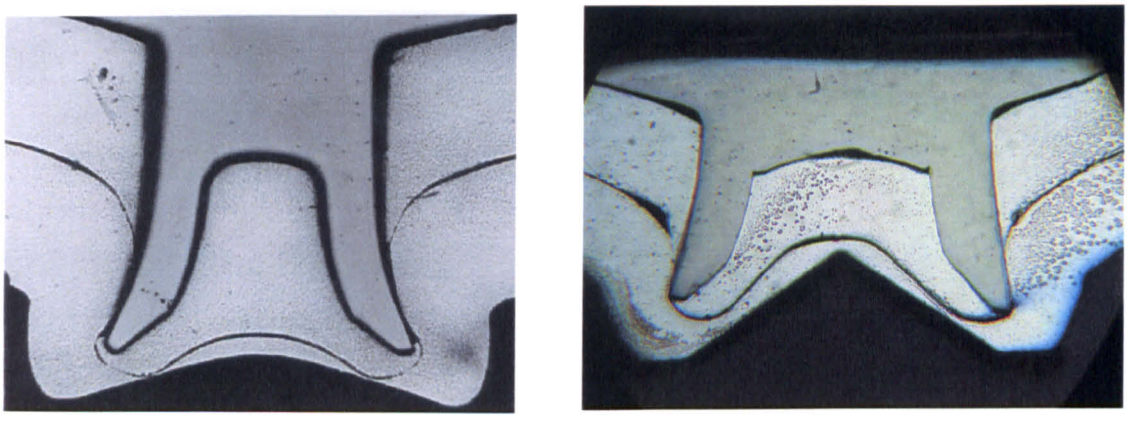

(a) **(b)**

Figure 3.2 (a) a cross-section of the FSN52 fastening
(b) a cross-section of the FSN55 fastening

Cross-sections of the FSN53 and FSN54 fastenings are shown in Fig.3.3. Examination using optical microscopy indicated that the deformation characteristics of the setting process were satisfactory and the setting parameters produced an FSN53 fastening of good quality. For the FSN54 fastening, the upper sheet was clearly not totally pierced and there was a significant gap between the two riveted sheets, while the lower sheet was fractured in the centre of the cavity of the anvil profile. This suggested that the setting parameters could not produce a good quality FSN54 fastening. Based on the cross-sectional examination, it was concluded that the FSN54 fastening would perform very poorly. Therefore, no mechanical testing was carried out for the FSN54 fastening.

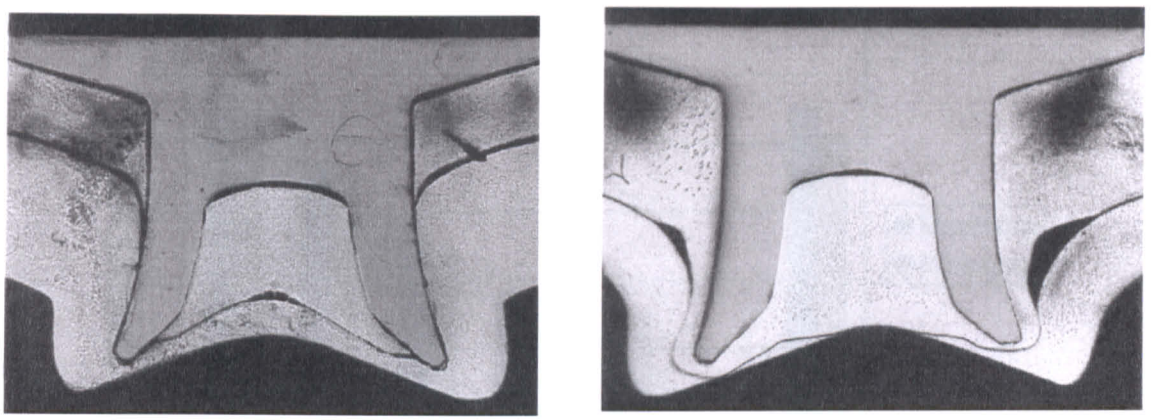

(a) **(b)**

Figure 3.3 (a) a cross-section of the FSN53 fastening
(b) a cross-section of the FSN54 fastening

3.1.2 Mechanical Test Results

3.1.2.1 Shear Test Results

Fig.3.4 shows the shear test results for the FSN5 series of fastenings. The FSN51 fastening exhibited the highest ultimate shear load and the FSN55 fastening had the lowest ultimate shear load. The ultimate load for the FSN51 fastening was higher than that for the FSN51* fastening indicating that the paint-baking cycle reduced the ultimate shear load of the fastening. The lower ultimate shear load for the FSN52 fastening compared with the FSN51 fastening suggested that the rivet and anvil design affected the ultimate shear load. The slightly higher ultimate shear load for the FSN51 fastening compared with the FSN56 fastening indicated the influence of the specimen size on the ultimate shear load. The fact that the FSN53 fastening had a lower ultimate shear load than the FSN52 fastening suggested that a reduction in the thickness of the upper sheet led to a decrease in the ultimate shear load.

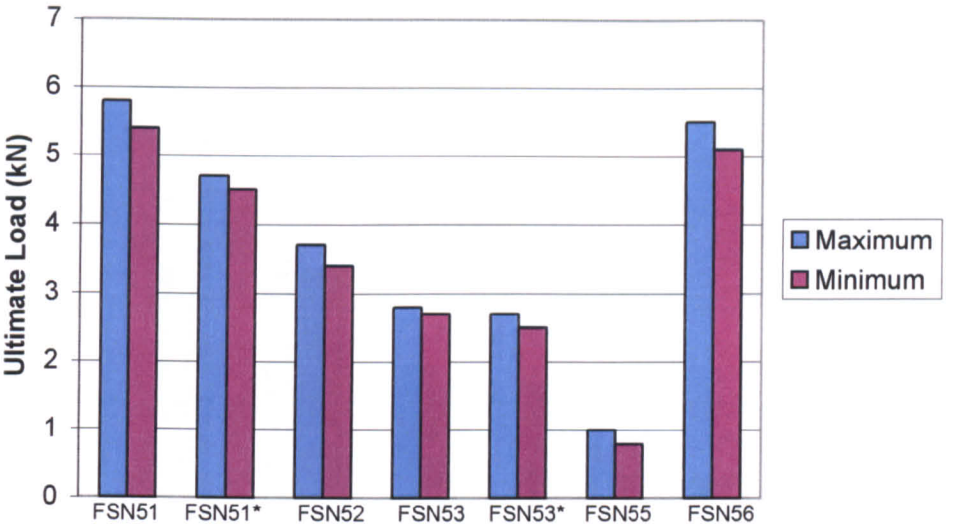

Figure 3.4 Shear test results for the FSN5 series of fastenings

3.1.2.2 Peel Test Results

The peel test results for the FSN5 series of fastenings are shown in Fig.3.5. The FSN51 fastening exhibited the highest ultimate peel load, while the FSN55 fastening had the lowest ultimate peel load. The ultimate peel load for the FSN52 fastening was lower than that for the FSN51 fastening indicating that the rivet and anvil design had an effect on the ultimate peel load. The lower ultimate peel load for the FSN53 fastening compared with the FSN52 fastening suggested that lowering the thickness of the pierced sheet led to a reduction in the ultimate peel load. The ultimate peel load for the FSN53 fastening was about 15% higher compared with the FSN53* fastening indicating that paint-baking led to a slight reduction in the ultimate peel load.

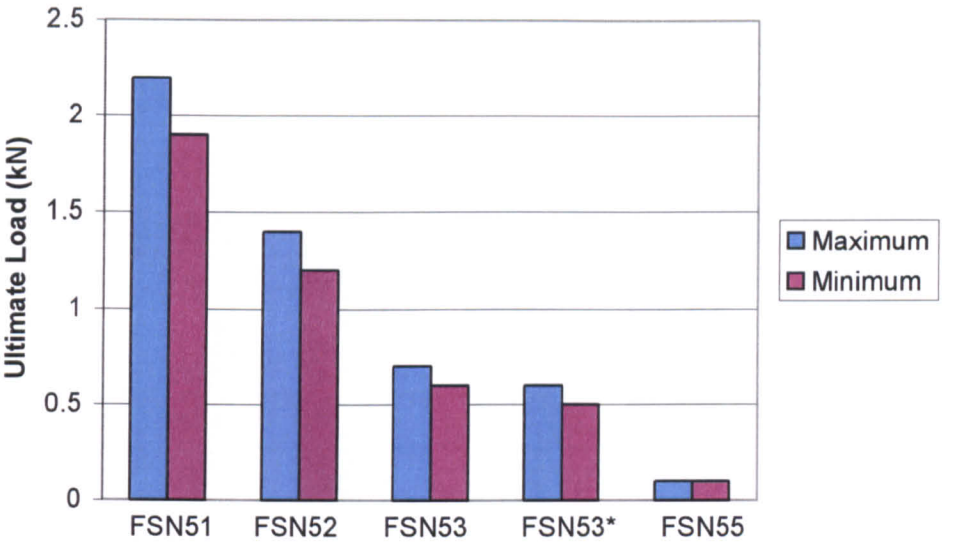

Figure 3.5 Peel test results for the FSN5 series of fastenings

3.1.2.3 Pull-out Test Results

Fig.3.6 shows the pull-out test results for the FSN5 series of fastenings. As for the shear and peel test results, the FSN51 fastening exhibited the highest ultimate pull-out load. The lower ultimate pull-out load for the FSN52 fastening compared with the FNS51 fastening suggested that the selection of rivet and anvil design had an effect on the pull-out strength. The higher pull-out strength of the FSN52 fastening compared with the FSN53 fastening indicated that a reduction in the thickness of the pierced sheet corresponded to a decrease in the pull-out strength. The ultimate pull-out load for the FSN53 fastening was almost the same as for the FSN53* fastening indicating that the paint-bake cycle had a marginal effect on the pull-out strength.

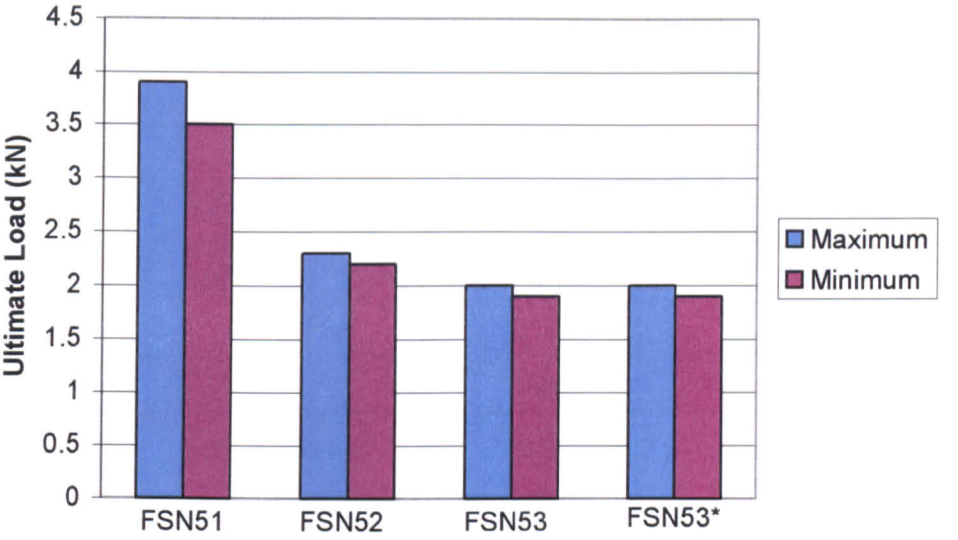

Figure 3.6 Pull out test result for the FSN5 series of fastenings

3.1.2.4 Fatigue Test Results

The fatigue test results for the FSN5 series of fastenings are shown in Fig.3.7. The FSN51 fastening exhibited the best fatigue behaviour in this series of fastenings. The S-N curves indicated that the FSN51 fastening had the longest fatigue endurance, whilst the fatigue endurance for the FSN53* fastening was the lowest. Compared with the FSN51 fastening, the fatigue endurance for the FSN56 fastening was shorter indicating that a reduction in the specimen size led to a decrease in the fatigue life. The shorter fatigue life for the FSN52 fastening compared with the FSN51 fastening indicated that the rivet and anvil design affected the fatigue endurance. The lower fatigue endurance for the FSN53 compared with the FSN52 fastening suggested that decreasing the upper sheet thickness led to a decrease in fatigue life. The fatigue endurance for the FSN53 fastening was marginally higher than that for the FSN53* fastening indicating that the paint-bake cycle had a marginal influence on the fatigue endurance.

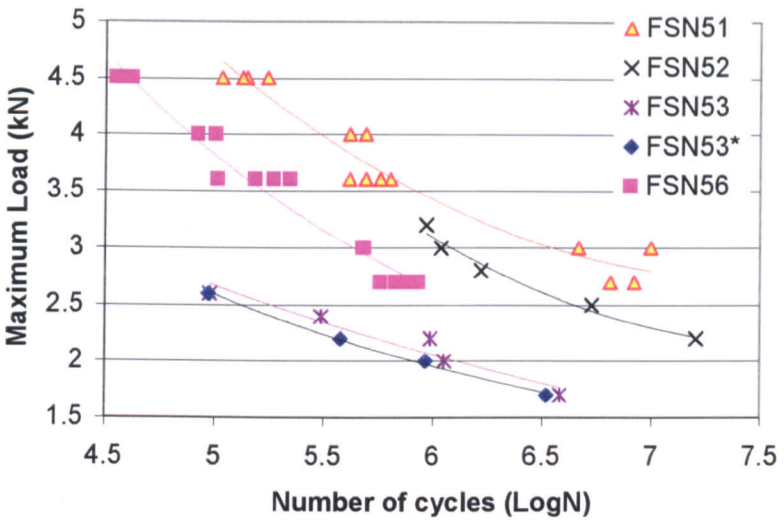

Figure 3.7 Fatigue test results for the FSN5 series of fastenings

3.1.3 Failure Modes

Three distinct failure modes were observed to occur in static and fatigue tests. These are described as *rivet pull-out, rivet fracture* and *sheet material failure. Rivet pull-out* involved sample failure due to the rivet pulling out during the tests. *Rivet fracture* describes the failure where the rivet fractured. S*heet material failure* simply implied that sample failure was due to fracture of the sheet material.

In shear tests, all samples failed by *rivet pull-out*. Fig.3.8 shows fractured samples having (1mm+2mm) and (2mm+2mm) thickness combinations. The rivet was pulled out of the locked sheet leading to a separation of the two riveted sheets, whilst the rivet was still attached to the pierced sheet. Both the pierced and the locked sheets had suffered some deformation and the 1mm pierced sheet suffered more distortion than the 2mm pierced sheet. For some fastenings with a (2mm+2mm) thickness combination, the rivet head also fractured, whilst the button remained intact, as shown in Fig.3.8(c). This indicated that the countersunk rivet head might be a stress concentration point.

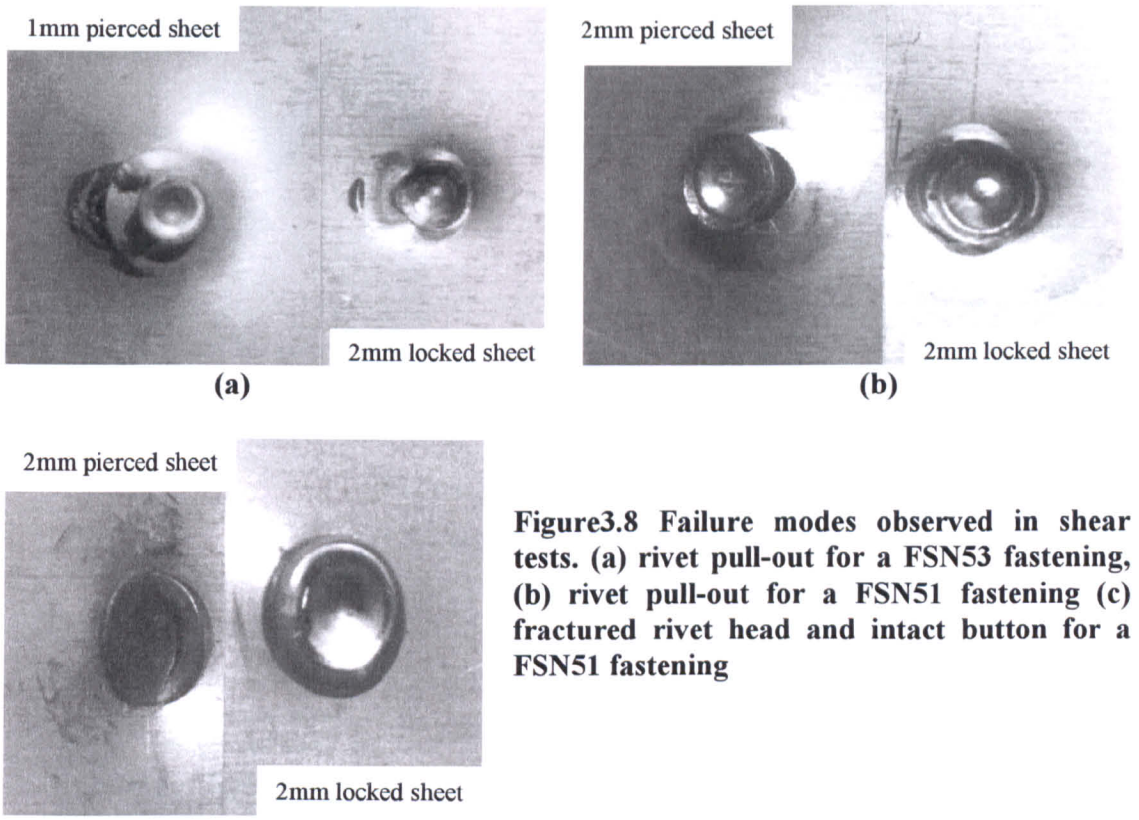

Figure3.8 Failure modes observed in shear tests. (a) rivet pull-out for a FSN53 fastening, (b) rivet pull-out for a FSN51 fastening (c) fractured rivet head and intact button for a FSN51 fastening

During peel testing, failure occurred by either *rivet pull-out* or *sheet material failure*. All the joints with a (2mm+2mm) thickness combination failed by the rivet being pulled out, whilst fracture of the thinner sheet occurred for all the joints with a (1mm+2mm) thickness combination. Fig.3.9 shows these two different failure modes.

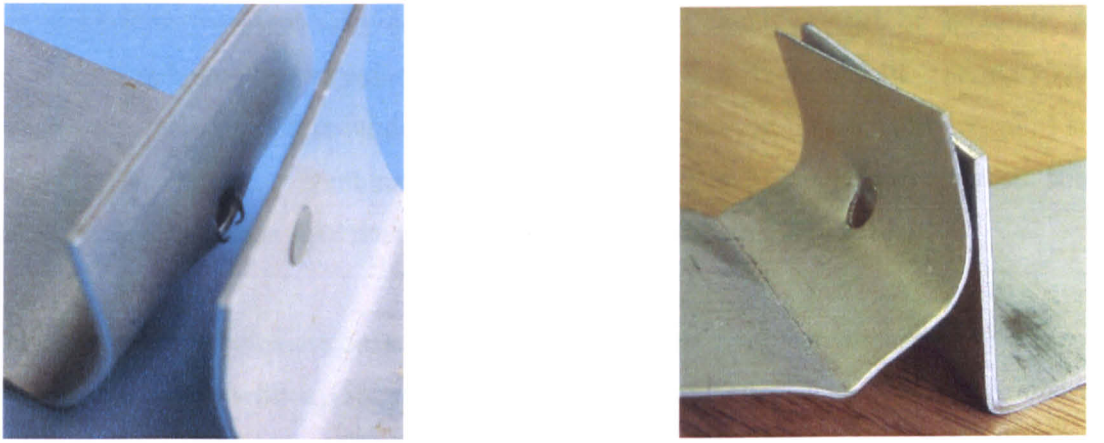

(a) (b)

Figure 3.9 Failure modes for the peel test,
(a) Rivet pull-out failure in (2mm+2mm) joint,
(b) Sheet material failure in (1mm+2mm) joint

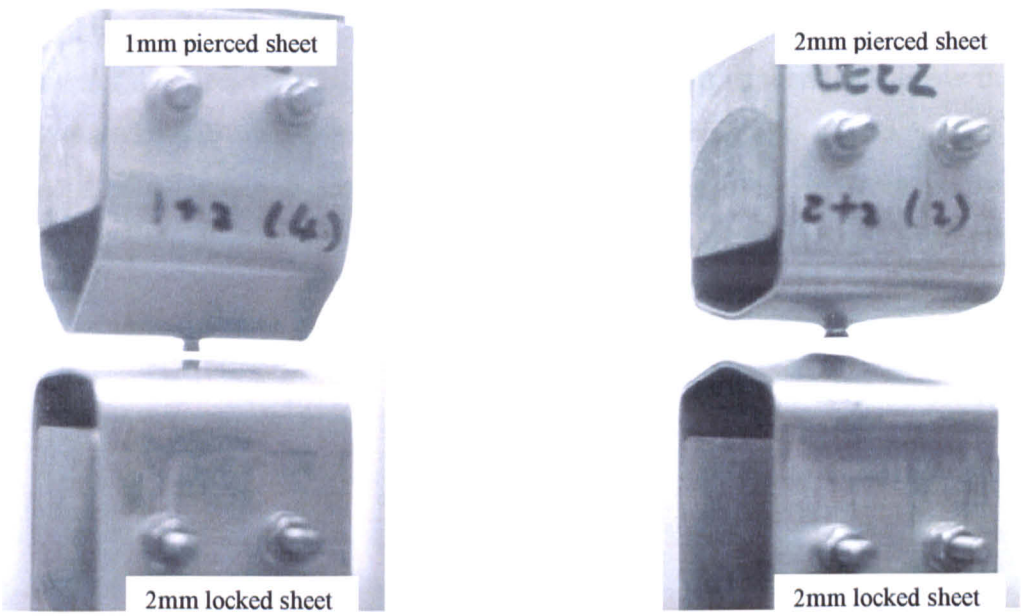

(a) (b)

Figure 3.10: Rivet pull-out failure in all the pull-out tests,
(a) a (1mm+2mm) joint, (b) a (2mm+2mm) joint

The pull-out test was specially designed to measure the clinch strength of the joints. All samples being tested by the pull-out test failed by means of rivet pull-out. Therefore *rivet pull-out* was the only failure mode observed for the pull-out test for both (2mm+2mm) and (1mm+2mm) thickness combinations, despite the fact that the thinner pierced sheet suffered more distortion than the thicker component, as shown in Fig.3.10.

The failure modes that were observed in fatigue tests were *rivet fracture* and *sheet material failure*. The joints with a (1mm+2mm) thickness combination failed by *sheet material failure* only, whilst either *rivet fracture* or *sheet material failure* occurred for the joints with a (2mm+2mm) thickness combination depending on the magnitude of the applied load. For joints with a (1mm+2mm) thickness combination, the 1mm thick pierced sheet suffered more distortion than the 2mm thick locked sheet. Eventually the thinner sheet fractured near the rivet head but the rivet remained undamaged still connecting the two sheets together, as shown in Fig.3.11 (a). For joints with a (2mm+2mm) combination, when the applied loads exceeded 3.6kN, rivet fracture dominated the failure mode together with fracture of the sheet material, as shown in Fig.3.11 (b). At applied loads lower than 3.0kN, sheet material fracture was the dominant mechanism of failure, as shown in Fig.3.11 (c). In addition, black-coloured scars were observed at the interface between the two riveted sheets, as presented in Figs.3.11 (b) and (c), indicating that fretting took place at the interface.

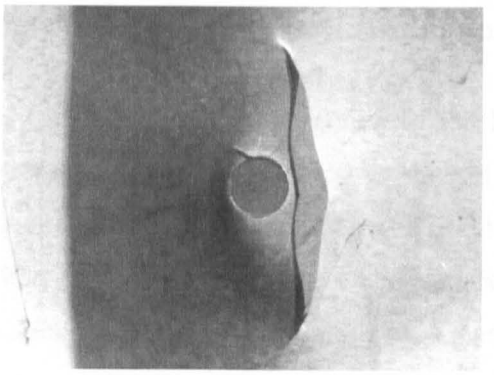

(a)

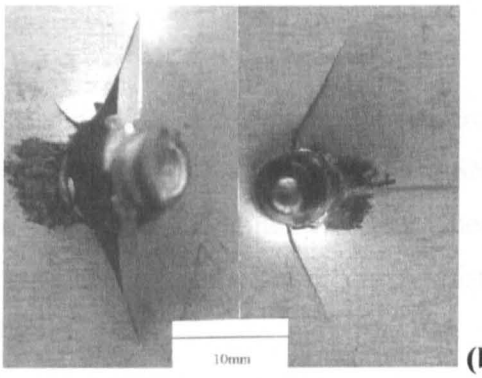

(b)

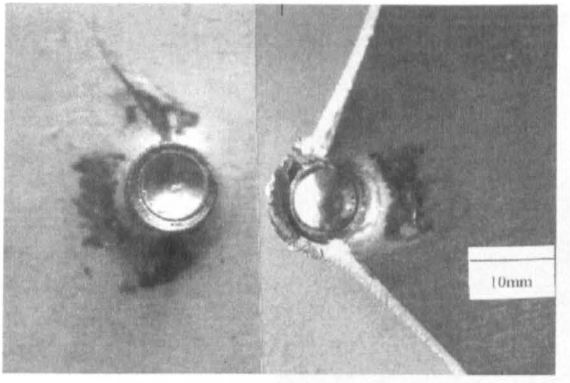

(c)

Figure 3.11: Failure modes for the fatigue test, (a) sheet material failure in (1mm+2mm) joint, (b) rivet fracture in (2mm+2mm) joint that failed at a maximum load of 3.6kN, (c) sheet material failure in (2mm+2mm) joint that failed at a maximum load of 2.7kN

3.2 FSH5 Series

The FSH5 series of fastenings was created specially for investigating the effect of the sheet surface condition on the fretting behaviour in light of the observation of fretting damage at the interface between the two riveted sheets. Alloy HS5754, which had the same mechanical properties as the NG5754 alloy but without the application of the wax-based surface lubricant, was used to produce the FSH5 series of fastenings with a (2mm+2mm) thickness combination. The FSH52 fastening was the same as the FSH51 fastening except that the former was prepared by inserting a PTFE tape at the interface between the two riveted sheets in order to examine if this could reduce or prevent fretting from taking place. The setting parameters used for the FSH5 series of fastenings was identical to those used for the FSN51 fastening.

3.2.1 Cross-sectional Examination

Fig.3.12 shows a cross-section of the FSH52 fastening. It was observed that the cross-sectional deformation characteristics of the FSH52 fastening were similar to the FSN51 fastening despite the insertion of PTFE tape at the interface between the two riveted sheets. The FSH51 fastening also had satisfactory cross-sectional deformation characteristics similar to the FSN51 fastening, as shown in Fig.3.1 (b).

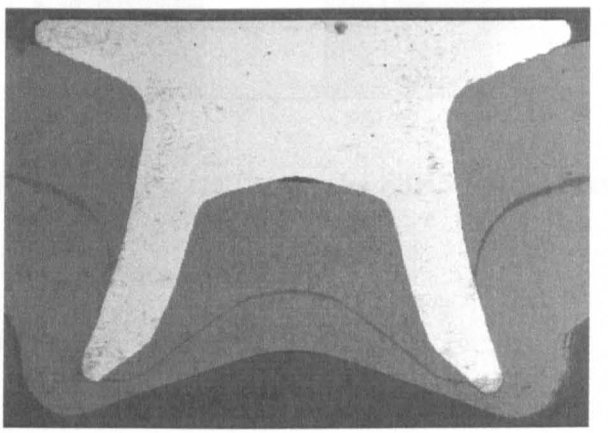

Figure 3.12 a cross-section of the FSH52 fastening

3.2.2 Mechanical Test Results

3.2.2.1 Shear Test Results

The shear test results for the FSH5 series of fastenings are shown in Fig.3.13. The FSH51 fastening exhibited higher shear strength than the FSH52 fastening indicating that the insertion of the PTFE tape reduced the shear strength.

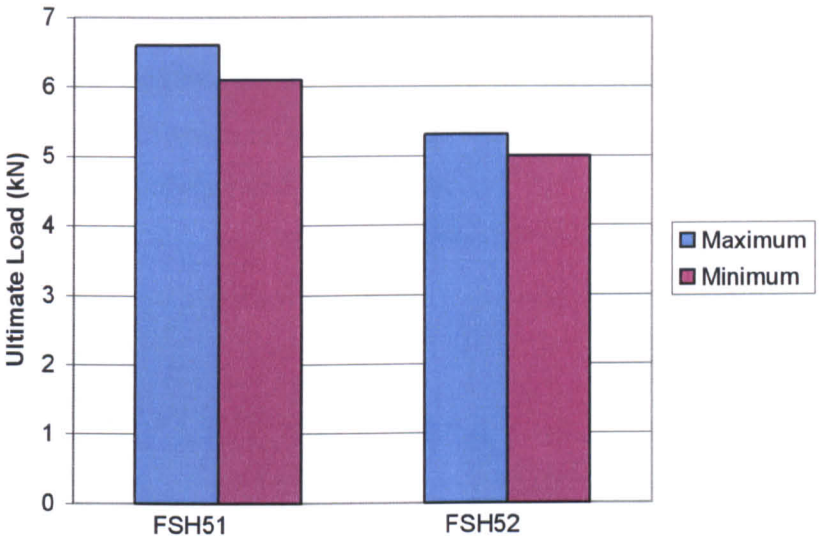

Figure 3.13 Shear test results for the FSH5 series of fastenings

3.2.2.2 Fatigue Test Results

Fig.3.14 shows the fatigue test results for the FSH5 series of fastenings. The FSH51 fastening exhibited longer fatigue endurance than the FSH52 fastening. This indicated that the insertion of the PTFE tape led to a reduction in the fatigue strength of the fastening.

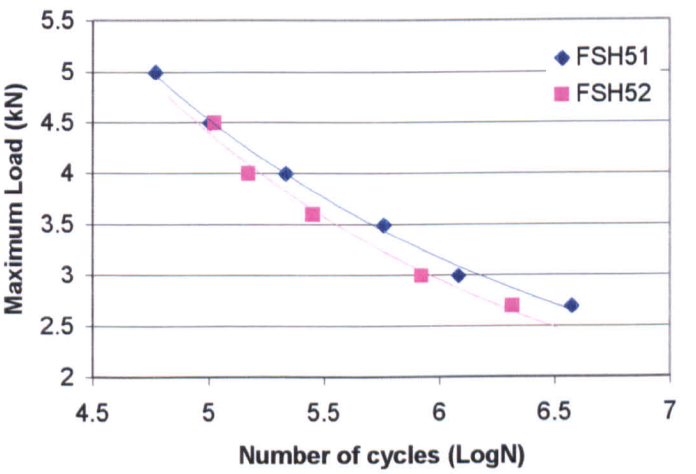

Figure 3.14 Fatigue test results for the FSH5 series of fastenings

3.2.3 Failure Modes

The failure mode that occurred during shear testing for the FSH5 series of fastenings was the same as for the FSN5 series of fastenings, as shown in Fig.3.15. The rivet was pulled out and led to separation of the two riveted sheets.

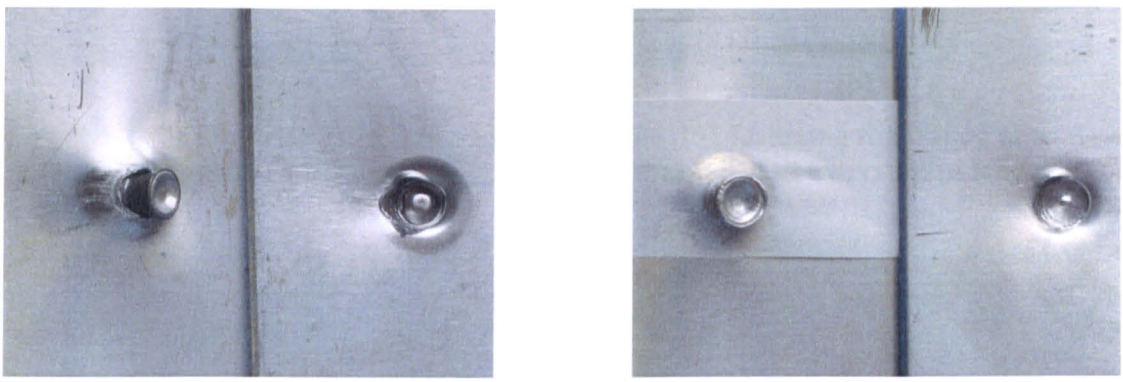

(a) (b)

Figure 3.15 Failure mode for the shear test, (a) rivet pull-out for a FSH51 fastening, (b) rivet pull-out for a FSH52 fastening

The failure mode that occurred during fatigue testing for the FSH51 fastening was the same as for the FSN51 fastening, whilst for the FSH52 fastening was different from the FSN51 fastenings. At high applied loads, *rivet fracture* occurred for the FSH51 fastening, while at low applied loads, the FSH51 fastening failed by *sheet material failure*. The black-coloured fretting scars formed at the interface between the two riveted sheets for the FSN5 series of fastenings also appeared at the interface of the FSH51 riveted sheets similar to the FSN51 fastening. However, for the FSH52 fastening *rivet fracture* dominated the failure mode at all applied loads. In addition, no visible black scars formed at the interface between the two riveted sheets for the FSH52 fastening except at a maximum load of 4.5kN. These observations indicated that the PTFE insert prevented the interface from suffering fretting damage, but in addition, the failure mechanism changed. Fig.3.16 shows the failure mode and the interface of the two riveted sheets for the FSH5 series of fastenings.

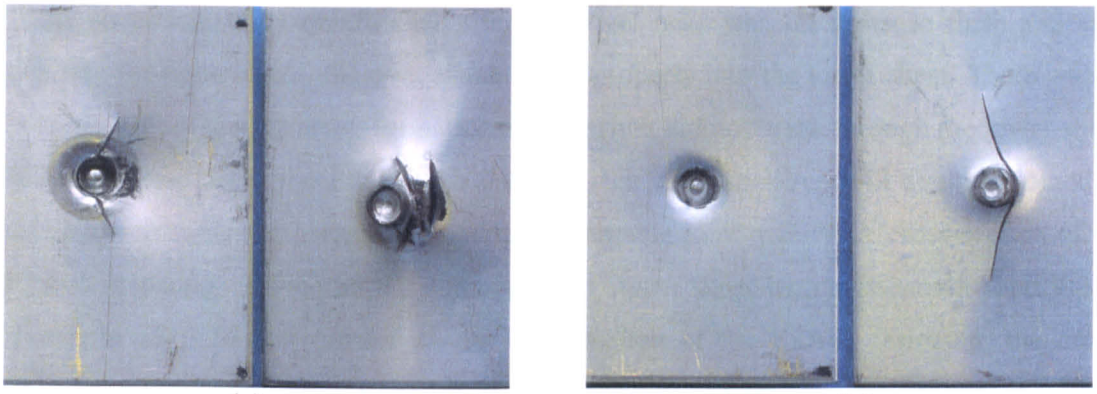

(a) (b)

Figure 3.16 Failure modes in fatigue tests: (a) a FSH51 fastening that failed at a maximum load of 3.0kN, (b) a FSH52 fastening that failed at a maximum load of 3.0kN

3.3 FSA6 Series

The FSA6 series of fastenings were made for joining AA6111 and NG5754 sheets together. For all the FSA6 series of fastenings, the upper sheet was either 2mm or 0.9mm thick AA6111 sheet with a variation in shelf-life. The lower sheet was a 2mm NG5754 sheet. The objective was to examine the effect of the shelf-life of the AA6111 sheet on the joint quality and behaviour. There were two different thickness combinations of (2mm+2mm) and (0.9mm+2mm) for the FSA6 series of fastenings. For each thickness combination, the setting parameters were kept identical. The FSA62 fastening was the same as the FSA62* except that the latter had been exposed to a paint-bake cycle. Apart from this, the only variation for the FSA6 series of fastenings was the shelf-life of the AA6111 sheet. Therefore any variation in joint quality and strength would be referred to as a different shelf-life of the AA6111 sheet.

3.3.1 Cross-sectional Examination

Cross-sectional examination was carried out on the FSA6 series of fastenings in order to clarify whether identical setting parameters could be used to join the AA6111 sheet with a variation in shelf-life and achieve good cross-sectional deformation characteristics. Fig.3.17 (a) shows a cross-section of the FSA63 fastening, which had a 2mm AA6111

upper sheet with a 21-month shelf life. The rivet head was set down to flush and after piercing the upper sheet, the rivet shank flared properly into the lower sheet. There was no evidence of any gap or crack formation and the rivet did not break through the lower sheet. This suggested that up to a 21-month shelf-life, the 2mm thick AA6111 could be joined by using identical setting parameters with an acceptable joint quality. A cross-section of the FSA66 fastening, which had a 0.9mm AA6111 upper sheet with a 10-month shelf-life, is shown in Fig.3.17 (b). Similar to the cross-section of the FSA63 fastening, the cross-sectional deformation characteristics of the FSA66 fastening were satisfactory indicating that up to a 10-month shelf-life, the 0.9mm thick AA6111 sheet could be joined by using identical setting parameters to material of a lower shelf-life.

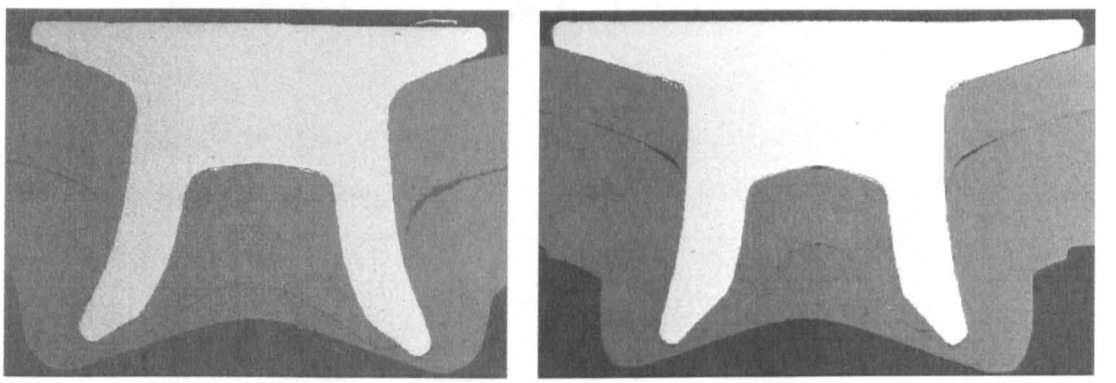

(a) **(b)**

Figure 3.17 (a) a cross-section of the FSA63 fastening
(b) a cross-section of the FSA66 fastening

3.3.1.1 Shear Test Results

Fig.3.18 shows the shear test results for the FSA6 series of fastenings with a (2mm+2mm) thickness combination. The ultimate shear load for the fastenings involving AA6111 sheet material with a different shelf-life did not change significantly indicating that the shelf-life of the sheet material had little influence on the ultimate shear load. The average ultimate shear loads for the FSA6 series of fastenings with a (2mm+2mm) thickness combination are shown in Fig.3.19. The FSA62 fastening exhibited about 6% higher average ultimate shear load than the FSA62* fastening. This indicated that the paint-baking cycle led to a small reduction in the ultimate shear load for the FSA6 series of fastenings.

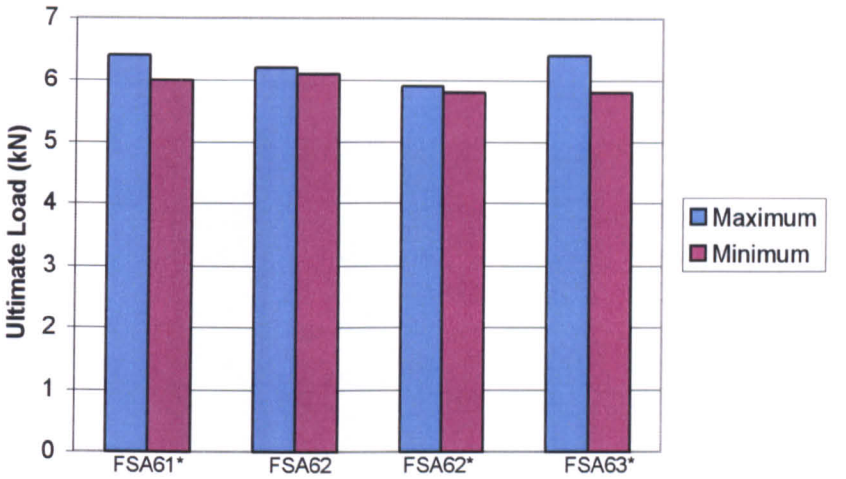

Figure 3.18 Shear test results for the FSA6 series of fastenings

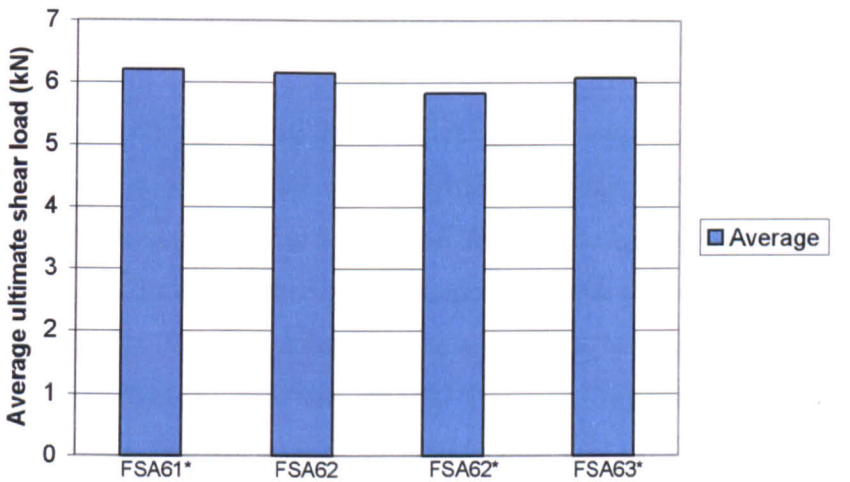

Figure 3.19 Average shear ultimate load for the FSA6 series of fastenings

The shear test results for the fastenings with a (0.9mm+2mm) thickness combination are shown in Fig.3.20. The FSA64* fastening exhibited a slightly higher shear strength than the FSA65* and the FSA66* fastenings indicating that the shelf-life of the 0.9mm thick AA6111 sheet had a minor influence on the shear strength of the fastenings.

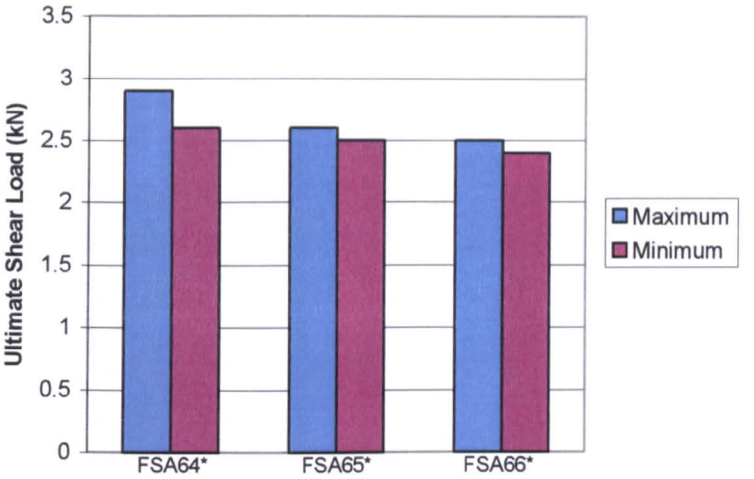

Figure 3.20 Shear test results for the FSA6 series of fastenings with a (0.9mm+2mm) combination

3.3.1.2 Peel Test Results

The peel test results for the FSA6 series of fastenings with a (2mm+2mm) thickness combination are shown in Fig.3.21. The FSA62 fastening exhibited the highest peel strength of all the fastenings. The corresponding FSA62* fastening, which had been paint-baked had about 15% lower peel strength. This indicated that the paint-bake cycle slightly reduced the peel strength of the fastenings. The slightly higher ultimate peel load for the FSA62* compared with the FSA61* and FSA63* fastenings suggested that the shelf-life of the 2mm AA6111 sheet only had a marginal effect on the peel strength of the fastenings.

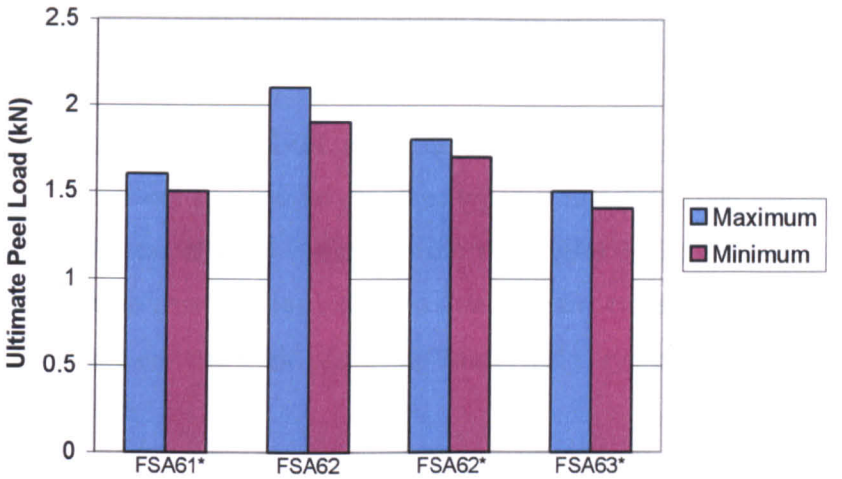

Figure 3.21 Peel test results for the FSA6 series of fastenings with a (2mm+2mm) combination

Fig.3.22 shows the peel test results for the FSA6 series of fastening with a (0.9mm+2mm) combination. The peel strength of the FSA65* fastening was the highest of the fastenings indicating that the shelf-life of the 0.9mm thick AA6111 sheet affected the peel strength of the fastening.

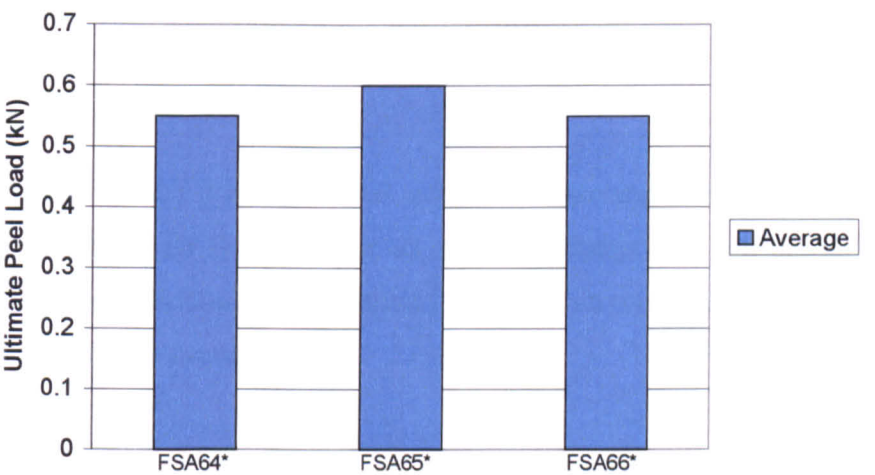

Figure 3.22 Peel test results for the FSA6 series of fastenings with a (0.9mm+2mm) combination

3.3.1.3 Pull-out Test Results

Fig.3.23 shows the pull-out test results for the FSA6 series of fastenings with a (2mm+2mm) combination. The FSA62 fastening exhibited the highest pull-out strength of the fastenings. The pull-out strength for the three types of fastenings that had been exposed to a paint-bake cycle was slightly different from each other and lower than that for the FSA62 fastening. These observations indicated that the paint-bake cycle led to a reduction in the pull-out strength and the shelf-life of the 2mm AA6111 sheet had a minor influence on the pull-out strength.

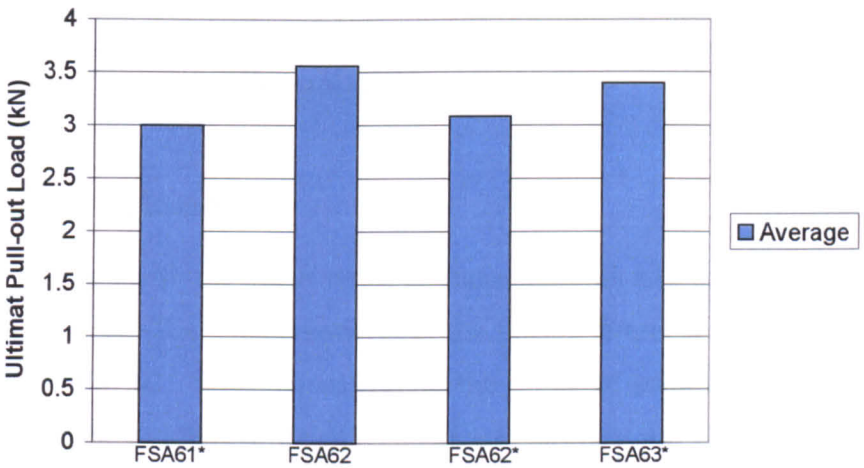

Figure 3.23 Pull-out test results for the FSA6 series of fastenings with a (2mm+2mm) combination

The pull-out test results for the FSA6 series of fastenings with a (0.9mm+2mm) combination are shown in Fig.3.24. For all three fastenings, the pull-out strength was similar to each other indicating that the shelf-life of 0.9mm thick AA6111 sheet had little influence on the pull-out strength.

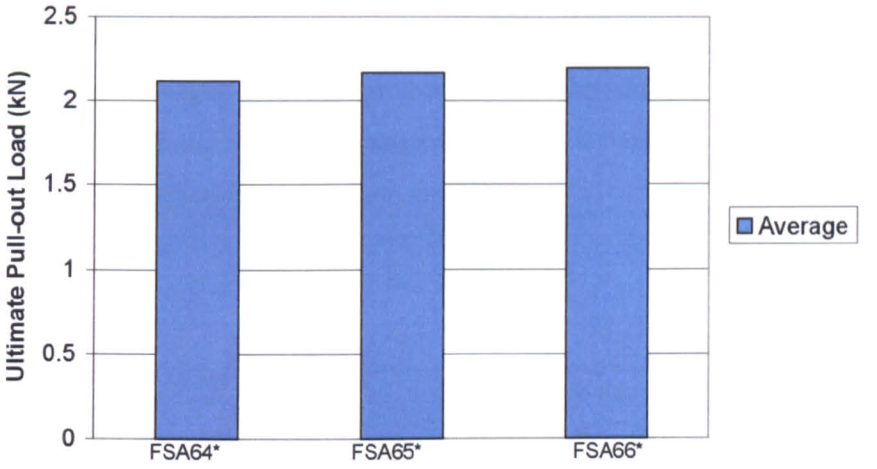

Figure 3.24 Pull-out test results for the FSA6 series of fastenings with a (0.9mm+2mm) combination

3.3.1.4 Fatigue Test Results

The fatigue test results for the FSA6 series of fastenings with a (2mm+2mm) combination are shown in Fig.3.25. The fatigue strength of the FSA62 fastening was marginally lower than that of the FSA62* fastening indicating the effect of paint-baking on the fatigue strength. The slightly different fatigue endurance between the FSA61*, FSA62* and FSA63* fastenings at a same applied load indicated that the shelf-life of the 2mm thick AA6111 sheet had only a minor influence on the fatigue endurance.

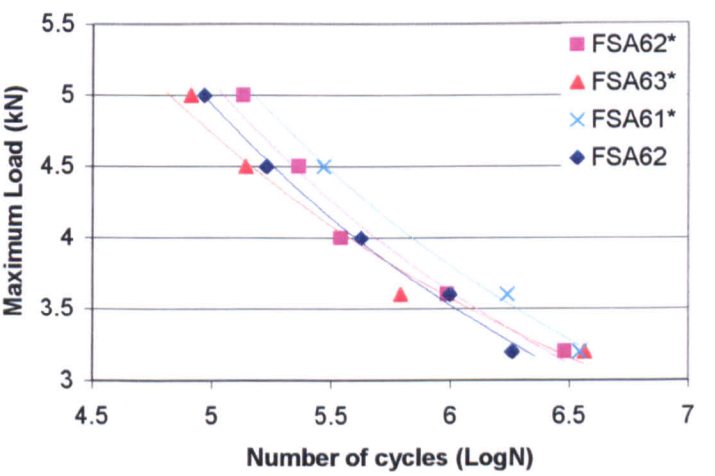

Figure 3.25 Fatigue test results for the FSA6 series of fastenings

Fig.3.26 shows the fatigue test results for the FSA6 series of fastenings with a (0.9mm+2mm) combination. From the figure, it is difficult to identify which fastening had the highest fatigue strength due to the overlap in the fatigue data under different conditions. This might indicate that the shelf-life of the 0.9mm thick AA6111 sheet had little influence on the fatigue strength of the fastenings.

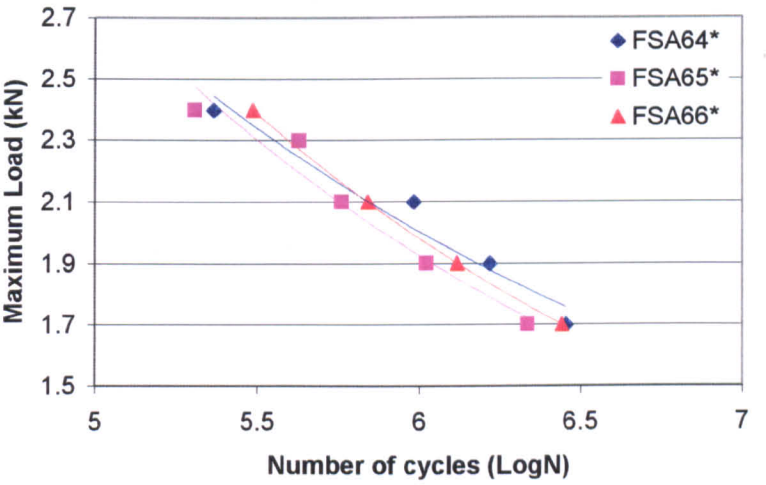

Figure 3.26 Fatigue test results for the FSA6 series of fastenings with a (0.9mm+2mm) combination

3.3.2 Failure Modes

The failure mode observed for the FSA6 series of fastenings during shear testing was *Rivet pull-out*. This behaviour was similar to that of the FSN5 series of fastenings. As shown in Fig.3.27, the rivet was pulled out of the locked sheet leading to a separation of the two riveted sheets, whilst the rivet was still attached to the pierced sheet. Both pierced and locked sheets suffered deformation with the 0.9mm sheet having more distortion. The failure mode for the peel and pull-out tests was also the same as for the FSN5 series of fastenings. For fastenings with a (0.9mm+2mm) combination, the thinner sheet fractured leading to *sheet material failure* during peel testing. For the pull-out test, *rivet pull-out* dominated the failure mode with more deformation suffered by the thinner sheet. For the fastenings with a (2mm+2mm) combination, all samples failed by the rivet being pulled

out of the lower sheet leading to the separation of the two riveted sheets. *Rivet pull-out* was the only failure system observed for fastenings with a (2mm+2mm) combination.

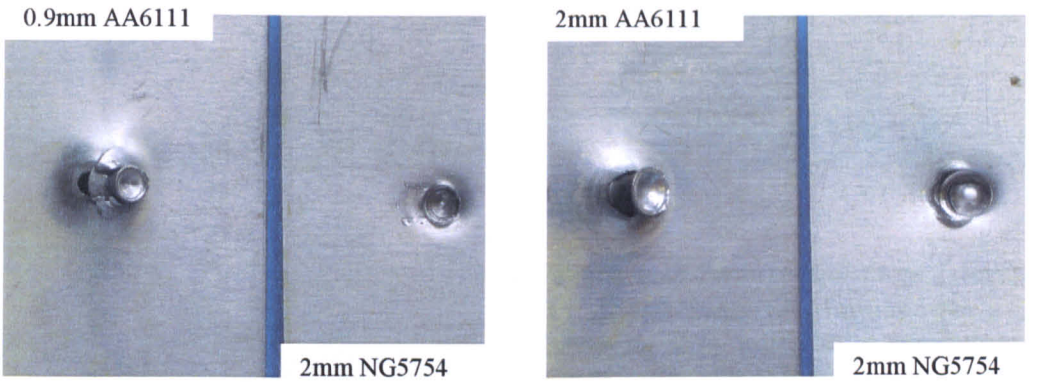

Figure 3.27 Rivet pull-out failure for the shear test

Fig.3.28 shows the failure modes that occurred during fatigue testing. Similar to the FSN5 series of fastenings with a (1mm+2mm) combination, the FSA6 series of fastenings with a (0.9mm+2mm) combination failed by *sheet material failure*, as shown in Fig.3.28 (a). The 0.9mm AA6111 pierced sheet fractured, while the rivet still connected the two sheets. At applied loads at and above 3.6kN, the FSA6 series of fastenings with a (2mm+2mm) combination failed by *rivet fracture*. At applied loads at and lower than 3.0kN, *sheet material failure* dominated the failure mode, as shown in Figs.3.28 (b) and (c). At all load levels, sheet material fracture was suffered only by the locked sheet, whilst the AA6111 pierced sheet underwent very little deformation. This was different from the observations of the failure mode for the FSN5 series of fastenings with a (2mm+2mm) combination. This indicated that the sheet material properties might affect the failure mode. Black-coloured fretting scars also formed at the interface between the two riveted sheets indicating that fretting had taken place.

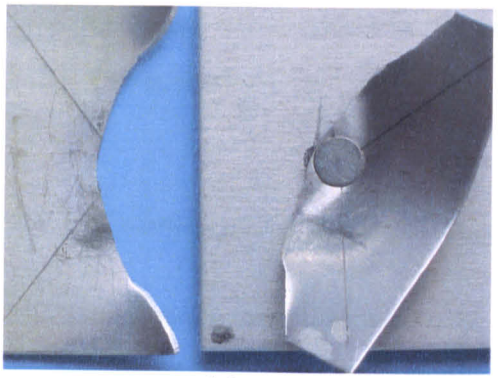

(a)

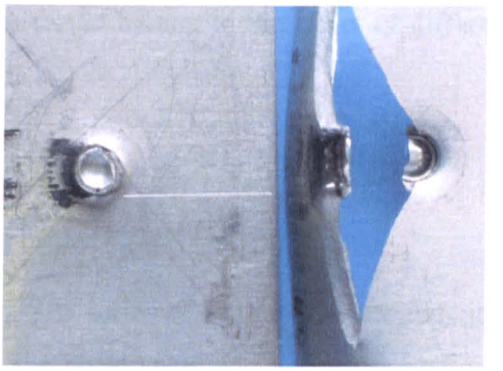

(b)

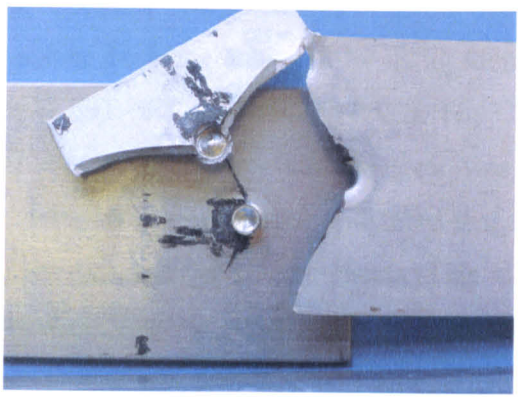

(c)

Figure 3.28 Failure modes in fatigue testing, (a) sheet material failure in a FSA64* fastening that failed at a maximum load of 2.0kN after 959,680 cycles, (b) rivet fracture in a FSA62* fastening that failed at a maximum load of 4.5kN after 230,570 cycles, (c) sheet material failure in a FSA61* fastening that failed at a maximum load of 3.2kN after 3,151,960 cycles

3.4 FSP5 Series

The FSP5 series of fastenings was created to join nominal 2mm NG5754 alloy sheets, which were pre-strained to different levels. The objective was to examine the effect of variations in the sheet strain level, which could occur during the sheet manufacturing procedure and the stamping process during car-body assembly, on the quality and behaviour of the joints. There were two groups in this series of fastenings. One group was exposed to a paint-bake cycle indicated by '*' in the fastening code, while the other was not. The setting parameters for all the FSP5 series of fastenings were identical to those of the FSN51 fastening, which was made from the 2mm thick NG5754 sheets with 0% pre-straining. The only variation for this FSP5 series of fastenings was the pre-straining level, which was indicated by the last number in the fastening code. For example, the fastening code FSP510 meant that the pre-straining level of the sheets joined by this fastening was

10%. Therefore any variation in the joint strength would be due to the effect of different pre-straining levels.

3.4.1 Cross-sectional Examination

The setting parameters that were used for all the FSP5 series of fastenings were identical despite the variation in pre-straining levels for the sheet material. The cross-sectional deformation characteristics of joints were assessed in order to examine whether good joint quality could be achieved by using identical setting parameters to join the sheet material with different pre-straining levels. Fig.3.29 shows a cross-section of the FSP510 fastening. It is clearly shown that the rivet was set down fully flush and flared properly. The microscopic examination indicated that there were no cracks in the sheet material and no gaps between the riveted sheets. This indicated that identical setting parameters could be used to join the NG5754 sheet at up to 10% pre-straining successfully leading to good cross-sectional deformation characteristics.

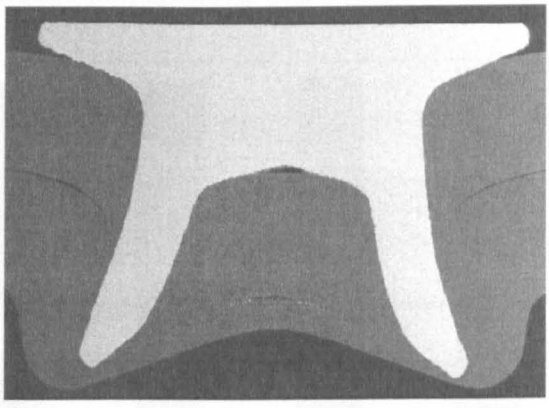

Figure 3.29 a cross-section of the FSP510 fastening

3.4.2 Mechanical Test Results

3.4.2.1 Shear Test Results

Fig.3.30 shows the shear test results for the FSP5 series of fastenings that had not been exposed to a paint-bake cycle. The FSP510 fastening exhibited the highest ultimate shear load indicating that the increase in the amount of pre-straining had led to an increase in the shear strength of the fastenings. The results show that the ultimate shear load increased as the amount of pre-straining increased. The shear test results for the FSP5 series of fastenings that had been exposed to a paint-bake cycle are shown in Fig.3.31. The ultimate shear load of the FSP50* fastening, which had not been pre-strained, was the lowest for the FSP5 series of fastenings. The results show that the higher pre-straining level, the higher the shear strength of the fastening even after paint-baking. Comparing Fig.3.30 with Fig.3.31, the FSP5 series of fastenings that had been exposed to a paint-bake cycle exhibited lower shear strength than the fastenings that had not been exposed to a paint-bake cycle. This indicated that the paint-bake cycle reduced the shear strength of the fastenings.

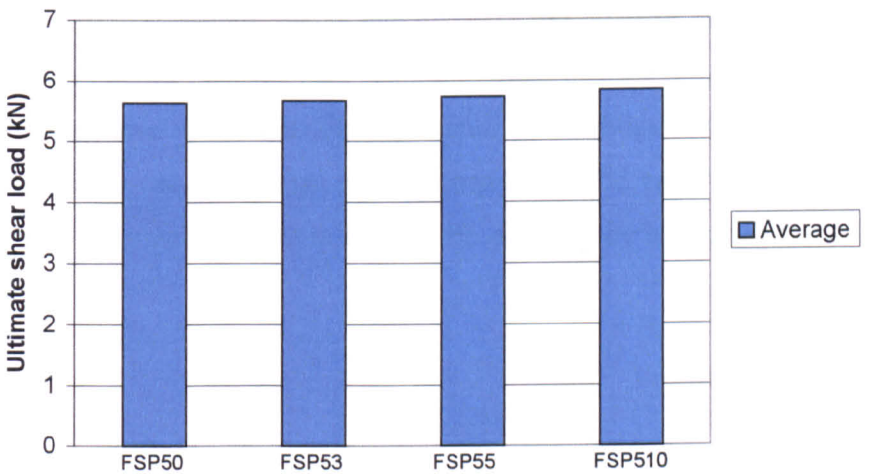

Figure 3.30 Shear test results for the FSP5 series of fastenings before paint-baking

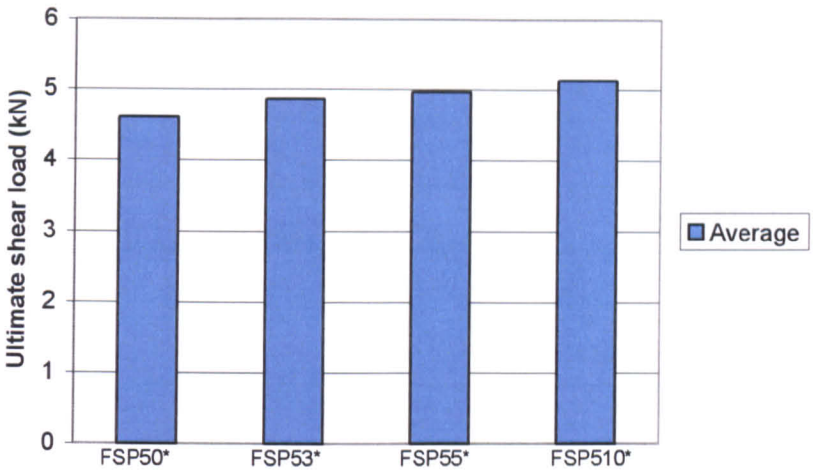

Figure 3.31 Shear test results for the FSP5 series of fastenings after paint-baking

3.4.2.2 Fatigue Test Results

The fatigue test results for the FSP5 series of fastenings that had not been exposed to a paint-bake cycle are shown in Fig.3.32. The FSP510 fastening exhibited the longest fatigue life, whilst the FSP50 fastening, which had not been pre-strained had the shortest fatigue life of all the FSP5 series of fastenings. This suggested that the fatigue strength increased as the pre-straining level increased. The difference in the fatigue life between the FSP50 and FSP53 fastenings was larger than that between the FSP55 and FSP510 fastening. This indicated that only a small increase in fatigue life occurred by increasing the pre-straining level above about 5%.

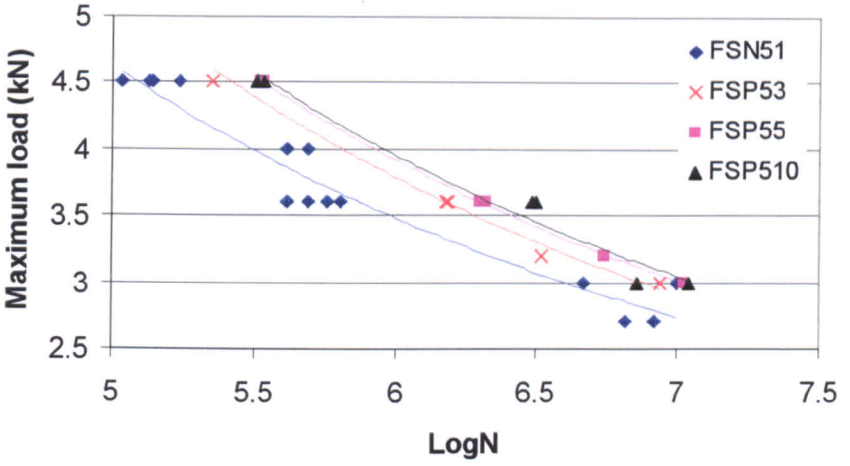

Figure 3.32 Fatigue test results for the FSP5 series of fastenings before paint-baking

Fig.3.33 shows the fatigue test results for the FSP5 series of fastenings that had been exposed to a paint-bake cycle. At maximum loads greater than 3.6kN, the FSP510* fastening exhibited the longest fatigue life. The increase in the pre-straining level led to an increase in the fatigue life after paint-baking. However, at maximum loads lower than 3.6kN, the increase in the pre-straining levels was not accompanied with an increase in the fatigue life. This was probably attributed to the scatter of the fatigue data and poor sampling.

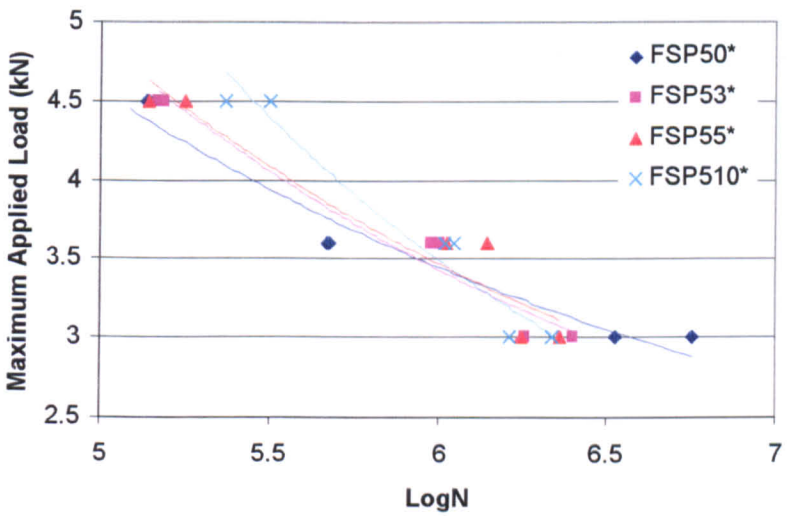

Figure 3.33 Fatigue test results for the FSP5 series of fastenings after paint-baking

3.4.3 Failure Modes

The failure mode that occurred for the FSP5 series of fastenings during shear testing was *rivet pull-out.* This behaviour was the same as for the FSN5 series of fastenings with a (2mm+2mm) combination. All fastenings failed by the rivet being pulled out of the locked sheet leading to the separation of the two riveted sheets, whilst the rivet still remained connected to the pierced sheet. During fatigue testing, at applied loads above 3.6kN, *rivet fracture,* that was accompanied by fracture of the riveted sheet, occurred for the FSP50 and FSP53 fastenings. At lower applied loads, only *sheet material failure* occurred. These observations were similar to those for the FSN51 fastenings. For the FSP55 and FSP510 fastenings, *sheet material failure* was the dominant failure mode at all applied loads. Fig.3.34 shows the failure modes that were observed during fatigue testing. At a maximum applied load of 4.5kN, the FSP53 fastening failed by rivet fracture with fracture of the locked sheet, whilst only fracture of the locked sheet occurred for the FSP510 fastening. The results indicated that the amount of pre-straining had an influence not only on the fatigue strength but also on the failure mode of the fastenings. Fretting was also observed to occur at the interface between the two riveted sheets indicated by the black-coloured fretting scars that formed at the interface.

The failure modes for the paint-baked samples were the same as without paint-baking.

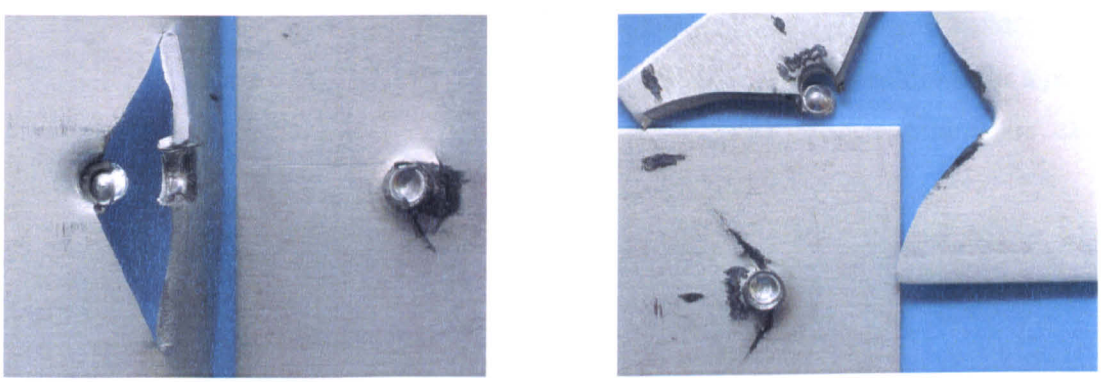

(a) **(b)**

Figure 3.34 Failure modes occurred during fatigue testing, (a) rivet fracture in a FSP53 fastening that failed at 4.5kN after 224,770 cycles, (b) sheet material failure in a FSP510 fastening that failure at 4.5kN after 321,210 cycles

CHAPTER FOUR

4. JOINT STRENGTH CHARACTERISTICS

The strength characteristics of self-piercing riveted joints depend on a variety of factors. The process parameters including the setting force, the rivet design and the anvil profile as well as the thickness and properties of the sheet material are believed to be the major influential factors. Drawing from past experience (King, [22]) and through microscopic examination, the optimum process parameters were identified during the initial part of the study. The joints that were used for mechanical testing were manufactured using these optimum parameters. It must be noted that any alteration of the influential factors requires a different combination of setting parameters for optimum setting conditions. As a result, a direct comparison of data from samples having different process parameters can be difficult.

4.1 Influence of Specimen Size

The specimen size has an influence on both the ultimate shear load and the fatigue endurance. Fig.4.1 shows the shear test results for the FSN51 and FSN56 fastenings that had a different specimen size from each other. The FSN51 fastening that joined sheets with

a 60mm width exhibited an ultimate shear load that was greater by about 35% than the FSN56 fastening, which joined sheets with a 48mm width.

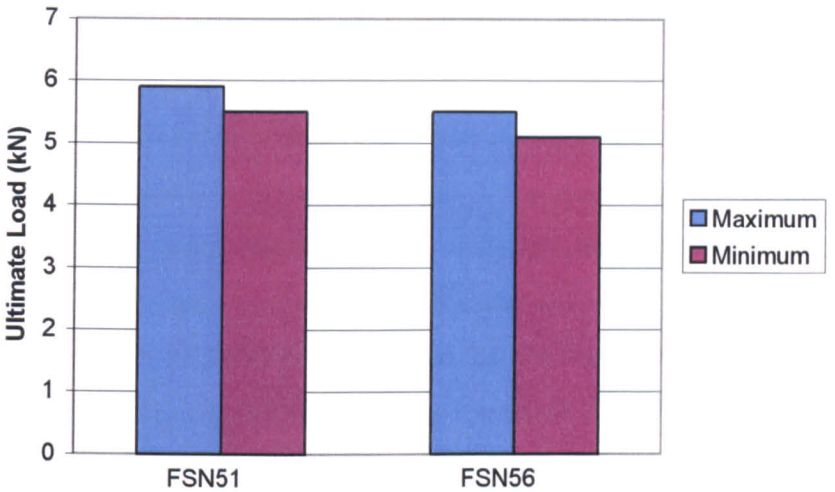

Figure 4.1 Comparison of shear ultimate load

During shear testing, the sheet material was subjected to a tensile stress with a non-uniform distribution along the discontinuous cross-section. Under the same load, the stress acting on the sheet for the FSN56 fastening was higher than that for the FSN51 fastening. Localised yielding might therefore occur earlier in the FSN56 fastening than in the FSN51 fastening as the load increased. In addition, the sheet material adjacent to the rivet was also subjected to a bearing stress since the rivet was in bearing against the side of the two sheets. Initially, the bearing stress was concentrated at the point of contact and then yielding of the sheet adjacent to the rivet occurred as the load increased. After yielding, the embedment of the rivet on a larger area of contact led to a more uniform stress distribution and concentrated on bearing the end of the sheet material. The development of bearing stresses for a self-piercing riveted joint is supposed to be the same as for a conventional riveted joint that was reported by Kulak et al. [34] and is shown in Fig.4.2.

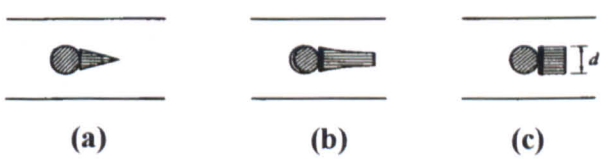

Figure 4.2 Distribution of bearing stresses: (a) elastic, (b) elastic-plastic, (c) nominal

Although the uniform stress distribution is not known, according to Kulak et al. [34], the maximum bearing resistance of the end of the sheet material σ_b can be expressed as

$$\sigma_b = (\frac{l}{0.715d} - 0.7)\sigma_t \qquad \textbf{Equation 4-1}$$

where l is the distance from the overlap end to the centre of the rivet, d is the diameter of the fastener and σ_t represents the tensile strength of the sheet material. As the FSN51 and the FSN56 fastenings joined identical sheet materials using identical rivets the two fastenings had the same value of d and σ_t. The value of l, which was half of the overlap length, was smaller for the FSN56 fastening than that for the FSN51 fastening. As a result, the FSN56 fastening had a much lower bearing resistance than the FSN51 fastening. The failure mode that occurred during shear testing for both the FSN51 and the FSN56 fastenings was rivet pull-out indicating that the bearing resistance of the riveted sheet was sufficient to prevent the rivet from tearing the riveted sheets. However, the lower bearing resistance for the FSN56 fastening led to more deformation at the end portion of the riveted sheets compared with the FSN51 fastening, as shown in Fig.4.3. In addition, the rivet was subjected to both a shear and a bending force. The bending moment tended to pull out the rivet by overcoming the frictional force between the rivet shank and the riveted sheets. The earlier yielding and the lower bearing resistance for the FSN56 fastening facilitated the rivet to overcome the frictional force and contributed to the reduction in the ultimate shear load for the FSN56 fastening.

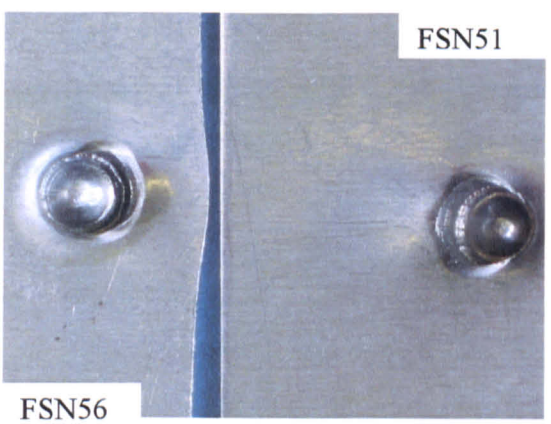

Figure 4.3 Deformation that occurred at the edge of the overlap for the FSN51 and FSN56 fastenings

The effect of the specimen size on the fatigue behaviour is shown in Fig.4.4. The FSN51 fastening exhibited a longer fatigue endurance than the FSN56 fastening.

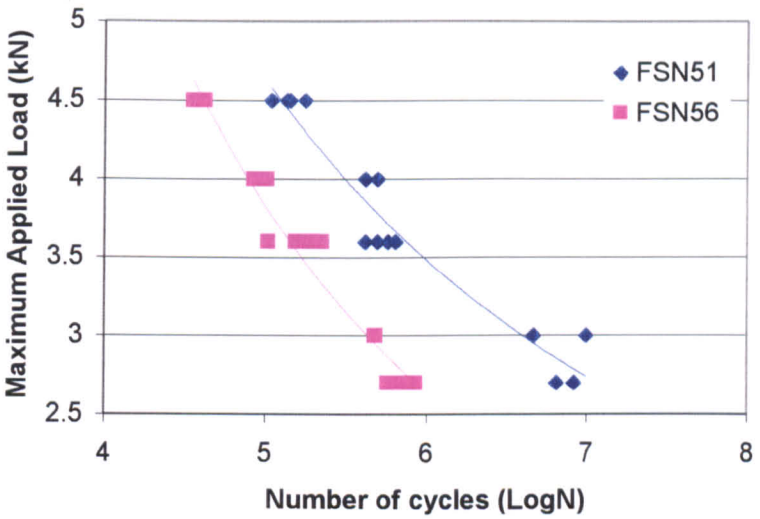

Figure 4.4 Comparison of fatigue endurance

The different specimen size of the two fastenings led to a different stress distribution on the cross-section of the sheet material. At a given applied load, the stress acting on the net section of the FSN56 fastening was higher than that of the FSN51 fastening due to the use of riveted sheets of a lower width. Fatigue, as a progressive failure phenomenon, proceeds by initiation and propagation of cracks to an unstable size. This is normally determined by the magnitude of the stresses and the presence of defects. At an equivalent load, the stress acting on the FSN56 fastening was greater than that acting on the FSN51 fastening. This led to quicker initiation and propagation of cracks in the FSN56 sample than in the FSN51 fastening. This contributed to the apparent shorter fatigue life of the FSN56 fastening.

Fig. 4.5 shows the fatigue data that was plotted as the ratio of the maximum applied load to the average ultimate shear load for the FSN51 and FSN56 fastenings. As shown in the figure, when the maximum applied load was 70% of the ultimate shear load, the fatigue endurance of the FSN51 fastening was about 10% higher than that for the FSN56

fastening. At 10^6 fatigue cycles, the FSN51 fastening sustained about 62% of its ultimate shear load, whilst the FSN56 fastening sustained only 52% of its ultimate shear load. This suggested that the FSN51 fastening had a better shear and fatigue performance than the FSN56 fastening.

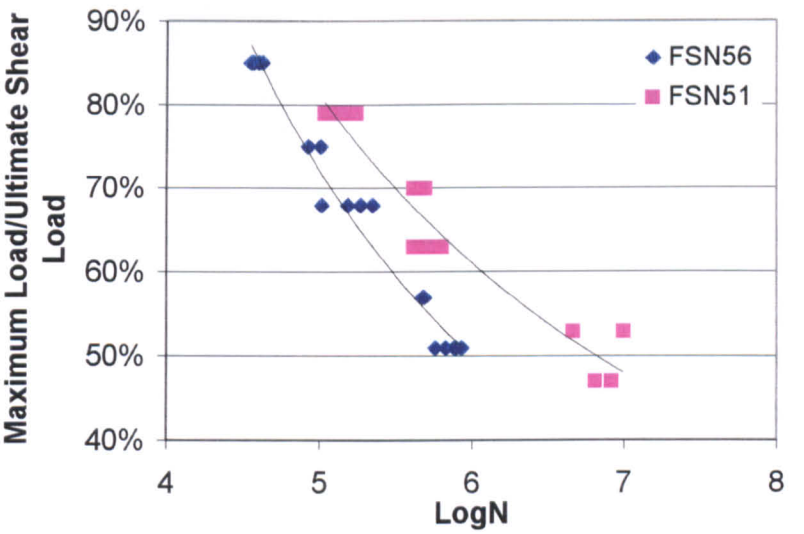

Figure 4.5 Ratio of max. applied load/ultimate shear load versus LogN

4.2 Influence of Sheet Material Strength

The sheet material strength had an influence on both the static and the fatigue behaviour of the fastenings. Fig.4.6 shows the shear, peel and pull-out test results for the FSN51 and the FSA62 fastenings. The FSA62 fastening exhibited a higher shear strength, but a slightly lower peel and pull-out strength compared with the FSN51 fastening.

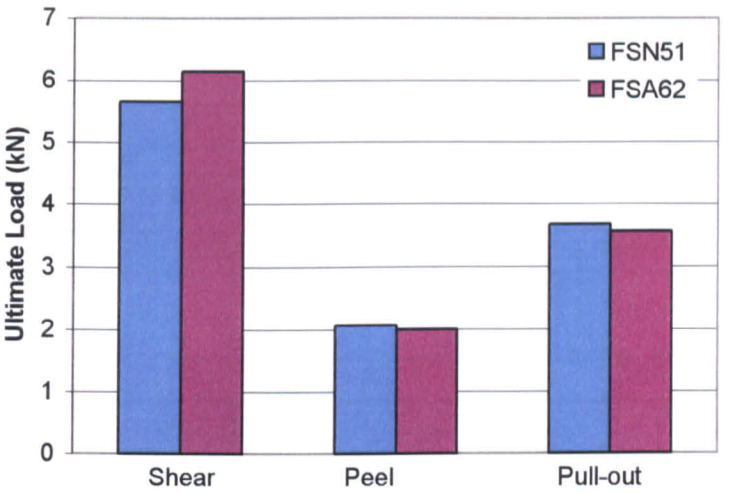

Figure 4.6 Influence of material properties on static tests

The only difference between the two fastenings was that the FSA62 fastening had a pierced sheet of 2mm-thick AA6111, whilst the FSN51 fastening had a 2mm-thick NG5754 sheet as the pierced sheet. The locked sheet for both fastenings was a 2mm-thick NG5754 sheet. Therefore the variation in the joint behaviour was due to the different mechanical properties of the pierced sheet.

As discussed in section 4.1, during shear testing, the tensile stress and the bearing stress acting on the sheet material affected the ultimate shear load. The 2mm-thick AA6111 pierced sheet for the FSA62 fastening had a higher tensile strength and a higher yield stress compared with the 2mm-thick NG5754 pierced sheet used for the FSN51 fastening, as shown in Fig.4.7. Therefore, the AA6111 sheet of the FSA62 fastening could withstand a higher stress before localised yielding occurred. In the meantime, the bearing stress of the sheet material is proportional to the tensile strength, as shown in Equation 4.1, and therefore the AA6111 sheet was able to take up a higher bearing load. The higher yield strength and the higher bearing resistance of the AA6111 sheet therefore contributed to the higher shear strength of the FSA62 fastening.

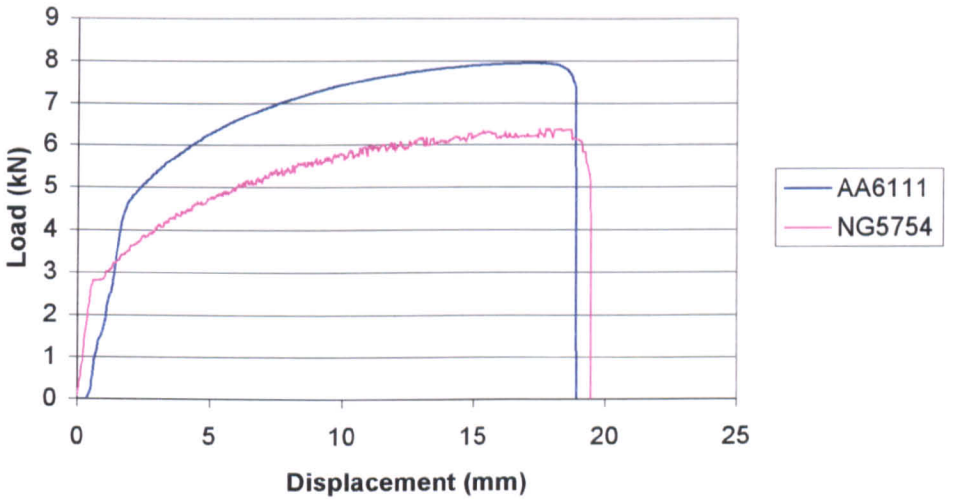

Figure 4.7 Tensile test results for AA6111 and NG5754

During peel and pull-out testing, the failure mode that occurred for the FSN51 and FSA62 fastenings, was by means of rivet pull-out with both riveted sheets suffering a small amount of deformation. This indicated that the peel and the pull-out forces concentrated on the clinch button of the fastening. The clinch strength, which was mainly governed by the frictional force between the rivet shank and the two riveted sheets, was eventually overcome by the load transferred by the sheet material to the clinch leading to separation of the two riveted sheets. Therefore, the frictional force, which was affected by deformation of the sheet material and the flare of the rivet into the lower sheet, had an influence on both the peel and the pull out strength. According to King [22], the mechanical properties of the sheet material affected the deformation characteristics of the fastening during the setting process. The harder and stronger material required a higher setting force to allow indentation and deformation of the sheet material, otherwise, the rivet would not flare properly and consequently the joint strength would be affected. As shown in Fig.4.7, the AA6111 sheet was stronger than the NG5754 sheet. In addition, the AA6111 alloy was also harder with a Vickers hardness value of 98 compared to 68 for the NG5754 alloy. Therefore a slightly higher setting force was probably required when joining AA6111 sheet. However, for comparison, the setting force used for the FSN51 and the FSA62 fastenings was identical. This could slightly affect the rivet flare into the lower sheet leading to a small reduction in the clinch strength. It should be noted here that the

surface of the AA6111 sheet differed from that of the NG5754 sheet in that the former was not covered by the wax-based solid lubricant. This could provide the interface between the rivet shank and the riveted sheet for the FSA62 fastening with a slightly higher coefficient of friction. However, the normal force (contact pressure) at the interface for the FSA62 fastening might be much lower than for the FSN51 fastening due to the use of an identical setting force. The frictional force at the interface for the FSA62 fastening, even with a slightly higher coefficient of friction, was still possibly lower than for the FSN51 fastening. As a result, the peel and pull-out strength of the FSA62 fastening were slightly, but not significantly, lower than that of the FSN51 fastening. These results suggested that the peel and the pull-out strengths were mainly dependent on the clinch strength, whilst the shear strength depended on both the sheet material properties and the clinch strength.

In addition to the effect on the static behaviour, the sheet material properties also affected the fatigue performance of the fastenings. Fig.4.8 shows the fatigue test results for the FSN51 and the FSA62 fastenings. At maximum loads greater than 3.5kN, the FSA62 fastening exhibited slightly longer fatigue endurance, whilst at a maximum load lower than 3.5kN, the fatigue endurance for both fastenings was almost the same. At loads exceeding 3.5kN, *rivet fracture* was observed for both the FSN51 and the FSA62 fastenings, as shown in Figs.3.11 (b) and 3.28 (b) indicating that the fatigue strength was dominated by rivet. At an identical applied load, the stress acting on the cross-section of the sheet material for the FSN51 fastening was more critical than it was for the FSA62 fastening due to the higher strength of the AA6111 sheet. This contributed to the initiation and propagation of cracks on the NG5754 sheet material. Fracture of the NG5754 sheet for both the FSN51 and the FSA62 fastenings was observed to occur during the fatigue test. The fracture of both the pierced and the locked sheet for the FSN51 fastening aided the rivet fracture. In the meantime, the lower yield stress and bearing stress of the NG5754 sheet for the FSN51 fastening facilitated the rivet pull-out. These factors contributed to a shorter fatigue life for the FSN51 fastening compared with the FSA62 fastening. By contrast, the AA6111 pierced sheet did not fracture even at the highest applied load, as shown in Fig.3.28 (c). Considering also the higher yield stress and bearing stress of the AA6111 sheet, the rivet pull-out for the FSA62 fastening did not occur as easily as for the FSN51 fastening. Therefore, the FSA62 fastening exhibited a longer fatigue life than the FSN51 fastening. At applied load levels below 3.5kN, the failure mode that occurred for

the two fastenings was *sheet material failure*, as shown in Figs.3.11 (c) and 3.28 (c). This indicated that the fatigue strength was mainly dominated by the initiation and propagation of cracks on the locked sheet that failed during fatigue testing. The use of a NG5754 lower sheet therefore led to almost the same fatigue life for both the FSN51 and FSA62 fastenings.

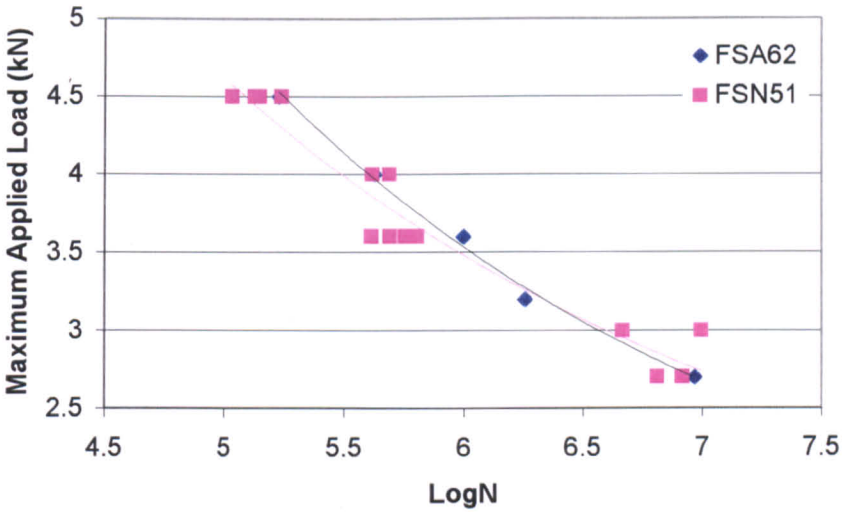

Figure 4.8 S-N curves for the FSN51 and the FSA62 fastenings

The fatigue behaviour between the two fastenings can also be compared by plotting the fatigue data in the form of the ratio of the maximum applied load to the average ultimate shear load against LogN (number of cycles), as shown in Fig.4.9. At an identical ratio, the FSN51 fastening exhibited better fatigue performance than the FSA62 fastening. This indicated that the FSN51 fastening had a better balance between the shear and fatigue behaviour compared with the FSA62 fastening. The high strength of the AA6111 sheet was probably not utilised efficiently during fatigue testing. This was also suggested by the fatigue failure mode that occurred for the FSA62 and the FSN51 fastenings. Rivet fracture and locked sheet fracture with no visible cracks on the AA6111 pierced sheet were the only failure system for the FSA62 fastening. In contrast, both locked sheet and pierced sheet fracture were involved in the failure mechanism for the FSN51 fastening, in addition to rivet fracture.

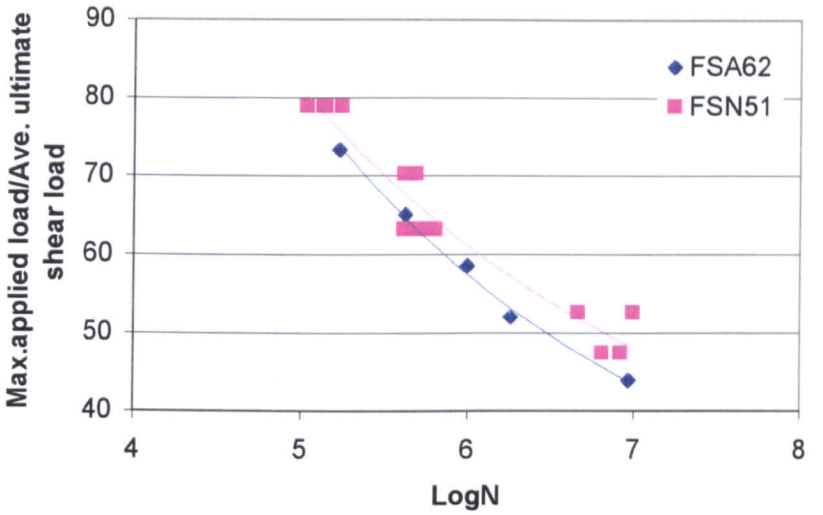

Figure 4.9 Ratio of Maximum applied load/Average ultimate shear load versus LogN

4.3 Influence of Sheet Material Thickness and Setting Force

Fig.4.10 shows the static test results for the FSN52 and the FSN53 fastenings. The upper sheet thickness differed between the two fastenings and consequently different setting pressure values were used, as listed in Table 2.6. The FSN52 fastening, which had a 2mm-thick pierced sheet and was pierced using a setting pressure of 120bar, exhibited a higher static strength than the FSN53 fastening, which had a 1mm pierced sheet and adopted a setting pressure of 100bar. This indicated that the sheet material thickness and possibly setting force had an influence on the static strength.

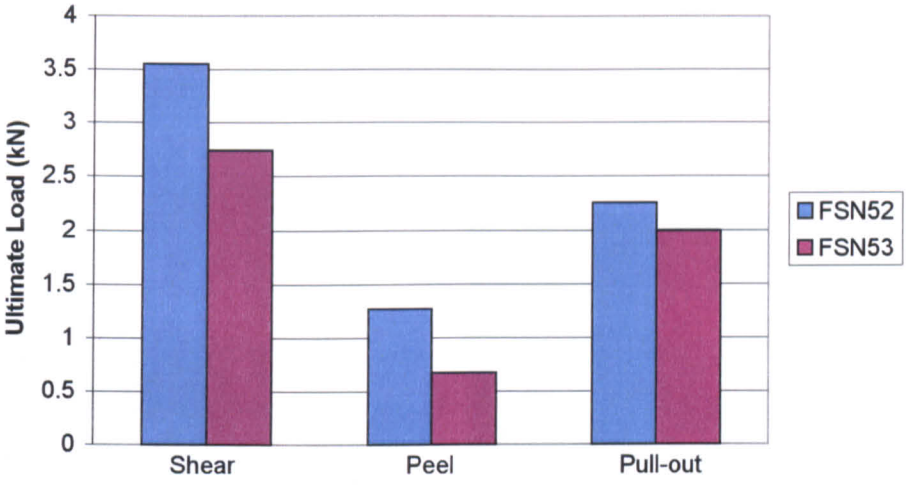

Figure 4.10 The influence of the thickness of the upper sheet

During shear testing, the tensile stress acting on the cross-section of the 1mm pierced sheet for the FSN53 fastening was twice the stress acting on the cross-section of the 2mm pierced sheet for the FSN52 fastening. In addition, according to Kulak et al [34], based on the assumption of a uniform stress distribution, the nominal bearing stress can be expressed as

$$\sigma_b = \frac{P}{dt} \qquad \textbf{Equation 4-2}$$

where P denotes the load sustained by the rivet, t the sheet thickness and d the rivet diameter. The FSN52 and the FSN53 fastenings had an identical rivet diameter d. Therefore, under the same shear load P, the bearing stress acting on the 1mm pierced sheet adjacent to the rivet for the FSN53 fastening was twice the bearing stress acting on the 2mm pierced sheet for the FSN52 fastening. These factors caused an earlier localised yielding and more distortion on the 1mm pierced sheet for the FSN53 fastening than on the 2mm pierced sheet for the FSN52 fastening, as shown in Fig.4.11. Once localised yielding occurred, the external load concentrated more on the rivet due to the embedment of the rivet which thus was in contact with a larger area of the riveted sheet leading to its pull out. The lower setting force that was used for the FSN53 fastening compared with the FSN52 fastening provided the joint with a lower contact pressure leading to a lower frictional force at the interface between the rivet shank and the riveted sheets. The rivet for the

FSN53 fastening was therefore pulled out more easily than for the FSN52 fastening. These factors contributed to the lower shear strength of the FSN53 fastening.

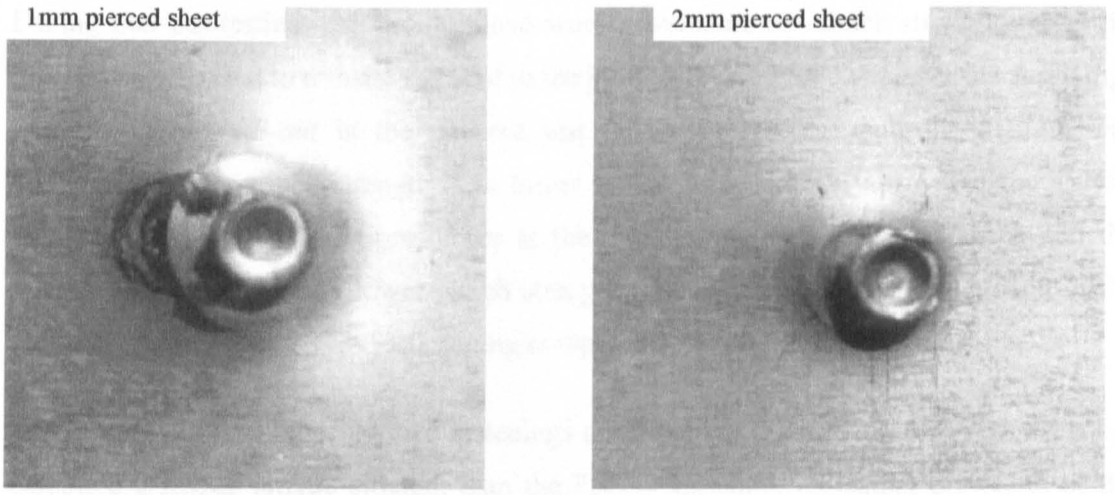

Figure 4.11 Deformation of the pierced sheet that occurred in shear test

During peel testing, peeling and bending of the sheet material around the rivet head dominated the process. According to bending theory, the maximum bending stress acting on a rectangular-section beam, which is subjected to a bending moment ***M*** about the z-axis, can be expressed as

$$\sigma_{\max} = \frac{M\frac{h}{2}}{\frac{bh^3}{12}} = \frac{6M}{bh^2} \qquad \textbf{Equation 4-3}$$

where ***b*** is the beam width and ***h*** is the beam height. The reverse square relationship between the maximum bending stress and the height, which was equal to the thickness of the sheet led to a very high bending stress on the 1mm sheet. Under an identical bending moment, the maximum bending stress on the 1mm-thick pierced sheet for the FSN53 fastening was 4 times the stress acting on the 2mm-thick pierced sheet for the FSN52 fastening. The 1mm-thick pierced sheet failed to sustain the very high bending stress leading to eventual failure of the FSN53 fastening by *sheet material failure*, as shown in Fig.3.9 (b). In this case, the effect of the setting force was less critical and had little effect on the joint strength. For the FSN52 fastening, the 2mm-thick sheet material could sustain

the bending moment and therefore transferred the load to the joint. The load on the joint concentrated on the clinch button of the fastening and eventually overcame the clinch strength of the FSN52 fastening leading to the rivet being pulled out.

During pull-out testing, the external load would overcome the clinch strength unless the sheet material failed to transfer the load to the joint. Both the FSN52 and FSN53 fastenings failed by *rivet pull-out* in the pull-out test indicating that the pull-out strength was dominated by the clinch strength. The lower setting force probably provided the FSN53 fastening with a lower frictional force at the interface between the rivet shank and the riveted sheets leading to a lower clinch strength. This contributed to the reduction in the pull-out strength for the FSN53 fastening compared with the FSN52 fastening.

The fatigue test results for the two fastenings are shown in Fig.4.12. The FSN52 fastening exhibited a higher fatigue strength than the FSN53 fastening indicating the effect of the sheet material thickness and the setting force.

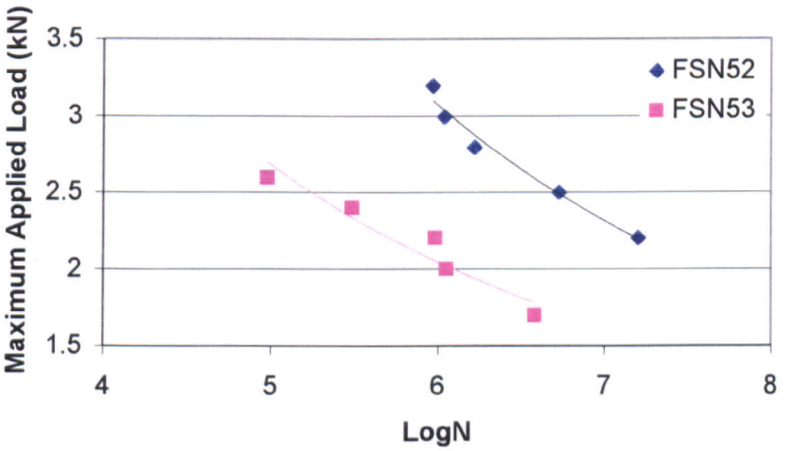

Figure 4.12The influence of the sheet material thickness on the fatigue test results

Similar to shear testing, during fatigue testing, the stress acting on the cross-section of the 1mm pierced sheet for the FSN53 fastening was twice the stress acting on the cross-section of the 2mm pierced sheet for the FSN52 fastening. This speeded up the initiation and propagation of cracks on the 1mm pierced sheet for the FSN53 fastening leading to

eventual failure by *sheet material failure*, as shown in Fig.3.11 (a). The 1mm-thick pierced sheet failed to sustain the fatigue loading resulting in a shorter fatigue life for the FSN53 fastening compared with the FSN52 fastening. This indicated that for the FSN53 fastening, the behaviour of the 1mm pierced sheet dominated the fatigue life rather than the clinch. It was therefore suggested that the setting force, which affected the clinch strength of the fastening might only have a minor effect on the fatigue strength of the FSN53 fastening.

4.4 Influence of Setting Parameters

The rivet and anvil design are normally selected in tandem. The setting force is generally selected based on the selection of rivet and anvil design as well as the properties of the sheet material to be joined. Details of the anvil profile are the property of Textron Fastening Systems and for confidential reasons cannot be reported here. This made it difficult to identify the factors that affected the joint behaviour individually. In this section the collective influence of the rivet and anvil design as well as the setting force is discussed.

The setting parameters were observed to have an influence on both the static and the fatigue strength of the fastenings. Fig.4.13 shows the static test results for the FSN51 and the FSN52 fastenings, which joined identical sheet materials by using a different rivet and anvil design and consequently a different setting pressure, as shown in Table 2.6. The fatigue test results for the two fastenings are shown in Fig.4.14. The FSN51 fastening exhibited a higher static strength and better fatigue behaviour than the FSN52 fastening indicating the effect of the setting parameters.

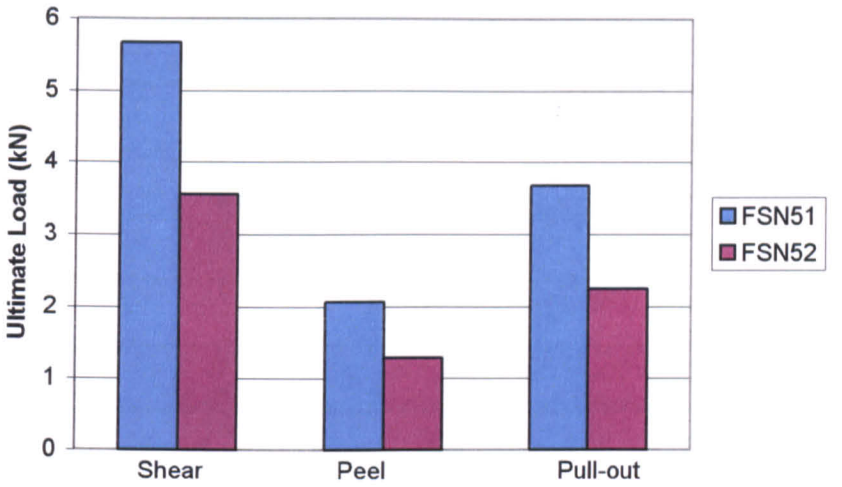

Figure 4.13 Static test results for the FSN51 and the FSN52 fastenings

During shear, peel and pull-out testing, the FSN51 and FSN52 fastenings failed by rivet pull-out with no fracture on the sheet material and the rivet. This indicated that the sheet material was strong enough to transfer external load to the rivet and the load capacity of the rivet itself was not exceeded. It was also concluded that the static strength of the two fastenings was mainly governed by the clinch strength, which was mainly dominated by the frictional force at the interface between the rivet shank and the riveted sheets. The sheet material used for both the FSN51 and the FSN52 fastenings was the same leading to an identical coefficient of friction. The rivet used for the FSN52 fastening was 1mm shorter in length and 0.9mm smaller in diameter than that for the FSN51 fastening. Therefore for the FSN52 fastening, the contact area between the rivet shank and the riveted sheets was smaller than for the FSN51 fastening. The lower setting force probably provided the FSN52 joint with a lower contact pressure between the rivet shank and the riveted sheets compared with the FSN51 fastening. These factors resulted in a lower frictional force at the interface between the rivet shank and the riveted sheets leading to a lower clinch strength for the FSN52 fastening compared with the FSN51 fastening. This contributed to the lower static strength of the FSN52 fastening. The different anvil profiles between the two fastenings might also have affected the rivet flare and consequently the clinch strength.

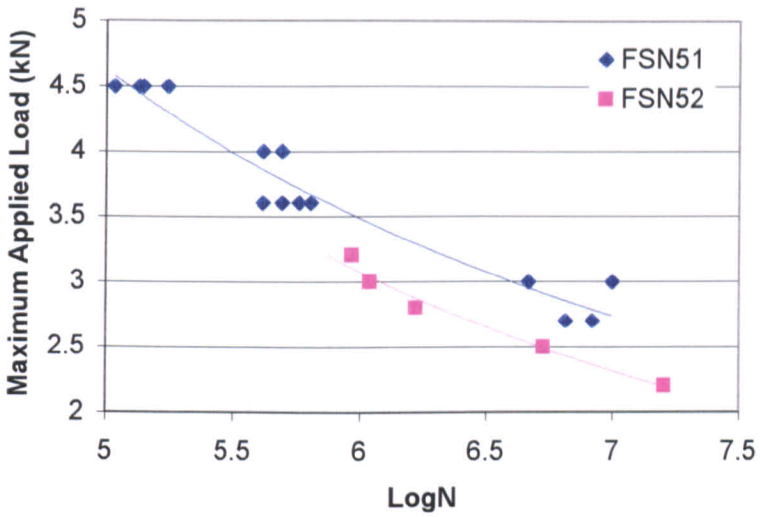

Figure 4.14 Fatigue test results for the FSN51 and the FSN52 fastenings

During fatigue testing, both *sheet material failure* and *rivet fracture* occurred for the FSN51 and the FSN52 fastenings, as described in Chapter Three. This indicated that the fatigue strength of the FSN51 and the FSN52 fastenings was governed by the behaviour of the sheet material and the rivet. Under a cyclic load, the frictional force at the interface between the two riveted sheets sustained a part of the cyclic load with a maximum value of μN, where μ is the coefficient of friction and N represents the normal load acting on the contacting surfaces. The higher the frictional force at the contacting surfaces the higher the load taken up by the interface. The lower setting force and the smaller rivet for the FSN52 fastening might provide a lower normal load and consequently a lower frictional force at the interface since the coefficient of friction was the same for both fastenings. Therefore, under an identical applied load, the load sustained by the contacting surfaces between the two riveted sheets was lower for the FSN52 fastening compared with the FSN51 fastening. As a result, the load sustained by the sheet and the rivet for the FSN52 fastenings was greater than that for the FSN51 fastening. The rivet that was used for the FSN52 fastening was smaller than that for the FSN51 fastening, whilst the sheet material was the same for both fastenings. Therefore, the stress acting on the cross-section of the sheet and on the rivet for the FSN52 fastening was greater compared with the FSN51 fastening leading to a quicker initiation and propagation of cracks on both the sheet and the rivet. These factors

explained why the FSN52 fastening failed at a lower number of fatigue cycles compared with the FSN51 fastening.

4.5 Influence of the Sheet Material Surface Condition

The sheet material surface condition had an influence on both the shear and the fatigue behaviour of the fastenings. Fig.4.15 shows the shear test results for the FSN51, FSH51 and FSH52 fastenings. The FSH51 fastening had the highest shear strength of the three fastenings.

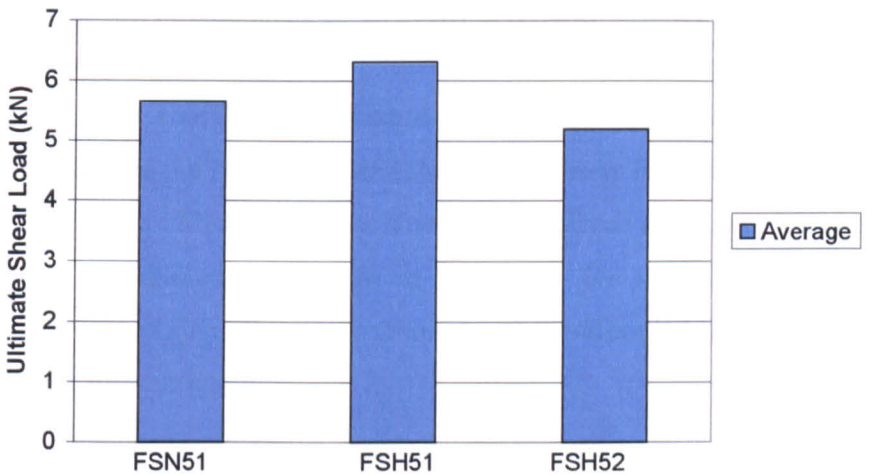

Figure 4.15 Shear test results for the FSN51, FSH51 and FSH52 fastenings

The three fastenings were created for joining 5754 alloy sheet of 2mm-thickness by using identical setting parameters, as listed in Table 2.6. The only difference between the three fastenings was the sheet material surface condition and as a result the coefficient of friction at the interface was different in each case. This meant that the frictional force at the interface between the two riveted sheets and at the interface between the rivet shank and the riveted sheet differed from one type of sample to the other. Cross-sectional examination suggested that the sheet material surface condition had an influence on the clinch strength of the fastenings. Fig.4.16 shows the locked sheet surface, which was in

contact with the rivet shank for the FSN51 fastening. The results of EDS analysis, shown in Fig.4.17, indicated that a high level of Carbon, which was the main constituent element of the surface lubricant, was present at that surface. The dark grey colour represented the wax-based surface lubricant in Fig.4.16. In addition, the wax-based surface lubricant was also detected on the surface of the pierced sheet surface, which was in contact with the rivet shank, as shown in Figs.4.18 and 4.19. The results suggested that after setting, the wax-based surface lubricant still remained at the interface between the two riveted sheets and the rivet shank. A part of a cross-section of the FSH52 fastening is shown in Fig.4.20. EDS analysis taken at the interface between the rivet shank and the locked sheet is shown in Fig.4.21. The presence of a high level of fluorine and carbon indicated the presence of PTFE. The inserted PTFE tape was located in fragments at the interface between the rivet shank and the riveted sheets. It was understood that both the lubricant and the PTFE tape reduced the coefficient of friction at the interface with the PTFE tape reducing it the most. The sheet material joined by the FSH51 fastening had no surface lubricant on its surface and this led a higher coefficient of friction at the contacting surfaces. Therefore, the frictional force between the rivet shank and the riveted sheets for the FSH51 fastening was higher than that for the FSN51 fastening. The frictional force at the interface between the rivet shank and the riveted sheets was at its lowest for the FSH52 fastening. This contributed to the reduction in the clinch strength and therefore led to the FSH52 fastening having the lowest static strength.

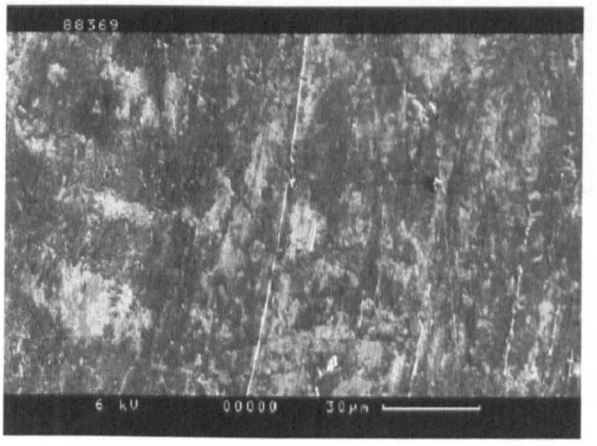

Figure 4.16 Locked sheet surface in contact with the rivet shank for the FSN51 fastening

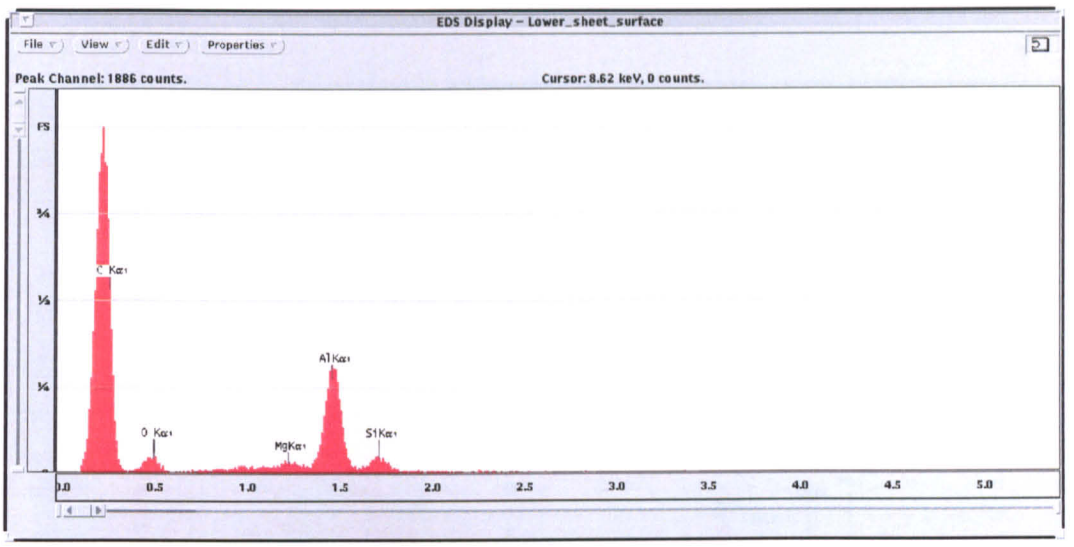

Figure 4.17 EDS analysis results for the locked sheet surface shown in Fig.4.16

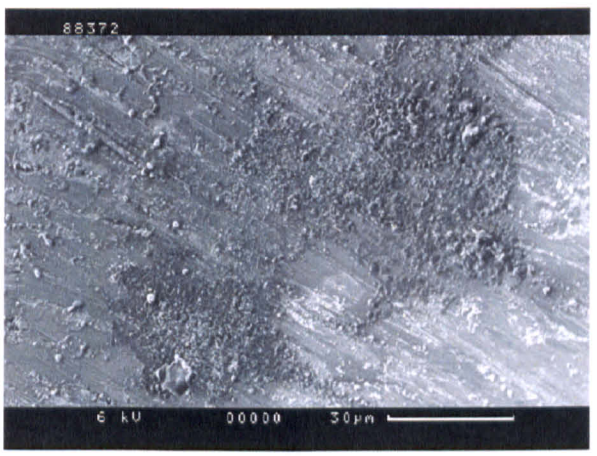

Figure 4.18 The surface of the pierced sheet in contact with the rivet shank for the FSN51 fastening

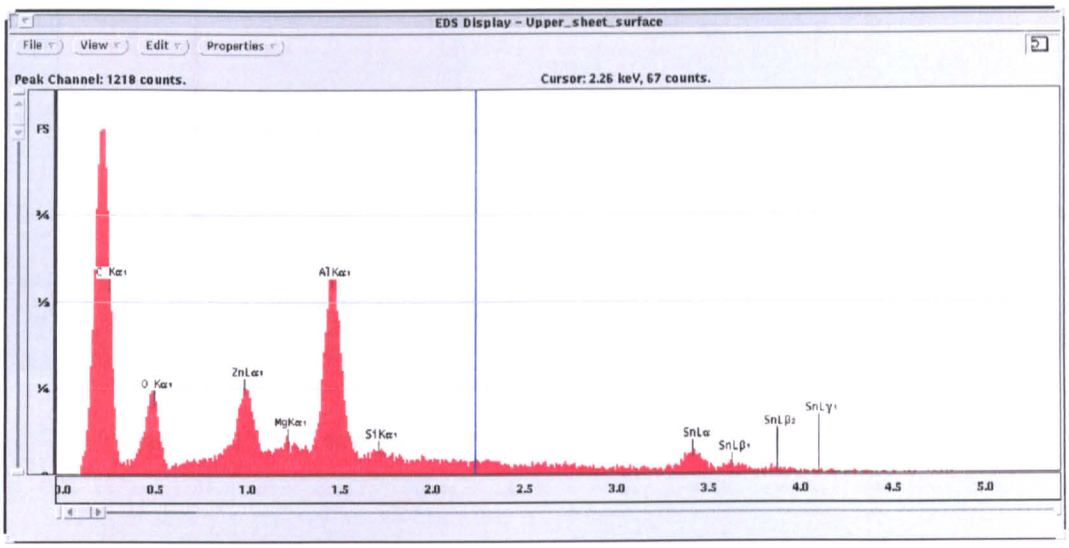

Figure 4.19 EDS analysis results for the pierced sheet surface shown in Fig.4.18

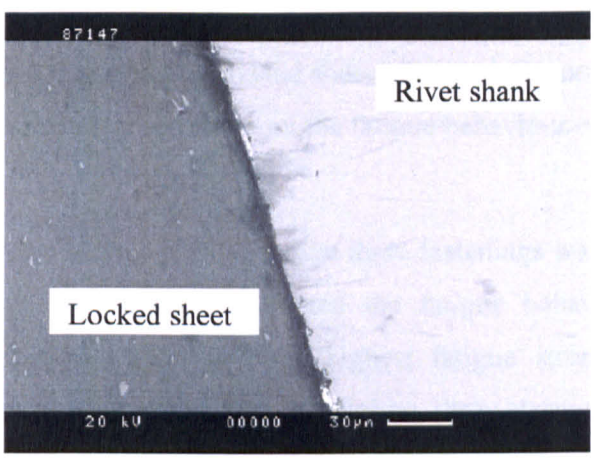

Figure 4.20 Interface between the rivet shank and the locked sheet for the FSH52 fastening

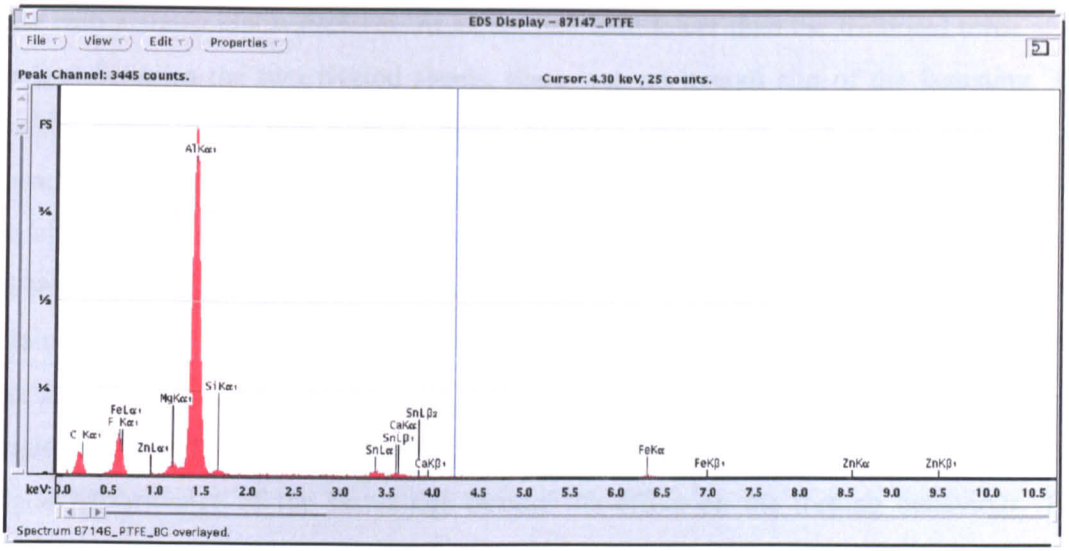

Figure 4.21 EDS analysis results for the interface shown in Fig.4.20

In addition to the effect on the clinch strength, the sheet material surface condition also affected the frictional force at the interface between the two riveted sheets. However, this did not influence the ultimate shear strength of the fastenings. During shear testing, the shear load was initially transferred by the frictional force at the interface between the two riveted sheets. As the shear load increased, the frictional force was exceeded and overall slip of the joint started to take place. From this stage, the shear load was mainly transferred by means of shearing of the rivet and bearing of the sheet material and therefore the frictional force did not affect the shear strength of the joints. Although the frictional force between the two riveted sheets did not influence the shear strength of the fastening, it had a significant influence on the fatigue behaviour of the fastening.

The fatigue strength of the three fastenings was different indicating that the sheet material surface condition affected the fatigue behaviour. As shown in Fig.4.22, the FSN51 fastening exhibited the highest fatigue strength of the three fastenings. The FSH51 fastening, which had the highest shear strength of the three fastenings, did not have the highest fatigue strength indicating that the highest shear strength was not accompanied with the highest fatigue strength. The fatigue test differs from the shear test in that the failure process in the fatigue test is governed by initiation and propagation of cracks. In addition, during fatigue testing, the applied load changed from its maximum to minimum

value with a sinusoidal waveform. At an applied load lower than the frictional force at the interface between the two riveted sheets, there was no overall slip of the fastening. The interface between the two riveted sheets therefore transferred part of the applied load depending on the magnitude of the applied load and the frictional force at the interface. The change of the interfacial conditions therefore led to a variation in the load transfer mechanisms. The higher the load transferred by the contacting surfaces the lower the load sustained by the rivet and the sheet material. This could lead to a longer fatigue life for the rivet and the sheet material. However, fretting occurred at the contacting surfaces during fatigue testing and made the analysis more complicated. The surface condition affected the fatigue performance of the fastenings through its effect on the fretting behaviour. This contributed to the variation in the fatigue strength of the three fastenings and will be further discussed in Chapter Five.

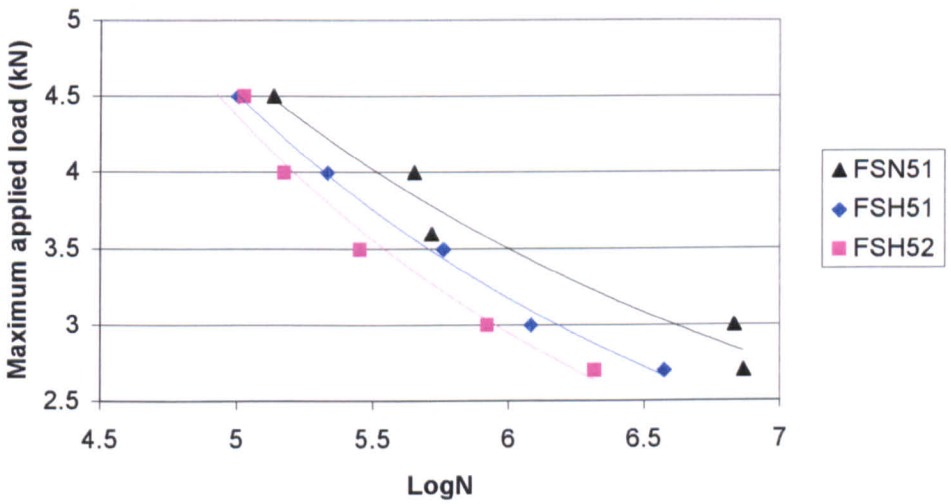

Figure 4.22 Fatigue test results for the FSN51, FSH51 and FSH52 fastenings

4.6 Influence of Pre-straining level

The pre-straining level had an influence on the ultimate shear load of the fastenings, as shown in Fig.3.30. The variation of the ultimate shear load of the FSP5 series of fastenings before paint-baking along with the pre-straining level is shown in Fig.4.23. The higher the pre-straining level the higher the ultimate shear load of the fastening.

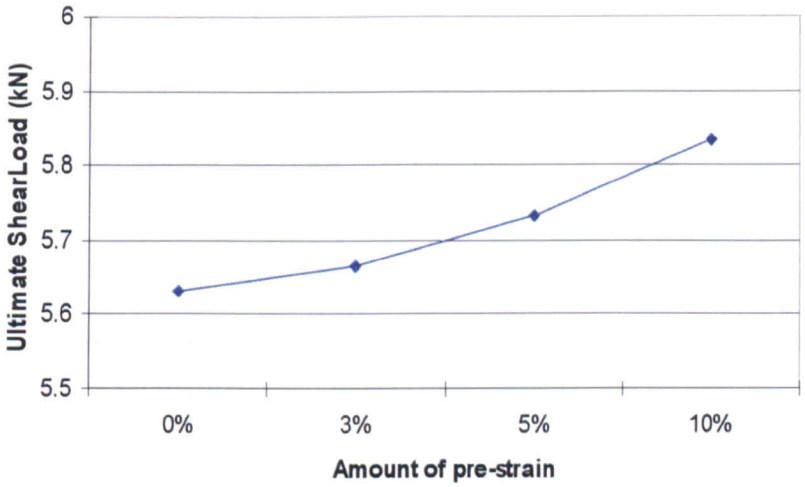

Figure 4.23 Shear strength versus amount of pre-straining

Pre-straining is a work-hardening process, which is accompanied with an increase in the strength and a decrease in the ductility of the material. Fig.4.24 shows the increase in the tensile strength and the reduction in the elongation for the pre-strained NG5754 alloy sheets with different amounts of pre-straining. The decrease in ductility could affect the cross-sectional deformation characteristics of the fastening during the setting process. It was observed that this did not cause obvious problems to the riveting process as shown in Fig.3.29 indicating that the reduction in the ductility of the pre-strained NG5754 alloy sheet was within acceptable limits. The shear test results suggested that the increase in the tensile strength of the pre-strained NG5754 sheet led to an increase in the shear strength of the fastening. This was due to the accompanying increase in the yield strength of the sheet material, which made the rivet more difficult to be pulled out. In addition, the higher tensile strength provided the sheet with a higher bearing resistance. These factors

contributed to the increase in the shear strength of the riveted samples as the amount of pre-straining level increased.

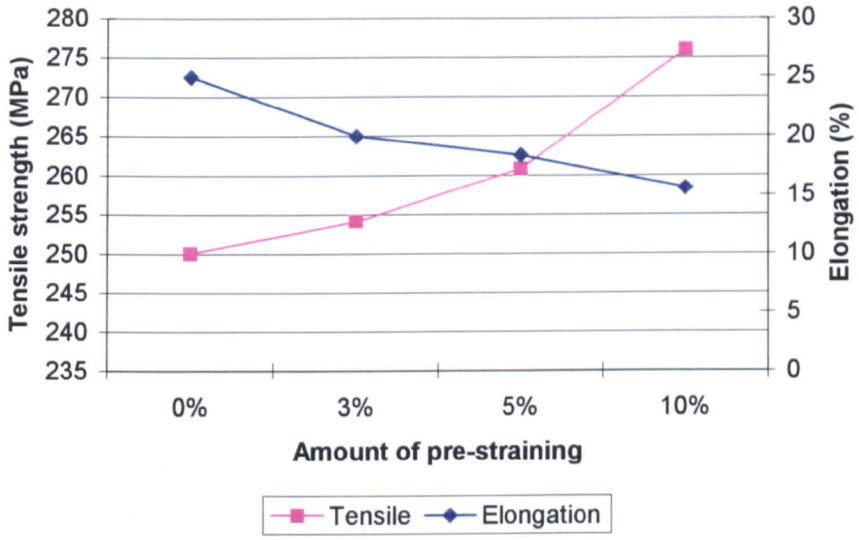

Figure 4.24 Properties of pre-strained NG5754 before paint-baking

The effect of the pre-straining level on the fatigue behaviour is presented in Fig.3.22, which shows the S-N curves for the FSP5 series of fastenings before paint-baking. The increase in the amount of pre-straining for the sheet material led to an increase in the fatigue strength of the fastenings. As a work-hardening process, pre-straining led not only to an increase in the yield strength, but also to an increase in the hardness of the sheet material. The hardness is considered to be one of the most important factors governing wear since hardness is the resistance of a material to plastic deformation. In addition, the true area of contact between the contacting surfaces is also related to material hardness. Bowden et al [42] reported that the real contact area A could be calculated as

$$A = \frac{N}{H} \qquad \textbf{Equation 4-4}$$

where N is the normal load and H represents the hardness of the softer of the two contacting materials. According to Waterhouse [43], wear is proportional to the real contact area, and therefore it is inversely proportional to the hardness. The harder the material the smaller the fretting area leading to less fretting damage and based on the experimental results, this was shown to be the true. Fig.4.25 shows the fretting scars that

formed on the surface of the pierced sheets of the FSP5 series of fastenings that were tested at a maximum applied load of 4.5kN for 20 minutes. The size of the fretting scar at the pierced sheet with 3% pre-straining was smaller than that at the pierced sheet without pre-staining, as shown in Fig.4.25 (a), but was greater than that at the pierced sheet with 5% pre-straining, as shown in Fig.4.26 (b). The relationship between the pre-straining levels and the fretting area was clearly defined. The higher the pre-straining the smaller the fretting scar. The increase in the hardness therefore reduced the wear rate during the fretting process leading to an increase in the fatigue strength of the fastenings.

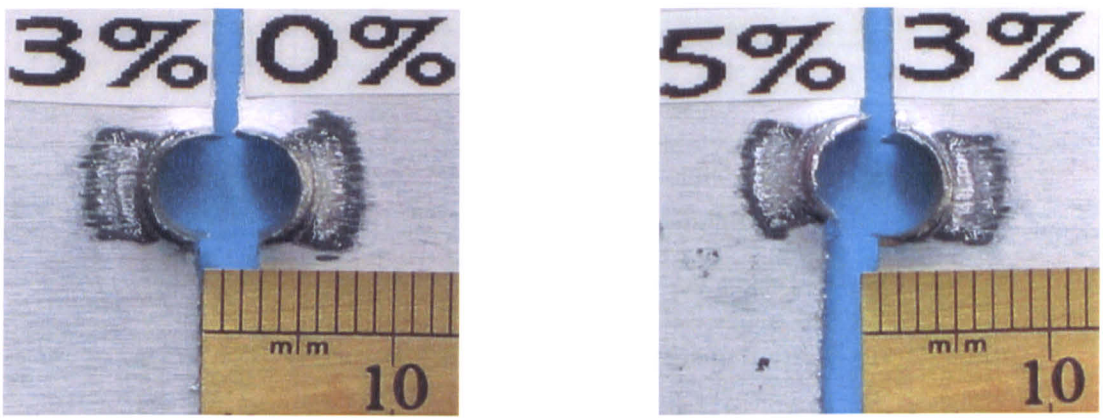

(a) **(b)**

Figure 4.25 Relationship between hardness and fretting area

The increase in the amount of pre-straining was accompanied with an increase in the fatigue resistance of the sheet material and this also led to an increase in the fatigue strength of the fastenings. However, the increase in the amount of pre-straining was not accompanied by proportionate improvements in the fatigue life of the sheet material and in the fatigue strength of the fastenings. Fig.4.26 shows the average number of cycles at maximum applied loads of 3.6kN and 4.5kN as a function of the amount of pre-straining. The slope of the line indicated the increase in the rate of the fatigue cycles from one pre-straining level to another. The different slope of the line between two different pre-straining levels suggested that the increase in the pre-straining level of the sheet material had not provided the fastening with a proportional increase in the fatigue strength. As shown in Fig.4.26, the slope was at its highest in going from 0% to 3% pre-straining. In

addition, the greatest amount of reduction in the fretting area also occurred from 0% to 3% pre-straining, as shown in Fig.4.25. This indicated that the fatigue endurance could be effectively increased by pre-straining the sheet material by up to 3%. Further increasing of the pre-straining level only led to a marginal increase in the fatigue strength of the fastenings.

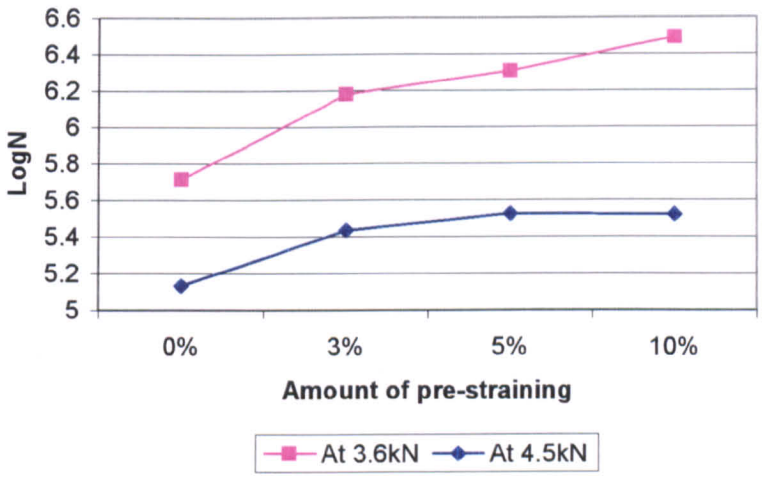

Figure 4.26 Average number of cycles versus amount of pre-straining

4.7 Influence of Paint-bake Cycle

4.7.1 The FSN5 series

The paint-bake cycle only had a minor influence on the static strength of the FSN5 series of fastenings. Fig.4.27 shows the static test results for the FSN53 and FSN53* fastenings. The only difference between the two fastenings was that the FSN53* fastening had been exposed to a paint-bake cycle, whilst the FSN53 fastening had not been. The FSN53 fastening had a slightly higher shear and peel strength and a slightly lower pull-out strength than the FSN53* fastening. The reasons for this were believed to be due to the softening of the NG5754 sheet material and the change of the interfacial conditions following paint-baking. Tensile and hardness tests that were carried out prior to and after paint-baking for the NG5754 alloy sheet indicated that the paint-baking treatment led to a decrease in the

strength and hardness of the alloy NG5754, as shown in Fig.4.28 and Table 4.1. The slight reduction in the yield strength and hardness of the NG5754 alloy sheet facilitated easier pull-out of the rivet during shear and peel testing leading to a marginal reduction in the shear and peel strength of the FSN53* fastening. In addition, during the paint-bake cycle the wax-based surface lubricant was removed and this led to an increase in the coefficient of friction at the interface between the rivet shank and the riveted sheets leading to a higher clinch strength. This probably contributed to the higher pull-out strength of the FSN53* fastening compared with the FSN53 fastening since the pull-out strength was mainly dominated by the clinch strength. The increase in the clinch strength following paint-baking did not lead to an increase in the shear and peel strength. This indicated that the increase in the clinch strength on its own was not sufficient enough to cause an increase in the shear and peel strength. It appears that the reduction in the yield strength and hardness of the sheet material were more influential factors in determining the shear and peel strength of the fastenings than the clinch strength.

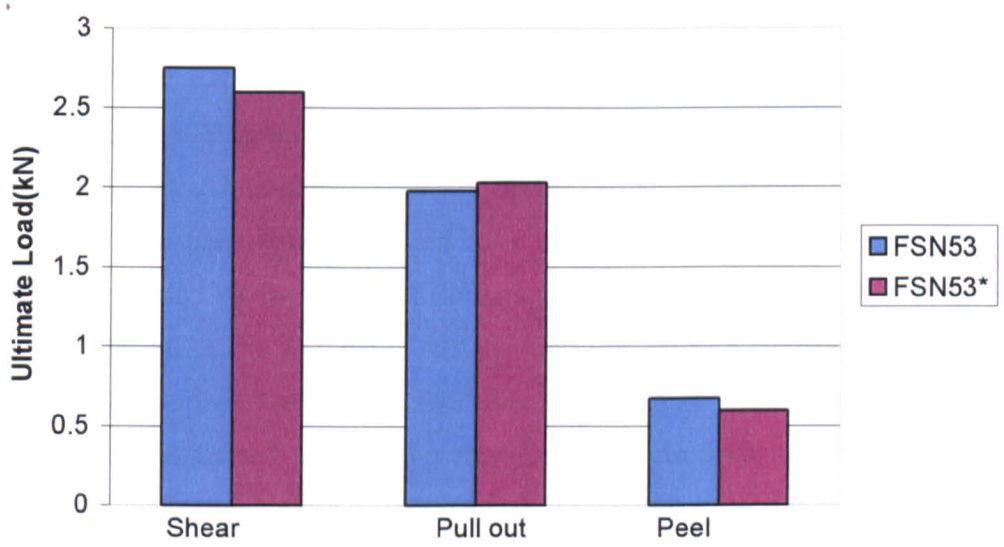

Figure 4.27 Static test results for the FSN53 and the FSN53* fastenings

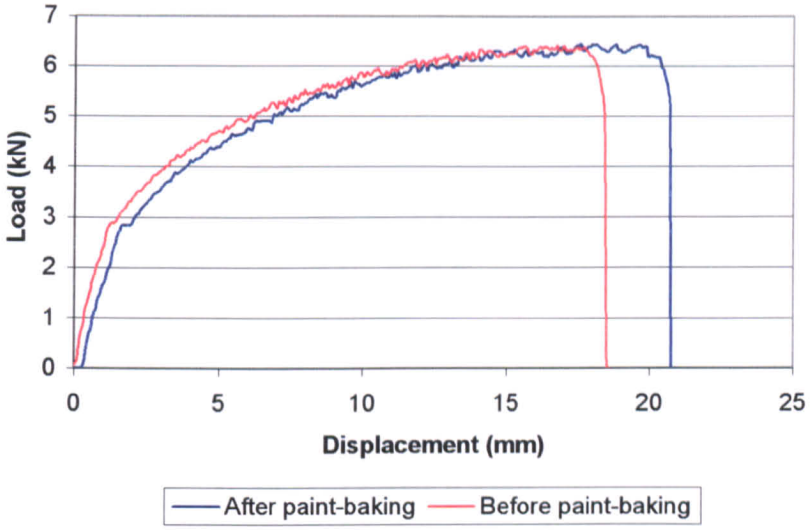

Figure 4.28 Tensile test results for the NG5754 sheet

Table 4-1 Vickers' Hardness test results for the NG5754

NG5754 (H_V)						Average
Before paint-baking	68.8	68.5	68.5	68.5	68.5	68.5
After paint-baking	66.3	65.2	65.2	66.6	66.6	65.9

The effect of paint-baking on the fatigue strength of the FSN53 and FSN53* fastenings is shown in Fig.4.29. The fatigue strength of the FSN53* fastening dropped slightly indicating that the paint-bake cycle led to a reduction in the fatigue strength of the fastening. In addition to the effect of softening of the NG5754 alloy following paint-baking, the removal of the wax-based surface lubricant led to a change of the interfacial condition at the interface between the two riveted sheets and at the interface between the rivet shank and the riveted sheets. The change of the interfacial condition affected the fretting behaviour and therefore contributed to the reduction of the fatigue strength. A detailed analysis will be presented in the next chapter.

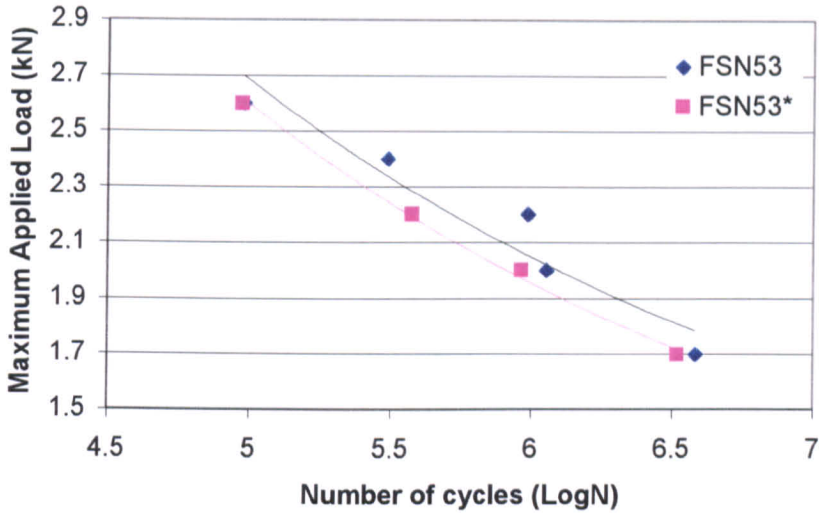

Figure 4.29 Fatigue test results for the FSN53 and the FSN53* fastenings

4.7.2 The FSA6 series

The FSA6 series of fastenings was created for joining AA6111 to NG5754 alloy sheets. In this joint combination, the AA6111 alloy was the pierced sheet and the NG5754 alloy was the locked sheet. During paint-baking, the NG5754 alloy underwent a recovery process, whilst precipitation hardening took place in the case of the AA6111 alloy leading to variations in the material properties for both the pierced and locked sheets. As a result, the paint-baking also had an influence on the FSA6 series of fastenings in addition to the effect of paint-baking on the FSN5 series of fastenings.

Fig.4.30 shows the static test results for the FSA62 and FSA62* fastenings. Similar to the behaviour of the FSN5 series of fastenings, the shear and peel strength of the FSA62 fastenings decreased following paint-baking. The softening of the NG5754 sheet, which facilitated the pull-out of the rivet during shear and peel testing also caused the reduction in the shear and peel strength of the FSA6 series of fastenings. Following the paint-baking treatment, precipitation hardening led to an increase in both the tensile and yield strength of the AA6111 alloy sheet, as shown in Fig.4.31. However, this did not lead to an increase in the shear and peel strength indicating that in this case, the shear and peel strength of the

fastenings were mainly dependent on the behaviour of the locked sheet and the clinch strength. Similar to the shear and peel strength, the pull-out strength of the FSA62* fastening was also lower than that of the FSA62 fastening indicating that the paint-bake cycle led to a reduction in the pull-out strength of the FSA6 series of fastenings. From a cross-section of the FSA6 series of fastenings shown in Fig.3.17 in Chapter Three, it was shown that the rivet shank was in contact mainly with the pierced sheet, which had no lubricant on its surface. After paint-baking, the coefficient of friction at the interface between the rivet shank and the pierced sheet would not change significantly. Therefore the clinch strength before and after paint-baking was expected to show hardly any variation for the two types of condition. The softening of the locked sheet facilitated the rivet being pulled out and contributed to the decrease in the static strength of the FSA62* fastening.

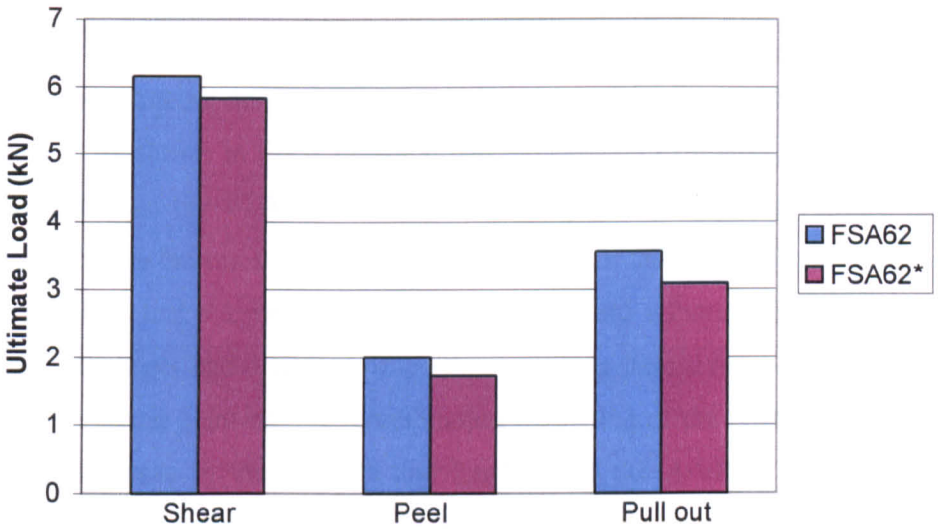

Figure 4.30 Static test results for the FSA62 and the FSA62* fastenings

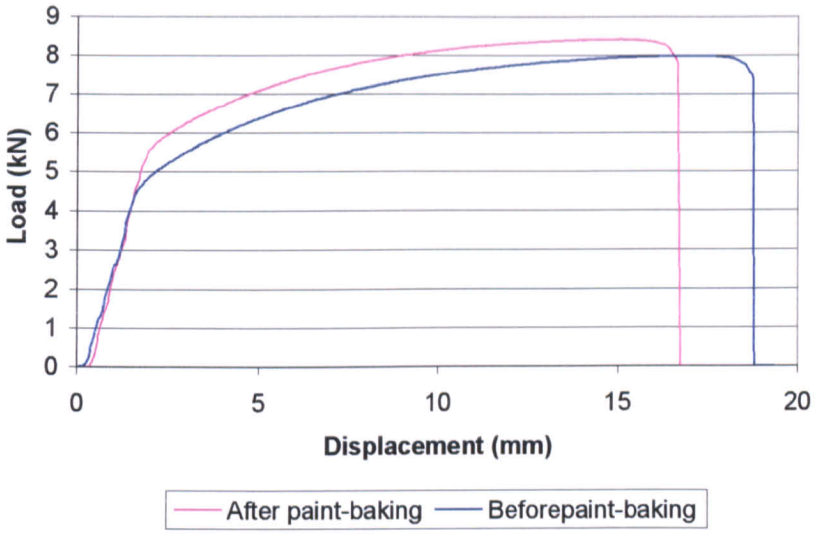

Figure 4.31 Tensile test results for the AA6111 alloy sheet

The effect of paint-baking on the fatigue behaviour of the FSA62 and FSA62* fastenings is not significant. As shown in Fig.4.32, the FSA62* fastening exhibited a marginally higher fatigue strength than the FSA62 fastening indicating that paint-baking might lead to a slight increase in the fatigue strength of the FSA6 series of fastenings. Both the FSA62 and FSA62* fastenings had a 2mm AA6111 pierced sheet and a 2mm NG5754 locked sheet. The two riveted sheets had different properties including hardness as shown in Table 4.1 and Table 4.2. During paint-baking, precipitation hardening of the AA6111 alloy occurred leading to an increase in the strength and hardness of the AA6111 alloy sheet. In the meantime, recovery of the NG5754 alloy sheet took place leading to a decrease in the strength and hardness. As a result, after paint-baking the wear resistance for the AA6111 alloy sheet increased, while it decreased for the NG5754 alloy sheet. The failure that occurred during fatigue testing for the FSA62 and the FSA62* fastenings was mainly dependent on the locked sheet as described in Chapter Three. Therefore it was reasonable to expect that the fatigue strength of the FSA62* fastenings would decreased. Therefore, the marginally higher fatigue strength of the FSA62* fastenings was unexpected. The fewer fatigue data that were collected for the FSA62* fastening and their high scatter could lead to inaccuracies. On the other hand, after paint-baking, the softer the locked sheet and the harder the pierced sheet led to a bigger difference in the hardness between the two

riveted sheets. According to Hogmark et al [44], who had carried out a study experimentally, the wear of the soft martensitic steel (500Hv) was less than that of a harder steel (700Hv) owing to the production of a protective black oxide on the soft material. However, whether wear of the softer locked sheet was less than that of the harder pierced sheet leading to an increase in the fatigue strength of the FSA62* fastening needs to be further investigated.

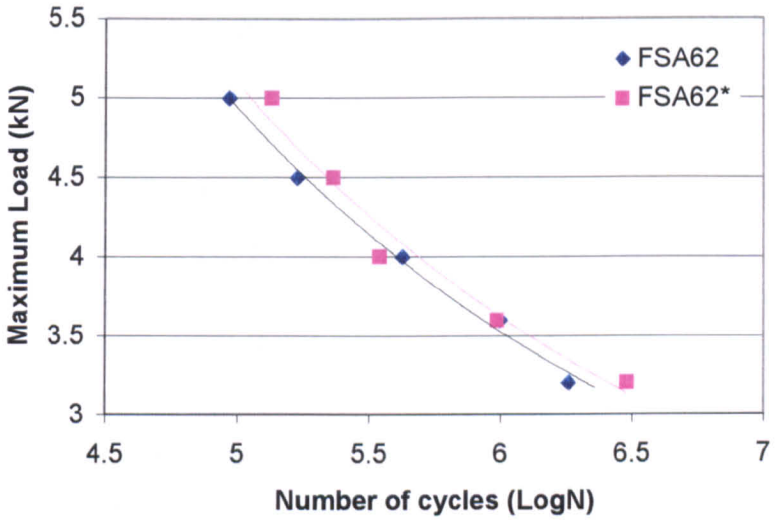

Figure 4.32 Fatigue test results for the FSA62 and the FSA62* fastenings

Table 4-2 Hardness test results for the AA6111 alloy sheet

	AA6111 (H_V)					Average
Before paint-baking	99.7	97.8	99	97.1	98.4	98.4
After paint-baking	102	100	102	105	105	102.8

4.7.3 The FSP5 series

The paint-bake cycle had an effect on the shear strength of the FSP5 series of fastenings, as shown in Fig.4.33. At all pre-straining levels, the shear strength for the FSP5 series of fastenings decreased following paint-baking. In addition, the paint-bake cycle also had an influence on the fatigue strength for the FSP5 series of fastenings, as shown in Figs. 4.34 – 4.37. Similar to the shear strength, at all pre-straining levels the fatigue strength of the FSP5 series of fastenings decreased following paint-baking. However, the amount of reduction in the fatigue strength differed at each pre-straining level. For the FSP50 fastening the fatigue strength decreased marginally following paint-baking, whilst for the FSP510 fastening the fatigue strength reduced significantly after the paint-bake cycle. During paint-baking, the pre-strained alloy sheet was subjected to a recovery process, which reduced the amount of dislocations and led to a reduction in the strength and an increase in elongation and ductility. Fig.4.38 and Fig.4.39 show the variation in strength and elongation of the pre-stained NG5754 sheet before and after paint-baking. Evidently the strength decreased and the elongation increased following paint-baking. At the same time, the hardness decreased, as shown in Fig.4.40. The reduction in the strength and the hardness of the riveted sheet material following paint-baking made the rivet pull out more easily during shear testing and probably speeded up crack initiation and propagation during fatigue testing. This led to the reduction in the shear strength and the fatigue strength of the fastenings. The higher the pre-straining level the greater the reduction in the strength of the sheet material following paint-baking, as shown in Fig.4.38. This contributed to the different amount of reduction in the shear and fatigue strength at each pre-straining level. The burning of the wax-based surface lubricant during paint-baking also contributed to the reduction in the fatigue strength of the fastenings and will be further discussed in Chapter Five.

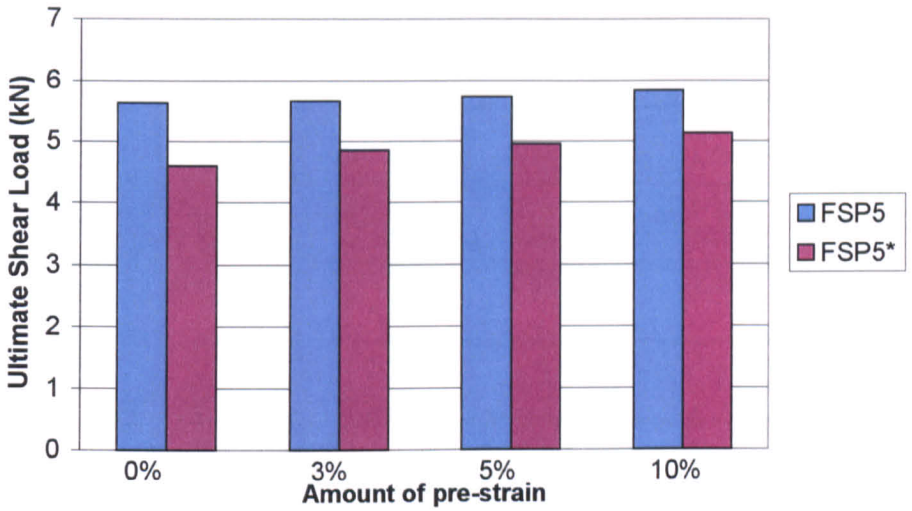

Figure 4.33 Shear test results for the FSP5 and the FSP5* fastenings

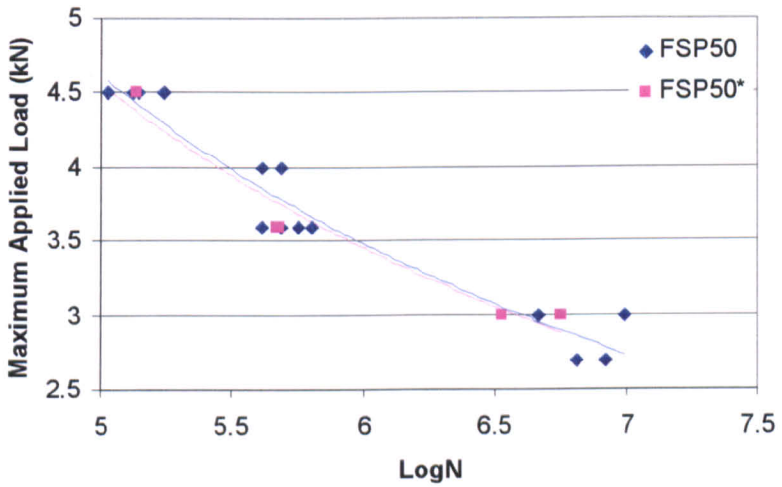

Figure 4.34 Fatigue test results for the FSP50 and the FSP50* fastenings

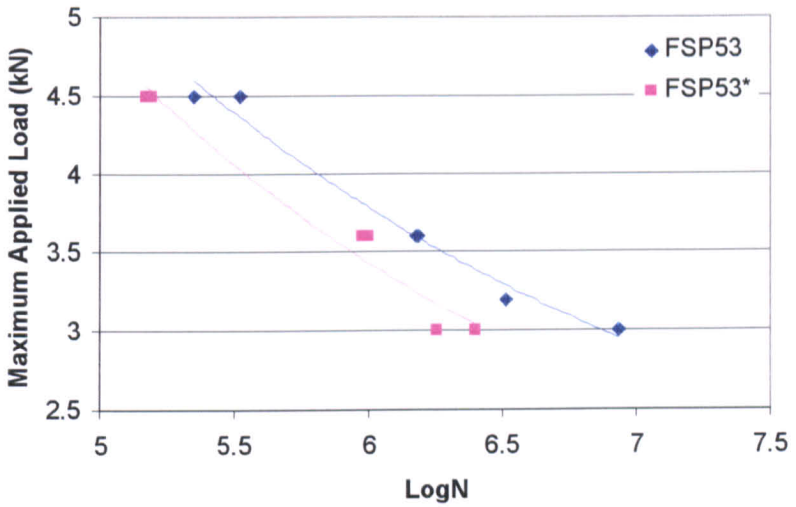

Figure 4.35 Fatigue test results for the FSP53 and the FSP53* fastenings

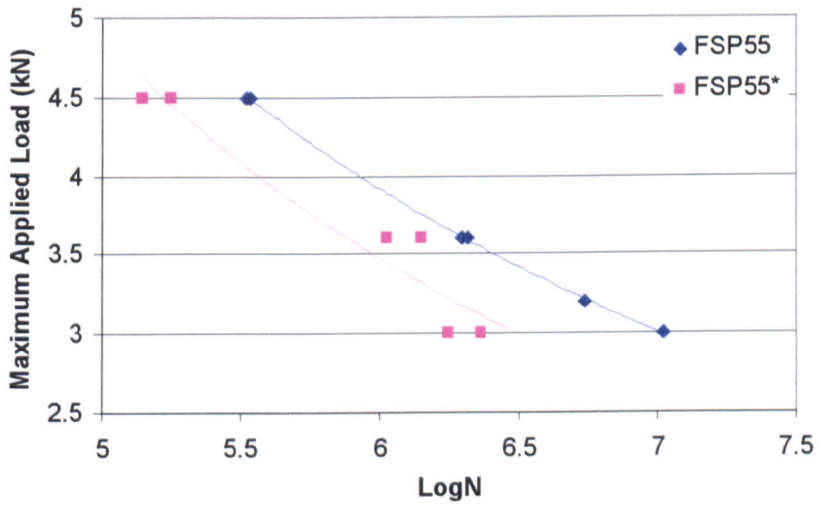

Figure 4.36 Fatigue test results for the FSP55 and the FSP55* fastenings

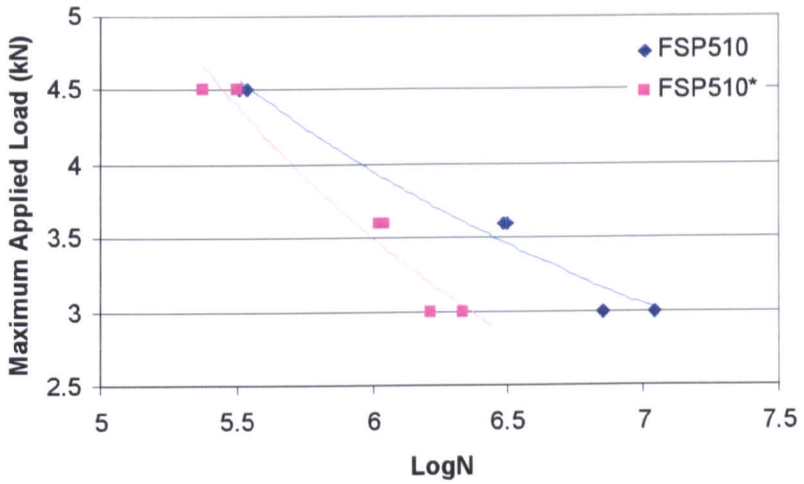

Figure 4.37 Fatigue test results for the FSP510 and the FSP510* fastenings

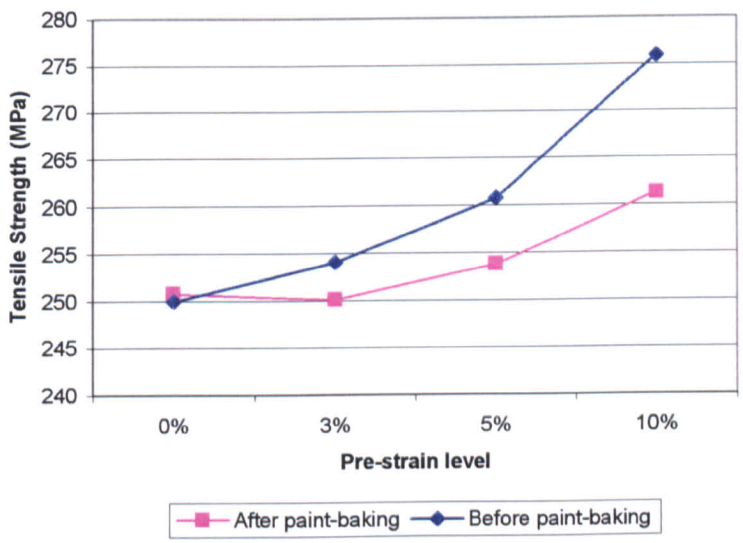

Figure 4.38 Tensile strength for the pre-strained NG5754 sheet material

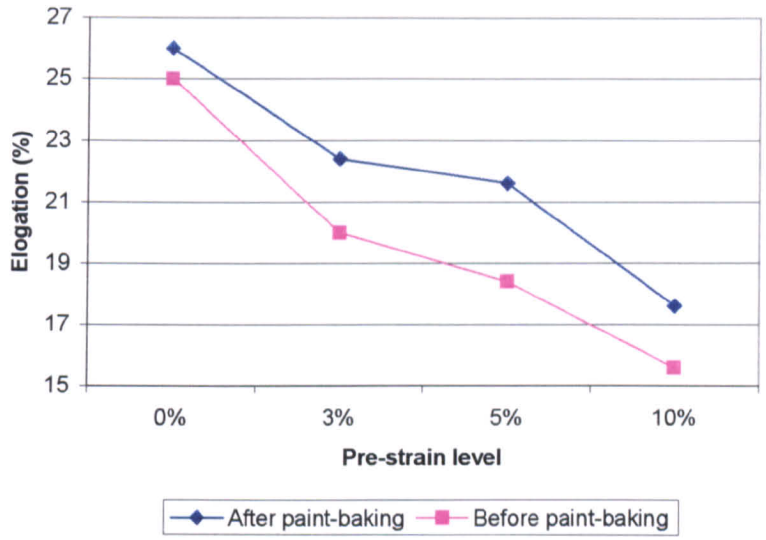

Figure 4.39 Elongation for the pre-strained NG5754 sheet

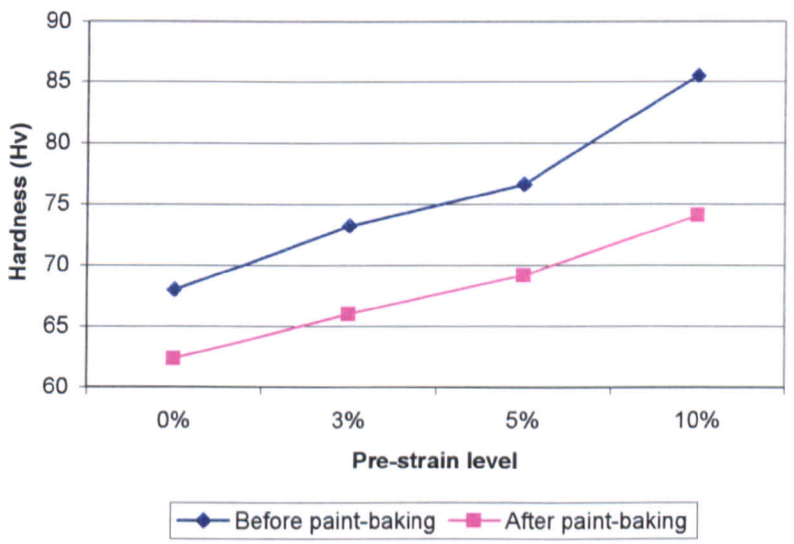

Figure 4.40 Hardness test results for the pre-strained NG5754 sheet

4.8 Influence of Shelf-life

The AA6111 alloy sheets that were used as the pierced sheet for the FSA6 series of fastenings were expected to simulate shelf-life conditions. From a manufacturing point of view, the AA6111 alloy sheet in T4 condition can be used at any time before the self-life expires. However, during storage, heat-treatable aluminium alloys can undergo natural ageing which is accompanied by an increase in the yield strength and hardness of the alloy. There are cases where the property changes of the alloy can be quite significant resulting in poor joint quality and therefore poor joint performance. Therefore it is important to examine whether identical setting parameters can be used to join the AA6111 alloy sheet and maintain a good joint quality that will enable the joint to perform satisfactorily. During this study, the conditions that were used to simulate the shelf-life conditions were not scientifically monitored in a lab setting, but involved time spent in storage at Alcan, the University of Hertfordshire and Textron Fastening Systems as well as time spent in transit. For each batch of samples, the conditions were not consistent with each other and there were also shelf-life variations within each individual batch of samples. Some of the sheet material had most of its shelf-life in storage at Alcan, some at the University laboratory, whilst others at the Textron workshop in Canada. The shelf-life also included time spent in transit. This could lead to inconsistent material properties for the AA6111 alloy. In addition, according to Polmear [1], the NG5754 alloy sheets that were used as the locked sheet for the FSA6 series of fastenings might undergo age softening at ambient temperatures. Over a period of time, the value of tensile properties of the NG5754 might drop due to localised recovery within the deformed grains. The variation in the time spent in storage and in transit probably led to inconsistent age softening conditions. As a result, the tensile properties of the NG5754 alloy might also not be consistent. Therefore, from a scientific point of view, it was difficult to clarify the effect of shelf-life on the joint behaviour accurately due to the inconsistent shelf-life conditions.

The shelf-life of the AA6111 alloy sheet had little effect on the fastening behaviour, as shown in Chapter Three. The static test results for the FSA6 series of fastenings with a (2mm+2mm) thickness combination following paint-baking are shown in Fig.4.41. The marginally higher shear strength of the FSA61* fastening, compared with the FSA62* and FSA63* fastenings could be due to the slightly higher tensile strength of the AA6111 sheet

after a 5-month shelf-life, as shown in Fig.4.42. However, the variation in the shear, pull-out and peel strength was not consistent and it was difficult to explain. The static strength of the fastenings was supposed to rely on the sheet material properties and the clinch strength. Therefore, the inconsistent variation in the static strength of the fastenings could be due to a number of possible reasons. One reason could be due to the variation of age softening of the 2mm NG5754 lower sheet since the age softening of the NG5754 sheet led to a reduction in the tensile strength and consequently affected the shear, peel and pull-out strength of the fastenings. In addition, the FSA61*, FSA62* and FSA63* fastenings were paint-baked at different times and the variation in each paint-baking process could lead to a variation in softening of the NG5754 sheet since recovery occurred during the paint-bake cycle. Another reason could be due to the variation in the mechanical properties of the AA6111 alloy sheet since the 2mm-thick AA6111 sheet spent its shelf-life under different conditions. This could lead to inconsistent mechanical properties of the sheet material and therefore contributed to the inconsistent variation in the static strength of the fastenings.

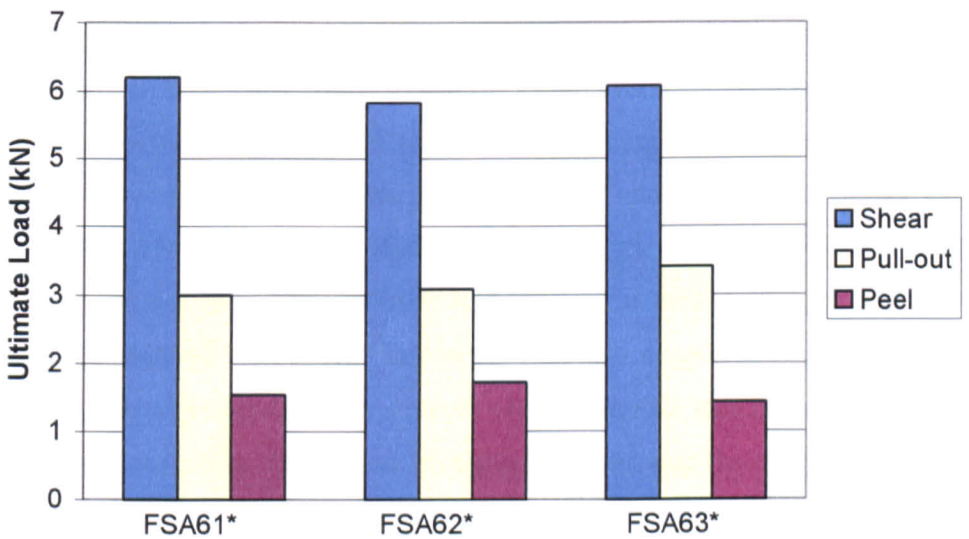

Figure 4.41 Static test results for the FSA61*, FSA62* and FSA63* fastenings

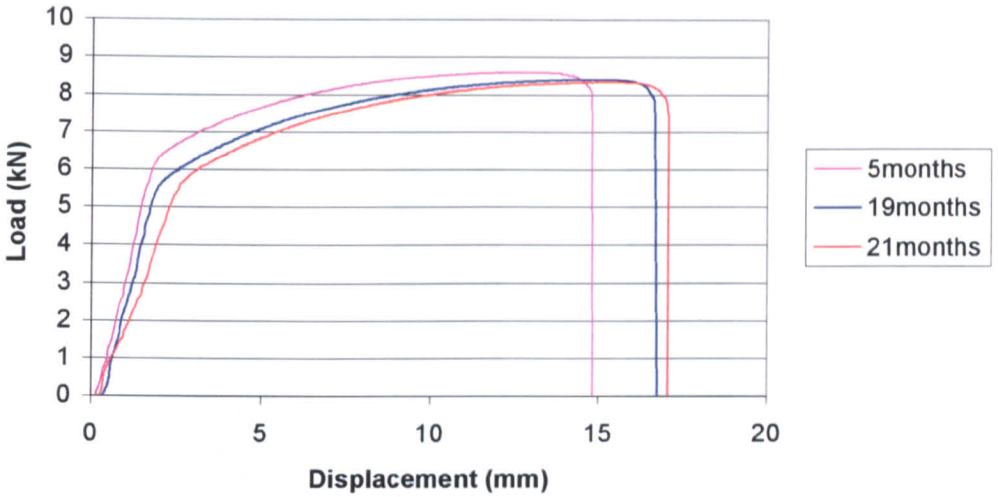

Figure 4.42 Tensile test results for 2mm AA6111 sheet after paint-baking

The effect of shelf-life on the fastening behaviour also can be seen from the experimental results for the FSA6 series of fastenings with a (0.9mm+2mm) thickness combination. Fig.4.43 shows all the static test results for these fastenings. The FSA64* fastening exhibited the highest shear strength of the three fastenings, whilst the peel and pull-out strength for the three fastenings were almost the same. The sheet material that was used for the FSA64* fastening had a 3-month shelf-life and exhibited the highest tensile strength compared with the sheet materials used for the FSA65* and FSA66* fastenings, as shown in Fig.4.44. This contributed to the highest shear strength of the FSA64* fastening. The sheet material with a 10-month shelf-life had the lowest tensile strength and led to the lowest shear strength of the FSA66* fastening. This also suggested that the pierced sheet material properties affected the shear strength of the fastening that had an identical locked sheet. The low variation in the pull-out strength indicated that the different properties for the AA6111 upper sheet did not affect the setting process significantly and therefore the clinch strength for the three fastenings was about the same. The failure mode that occurred for the three fastenings during peel testing indicated that the peel strength of the fastening was dominated by the fracture of the thinner AA6111 sheet. However, the low value of the peel strength and the variation in the material properties made it difficult to explain the effect of shelf-life on the peel strength.

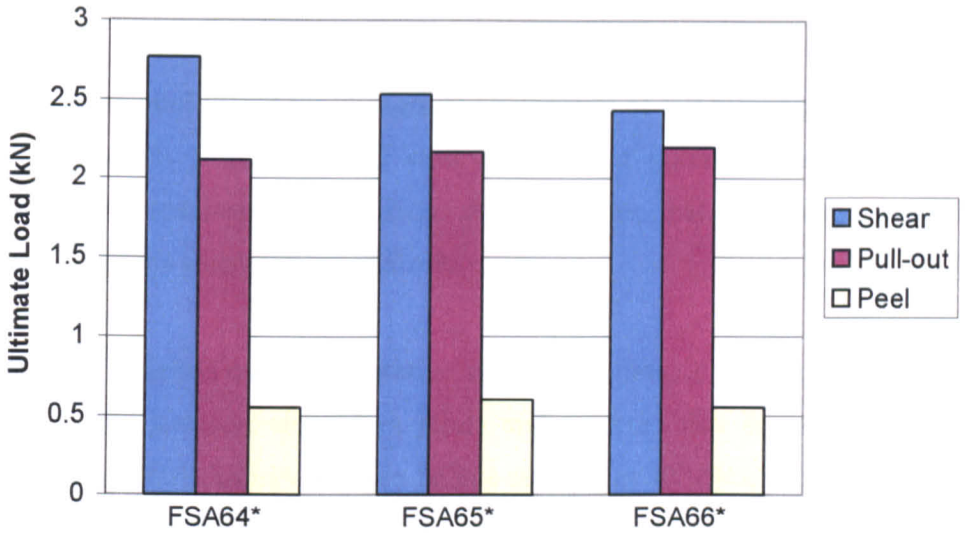

Figure 4.43 Static test results for the FSA64*, FSA65* and FSA66* fastenings

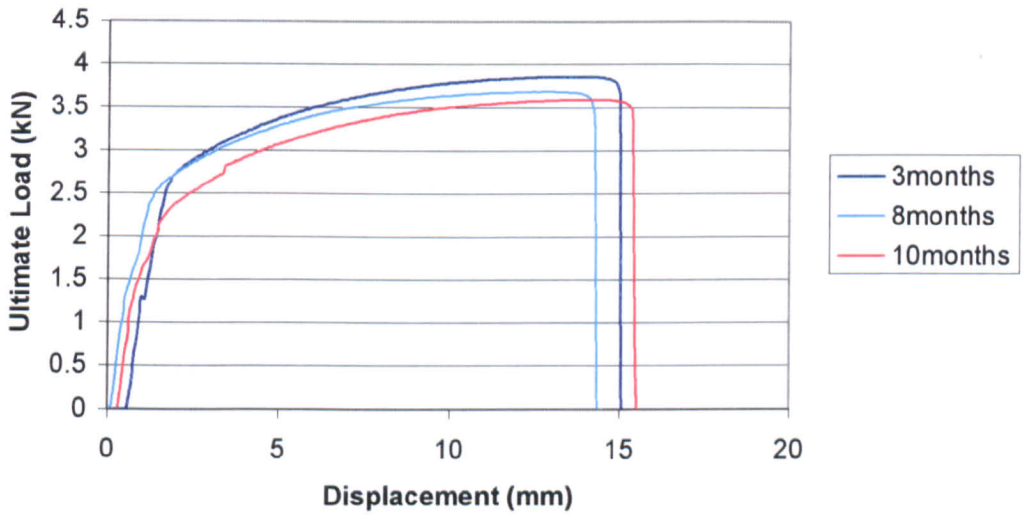

Figure 4.44 Tensile test results for 0.9mm AA6111 sheet after paint-baking

The effect of shelf-life on the fatigue behaviour of the fastenings was difficult to identify due to the small number of tests that were carried out and the wide scatter of the data, in addition to the influence of the inconsistent shelf-life and age softening conditions.

4.9 Comparison between this study and literature

In order to further understand the strength characteristics of self-piercing riveted joints, the experimental results were compared with the relevant published data. However, the diversity of test specimens and testing methodologies that were used by different researchers has made a comparison difficult.

Krause et al [27] carried out a comparative study of the fatigue behaviour of spot-welded and mechanically fastened aluminium joints and reported that the self-piercing rivets offered the joints 100% improvement in fatigue strength at 10^6 cycles compared with spot-welds. The joints were therefore supposed to be optimised and it was worth comparing with the data obtained from the FSN51 fastenings by the current experimental work. In the study by Krause et al. [27], two 5754-O aluminium alloy sheets in 2mm-thickness and 25mm width with an overlap of 20mm were joined by a steel rivet. The 5754-O alloy was also supplied by Alcan International Limited. Although the NG5754 alloy that was used in the current project was an updated type of the 5754-O alloy, the mechanical properties of the two types of 5754 alloy did not differ significantly. The tensile strength of the NG5754 was about 250MPa, while 220MPa was reported for the 5754-O. The steel rivets were manufactured by the Henrob Corporation, who also produced all the self-piercing riveted samples for the study by Krause et al. [27]. The rivets had a 6mm diameter and the shank length, although not given, was unlikely to be shorter than 7mm. The shear test for both projects was carried out at a 10mm/min speed. The fatigue test for the study by Krause et al. [27] was performed at a test frequency that varied from 0.5 to 20Hz depending on the magnitude of the applied load. The different setting parameters and test conditions between the two projects are listed in Table 4.3.

Table 4-3 Different setting parameters and test conditions

Project	Sheet (2mm)	Rivet (mm)	Setting pressure (bar)	Anvil	Test frequency (Hz)
Krause et al	5754-O	∅6 × ≥7	Unknown	Unknown	0.5-20
UH	NG5754	∅4.8 × 7	240	64015	20

Note: UH represents the University of Hertfordshire, where the current project has been carried out.

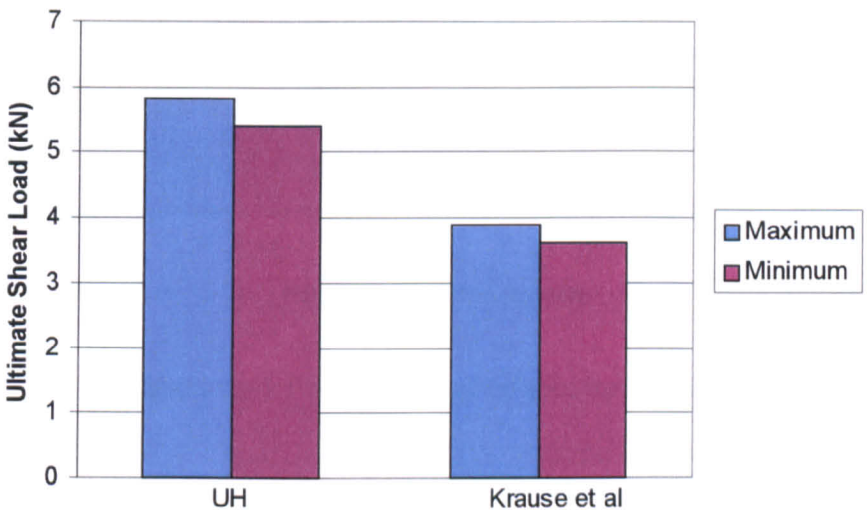

Figure 4.45 Comparison of shear test results

Fig.4.45 shows a comparison of the shear test results obtained by the two studies. The ultimate shear load obtained from the current project was higher than that obtained by Krause et al. [27] indicating the effect of setting parameters. According to King [22], the use by Krause et al. [27] of a bigger diameter and a longer rivet shank of the rivet should have provided the joint with a higher ultimate shear load. However, the slightly lower strength of the riveted sheet and the unknown anvil profile as well as the smaller samples that were used by Krause et al. [27] probably contributed to the lower ultimate shear load.

A comparison of the fatigue data from the two projects is shown in Fig.4.46. The fatigue endurance for the FSN51 fastening in the current project was longer at an identical applied load compared with the samples tested by Krause et al. [27]. The slightly lower sheet

material strength and the different anvil profile as well as the narrower specimen size, contributed to the lower fatigue endurance for the samples that were tested by Krause et al. [27]. The different frequency that was used by the two studies was probably another reason for the observed variation in the fatigue strength.

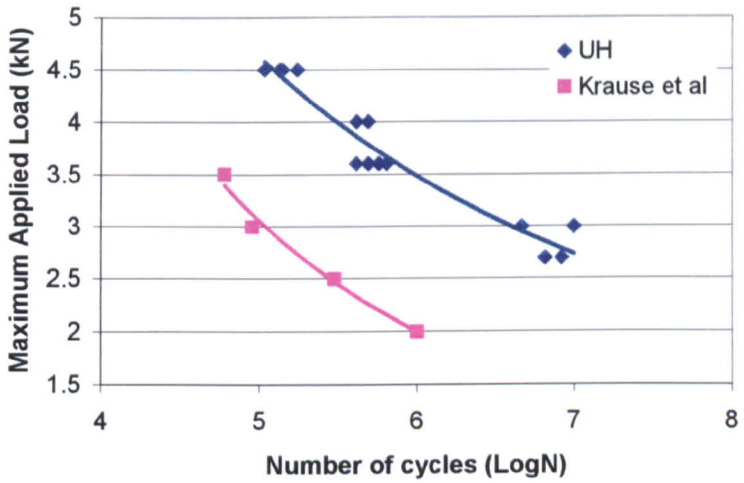

Figure 4.46 Comparison of fatigue test results

Similar comparison was also made between the FSN51 fastening from the current project and the data published by Booth et al [28], who joined two 5754 aluminium alloy sheets of 2mm gauge by using a steel rivet of a 5.3mm diameter and a 7.0mm length. The rivets used by Booth et al. [28] were bigger than the rivets used by the current project in both diameter and length. The setting pressure used by Booth et al. [28] was 275bar compared to 240bar used by the current project. The anvil profile differed for the two projects. A comparison of the shear test results for the two projects is shown in Fig.4.47. The ultimate shear load for the current project was higher than that obtained by Booth et al. [28] indicating the effect of setting parameters.

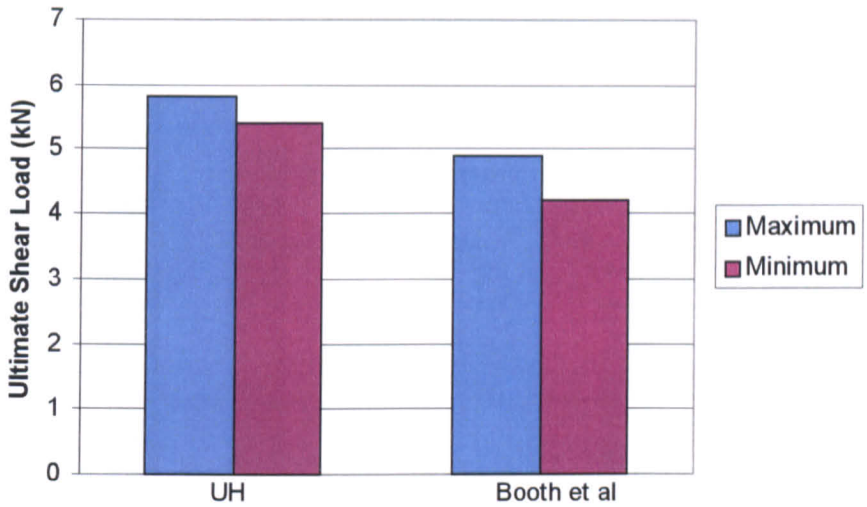

Figure 4.47 Comparison of shear test results

A study that was similar to the current project has been carried out by Fu and Mallick [29] at the University of Michigan (UM). In the UM study, two 5754-O alloy sheets in 2mm gauge and 25.4mm width were joined by a steel rivet using a slightly lower setting force compared with the current project. The anvil profile also differed from that of the current project. A comparison of the ultimate shear load and the fatigue endurance together with the thickness combination and rivet parameters are shown in Fig.4.48 and Fig.4.49 respectively. Both the ultimate shear load and the fatigue endurance for the UM study were lower than those for the current project. At an identical applied load, the fatigue endurance of the samples having rivets with a 3.9mm diameter and a 6.0mm length in the current project was even higher than that of the samples having rivets with a 5mm diameter and a 6.5mm length in the UM study. This indicated the effect of the specimen size on the shear and fatigue strength of the joints. The best performance of self-piercing riveted joints is dependent on the combination of all the setting parameters.

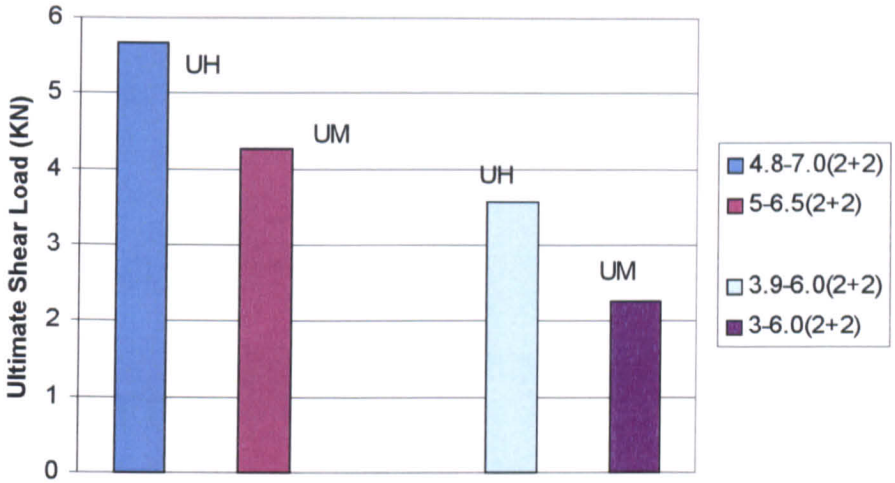

Figure 4.48 Comparison of shear test results

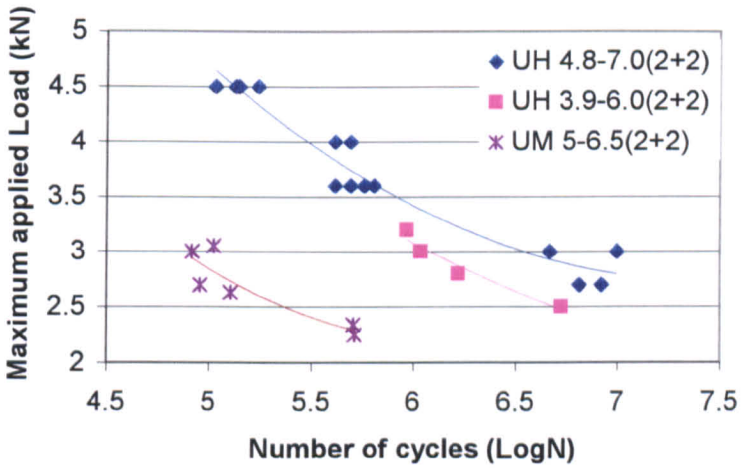

Figure 4.49 Comparison of fatigue test results

CHAPTER FIVE

5. FAILURE MECHANISMS

5.1 Failure Modes

Three distinct failure modes, defined as *rivet pull-out, rivet fracture* and *sheet material failure* were observed to occur in static and fatigue tests, as described in Chapter Three. *Rivet pull-out* refers to fastening failure that is due to the rivet being pulled out. *Rivet fracture* refers to fastening failure that is due to the fracture of the rivet. *Sheet material failure* refers to fracture of the sheet material leading to eventual sample failure. The examination of the failure mode that occurred during shear, peel, pull-out and fatigue testing identified the main influential factors on the joint strength characteristics.

5.1.1 Failure Mode in Shear Tests

In shear tests, all samples failed by the rivet being pulled out of the locked sheet, while deformation of the two riveted sheets had also taken place, as shown in Figs.3.8, 3.15 and 3.27. *Rivet pull-out* was the only failure mechanism for the shear test and this was related

to the load transfer mechanism of the fastening. According to Kulak et al [34], when a conventional riveted lap joint was subjected to a shear load, the shear load was mainly transferred by the rivet and the sheet material by means of shear and bearing after overall slip of the joint took place. For a self-piercing riveted lap joint, shearing of the rivet and bearing of the riveted sheets are also expected to occur during the shear test. In addition, for the rivet with a countersunk head, tilting of the rivet also took place during shear testing. As illustrated in Fig.5.1, when a shear force S was applied, two components, S_1 and S_2, were created and formed a couple acting on the rivet. As a result, the rivet tended to tilt up by overcoming the frictional force between the rivet and the two riveted sheets. In the meantime, secondary bending also tended to pull out the rivet, as shown in Fig.1.2. Therefore, for a self-piercing riveted lap joint, during shear testing, both the pierced and the locked sheets were in bearing against the rivet, while the rivet was subjected to a shear and a pull-out force due to tilting and the effect of secondary bending. The bearing force was initially concentrated on the contact point between the riveted sheet and the rivet. As the loading process proceeded, the riveted sheets suffered localised yielding leading to a large contact area between the riveted sheet and the rivet. A more uniform bearing stress therefore acted on the riveted sheet material adjacent to the rivet leading to more deformation of the sheet material. In the mean time, the shear and pull-out forces acting on the rivet also increased. The shear force was not sufficient to fracture the rivet, whilst the increase in the pull-out force enabled the rivet to overcome the frictional force at the interface between the rivet shank and the riveted sheets. Failure therefore occurred by the rivet being pulled out with some deformation of the riveted sheets. Figs.3.8 (a) and (b) clearly show that the sample failed by rivet pull-out with localised yielding and deformation on both the locked and the pierced sheets. The 1mm thick pierced sheet suffered more deformation than the 2mm-thick pierced sheet since the bearing resistance of the 1mm thick sheet, as obtained from equation 4-2, was smaller. More deformation was experienced by the FSN56 fastening than the FSN51 fastening, as shown in Fig.4.3. The reason for this was the fact that the FSN56 fastening had a shorter end-distance (or half of the overlap length) than the FSN51 fastening. The actual failure mode in shearing indicated that the yield strength and the bearing resistance of the sheet material as well as the clinch strength affected the shear strength of the fastening.

In addition, the side of the rivet head that had not been subjected to the shear component S_1 also fractured for most of the fastenings with a (2mm+2mm) thickness combination, as shown in Fig.3.8 (c). This was because the rivet had a rotating tendency and this side probably sustained most of the load as it pressed against the pierced sheet. Fracture of the rivet head therefore occurred.

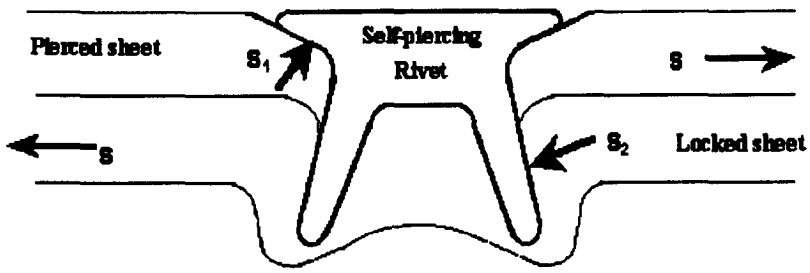

Figure 5.1 Loading process of shear test

It should be noted here that the failure mode for a self-piercing riveted joint during shear testing was different from that for a conventional riveted joint. Iyer et al [45] reported that in a conventional riveted joint with a countersunk head rivet, rivet tilting also occurred. However, the tilting could not lead to rivet pull-out due to the existence of the forged button on the bottom sheet. Instead of pull-out, a tensile stress was introduced to the rivet. The rivet was therefore under both shear and tension. As a result, during shear testing rivet fracture was the most common failure system for a conventional riveted joint, compared to rivet pull-out for a self-piercing riveted joint.

5.1.2 Failure Modes in Peel Tests

Failure during peel testing occurred by either *rivet pull-out* or *sheet material failure*. The fastenings with a (2mm+2mm) thickness combination failed by rivet pull-out. The fastenings with a (1mm+2mm)/(0.9mm+2mm) thickness combination failed by fracture of the thinner sheet. During the peel test process, bending and peeling of the sheet material around the rivet head were observed. The bending stress was inversely proportional to the square of the sheet thickness, as shown in equation 4-3. Therefore under an identical bending moment, the bending stress acting on the thinner sheet was much higher than that on the thicker sheet. As a result, the peel samples with a (1mm+2mm)/(0.9mm+2mm)

thickness combination produced considerable distortion in the thinner sheet. The thinner sheet peeled off the rivet head and failed to transfer the peel load to the clinch leading to final failure of the fastening by *sheet material failure*, as shown in Fig.3.9 (b). This result suggested that for the (1mm+2mm)/(0.9mm+2mm) sheet combination, the thinner sheet acted as a stress concentrator and the joint itself could withstand a higher peel load than the 1mm/0.9mm sheet. For the fastenings of (2mm+2mm) combination, the pierced sheet transferred the peel load to the clinch while the pierced sheet underwent deformation, as shown in Fig.3.9 (a). Peeling then concentrated on the clinch button and caused the flared rivet shank to eventually be pulled out of the locked sheet. Thus *rivet pull-out* occurred for this combination. Therefore, in the case of the peel test, the determining factor that controlled the failure mode was the pierced sheet thickness.

5.1.3 Failure Mode in Pull-out Tests

The pull-out test was specially designed for measuring the clinch strength of the fastenings. Samples being tested by the pull-out test failed by means of rivet pull-out. Therefore *rivet pull-out* was the only system of failure in the pull-out test for all fastenings of both thickness combinations. In the case of the (1mm+2mm)/(0.9mm+2mm) combination, the thinner pierced sheet suffered more distortion than the thicker component, as shown in Fig.3.10. It was concluded that for the pull-out test, the behaviour was mainly dependent on the rivet retention and the flare into the material.

5.1.4 Failure Modes in Fatigue Tests

Rivet fracture and *sheet material failure* occurred in fatigue testing. The fastenings with a (2mm+2mm) thickness combination failed by *rivet fracture* or *sheet material failure* depending on the magnitude of the applied load, whilst only *sheet material failure* occurred for the fastenings with a (1mm+2mm)/(0.9mm+2mm) thickness combination. For the fastenings with a 1mm/0.9mm thick pierced sheet, the thinner pierced sheet suffered more distortion than the thicker one and this eventually led to failure. The thinner sheet fractured near the rivet head but the rivet remained undamaged still connecting the two sheets together, as shown in Fig.3.11 (a). This suggested that the clinch strength was sufficiently

high and therefore the fatigue endurance for the fastenings with a (1mm+2mm)/(0.9mm+2mm) combination was determined by the thinner sheet material. For all the fastenings with a (2mm+2mm) thickness combination, at high applied loads, rivet fracture and pull-out dominated the failure mode and fracture of the riveted sheet was also observed. At low applied loads, locked sheet fracture dominated the failure of the fastenings, as shown in Fig.3.11 (b), (c). The results indicated that the rivet and the sheet material properties as well as the clinch strength had an influence on the fatigue strength of the fastenings. All samples that were fatigue tested formed visible black-coloured fretting scars at the interface between the two riveted sheets. This observation indicated that the failure mode in fatigue testing might also depend on the fretting behaviour and therefore further investigation of the fatigue failure mechanisms was carried out.

5.2 Fatigue Failure Mechanisms

5.2.1 Occurrence of Fretting

Examination of the interface between the two riveted sheets and the interface between the rivet shank and the locked sheet of a fastening that was subjected to fatigue testing revealed the presence of fretting. A cross-section of a self-piercing riveted joint in Fig.5.2 clearly shows the positions where fretting was observed. As shown in Figs.3.11 (b) and (c), black-coloured fretting scars formed at the interface between the two riveted sheets. Fretting, at position A in Fig. 5.2 took place as a result of repeated loading, which led to a relative movement at the contacting surface between the two riveted sheets. At position B, secondary bending and rivet tilting acted as oscillatory sources and caused fretting at the point of contact between the rivet shank and the locked sheet. Fig.5.3 shows fretting scars that formed at the surface of the rivet shank and at the surface of the locked sheet, which was in contact with the rivet shank after 10,552,000 cycles at a maximum applied load of 2.7kN. Under the effect of secondary bending and tilting of the rivet, the rivet head on the right-hand side of the joint (Refer to Fig.2.5) pressed its head against the pierced sheet leading to fretting at position C, the interface between the edge of the rivet head and the pierced sheet, as shown in Fig.5.4.

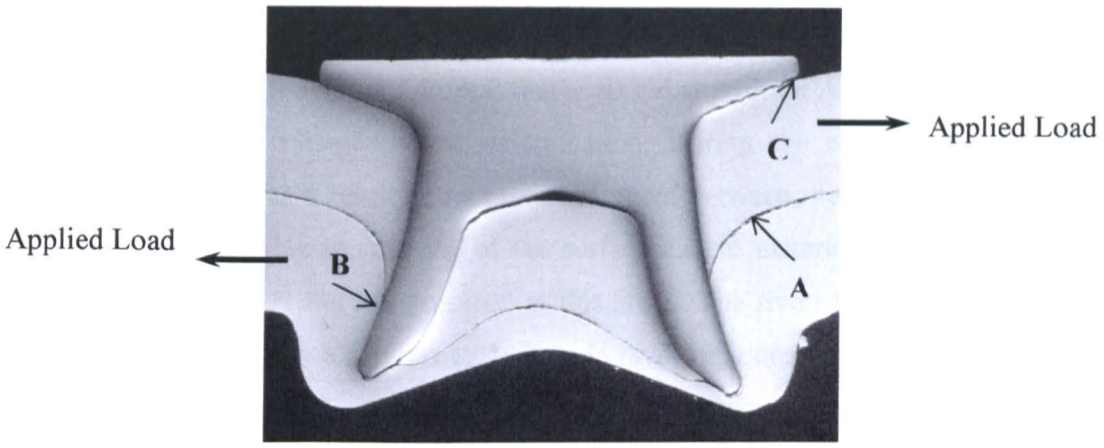

Figure 5.2 The three positions where fretting occurred

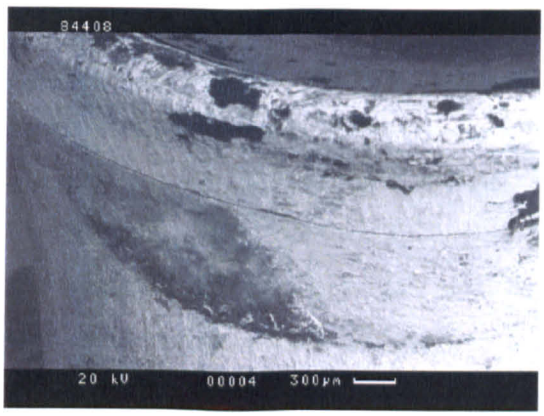

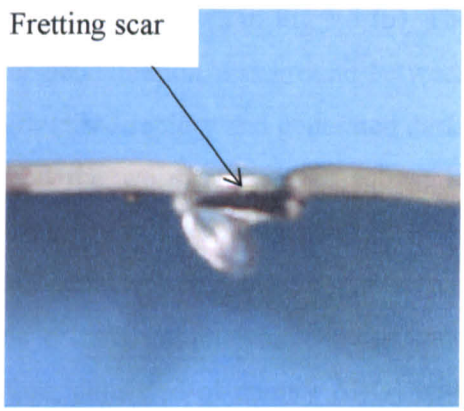

Figure 5.3 Fretting scar formed at: (a) the surface of the rivet shank, (b) the surface of the locked sheet

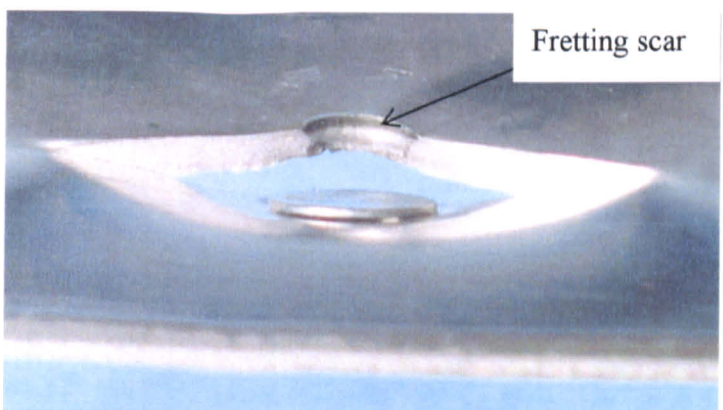

Figure 5.4 Fretting scar formed at the pierced sheet in contact with the edge of rivet head

5.2.2 Fretting Mechanisms

The investigation of the fretting process that occurred at position A and position B revealed the involvement of ploughing and delamination. During the early stages of fretting, ploughing occurred as a result of relative movement between the two riveted sheets and this led to considerable roughening of the surface and to material transfer, as shown in Fig.5.5 (a). Two-body fretting occurred at this stage. The riveted aluminium alloy sheet was initially covered by a thin protective oxide layer in addition to the surface lubricant. After wearing off the surface lubricant, the ploughing process dispersed the oxide layer and promoted further contact leading to acceleration in the amount of surface damage. The debris was trapped on the fretted surface and acted as an abrasive leading to third-body fretting. As the fretting process proceeded, material was removed from the surface by a delamination process producing plate-like particles of debris, as shown in Fig.5.5 (b). The material transferred or removed by either ploughing or delamination was ground between the two contact surfaces to form finer particles, which oxidised rapidly and generated dark-coloured fretting debris that could be seen clearly on the worn surface, as shown in Figs.3.11 (b) and (c). The accumulated debris on the fretting surface was detected by SEM and is shown in Fig.5.5 (c). EDS analysis of the debris is presented in Fig.5.6 and shows high levels of aluminium and oxygen and low levels of magnesium which is the main alloying element in the 5754 alloy. The debris therefore, consisted of mainly Al_2O_3 with small amounts of MgO. This confirmed that the oxidation process had taken place during fretting.

(a)

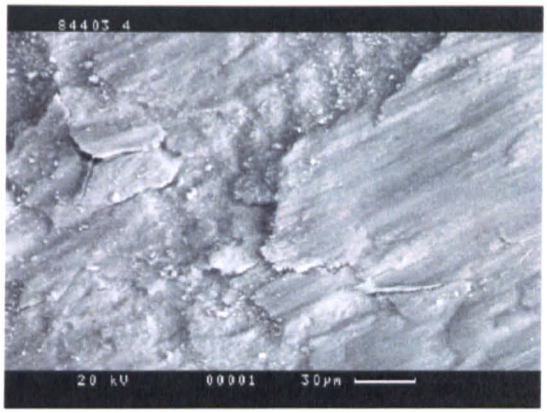

(b)

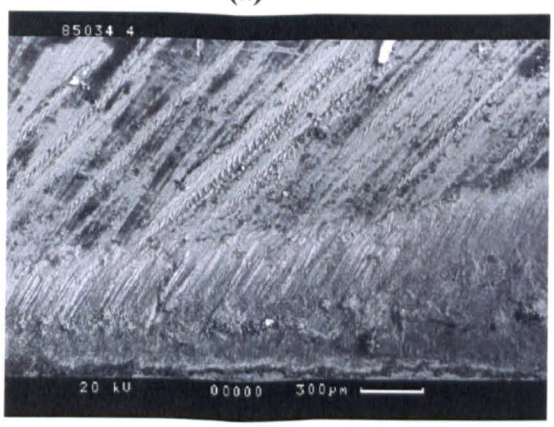

(c)

Figure 5.5 (a) ploughing occurred at a locked sheet after 2.1×10^5 cycles at 4.5kN, (b) delamination occurred at a locked sheet after 173,200 cycles at 4.5kN, (c) accumulated debris at a locked sheet after 173,200 cycles at 4.5kN

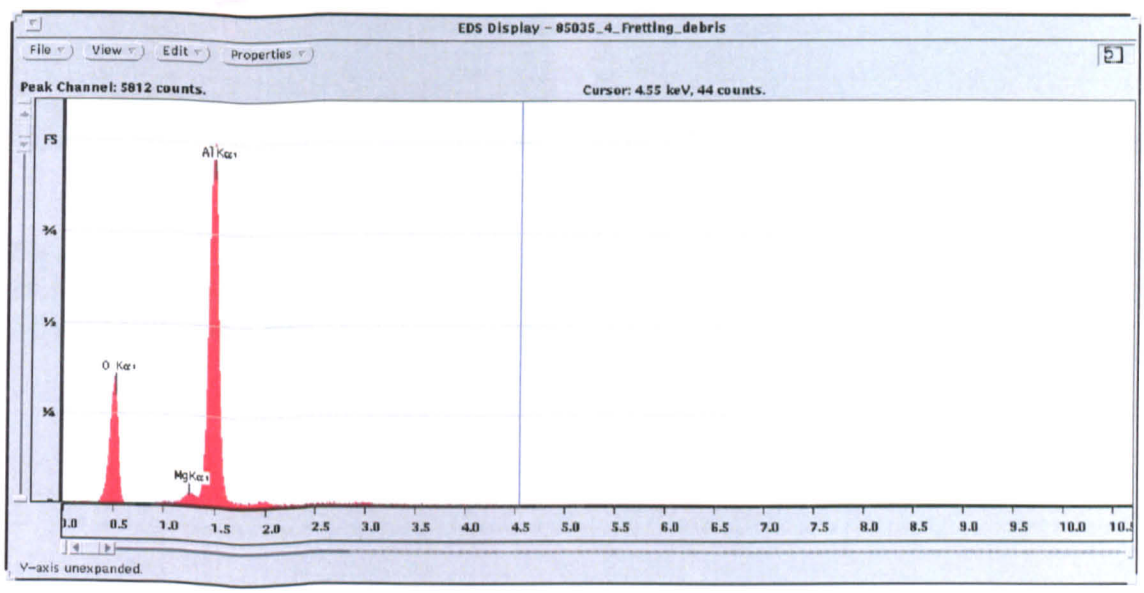

Figure 5.6 EDS spectrum of the accumulated debris at the riveted sheet

Fig.5.7 (a) shows the fretted surface of the rivet shank. It was apparent that the delamination process also took place at the surface of the rivet shank as a result of fretting at the interface between the rivet shank and the riveted sheet. Debris that accumulated at the end of the rivet shank was also observed under SEM, as shown in Fig.5.7 (b). A spectrum from EDS analysis of the debris is presented in Fig.5.8 revealing the presence of aluminium, magnesium, oxygen, carbon, iron, zinc and tin. The presence of iron in the debris suggested that the steel rivet had suffered from fretting damage following damage of the rivet coating that consisted of zinc and tin. The involvement of a high volume of carbon indicated that the wax-based surface lubricant was worn off in the initial stages. In addition to the rivet shank, the riveted alloy sheet that was in contact with the rivet shank also suffered from fretting damage indicated by the involvement of aluminium and magnesium. The high levels of oxygen in the EDS analysis suggested that oxidation of the worn metal also took place during the fretting process.

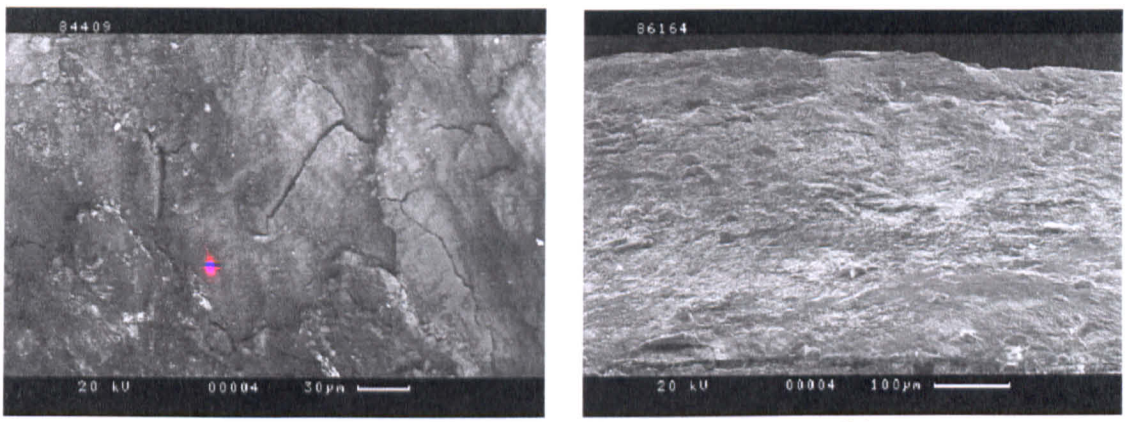

(a) **(b)**

Figure 5.7 (a) delamination and associated fatigue cracks at the rivet shank after 10,552,000 cycles at 2.7kN, (b) accumulated fretting debris at the rivet shank after 139,200 cycles at 4.5kN

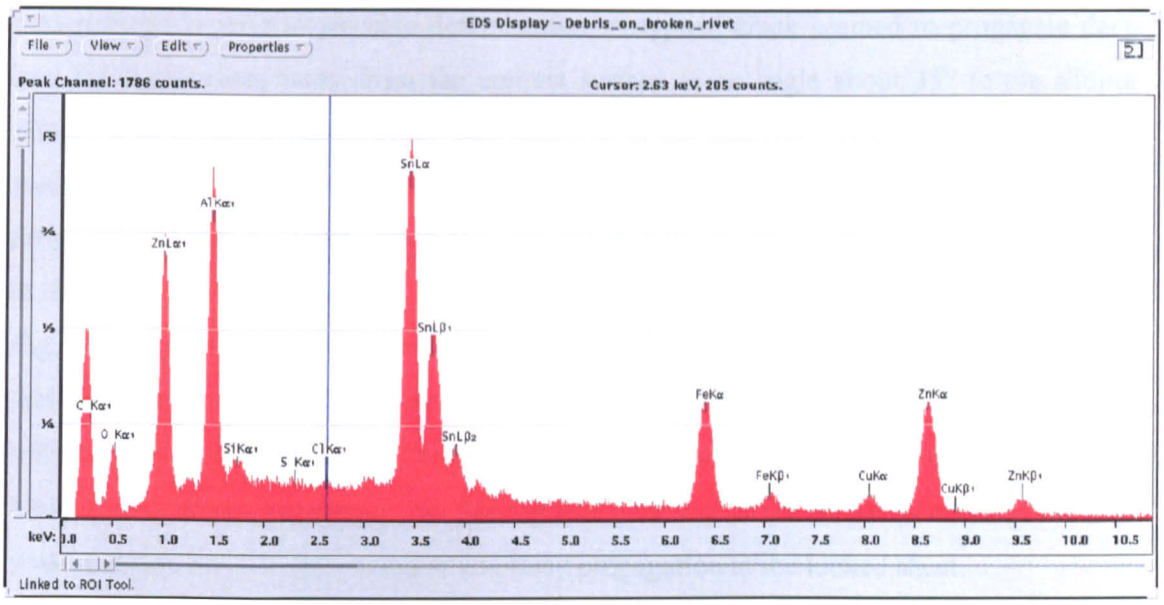

Figure 5.8 EDS spectrum of the debris at the rivet shank

5.2.3 Fretting Damage

5.2.3.1 Crack Initiation and Propagation

Visible cracks generated from the buttonhole at the 3 and 9 o'clock positions in relation to the loading direction on the locked sheet can be seen in Figs.3.11, 3.28 and 3.34. In addition, all cracks that initiated and propagated on the sheet material were observed to be located at the interface between the two riveted sheets or at the interface between the locked sheet and the rivet shank where fretting had taken place.

The micrograph of a locked sheet that failed after 489,300 cycles at a maximum load of 3.6kN is presented in Fig.5.9 (a). Evidently the rivet has fractured and cracks that formed at the buttonhole at the 3 and 9 o'clock positions in relation to the loading direction are visible. A section in the vertical direction of this sample was taken and presented in Fig.5.9 (b) which shows the surface of the locked sheet that was initially in contact with the shank of the rivet at the position designated as B in Fig.5.2. Fig.5.9 (b) also shows lots of small cracks that initiated on the fretting worn surface of the locked sheet. All cracks were generated and propagated oblique to the sliding direction. Most of the cracks propagated to

closed loops leading to possible delamination. A typical crack seemed to propagate deep into the metal sheet away from the contact surface at an angle about 35° to the sliding direction. It appeared that fretting, that occurred at the interface between the shank of the rivet and the locked sheet, resulted in the initiation and propagation of cracks. In addition, fatigue cracks due to fretting were also generated at the contact surface of the locked sheet at the point of contact with the pierced sheet, that is position A, in Fig.5.2. As shown in Fig.5.10, a crack formed and propagated into the locked sheet after 89,000 cycles, which was equivalent to 65% of the average fatigue life at a maximum load of 4.5 kN. The crack initiated about 35° oblique to the sliding direction and propagated to a depth of about 120μm. The results suggested that fretting that occurred at the interface between the two riveted sheets led to crack initiation and early propagation at the locked sheet.

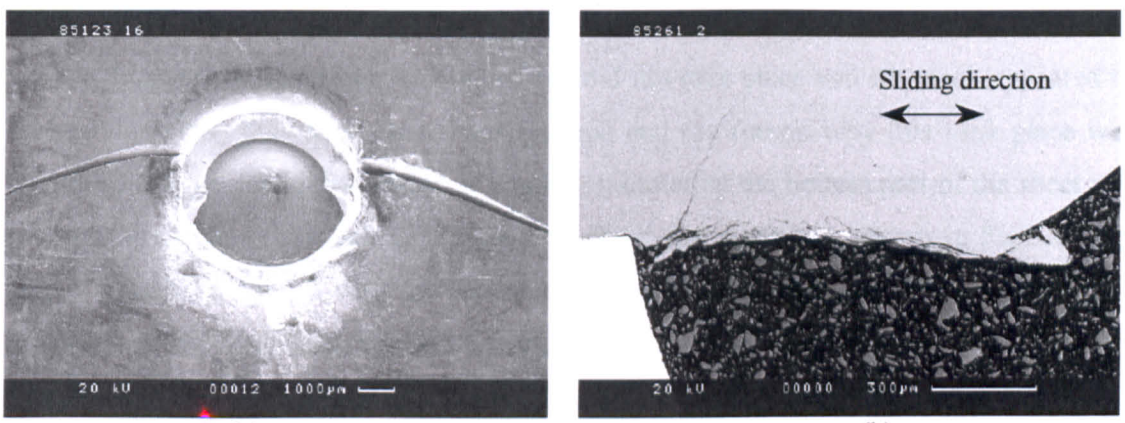

(a) (b)

Figure 5.9 (a) the locked sheet after 489,300 cycles at a peak load of 3.6kN with a part of broken rivet; (b) small cracks that initiated at the surface of the locked sheet in contact with the rivet shank

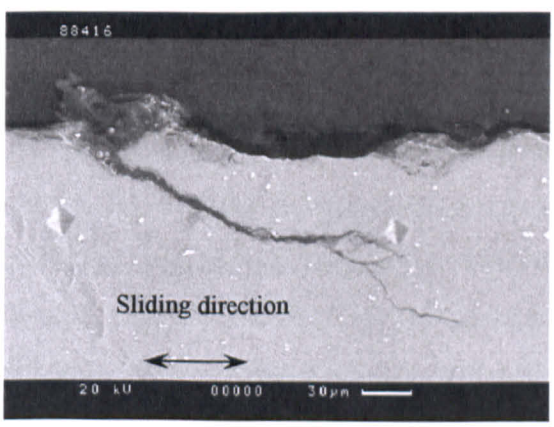

Figure 5.10 cracks generated at the surface of the locked sheet in contact with the pierced sheet after 89,000 cycles at a maximum load of 4.5kN

Crack initiation and propagation due to fretting were also observed on the surface of the pierced sheet. Fig.5.11 (a) shows the fretting surface as well as a crack designated as crack 1 on the pierced sheet after 133,800 cycles at a maximum load of 4.5kN. In Fig.5.11 (b), evidence is presented of another crack in the same sample designated as crack 2. It appears that the two cracks initiated at the edge of the fretted area close to the rivet and propagated out of it. A cross-section of the two cracks is presented in Fig.5.11 (c) and shows that both cracks initiated at the fretting surface at an angle of about 40° to the sliding direction. Following early propagation of crack 2, part of the sheet material dropped off along the crack as circled in Fig.5.11 (c). Crack 1 grew into the subsurface about 300μm deep, oblique to the sliding direction. This was followed by the formation of a knee-point with the crack changing direction and continuing to propagate perpendicular to the sliding direction through the thickness of the sheet. This crack was expected to continue to propagate in a straight line and to develop a crack tip, which is what would normally happen during fretting fatigue. However, this did not take place and the crack appeared to change direction. This observation was unusual and the reason why this took place was because a fatigue crack, designated as crack 3, initiated at the bottom part of the sheet and propagated to meet the crack 1. It should be noted that surface **A** shown in Fig.5.11 (c), was originally in contact with the locked sheet, while surface **B** was in contact with the underside of the rivet head. Crack 3 initiated at surface **B** and propagated to meet crack 1. These observations suggested that the damage of the pierced sheet was caused by fretting at the interface between the two riveted panels and was assisted by failure at the interface between the underside of the rivet head and the pierced sheet.

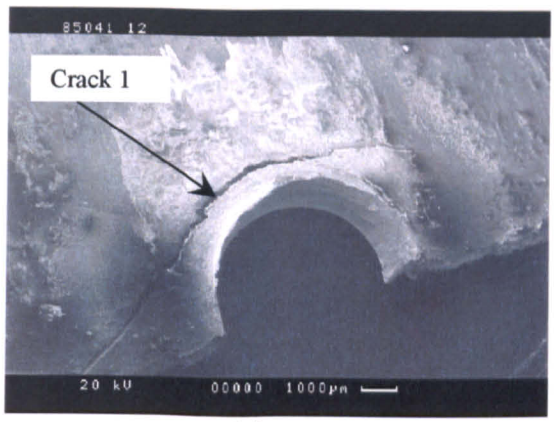

(a)

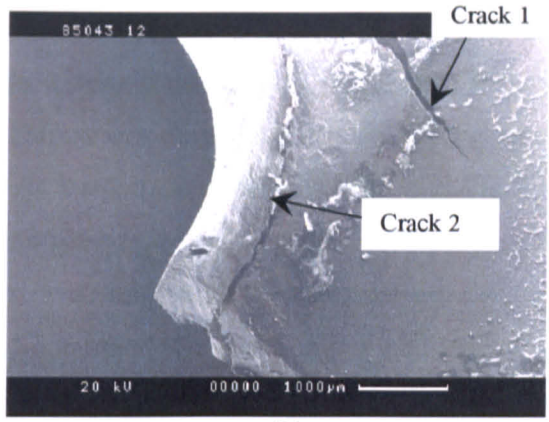

(b)

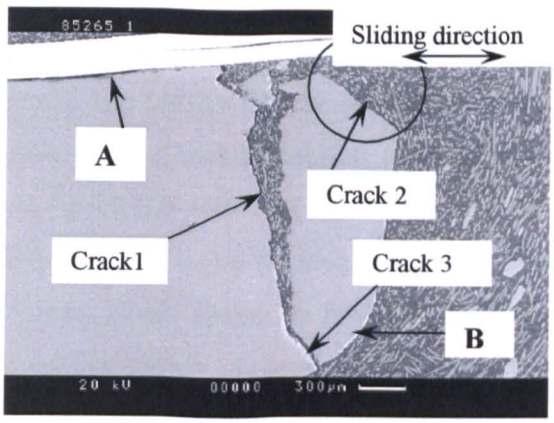

(c)

Figure 5.11 Cracks formed at the pierced sheet after 133,800 cycles at a maximum load of 4.5kN (a) crack located at the edge of fretted area; (b) cracks emerged at the edge of deformed sheet; (c) section across the cracks.

Fatigue cracks initiated at the contact surface oblique to the sliding direction and this was due to the combined effect of the tangential force and the applied load. In the case of fretting, an alternating tangential stress was applied to the contact surface due to the existence of a frictional force. Based on the elastic stress analysis in the interpretation of fretting fatigue failures that was carried out by O'Connor [46], the tangential force tended to put the sheet material ahead of the contact area into compression and the material behind into tension. In the meantime, a tensile stress was introduced to the sheet material by the tension-tension applied load. The contact surface was therefore in a state of compression at the contact area and in tension outside it. The combined effect of the compression and the tension led to crack initiation oblique to the sliding direction. As reported by Endo and Goto [47, 48], the initiation of a crack relieved the stress concentration at the contact surface. Fig.5.9 (b), Fig.5.10 and Fig.5.11 (c) show that fatigue cracks initiated at the contact surface oblique to the sliding direction at both positions A and B. These characteristics of crack initiation are different from what would happen in normal fatigue

due to the effect of the tangential stress. However, according to Endo and Goto [47, 48], the tangential stress was only effective within a certain depth from the contact surface. After early growth, the effect of the tangential stress was eliminated and the applied stress dominated further propagation of the cracks. As a result, at position A shown in Fig.5.11 (c), a knee-point in the propagation curve was generated and then the crack propagated perpendicular to the sliding direction. This was because before the knee-point, the tangential stress was sufficiently effective and combined with the applied load leading to the cracks oblique to the sliding direction. Afterwards, as the effect of the tangential stress became less and less, the applied load eventually took over and dominated the propagation of the cracks. The direction of the applied load was parallel to the sliding direction at position A and therefore the cracks propagated perpendicular to the sliding direction leading to tensile type of cracks. At position B, the applied load acted as a normal load rather than a tension-tension cyclic load which was the case at position A. Therefore no obvious knee-point and tensile-type cracks appeared in the propagation curve, as shown in Fig.5.9 (b). Fig.5.9 (b) also shows that most of the cracks propagated a short distance and formed closed loops. As fretting wear proceeded, the closed-loop material would be worn by delamination. According to Hurricks [49], the fretting process continues leading to new crack initiation and propagation following delamination. The crack that seemed to propagate deep and change direction shown in Fig.5.9 (b) was probably caused by new crack initiation.

According to O'Connor [46] and Endo [48], the combined stress of the tangential force and the cyclic load is known to reach a maximum value at the edge of the contact area or at the slip/non-slip boundary. That is why fatigue cracks generated at the edge of the contact area on the pierced sheet. This was also the reason why cracks generated at the 3 and 9 o'clock positions of the locked sheet in relation to the direction of the applied load since these positions formed the slip/non-slip boundary. In addition, during the riveting process, these positions of the locked sheet suffered more deformation than other parts in order to produce the buttonhole under the effect of the upset anvil. Weaker points were therefore produced at the locked sheet around the buttonhole. This could also contribute to crack initiation at these positions. It was therefore concluded that in a self-piercing riveted joint, crack initiation and early propagation were due to the combination of the applied stress and

the tangential stress at the contact surface, while further propagation of the crack was dominated by the applied load.

5.2.3.2 Surface Work-hardening and Depth of Damaged Layer

The microhardness across the section of a fretting scar that formed on the locked sheet for the FSN51 fastenings was measured 20μm below the fretting surface with a Leitz micro-hardness tester. The testing load was 15g and the loading time was 20 seconds. Fig.5.12 shows the variation of microhardness with the number of fatigue cycles. The average microhardness increased as the number of cycles increased until eventually failure was reached. This suggested that the fatigue test had led to considerable surface work-hardening of the riveted sheet. One of the factors that contributed to the increase in microhardness was the repeated loading that led to strain hardening of the alloy sheet. However, the fretting action was the most significant contributor to the increase in the microhardness.

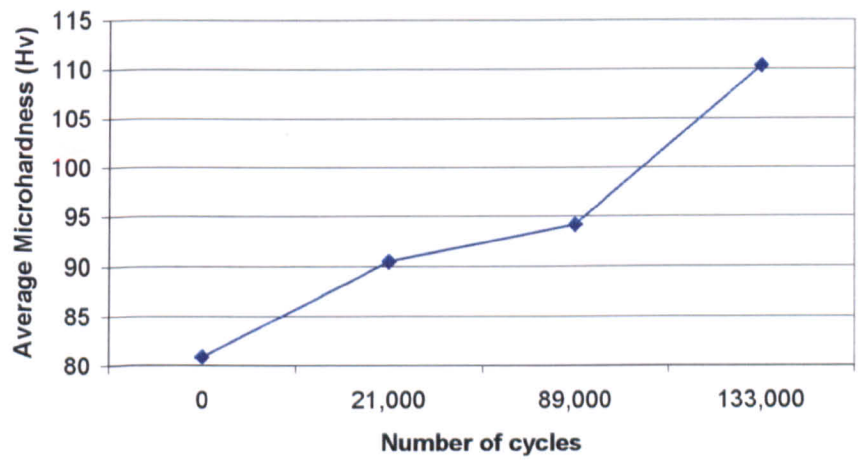

Figure 5.12 Effect of the surface work-hardening of the locked sheet

Fig.5.13 shows the distribution of the microhardness that was obtained from two sectioned samples. One of the samples had been fatigue tested and failed after 133,800 cycles at a maximum load of 4.5kN, whilst the other had not been fatigue tested. The microhardness test for the sample that underwent fatigue testing was performed at the cross section of a

fretting scar that formed on the locked sheet. For the untested sample, the microhardness was obtained from the same position as for the sample that underwent fatigue testing. As shown in Fig.5.13, after fatigue testing, the microhardness was much higher than before testing indicating that work-hardening of the riveted sheet had taken place during the test. The microhardness within the fretted area ranged from about 95Hv to 125Hv and was higher than it was outside the fretted area. The increase in the hardness outside the fretted area was caused by repeated loading, whilst within the fretted area this was due to fretting. This result indicated that fretting had led to a significant surface work-hardening of the riveted sheet. During fretting, debris was produced and built up between the contacting surfaces. The escape of the accumulated debris was restricted and as a result it became compacted and formed an oxide bed at the interface between the two riveted sheets, as shown in Fig.5.5. Consequently the compacted oxide indented the contacting surface of the joint and caused plastic scratching leading to surface work-hardening. This is in agreement with the third-body approach of wear described by Godet [50], who established that compacted fretting debris might lead to surface work-hardening at the fretting surface. The increase in the number of cycles was accompanied with the increase in the fretting debris and led to an increase in the microhardness of the sheet material.

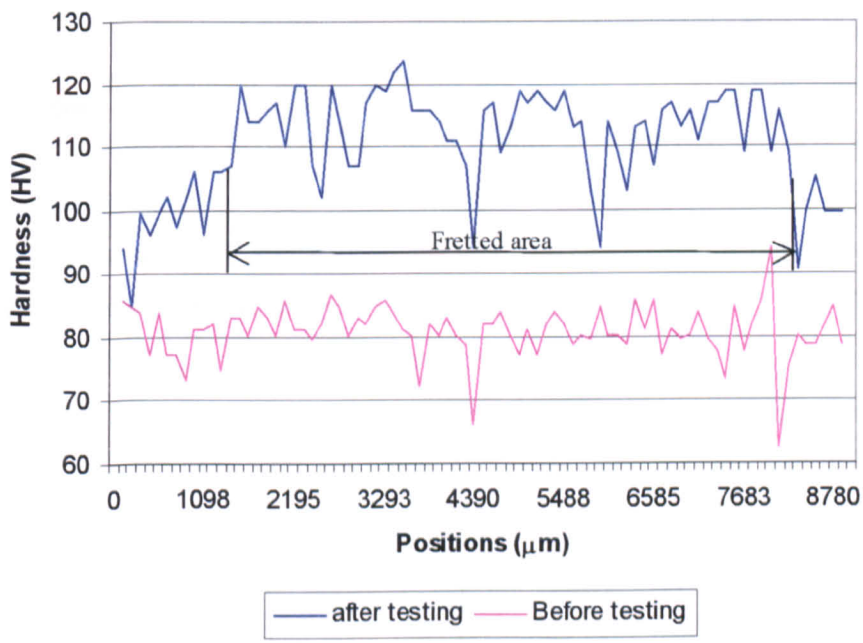

Figure 5.13 Distribution of the microhardness of the locked sheet

The microhardness was also measured along the distance from the fretting surface and the results are shown in Fig.5.14. The microhardness decreased as the distance from the fretting surface increased. A rapid reduction in the microhardness took place near the fretting surface. Fretting occurred as a result of the combined effect of the repeated load and the tangential force. During the fretting process, the combination of the tangential stress and the repeated stress was at a maximum at the top of the contact surface leading to a significant amount of surface work-hardening at that area. As the distance from the contacting surface increased, the effect of the tangential force decreased. As a result, the combined magnitude of the two stresses decreased and this contributed to the reduction in the microhardness. The gradient of the plots in Fig.5.14 became more negative at a short distance from the fretting surface, as the number of fatigue cycles increased. From an inspection of Fig.5.14, it is evident that the rate of change of microhardness with distance from the fretting surface is almost constant at a low distance from the surface. At intermediate distance values from the surface, the gradient gradually becomes less negative and almost constant as the distance from the surface increases. The intermediate distance values represent the area where the gradient undergoes a transition from a high to a low negative value. From Fig.5.10, it was established that the depth of crack propagation due to fretting for a sample that was subjected to fatigue testing at a maximum load of 4.5kN was about 120μm after 89,000 cycles. The direction of the crack changed after propagation to a depth of 120μm. The gradient in Fig.5.14 for the plot at 89,000 cycles lies within its transition value at a distance between 100μm to 150μm from the fretting surface, as shown in Fig.5.15. This transition value coincides with the depth of fretting fatigue crack propagation for this sample. A similar analysis was also conducted for the pierced sheet of a sample that was subjected to fatigue testing at a maximum load of 4.5kN for 133,800 cycles. As shown in Fig.5.16, the intermediate gradient value in this figure lies at a distance of around 250μm to 300μm. The depth of crack propagation due to fretting for this sample was established to be around 300μm from Fig.5.11 (c). The value of the depth of damage due to fretting deduced from microhardness and microscopic examination was almost the same for both the pierced sheet and the locked sheet. The results therefore indicated the depth of the damaged layer due to fretting. The damage was caused by the combined effect of the repeated load and the tangential force. However, only the effect of the tangential force varied as the depth from the contacting surface changed and therefore

the results indicated the distance value up to which the tangential force had its greatest influence. As the number of cycles increased, the depth of the damaged layer also increased and this was attributed to the increasing debris that became compacted at the fretting surface. The microhardness at a distance of more than 500μm from the fretting surface was still higher than at the centre of specimen indicating that the depth that was affected by the combined effect of the tangential force and the repeated stress was considerably large. In addition, at the other side of the locked sheet where no fretting occurred, the microhardness also increased as the number of cycles increased indicating the effect of the work-hardening due to the repeated loading.

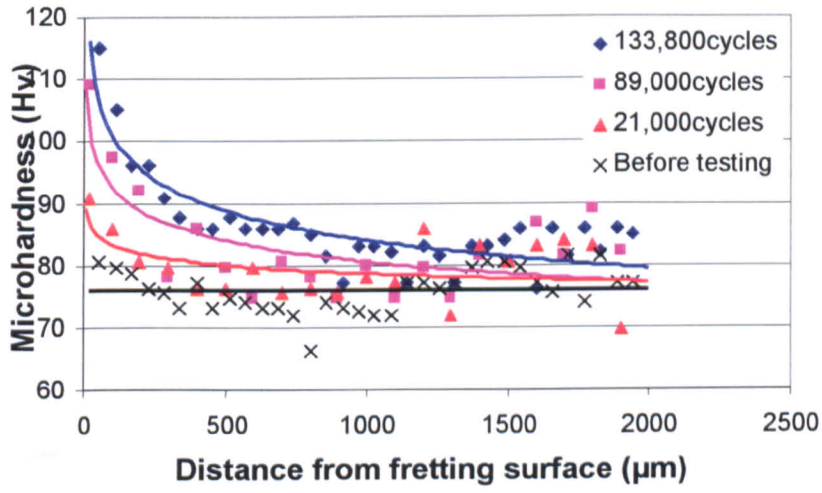

Figure 5.14 Microhardness measurements on the locked sheet

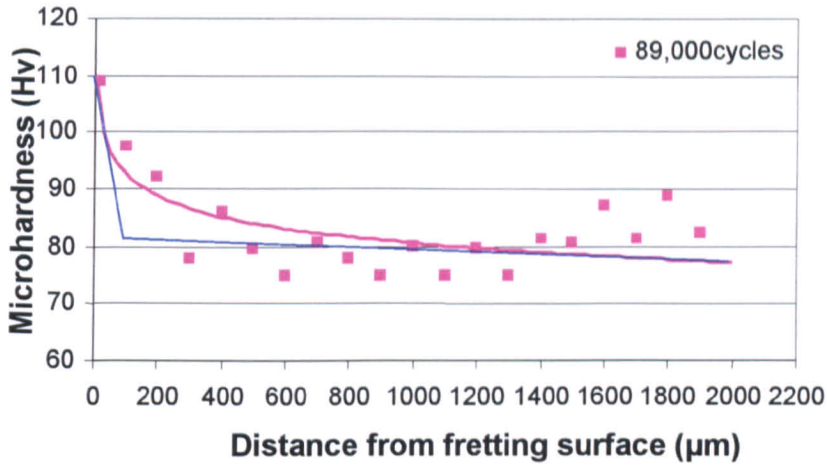

Figure 5.15 Variation of gradient versus distance from fretting surface

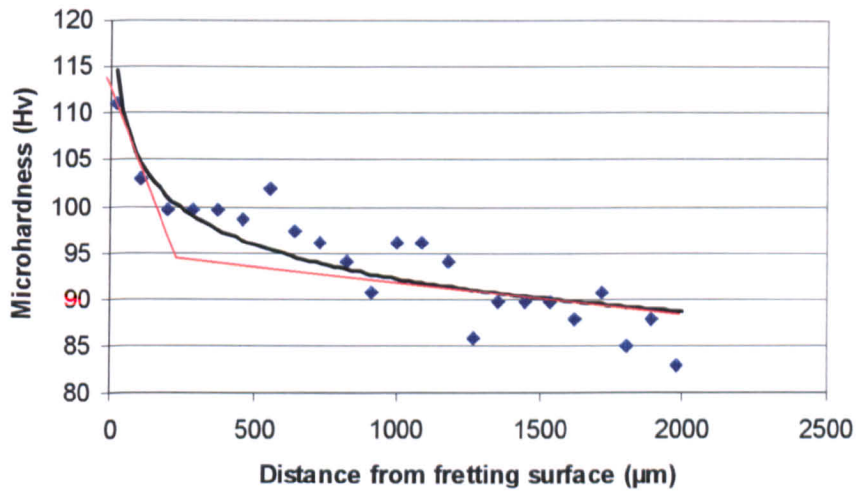

Figure 5.16 Microhardness measurements for the pierced sheet

5.2.4 Combination of Fretting and Fatigue

In addition to fretting fatigue, evidence of normal fatigue that was not associated with fretting was observed. Fig.5.17 (a) presents the right-hand side part of the rivet head of a joint, after 133,800 cycles at a maximum applied load of 4.5kN and shows fatigue cracks that formed on the underside of the rivet head. A cross-section of these fatigue cracks, as presented in Fig.5.17 (b), indicated that the cracks initiated and propagated perpendicular to the interface between the underside of the rivet head and the pierced sheet. It should be noted that surface **B** shown in Fig.5.11 (c) was in contact with the underside of the rivet head. The crack that formed at surface **B** was also perpendicular to the contact surface. This observation suggested that normal fatigue occurred at the interface between the underside of the rivet head and the pierced sheet and contributed to the fracture of the pierced sheet and the rivet head. During fatigue testing, the rivet head on the right-hand side of the joint pressed its head against the pierced sheet due to the effect of secondary bending and rivet tilting. Under the concentrated cyclic compression stress, cracks formed at both the rivet head and the pierced sheet. As a result of the deformation of the pierced sheet, the interface between the edge of the rivet head, and the pierced sheet along the thickness direction, was created. Fretting occurred as the rivet head continued to press its head against the pierced sheet. Normal fatigue produced fretting at position C, designated in Fig.5.2 and led to the damage on the pierced sheet and the rivet head. Therefore, normal fatigue dominated the damage at position C, rather than fretting.

Apparent fatigue striations and secondary cracks were also observed outside the fretting area, whilst, near the fretting surface, no obvious fatigue striations were found. An example is shown in Fig.5.17 (c), which presents the fatigue striations and secondary cracks formed outside the fretting area of the fractured pierced sheet after 489,300 fatigue cycles at a maximum load of 3.6kN. These observations suggested that for a self-piercing riveted joint, failure during fatigue was due to the combination of fretting and fatigue.

(a)

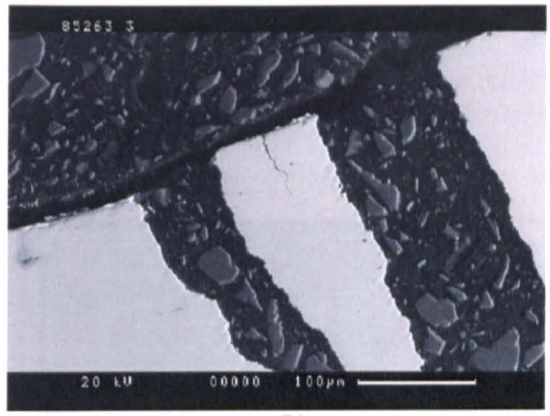

(b)

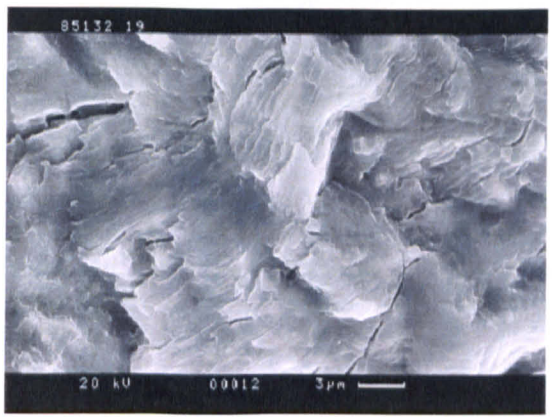

(c)

Figure 5.17 (a) Fatigue crack on the underside of the rivet head; (b) initiation of fatigue cracks on the underside of the rivet head; (c) fatigue striations and secondary cracks formed at the fractured pierced sheet after 489,300 at a maximum load of 3.6kN.

5.2.5 Effect of the Number of Cycles on Fretting Damage

The number of fatigue cycles had an important effect on the degree of fretting damage. Fig.5.18 (a) shows a light micrograph of the contact surface between the two riveted sheets after 21,000 cycles, which was equivalent to 15% of the average fatigue life at a maximum applied load of 4.5kN. Clearly defined fretting scars were noticeable on the surface of both sheets, with the central areas appearing to be bright, while the surrounding scars were dark. EDS analysis revealed the presence of a high carbon content within the bright area, indicating that the wax-based lubricant was still on the surface of the alloy, while the dark area consisted mainly of fretting debris of Al_2O_3. As the fatigue cycles increased to 89,000, equivalent to 65% of the average fatigue life at a maximum applied load of 4.5kN, the bright central area that was present after 21,000 cycles had vanished, whilst the oversize

size of the surface damaged area remained the same, as shown in Fig 5.18 (b). Only one fretting region existed at this stage.

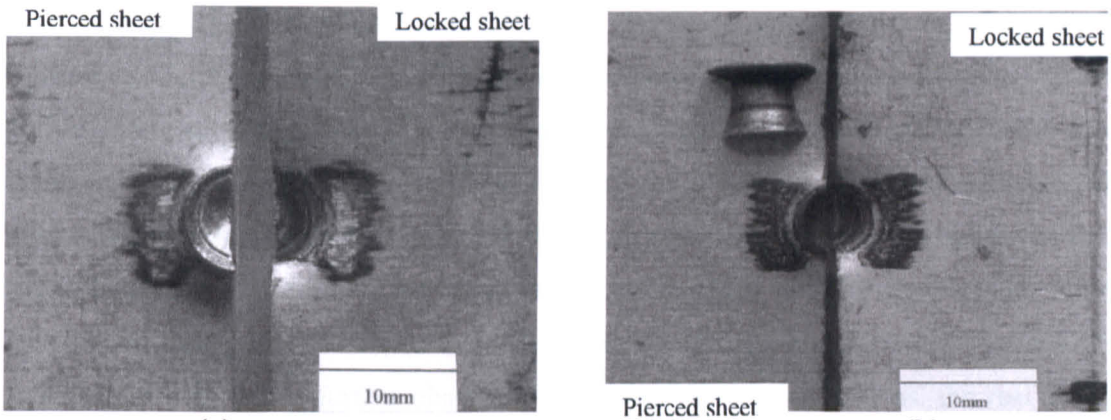

Figure 5.18 Fretting scars at the interface between the riveted sheets: (a) two regions emerged after 21,100 cycles at 4.5kN, (b) one region existed after 89,000 cycles at 4.5kN

According to Mindlin's [51] theory that has been widely used to describe elastic contact, for sphere-plane contact, under tangential loading before incipient gross slip, a slip annulus and a stick zone develop at the contact surface. During the initial stages of fretting a slip region and a stick region developed at the interface between the two riveted sheets. The bright central region in Fig.5.18 (a) is the stick region where no slip occurred, while the outer dark region is the slip region and contained debris. The fretting process within the slip region was accompanied by micro-slip. These two regions developed during the fretting process and their size can be calculated using the following equation derived by O'Connor [46],

$$\frac{a'}{a} = \left[1 - \left(\frac{T}{\mu N}\right)\right]^{1/3} \qquad \textbf{Equation 5-1}$$

where, **a'** represents the radius of the central region, **a** is the radius of the outer region, **T** is the tangential force, **N** is the value of the normal load and **μ** is the coefficient of friction at the interface between the two contacting surfaces. In the present investigation, **N** was proportional to the principal cyclic load, **S** in addition to the effect of setting force. As the

number of cycles increased, the decrease in the bright central area meant that the **a'** term decreased, while the fretted area remained the same indicating that **a** was constant. Therefore the value of (a'/a) decreased as the number of cycles increased. An explanation for this comes from consideration of the effect of the fretting debris. According to Waterhouse [43], due to the effect of the debris that forms and becomes compacted at the fretting interface, the coefficient of friction, μ, increases during the early stages of fretting before it reaches a constant value at a steady-wear state. As a result, the tangential force increased as the number of cycles increased until the μ reached a constant value and the tangential force approached the value of μN. From equation 5.1, when the tangential force reached μN, $a_1=0$. Therefore, the bright central area, which was the stick region, can be expected to disappear and macroscopic sliding to commence over the entire contact area, as was observed. It was further observed that during the fretting process, the real contact area, **A**, which can be described by **a**, remained constant. This is also consistent with the local conditions suggested by Waterhouse [43], that the relationship between the real contact area and the normal load can be expressed as

$$A = \frac{N}{N_0} \qquad \textbf{Equation 5-2}$$

where N_0 is related to the material properties. The value of **N** is proportional to the applied load, leading to a fixed maximum contact area **A**. In other words, the value of **A** and **a** remained constant as the number of cycles increased. The number of fatigue cycles therefore had an important effect on the fretting damage by increasing the tangential force leading to a reduction in the stick region during the early fretting process.

5.2.6 Effect of Applied Load on Fretting

The interface of the sheets in a joint that was subjected to a maximum applied load of 2.7kN for 845,900 cycles, which was equivalent to 10% of the average fatigue life, is presented in Fig.5.19. Compared with Fig.5.18, the fretting scars at the lower fatigue load were less clearly defined and covered a smaller area than at the higher fatigue load. This indicated the effect of the applied load on fretting damage.

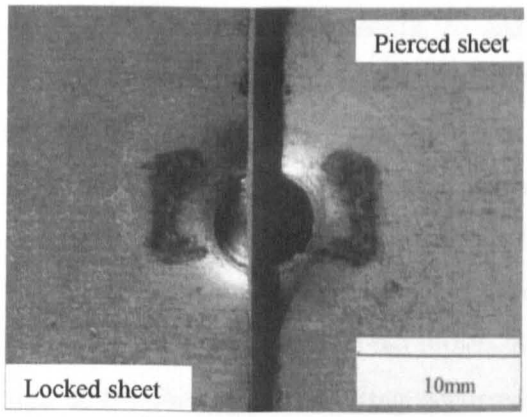

Figure 5.19 Fretting scars at the interface between the two riveted sheets after 845,900 cycles at 2.7kN.

A number of contact surfaces exist for a self-piercing riveted sample. It is understood that after joining, a closure load provided by the setting force exists in the joint between the riveted components and holds them together. This induces the possibility of fretting at these contact surfaces when the sample is subjected to cyclic loading. According to Forsyth [52], most examples of fretting that are associated with fasteners can be resolved into two types: flange-face fretting and pin-bore fretting. The reason for making a distinction between the two classes of fretting is not that the local physical process of fretting is different, but that in flange-face fretting the normal load is virtually independent of the cyclic load, whereas in pin-bore fretting the normal load and the cyclic load are interdependent. For a self-piercing riveted joint, the closure load acted as the normal load at the interface between the two riveted sheets and was therefore led to flange-face fretting, which was not affected by the magnitude of the principal cyclic load. However, the experimental results showed that the fretting damage at the interface between the two riveted sheets was in fact affected by the principal cyclic load, as shown in Figs 5.18 and 5.19.

The applied load (S) affected the fretting damage at the interface between the riveted sheets through its effect on the normal load at the interface. In addition to the effect of secondary bending, tilting of the rivet occurred during the fatigue loading process. As shown in Fig.5.1, once the load S was applied, two components, S_1 and S_2, were induced at the head and the flared shank of the rivet respectively. The two components can be determined by the principal load, S, and by the geometry of the rivet. For joints with

identical thickness combination and setting parameters, the principal load, S, was the only variable. These two components, S_1 and S_2, which increased with the principal load S, formed a couple and caused a tendency for the rivet to tilt. Due to the absence of a pre-drilled hole, the rivet head was forced to lift on the left-hand side and press on the right-hand side against the upper sheet. As a result, on the left-hand side of the joint, the interface between the riveted sheets lost contact, while on the right-hand side of the joint, the normal load at this interface increased as the principal load increased. Consequently, fretting did not take place at the interface between the two riveted sheets on the left-hand side of the joint, whilst fretting occurred at the interface between the two sheets on the right-hand side of the joint and was affected by the cyclic load. According to Waterhouse [43], the real contact area, A, is directly proportional to the normal load, N, as shown in equation 5.2. This implies that an increase in the normal load results in an increase in the contact area. Since fretting only occurs at the contact area, it is expected that this will be accompanied with an increase in the fretted area. Therefore, the fretted area between the riveted sheets increased as the principal cyclic load increased, as shown in Figs.5.18 and 5.19. Furthermore, fatigue cracks were initiated on both the pierced and the locked sheets at a higher load level since a higher normal load resulted in more severe fretting damage and fatigue damage.

The principal cyclic load also affected the fretting damage at the interface between the shank of the rivet and the sheets. In addition to the effect of secondary bending, tilting of the rivet and bearing against the riveted sheets adjacent to the rivet led to pin-bore fretting at the interface between the rivet shank and the riveted sheets. Tilting acted as an oscillatory source and caused the relative movement at the interface between the rivet shank and the riveted sheets on the left-hand side of the joint (refer to Fig.2.5), while the principal cyclic load still acted as a normal load to this interface. As a result, fretting took place on the left-hand side of the interface between the shank of the rivet and the locked sheet. The oscillatory force and the normal load at this interface increased as the principal cyclic load increased. Therefore, at a relatively higher load level, more severe fretting and fatigue occurred, leading to crack initiation and propagation at the rivet shank. The samples therefore failed by rivet fracture at a high applied load during fatigue testing. At a lower load level, fretting and normal fatigue were not sufficient to lead to fracture of the rivet. As a result, the sheet material fractured and dominated the failure mode that occurred

at lower applied loads during fatigue testing. In addition, the experimental results indicated that fretting did not take place at the interface between the rivet shank and the riveted sheets on the right-hand side of the joint. This was because the relative movement between the rivet shank and the riveted sheets on the left-hand side of the joint was stopped by the rivet head on the right-hand side of the joint. Instead of sliding at the interface between the rivet shank and the riveted sheet, the rivet head was subjected to a high pressure leading to fracture of the rivet head, as shown in Figs.5.17 (a) and (b). Consequently, the 3 and 9 o'clock positions formed the boundary between the fretting and the non-fretting region, where the combined stress of the tangential force and the cyclic load reached a maximum value. In order to relieve the high stress concentration, fretting cracks initiated at the 3 and 9 o'clock positions of the locked sheet in relation to the direction of the applied load.

In addition to the effect on the normal load, the principal cyclic load also affected the initiation and propagation of fatigue cracks. At the interface between the riveted sheets, fatigue cracks initiated obliquely to the sliding direction. After early growth, the direction of crack propagation became perpendicular to the sliding direction and therefore, a tensile-type crack, also referred to as a stage II crack by Waterhouse [53], was formed. The reason why fretting cracks initiated at an angle to the sliding direction was due to the combination of the tangential force and the cyclic load, as explained above. The higher the applied load the easier the crack initiation and propagation. It should be noted that the sliding direction at the interface between the two riveted sheets was parallel to the principal cyclic load, which directly acted as a tensile stress on the riveted sheets. After early crack growth the effect of the tangential force was less effective and normal fatigue dominated the propagation of the cracks leading to a tensile type of crack. At the interface between the shank of the rivet and the locked sheet, fretting cracks initiated at the fretting surface of the locked sheet at an angle of about 35° to the sliding direction, as shown in Fig.5.9 (b). This was also due to the combination of tangential force and the cyclic load. However, no tensile-type crack was formed at this interface and this was because at this interface, the principal cyclic load was perpendicular to the tangential force rather than parallel to it.

It should be noted here that the variation in the normal load was also accompanied with a change in the tangential force. According to O'Connor [46], for the limiting case of

incipient sliding, the maximum tangential force is equal to μN. Therefore, as the normal load increased the maximum tangential force also increased leading to possible worse fretting damage by promoting crack initiation and propagation. On the other hand, according to Waterhouse [43], the increase in the normal load might reduce the slip region by reducing the slip-amplitude leading to a possible reduction in the fretting damage. Therefore the change of the normal load triggered these two reverse tendencies. The present investigation has shown that the morphology of the fretting scars varied with different applied load levels. The trace of the micro-slip was more obvious at high load levels, as shown in Figs.5.18 and 5.19, suggesting that the slip-amplitude might be greater at higher load levels than at low levels. Based on these observations, the larger principal cyclic load probably created more serious fretting damage by increasing the normal load and the slip amplitude. As a consequence of this, two different failure modes took place depending on the level of the applied load. However, the effect of the normal load and the cyclic load on the slip-amplitude needs to be further investigated.

5.2.7 Effect of Interfacial Conditions on Fretting

The observation of fretting damage during this study led to an investigation to examine ways to prevent this type of fretting damage. Since fretting only occurs at contacting interfaces the condition of the contact surface might affect the fretting behaviour. Therefore the FSH5 series of fastenings was created for examining the effect of the sheet surface condition on the fretting behaviour.

Fig.5.20 shows the fatigue test results for the FSN51, FSH51 and FSH52 fastenings that had different interfacial conditions at the interface between the two riveted sheets. The FSN51 fastening, which joined sheets that had been coated with a wax based lubricant exhibited the longest fatigue life. At 1×10^6cycles, the fatigue strength of the FSH51 fastening, which joined uncoated sheets, was at least 10% lower than that of the FSN51 fastening. The FSH52 fastening, which had a PTFE insert at the interface between the two riveted sheets, had the shortest fatigue life. At 1×10^6 cycles, the fatigue life of the FSH52 fastenings was almost 7% shorter than that of the FSH51 fastening.

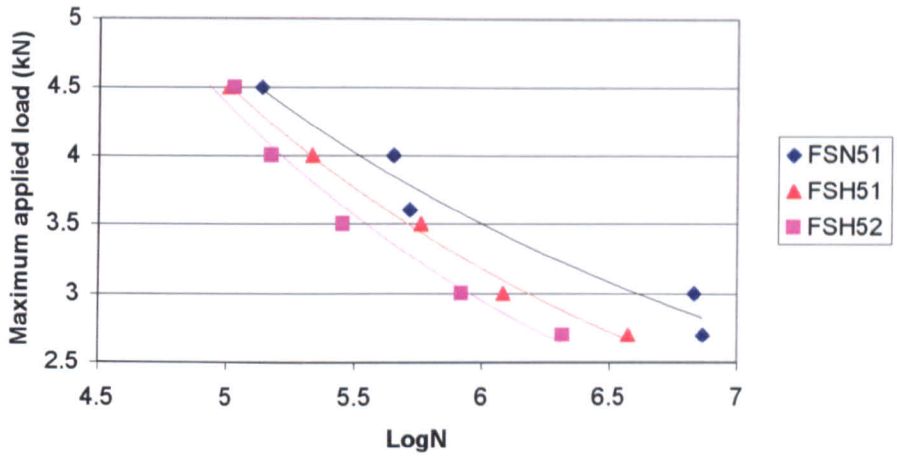

Figure 5.20 Fatigue test results for the FSN51, FSH51 and FSH52 fastenings

5.2.7.1 Fretting Behaviour

Typical fretting scars at the interface between the two riveted sheets for the FSN51 fastening are shown in Figs.3.11, 5.18 and 5.19. The fretting regimes vary from 5 to 8 mm in length and from 2 to 4 mm in width at a maximum load of 4.5kN. The figures also show the effect of the number of cycles and the magnitude of the applied load on the fretting damage. Ploughing and delamination were observed to occur at the interface between the two riveted sheets for the FSN51 fastening, as shown in Figs.5.5 (a) and (b). The fretting behaviour for the FSH51 fastening was very similar to the FSN51 fastening. Fretting scars developed at all applied load levels during fatigue testing for the FSH51 fastening. Figs.5.21 (a) and (b) present evidence of fretting scars on the surface of the pierced sheet and delamination occurred on the surface of the locked sheet of a FSH51 fastening after 215,060 cycles at a maximum applied load of 4.0kN. However, the fretting behaviour for the FSH52 fastening was somewhat different from the FSN51 and FSH51 fastenings. Inserting a PTFE tape at the interface between the two riveted sheets prevented direct contact between the two riveted sheets. Examination of the interface between the two sheets following fatigue testing at a maximum load of 4.5kN, revealed the presence of small fretting scars on both the pierced sheet and the locked sheet, as shown in Figs.5.22 (a) and (b). The size of the fretting region was 5mm in length and 2mm in width and this

was much smaller than that observed for the FSN51 fastenings. In spite of the fact that the two sheets were separated by the PTFE layer, surface damage characterised by delamination was also observed, as shown in Figs.5.22 (c) and (d). At a maximum load of 3.0kN, there were no visible fretting scars on the surface of the two riveted sheets after fatigue fracture of samples. Fig.5.23 (a) shows the surface of the pierced sheet indicating that the presence of PTFE prevented the formation of any fretting scars on the riveted sheets tested at a maximum load of 3.0kN. SEM examination of samples that fractured at a maximum load of 3.0kN in Fig.5.23 (b) revealed surface damage of the PTFE tape even though no fretting scars formed on the riveted sheets for this sample.

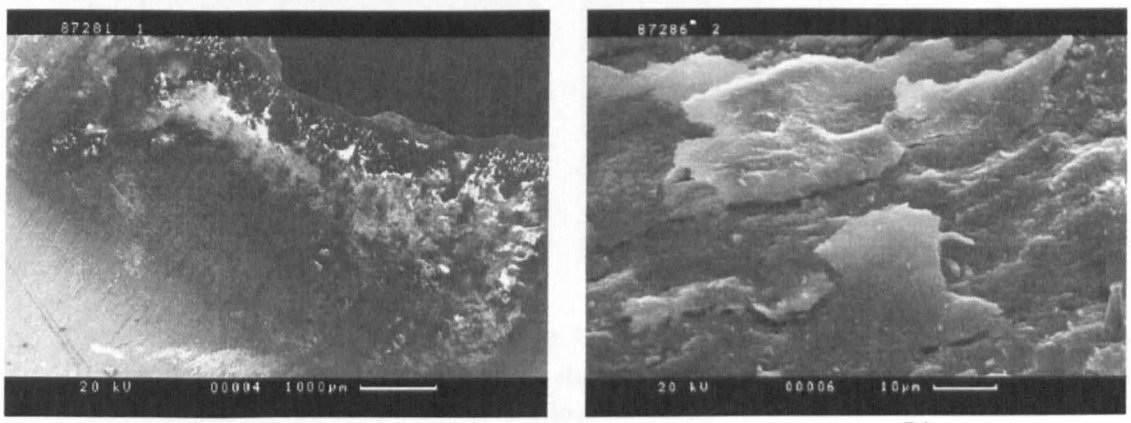

(a) (b)

Figure 5.21 After 215,060 cycles at 4.0kN for a FSH51 fastening, (a) fretting debris on the pierced sheet, (b) delamination on the locked sheet.

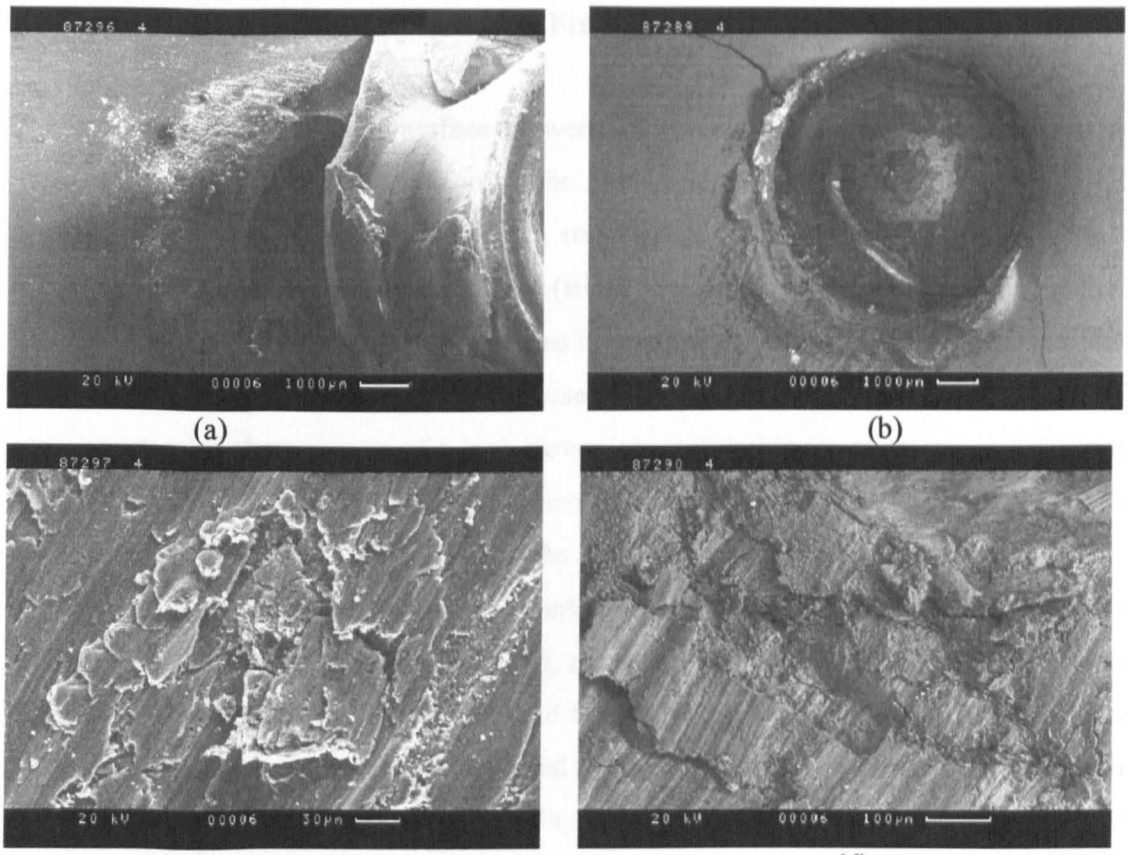

Figure 5.22 Contact surfaces of a FSH52 fastening after 97,890 cycles at 4.5kN, (a) fretting scars on the pierced sheet, (b) on the locked sheet, (c) damaged surface of the pierced sheet, (d) damaged surface of the locked sheet.

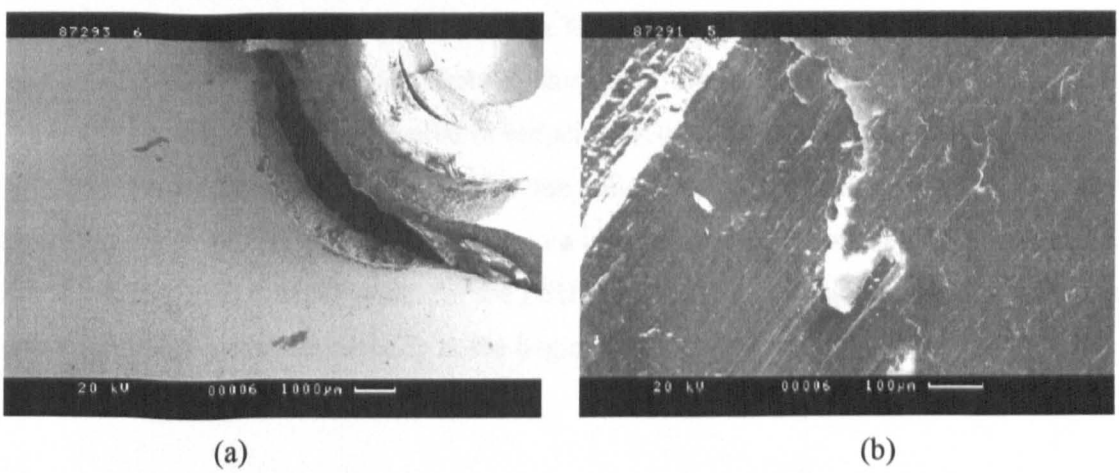

Figure 5.23 after 604,403 cycles at 3.0kN of a FSH52 fastening (a) no fretting scars on the pierced sheet, (b) damaged surface of the PTFE tape.

5.2.7.2 Effect of the Solid Lubricant on Fretting

The fretting damage at the interface between the piercing and the locked sheets was observed to occur in two stages. During the first stage, ploughing took place due to the cyclic micro-sliding movement leading to roughening of the alloy surface as shown in Fig.5.5 (a). At this stage, slip and non-slip (stick) regions developed as shown in Fig.5.18 (a). An SEM, micrograph of the two regions is presented in Fig.5.24 (a). Under the SEM, the appearance of the two regions was reversed with the stick region appearing dark. EDS analysis revealed the presence of a high carbon content within the stick region indicating that the wax-based lubricant still covered most of the alloy surface at this region. The light grey areas represented the regions where the alloy surface had been exposed. Analysis of the white particles showed that they represented fretting debris of Al_2O_3. As the number of cycles increased the stick region vanished, as shown in Fig.5.18 (b) indicating that the wax-based solid lubricant had been removed from the alloy surface. Once the alloy surface became exposed, the aluminium alloy started to suffer from fretting damage. Delamination of the alloy material occurred as a result of a continuous wear process, as shown in Fig.5.5 (b). This produced more debris as shown in Fig.5.5 (c) and Fig.5.24 (b). EDS analysis of the debris shown in Fig.5.24 (b) revealed that the black-coloured debris represented the solid lubricant, as shown in Fig.5.25. The grey-coloured area represented the exposed alloy surface, as revealed by the EDS analysis in Fig.5.26. The debris produced by the wear process accumulated at the contact surface and formed a third-body particle to promote further three-body fretting. For the FSN51 fastening, the sheet material prior to testing was covered by the solid lubricant and therefore the fretting process initially involved removal of the solid lubricant followed by fretting damage of the alloy surface. The presence of the solid surface lubricant was effective in reducing fretting damage during the early stage of the test. It was therefore concluded that the solid surface lubricant delayed the onset of fretting wear at the alloy surface leading to a higher fatigue life for the FSN51 fastenings. On the other hand, it appears that for the FSH51 fastenings, fretting damage started to take place at the alloy surface virtually at the beginning of the dynamic test, resulting in a short fatigue life.

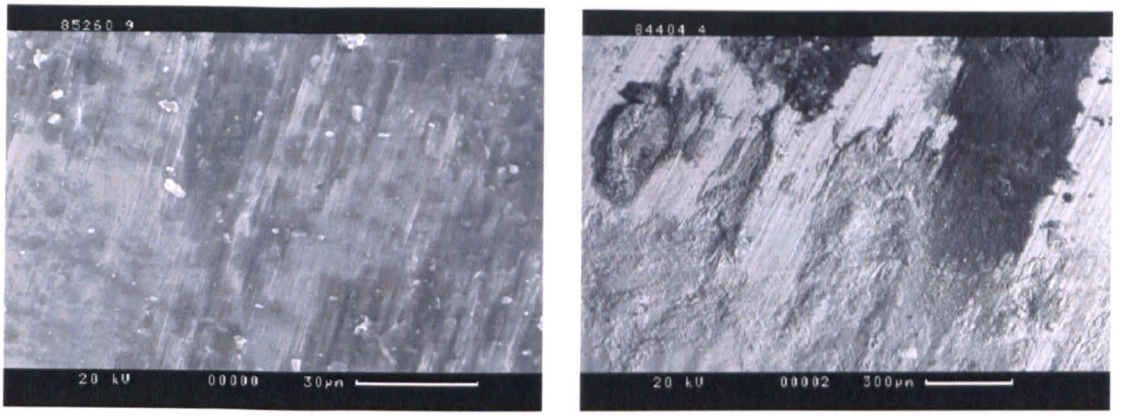

(a) **(b)**

Figure 5.24 (a) Wearing of the wax-based lubricant,
(b) accumulated debris on the contact surface after 173,200 cycles at 4.5kN.

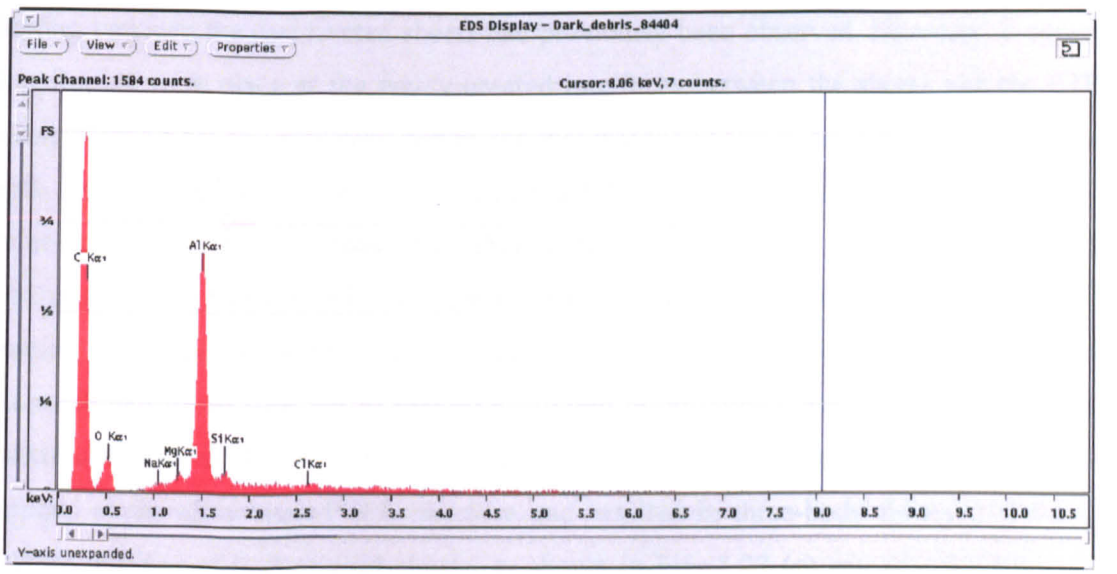

Figure 5.25 EDS analysis of dark area shown in Fig. 5.24 (b)

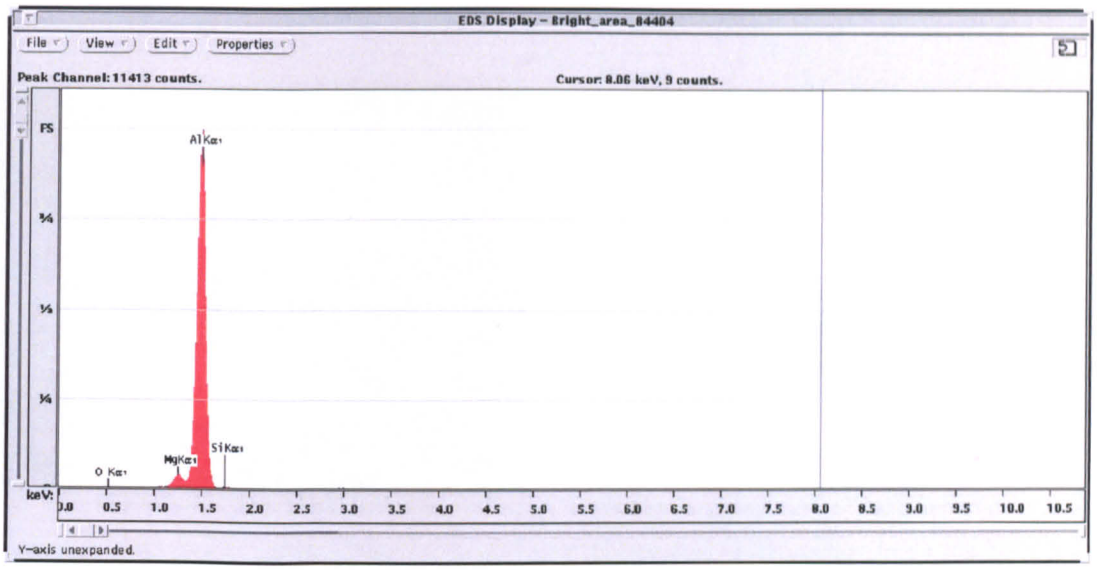

Figure 5.26 EDS analysis of grey area shown in Fig. 5.24 (b)

5.2.7.3 Effect of the PTFE Insert on Fretting

The PTFE tape prevented direct contact of the two riveted sheets at the critical zone where fretting between the two riveted sheets had previously been observed. However, it appears that fretting took place at the newly-created interfaces between the sheets and the PTFE insert. Support for this was provided by the fact that the accumulated debris was located on both sides of the PTFE tape as shown in Fig.5.27. The EDS analysis shown in Fig.5.28 revealed that the debris consisted of aluminium oxide particles and fragments of PTFE. The presence of fluorine indicated that the PTFE tape also suffered from damage due to fretting that occurred at the interface between the two riveted sheets. The initial cyclic micro-sliding movement led to two-body fretting at the alloy sheet/PTFE interface. At a maximum load of 4.5kN, the two-body fretting created fretting debris which became trapped at the alloy sheet/PTFE interface and resulted in three-body fretting, leading to surface damage of both riveted sheets, as shown in Figs.5.22 (c) and (d). Therefore, the PTFE tape could not prevent fretting at a maximum load of 4.5kN. At the lower load level, two-body fretting led to the surface damage of the PTFE tape, as shown in Fig.5.23 (b). However, under these conditions, the two-body fretting was less severe and did not produce enough debris for three-body fretting. Therefore there was no fretting damage of the riveted sheets at a maximum load of 3.0kN and below.

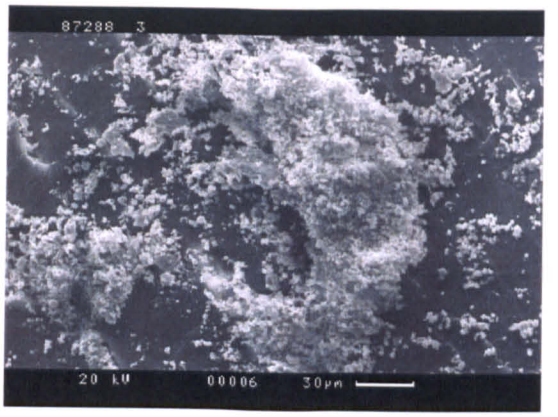

Figure 5.27 Debris accumulated on the PTFE tape of a FSH52 sample after 97,890 cycles at a maximum load of 4.5kN

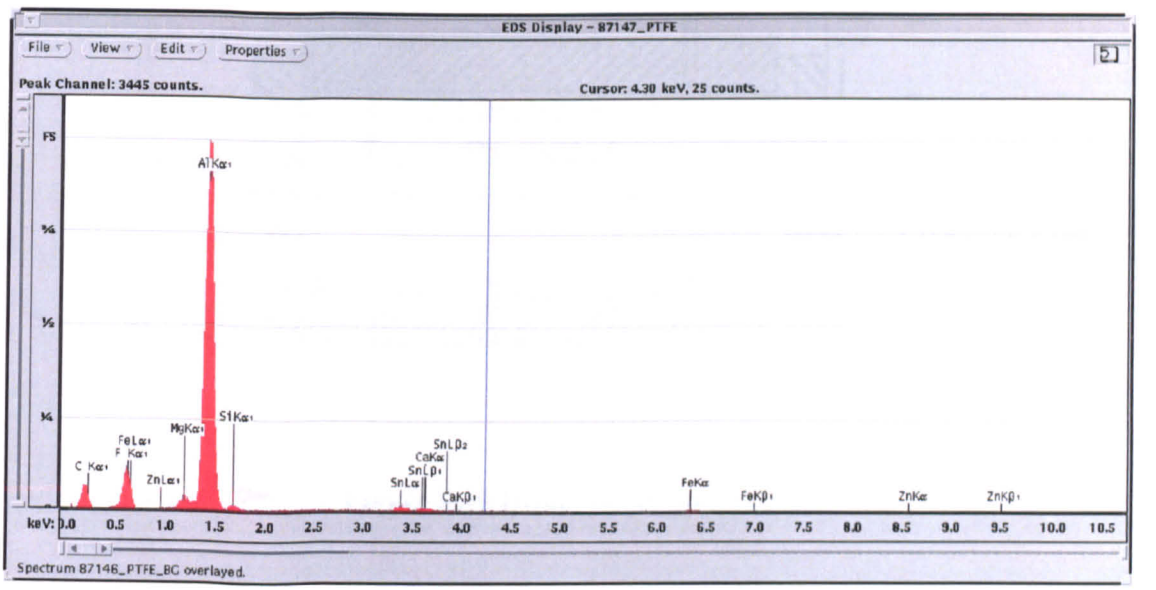

Figure 5.28 EDS analysis of the debris shown in Fig.5.27

5.2.7.4 Effect of Coefficient of Friction on Fretting

The coefficient of friction between the pierced and the locked sheet for the FSN51, FSH51 and FSH52 fastenings was measured using a direct shear apparatus. The objective of this part of the work was to examine the effect of the coefficient of friction on the fretting behaviour. The essential features of the apparatus are shown diagrammatically in Fig.5.29. A vertical (normal) force, **N**, is applied to the specimen through a loading plate and a shear stress is gradually applied on a horizontal plane by causing the two halves of the box to

move against each other. The shear force, T, is measured when a relative movement occurs and reaches a steady state. The coefficient of friction is then calculated by using equation 5.3:

$$\mu = \frac{T}{N} \qquad \textbf{Equation 5-3}$$

Three pairs of specimens for each fastening were tested and the average of the three values was adopted as the coefficient of friction at each interface. The test results are shown in Table 5.1.

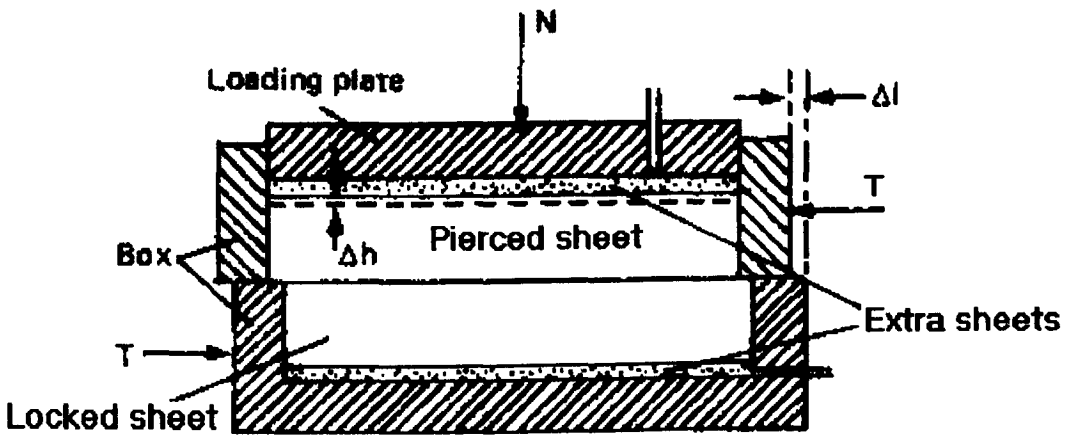

Figure 5.29 Direct shear apparatus

Table 5-1 Coefficient of friction at different interfaces

Fastenings	Interface	Coefficient of friction
FSN51	Pierced sheet/Locked sheet	0.26
FSH51	Pierced sheet/Locked sheet	0.24
FSH52	Pierced sheet/PTFE//Locked sheet	0.03

In a self-piercing riveted joint, the normal load is directly proportional to the applied load. The lower the applied load the lower the normal load leading to a smaller fretting area, as discussed in section 5.2.6. This also suggested that the lower the frictional force the smaller the fretting area. The inserted PTFE tape induced a very low coefficient of friction

at the interface between the PTFE tape and the riveted sheet, as shown in Table 5.1. Consequently, the frictional force at this interface was about 10 times less than that at the interface between the two riveted sheets at an identical normal load. This resulted in a much smaller fretting area in the PTFE-insert samples. In addition, the frictional force is directly related to the tangential force in the case of incipient sliding. The lower frictional force therefore led to a lower tangential force at the contact surface. According to Alaham et al [54], when the tangential stress was small, the amount of ploughing and delamination would be expected to be less since the probability of asperity interactions drops and the amount of adhesive transfer is less. However, in a fretting fatigue degradation process, ploughing and delamination are important in establishing a surface morphology, which is long-lasting and therefore influences the future course of wear. The third-body of fretting is produced mainly at this stage. For a PTFE-insert sample, ploughing is unable to occur at the interface between the PTFE tape and the alloy sheet since the PTFE tape is very soft and the tangential force was very low in the case of incipient sliding. However, delamination might occur depending on the cyclic normal load and the cyclic frictional force. At a higher applied load, the normal load was higher resulting in a higher frictional force at the interface between the PTFE tape and the riveted sheet. Consequently, delamination occurred at the alloy surface and produced oxide debris leading to three-body fretting. Therefore fretting scars were observed at a maximum load of 4.5kN although the fretting area was much smaller compared to tests without PTFE. In contrast, at a lower applied load the normal load and the frictional force were also lower and therefore delamination at the sheet surface did not take place. As a result, there was insufficient oxide debris production to carry out three-body fretting. The low frictional force at the interface between the PTFE tape and the riveted sheet reduced the fretting damage.

Based on the load transfer mechanism of a lap joint, the lower the frictional force the lower the load transferred by the interface. As a result, the load transferred by the rivet was increased leading to an increase in the normal load at the interface between the rivet shank and the sheet. The increase in the normal load at this interface was accompanied with an increase in the shear stress acting on the rivet shank leading to severe fatigue of the rivet. In addition, the tangential force at this interface increased as the normal load increased leading to severe fretting at this interface. EDS analysis of the debris shown in Fig.5.27 also revealed the presence of small amount of zinc and tin. The presence of zinc and tin

indicated that the rivet coating had worn off due to fretting and the debris that formed at the interface between the rivet shank and the sheet had been transferred to the interface between the riveted sheet and the PTFE tape. A PTFE insert induced a small frictional force at the interface between the PTFE insert and the riveted sheet, resulting in a short fatigue life for the FSH52 fastening due to the load transfer requirements of the lap joint.

5.3 Comparison between this study and literature

The failure modes that were reported by previous studies and the current project were compared in order to obtain a better understanding of the failure mechanism of self-piercing riveted joints. King [22] has summarised the failure modes that occurred during static tests in his study. The most prominent failure mode that was observed by King [22] for both shear and peel tests is shown in Fig.5.30 (a). The rivet together with part of the locked sheet were pulled out from the buttonhole. This was due to the fact that breaking-through took place in many of his samples. Failure by rivet pull-out, shown in Fig.5.30 (b) was believed by King [22] to occur in poor quality joints. For the joints with different sheet thickness combination, the thinner sheet was torn for both shear and peel tests, as shown in Fig.5.30 (c). These observations from King's [22] study differ from observations from the current project. Failure by tearing of the thinner sheet was only observed to occur in the peel test in the current study. The smaller overlap length used by King [22] provided the riveted sheets with a smaller bearing resistance. This factor, coupled with the effect of thickness on the bearing resistance, led to tearing of the thinner sheet during the shear test in King's study [22]. The failure mode that was believed to occur in poor quality joints by King [22] and shown in Fig.5.30 (b) was the only failure system that occurred for the joints with an equal sheet thickness combination in shear and peel tests in the current project. The most prominent failure mode, that occurred in King's study and is presented in Fig.5.30 (a), did not take place in the current project. According to cross-sectional examination, there was no breaking-through in any of the samples tested in the current project and the failure mechanism observed during shear and peel testing did not involve separation of part of the locked sheet from the buttonhole.

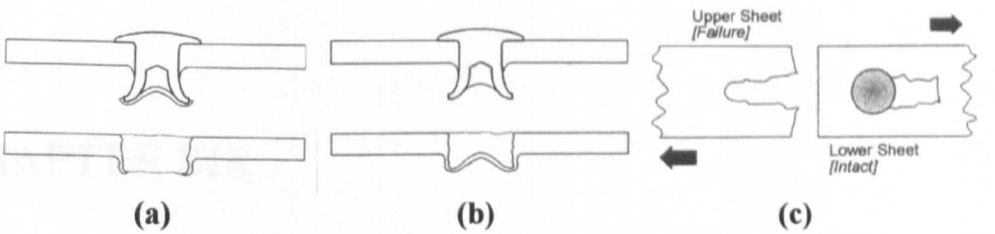

Figure 5.30 Failure modes (After King [22])

Fatigue failure modes were also reported by previous studies although there was no detailed analysis. Krause et al [27] described the failure mode that occurred in the fatigue test for aluminium self-piercing riveted specimens as an eyebrow crack. In the study by Westgate et al [26], different failure modes were observed to occur in steel and aluminium specimens. Fracture of the upper sheet around the head of the rivet led to failure of the aluminium joints. Fu and Mallick [29, 30], who carried out a similar project to the current project, also reported that fracture of the upper sheet dominated the fatigue failure. In the current project, different failure modes were observed depending on the magnitude of the applied load. At high applied loads, fracture of the rivet shank dominated the failure mode, whilst at low applied loads, sheet material fracture was the only failure system. The different failure modes that occurred in previous studies and the current project were probably due to the different specimen size and test methodologies. In the current project, the highest magnitude of the applied load was about 80% of the average ultimate shear load and this contributed to the fracture of the rivet shank. The narrower the sheet material the higher the stress acting on the sheet under an identical load and this could lead to failure of the sheet rather than the rivet. In addition, the criterion for ultimate failure in the current project was fracture of the joint, whilst in other studies it may have been a specific displacement value experienced by the joint. This difference in the failure criterion may have led to the observation of different failure modes. It is therefore further suggested that the specimen geometry and testing methodology need to be standardised in order to relate test performance to in-service performance.

CHAPTER SIX

6. EXAMINATION AND ANALYSIS OF SECONDARY BENDING

6.1 Aims of the Examination and Analysis

Secondary bending is an inherent feature of single lap joints like those that were used throughout this study. It is important to examine and analyse the effect of secondary bending on the mechanical behaviour and in particular on the fatigue performance of self-piercing riveted single lap joints, because fatigue fracture usually occurs on a cross-sectional discontinuity. In addition, the resulting bending stress can locally exceed the axial stress by several times and can have a decisive effect on the fatigue behaviour. Previous studies investigated the influence of secondary bending on the fatigue behaviour of conventional single lap joints by comparing results between specimens without secondary bending and single lap joints with secondary bending. In both studies by Hartman [35] and Schütz et al [36], the specimens without secondary bending were either symmetric butt-joints or double-shear joints that were produced by using the same setting parameters as for single lap joints. However, it is difficult to retain the same rivet quality as for single lap joints by using the same parameters to make double-shear specimens and symmetric butt-joints. According to Schütz et al [36], the load transfer mechanisms of symmetric butt-joints and double-shear joints differ from that for single lap joints. In addition, the pressure distribution is different in single lap joints compared to symmetric butt-joints and double-shear joints. In symmetric butt-joints and double-shear joints, a higher applied load is

transferred by the frictional force between the riveted sheets, whilst in single-shear joints this is encountered far less frequently. This leads to a significant difference in the fatigue strength between either symmetric butt-joints or double-shear joints and single-shear joints. These differences in behaviour are inseparable and in the case of single lap joints they are affected by secondary bending. As a result, the data obtained from symmetric butt-joints and double-shear joints would be incomparable to the data for single lap joints and could not reflect the effect of seconding bending. For a self-piercing riveted lap joint, it is even more difficult to make a symmetric butt-joint or a double-shear joint by using the same setting parameters as for a single-shear joint. Therefore, a single lap joint was used to examine the effect of secondary bending.

Rivet-bonding joints were introduced for strain measurement by combining riveting and adhesive bonding. This was carried out in order to compare the strain measurement results and to identify the effect of adhesive bonding on secondary bending.

The purpose of the examination and analysis reported in this chapter is to determine the distribution of secondary bending in some representative fastenings. The principal aims of the examination and analysis are listed below:

1. To determine the distribution of secondary bending of the fastenings.
2. To determine the secondary bending ratio k ($k = \frac{\sigma_{bending}}{\sigma_{nominal}}$).
3. To identify the factors that influence the secondary bending ratio.
4. To clarify the effect of bonding and riveting for a rivet-bonding joint.
5. To predict the effect of secondary bending on the mechanical behaviour and in particular on the fatigue strength.

6.2 Procedure of the Examination and Analysis

Secondary bending is not constant over the whole of the cross-section of samples. The maximum secondary bending for a single riveted lap joint occurs at the central cross-section of the rivet. The value of the secondary bending can be determined mathematically or empirically. As defined in Fig.1.2, for a single lap joint, the maximum secondary bending can be expressed as

$$M_x = PW = EI\frac{d^2w}{dx^2} \qquad \textbf{Equation 6-1}$$

By using computer techniques and introducing some assumptions, it is possible to determine the value of the bending. However, the calculated results can be very inaccurate due to the complex deformation and load transmission mechanisms of single lap joints. Secondary bending is mostly restricted to a very small region, where localised yielding occurs due to stress concentrations. The deformation and load transmission mechanisms are rather complicated and not amenable to calculation. Alternatively, an empirical measurement using a bending-strain gauge can be employed to determine the bending distribution. The problem with this approach is the fact that the cross-section of interest is usually accessible only from one side. Both of these methods for determining the secondary bending on riveted single lap joints have been examined by Schütz et al [36], who indicated that the results from the empirical measurement were more accurate than those obtained from the mathematical determination. Bending-strain gauges were therefore used in the present study to quantify the bending distribution in self-piercing riveted single lap joints.

The position where maximum bending occurs can only be accessed from one side since the other side is covered by the riveted sheet. Therefore, two bending-strain gauges were placed on the pierced sheet at each side of the rivet head, as shown in Fig.7.1 in order to obtain the most accurate results.

Two bending-strain gauges (FLA-6.350-11) with a length of 6mm and a gauge factor of 2.13±1% at 23°C were bonded on a clean surface of the pierced sheet at each side of the

rivet head, as shown in Fig.7.1. The gauge factor represents the percentage change in the electrical resistance of the wire and corresponds to a change of 2.13±1% in length.

After the strain gauges were bonded, they were then connected to a data logger. An Orion Delta 3530 Data logging system was used to record the resulting strains at 0.2 seconds intervals. Each specimen was placed in the tensile test rig and the strain gauges were calibrated to zero before commencement of the test. The data logger recorded the results for the strain in micrometers and the external load in kN. The tensile test rig used for the strain measurement was an Avery Denison tensile test rig with a load capacity of 500kN.

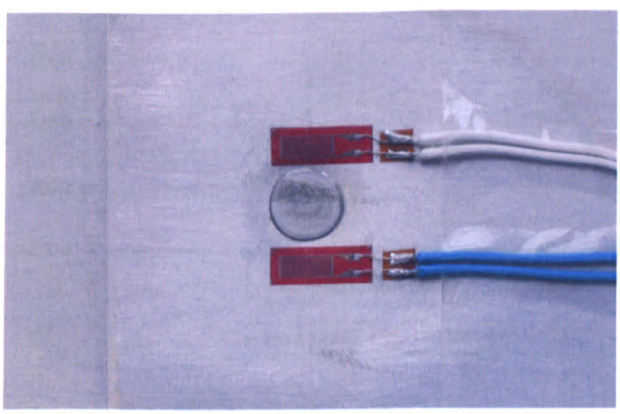

Figure 6.1: Positions of strain gauges

The rivet-bonding samples were produced in two stages. Both the pierced sheet and the locked sheet were cleaned with acetone to remove all traces of oil, grease and dirt at the overlap area. Araldite 420 A/B Aerospace Adhesives was then applied at the overlap area with a layer of adhesive 0.05 to 0.1mm thick. Curing was performed at room temperature for 24 hours under a 5kg load followed by treating at 70°C for 30 minutes. Riveting was then performed using the same setting parameters as for the fastenings without adhesive bonding. The geometry of the rivet-bonding samples was also the same as for the fastenings without adhesive bonding.

6.3 Results and Discussion

6.3.1 Bending Distribution of the FSN51 and the FSN56 Fastenings

Fig.7.2 shows the strain measurement results against the external load for the FSN51 and the FSN56 fastenings. The strain values of the FSN56 fastening were slightly higher than those of the FSN51 fastening.

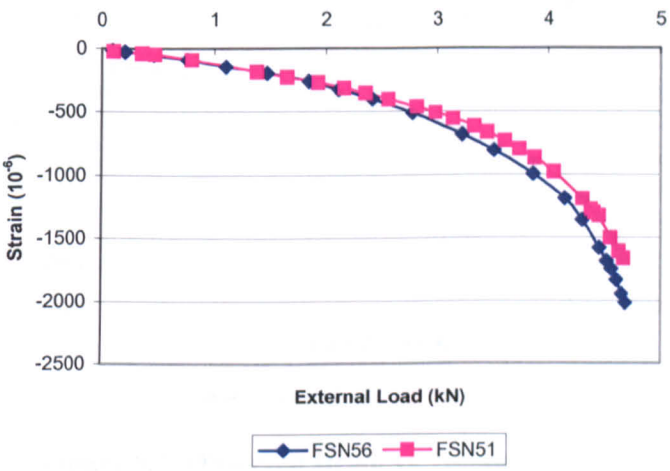

Figure 6.2: Strain gauge measurement results

The external loads can be converted to axial nominal stress, $\sigma_{nominal}$, by dividing by the gross cross-sectional area. At an external load of 4.5kN, the axial nominal stress was 46.9MPa for the FSN56 fastening and 37.5MPa for the FSN51 fastening which was larger in size. Based on these data, it is reasonable to assume that the sheet material is still within its elastic range. Therefore, the strain, $\varepsilon_{nominal}$, corresponding with the axial nominal stress could be calculated from equation 7.2:

$$\varepsilon_{nominal} = \frac{\sigma_{nominal}}{E} \qquad \textbf{Equation 6-2}$$

where E is the Young's Modulus of the sheet material. By using this equation, the nominal strain values were calculated and plotted in Fig.7.3 against the observed strain values. Under the axial nominal stress, the nominal strain value was positive. Under a combination

of the axial nominal stress and the secondary bending, the observed strain value changed from positive to negative leading to a compressive stress, which was imposed on the axial nominal stress. These results showed that the secondary bending compensated the positive strain value and resulted in a negative strain value. The difference between the nominal strain value and the observed strain value represents the strain that was caused by secondary bending and is shown in Fig.7.4. The bending strain value of the FSN56 fastening was slightly higher than that of the FSN51 fastening.

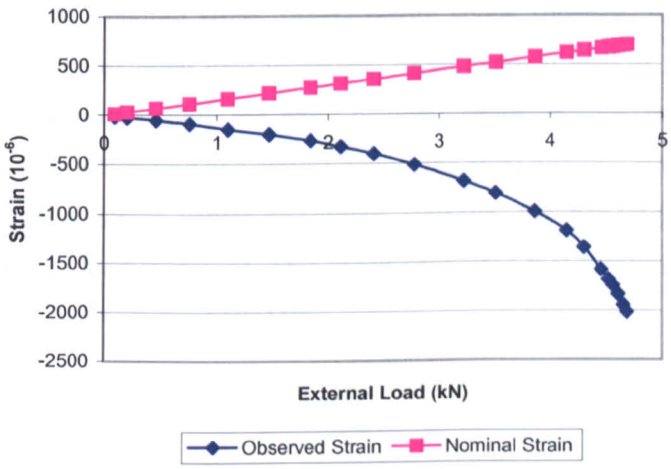

Figure 6.3: Observed strain vs. Nominal strain

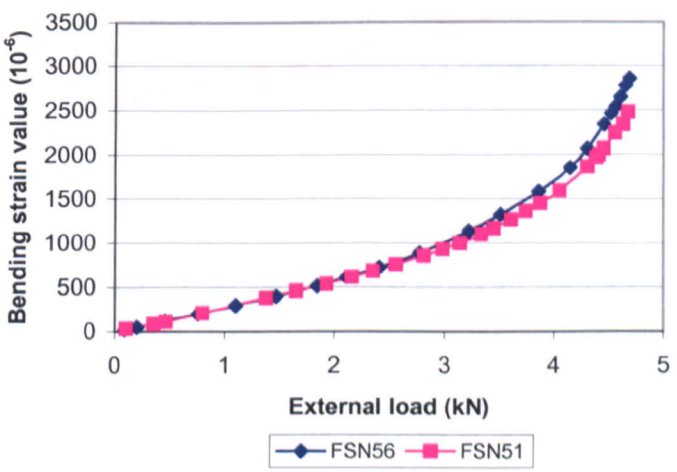

Figure 6.4: Secondary bending strain distribution

By using the bending strain values shown in Fig.7.4 and assuming elastic behaviour, the bending stress, $\sigma_{bending}$, can be calculated by using equation 7.3:

$$\sigma_{bending} = \varepsilon_{bending} \times E \qquad \textbf{Equation 6-3}$$

where $\varepsilon_{bending}$ is the bending strain. The bending distribution of the FSN51 fastening can then be presented by the axial nominal stress, $\sigma_{nominal}$, and the bending stress, $\sigma_{bending}$, against the external load, as shown in Fig.7.5. The bending stress was higher than the axial nominal stress. An extra stress was therefore imposed on the axial nominal stress due to secondary bending. At bending stress values below about 100MPa, the bending stress increased linearly as the external load increased. At an external load of 2kN, the bending stress, $\sigma_{bending}$, was almost double the axial nominal stress, $\sigma_{nominal}$, indicating that the imposed stress due to the bending had almost double the axial nominal stress, $\sigma_{nominal}$ at this load level. At bending stress values exceeding 100MPa, the bending stress increased sharply as the external load increased. This result suggested that localised yielding of the sheet material might occur at about 100MPa.

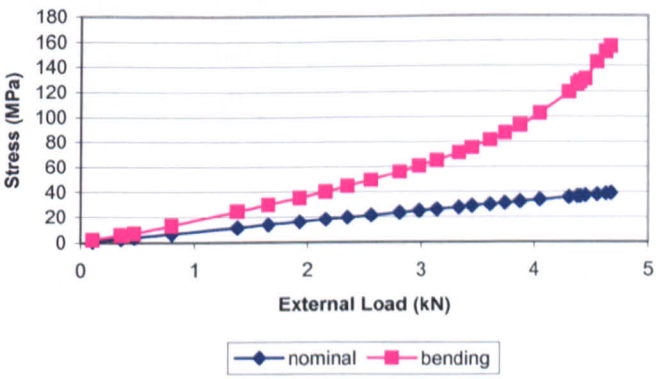

Figure 6.5: Bending stress and Nominal stress for the FSN51 fastening

Fig.7.6 shows the bending distribution for the FSN56 fastening. Similar to the FSN56 fastening, the bending stress, $\sigma_{bending}$, was greater than the axial nominal stress, $\sigma_{nominal}$ leading to an imposed stress on the sheet material. At bending stress values exceeding 100MPa, the bending stress increased sharply with the external load. This was the same

result as for the FSN51 fastening suggesting that localised yielding of the sheet material occurred at about 100MPa.

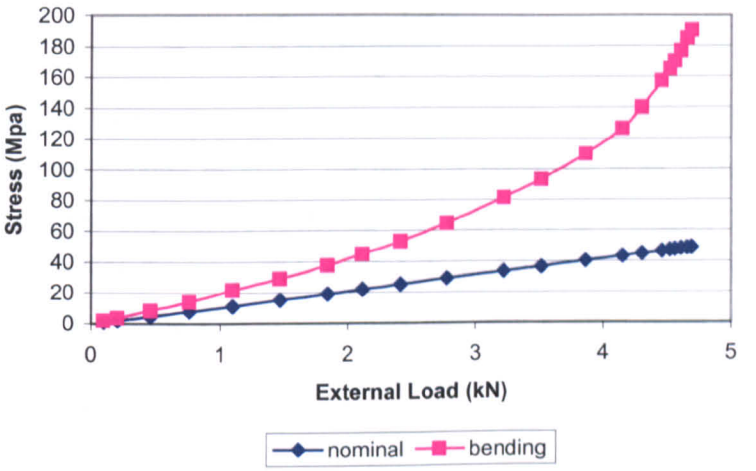

Figure 6.6: Bending stress and Nominal stress for the FSN56 fastening

Fig.7.7 shows the tensile test results of the sheet material used for the two fastenings. The result indicates that the yield stress of the sheet material was about 110MPa. This explains why localised yielding of the sheet material started to take place at about 100MPa, which is close to the yield stress of the sheet alloy.

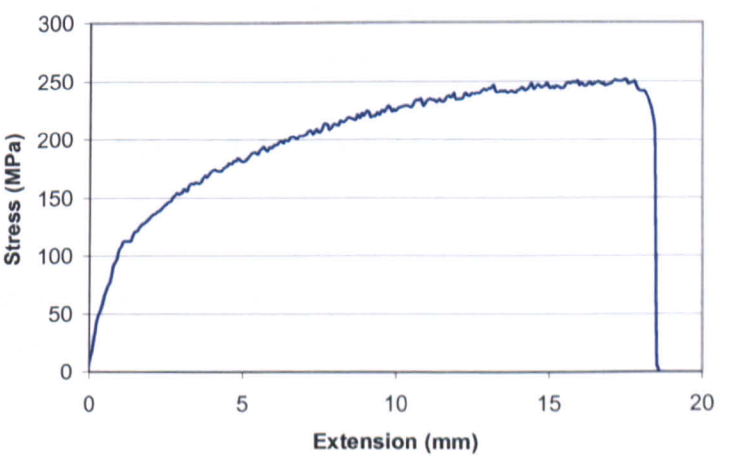

Figure 6.7: Tensile test results of NG 5754 sheet

Based on bending theory, the maximum bending moment about the z-axis, which resulted in the bending stress at the sheet with a rectangular-section, can be calculated by equation 7.4:

$$M_{\max} = \frac{\sigma I}{y} = \frac{\sigma_{bending} bt^2}{6} \qquad \textbf{Equation 6-4}$$

where ***b*** is the width of the sheet and ***t*** represents the thickness of the sheet. By using the above equation, the bending moments for the two fastenings were calculated and are shown in the Fig.7.8. The FSN56 fastening was subjected to a slightly lower bending moment than the FSN51 fastening. This result indicated that the specimen sizes that were used for the FSN51 and the FSN56 fastenings had only a small effect on the bending moment.

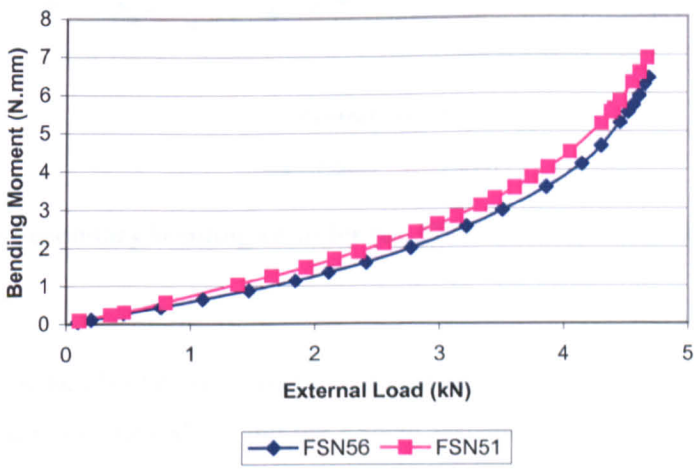

Figure 6.8: Maximum bending moment

The distribution of secondary bending can also be presented by the secondary bending ratio *k*, which is defined as

$$k = \frac{\sigma_{bending}}{\sigma_{nominal}} \qquad \textbf{Equation 6-5}$$

By using this equation, the secondary bending ratio for both the FSN56 and the FSN51 fastenings can be calculated and the results are shown in Fig.7.9. For instance, at an external load of 2kN, the axial stress of the FSN51 fastening is $\sigma_{nominal}=\frac{2000}{2\times 60}=16.67\,MPa$ and the bending stress is $\sigma_{bending}=\sigma_{nominal}\times k=16.67\times 2.1=35MPa$. By using the bending ratio, the bending stress can be calculated.

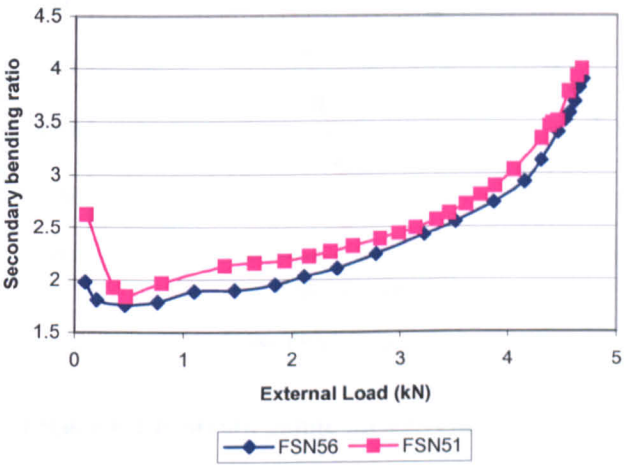

Figure 6.9: Secondary bending ratio for the FSN51 and the FSN56 fastenings

Fig.7.9 also shows the effect of specimen size on the secondary bending ratio. The slightly different ratios between the FSN51 and the FSN56 fastenings indicated that based on the fastening conditions, the specimen size had a little influence on the bending ratio of the fastenings. However, Schűtz et al [36] reported that a bigger overlap length was accompanied with a smaller bending ratio if the overlap length was the only variation between samples. In this case, the sample size of the FSN56 fastening differed not only in overlap length but also in specimen length and width which also affected the bending ratio. Therefore it is difficult to identify the major influential factors on the bending ratio for these two fastenings.

6.3.2 Bending Distribution of the FSA61* and the FSA64* Fastenings

The strain measurement results for the FSA61* and the FSA64* fastenings are shown in Fig.7.10. At an identical external load, the FSA64* fastening suffered more straining than the FSA61* fastening.

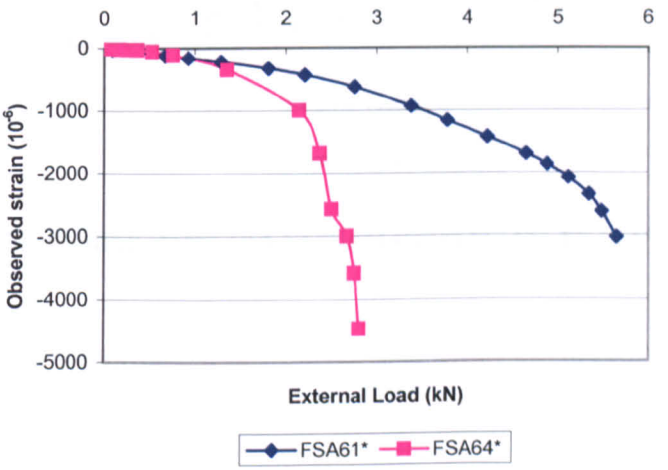

Figure 6.10: Strain gauge measurement results

By performing the same analysis and calculation as for the FSN51 and the FSN56 fastenings, the stresses acting on the pierced sheets due to the axial external load and the bending moment for the FSA61* are shown in Figs.7.11. The stress due to bending was much higher than that due to the axial load and the point where the bending stress increased sharply was about 200MPa. This value is approximately equal to the yield stress of the AA6111 alloy, as shown in Fig.7.12. This indicated that yielding of the sheet material would take place at that point.

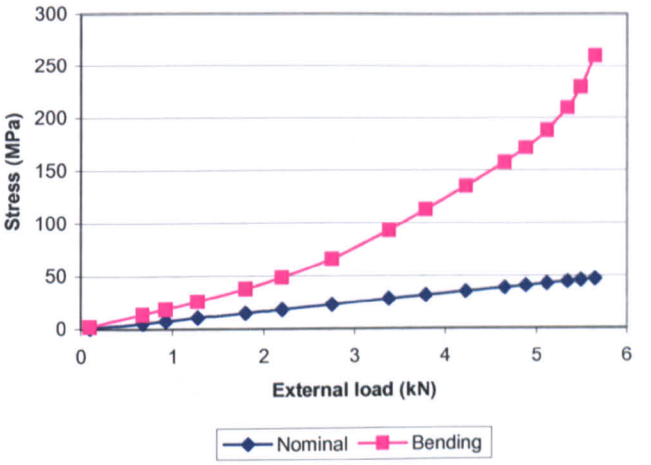

Figure 6.11: Bending stress and Nominal stress for the FSA61* fastening

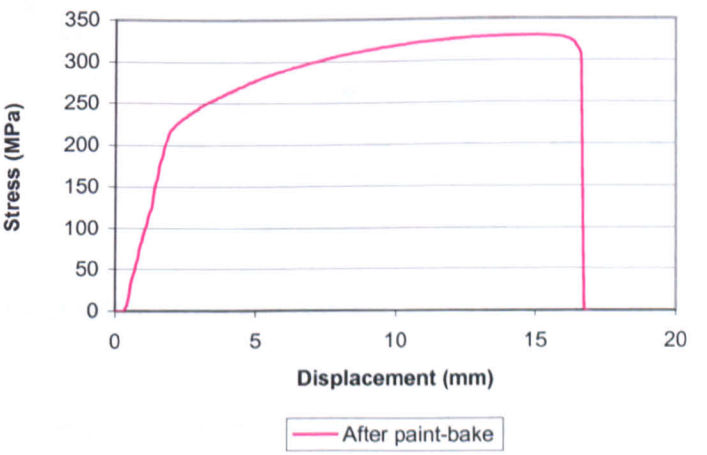

Figure 6.12: Tensile test result for the AA6111 sheet

Fig.7.13 shows the bending stress and the nominal stress for the FSA64* fastening. The bending stress increased sharply above 100MPa. This value is much lower than the yield point of the AA6111 alloy. The reason for this discrepancy was due to the effect of the thickness on the bending stress. In this case the bending stress is inversely proportional to the square of the thickness of the riveted sheet, as shown in equation 4.3. The FSA64*

fastening had a 0.9mm sheet thickness, whilst the other samples that were examined had a 2mm thickness. The square value of the 0.9 resulted in a rapid increase in the bending stress as the bending moment increased and this probably led to inefficient elastic behaviour. In addition, the average ultimate shear load for the FSA64* fastening was only 2.7kN. Therefore at an external load of 2.1kN, where a rapid increase in the bending stress started to take place, bearing of the 0.9mm sheet might have occurred due to the relative lower bearing resistance of the 0.9mm sheet. As a result, the point where the bending stress increased sharply was not the yield point of the sheet material. This observation also indicated that the sheet thickness had a significant effect on the bending distribution.

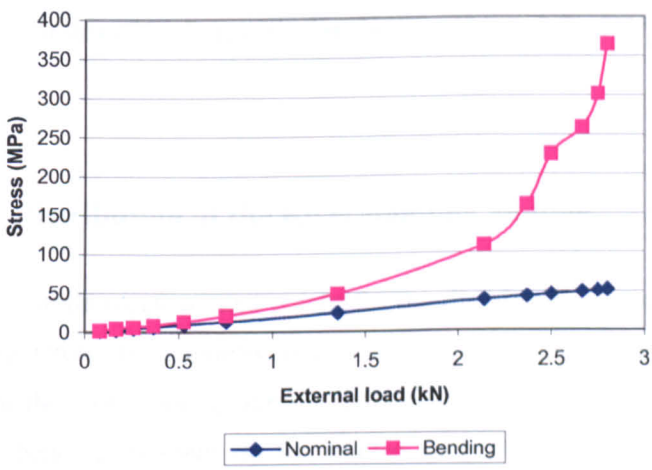

Figure 6.13: Bending stress and Nominal stress for the FSA64* fastening

The secondary bending ratio for the FSA61* and the FSA64* fastenings is shown in Fig.7.14. At an external load of 2.1kN, the bending stress was almost 2.5 times of the nominal stress for the FSA61* and the FSA64* fastenings. When above 2.1kN, due to inefficient elastic behaviour for the FSA64* fastening, the bending ratio shown in Fig.7.14 was probably not accurate enough. However, the effect of the increasing load on the bending ratio for the FSA64* fastening suggested that the sheet thickness had a significant effect on the bending distribution.

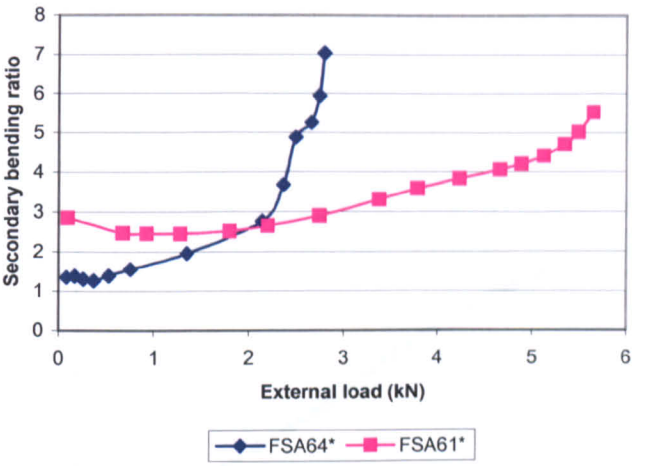

Figure 6.14: Secondary bending ratio for the FSA61* and the FSA64* fastenings

6.3.3 Bending Distribution of the Rivet-bonding Sample

Fig.7.15 shows the strain measurement results for the rivet-bonding sample which had the same riveting parameters and geometry as for the FSN51 fastening. Positive strain values were observed for the rivet-bonding sample indicating that the adhesive layer eliminated the effect of the bending moment on the riveted sheet. Under elastic assumption, the nominal strain values of the riveted sheet were calculated and compared with the observed strain values, as shown in Fig.7.16. The nominal strain value at each load was higher than the observed strain value indicating that the adhesive layer sustained not only the bending moment but also part of the external load leading to a smaller positive strain value for the riveted sheet.

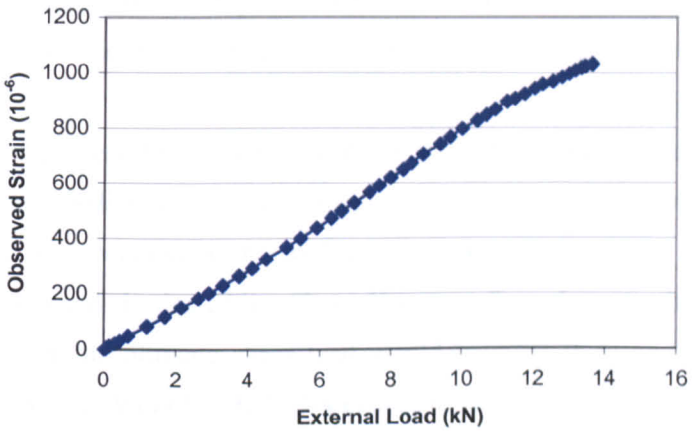

Figure 6.15: Strain measurement results for the rivet-bonding sample

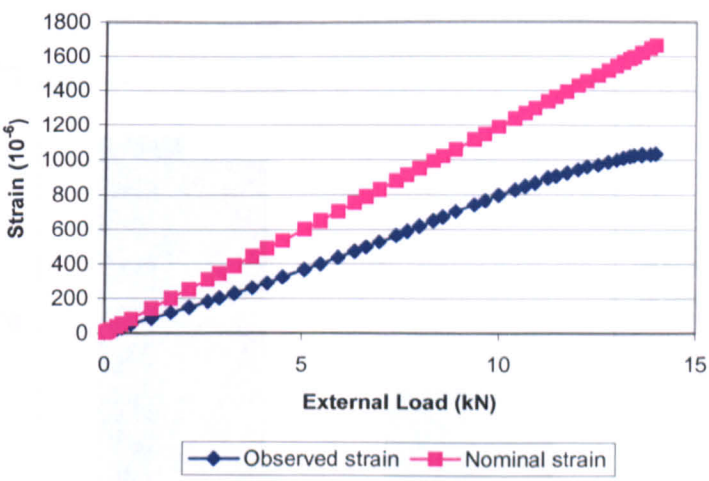

Figure 6.16: Observed strain vs. Nominal strain

6.4 Effect of Secondary Bending

As a result of the inherent eccentricity of the lap joints, secondary bending was induced. The secondary bending led to an additional axial stress acting on the sheet material discontinuities, whilst a tensile component was also introduced to the rivet. Consequently, the mechanical behaviour of the fastenings was affected by the secondary bending.

Fig.7.17 shows the shear test results for the FSN51 fastening and the rivet-bonding samples. The rivet-bonding samples exhibited much higher ultimate shear load than the FSN51 fastening. This was due to the application of the adhesive layer, which withstood the bending moment and eliminated its effects. However, from these results, it was difficult to conclude whether the ultimate shear load would increase if secondary bending was prevented or minimised. According to Kulak et al [34], the shear strength of a conventional riveted single lap joint was about 10% less than that for a symmetric butt-joint, which was formed using the same setting conditions. The design of a symmetric butt-joint is such that it eliminates secondary bending. It is therefore reasonable to assume that elimination of secondary bending could lead to a high ultimate shear load for a self-piercing riveted joint.

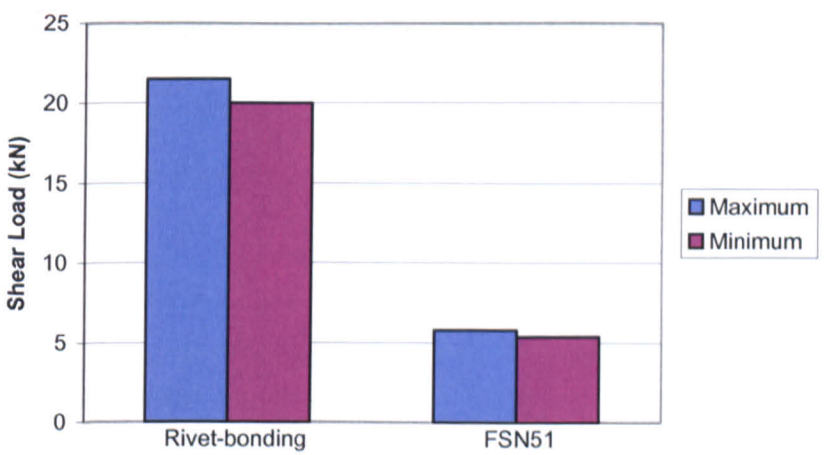

Figure 6.17: Shear test results for the rivet-bonding and the FSN51 samples

The failure mode that occurred during the shear testing of a self-piercing riveted sample was also affected by secondary bending. As discussed in Chapter 5, pull-out of the rivet was the only failure system for the shear tests. In addition to the effect of tilting of the rivet and yielding as well as bearing of the sheet material, the introduction of the additional secondary tensile component which acted on the rivet, facilitated the rivet pull-out leading to eventual failure of the fastenings. This behaviour was different from that for a conventional riveted joint. According to Kulak et al [34], for a conventional riveted lap joint, rivet fracture was the most likely failure system during shear testing. The secondary tensile component facilitated the fracture of the rivet rather than pull-out of the rivet due to the existence of a forged button on the lower sheet.

In addition to the effect of secondary bending on the shear behaviour, secondary bending also affected the fatigue behaviour. The additional secondary tensile component was believed to facilitate the fracture of the rivet. The additional axial bending stress combined with the nominal stress and resulted in high local stresses at areas of discontinuities of the sheet. This facilitated crack initiation and propagation within the sheet material. The higher bending stress that was suffered by the 0.9mm sheet due to the effect of the low thickness on the bending moment contributed to the fracture of the 0.9mm sheet at all applied loads during fatigue testing. The combination of the bending stress and the nominal stress contributed to the failure of the joints during fatigue testing. The bending stress therefore needed to be taken into account in order to understand the fatigue behaviour of samples.

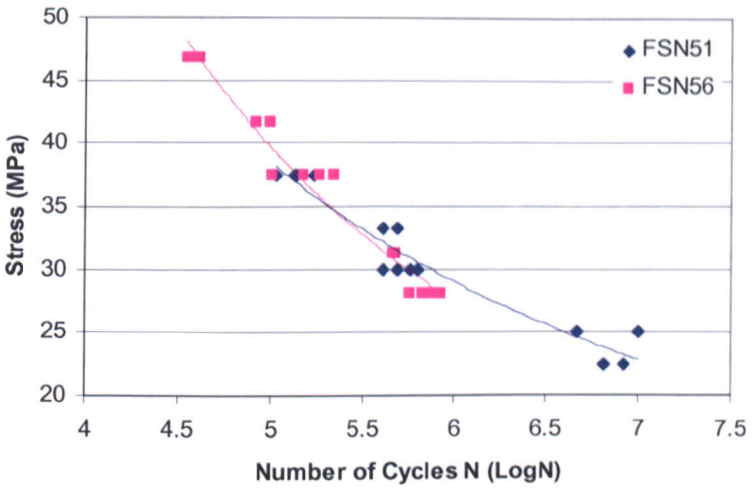

Figure 6.18: Fatigue strength of the FSN51 and the FSN56 fastenings

Fig.7.18 shows the fatigue strength of the FSN51 and the FSN56 fastenings using stress versus the number of cycles. The stress was obtained by using the maximum applied load divided by the gross area of the sheet and can be presented by the equation $\sigma_{nominal} = \frac{P}{A}$.

The actual stress of the critical area of the sheet material was a combination of the nominal stress and the bending stress and could be expressed as

$$\sigma_{combined} = \frac{P}{A} + \frac{My}{I} \qquad \textbf{Equation 6-6}$$

As discussed in section 7.3.1, the combined stress could also be obtained by using the equation,

$$\sigma_{combined} = \sigma_{nominal} + \sigma_{bending} = \sigma_{nominal}(1+k) \qquad \textbf{Equation 6-7}$$

From this equation, it was reasonable to predict that when considering the effect of secondary bending, the fatigue strength for a self-piercing riveted single lap joint was higher by (1+k) times. For example, at an external load of 2kN, the predicted fatigue strength for the FSN51 fastening would be

$$\sigma_{predicted} = \sigma_{combined} = \sigma_{nominal}(1+k) = \sigma_{nominal}(1+2.1) = 3.1\sigma_{nominal}$$

whilst for the FSN56 fastening,

$$\sigma_{predicted} = \sigma_{combined} = \sigma_{nominal}(1+k) = \sigma_{nominal}(1+2.0) = 3.0\sigma_{nominal}$$

The slightly higher bending ratio for the FSN51 fastening led to a higher fatigue strength value by taking secondary bending into consideration. Fig.7.19 shows the nominal stress and the predicted (combined) fatigue stress versus the number of cycles for the FSN51 and the FSN56 fastenings. It was suggested that the secondary bending led to a significant reduction in the fatigue strength depending on the magnitude of the secondary bending ratio.

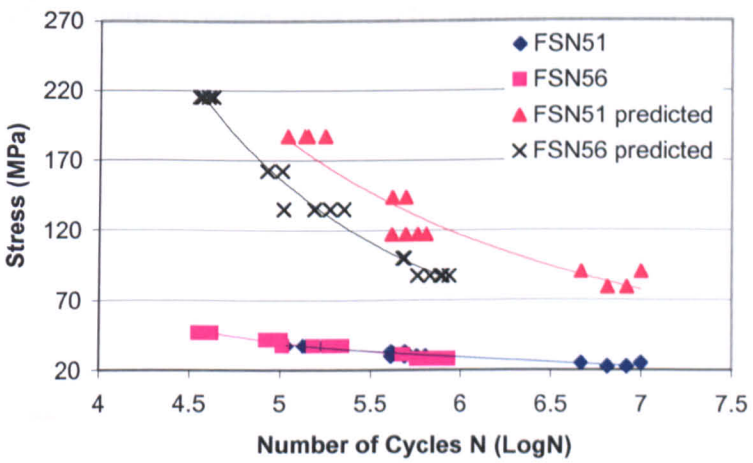

Figure 6.19: Fatigue strength presented by nominal stress and combined stress

By performing the same calculation as for the FSN51 and the FSN56 fastenings and considering the effect of secondary bending, the fatigue strength of the FSA61* and the FSA64* fastenings are presented in Fig.7.20. Since the nominal fatigue strength of the FSA64* fastening was calculated by using the maximum applied load divided by the gross area of the 0.9mm pierced sheet and taking into account the effect of the high bending ratio, a very high fatigue strength was predicted for the FSA64* fastening.

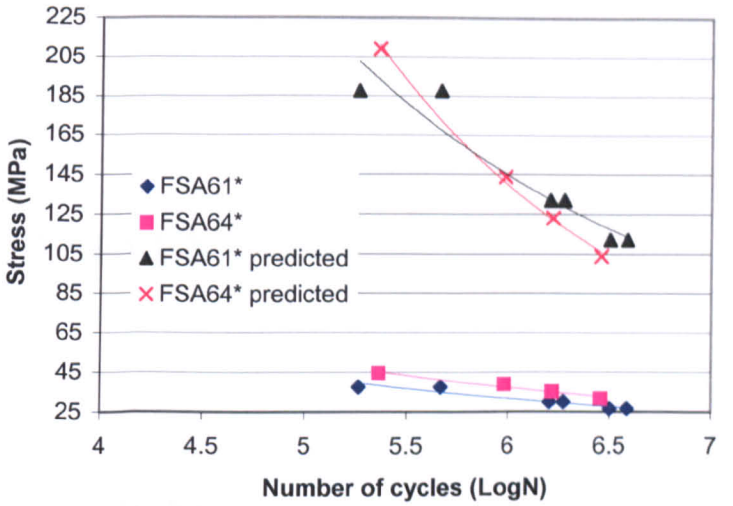

Figure 6.20: Fatigue strength presented by nominal stress and combined stress

CHAPTER SEVEN

7. CONCLUSIONS

7.1 Cross-sectional Deformation Characteristics

The cross-sectional deformation characteristics of the riveted joints were examined by standard optical and scanning electronic microscopy prior to testing. Based on this examination, the following conclusions can be drawn:

1. The processing conditions can be optimised to achieve good-quality joints.
2. Any variation in rivet geometry size, anvil profile and sheet thickness as well as the setting force will alter the joint quality and in turn affect the strength characteristics of the joints.
3. The change of the thickness combination from (1mm+2mm) to (2mm+1mm) will lead to a poor cross-sectional deformation of the joint.
4. The pre-straining levels of the 5754 alloy and the shelf-life time of the 6111 alloy do not affect the cross-sectional deformation characteristics significantly.
5. Identical setting parameters can be used to join the 5754 alloy sheet with up to 10% pre-straining and still achieve good-quality joints.
6. The AA6111 sheet can be joined satisfactorily after a shelf-life of 21 months by using the same setting parameters as for fresh AA6111.

7.2 Strength Characteristics

The strength of riveted joints was measured via standard shear, peel and fatigue tests and also by a specially developed pull-out test. The strength characteristics of riveted joints were thus identified.

The shear strength of the riveted joints of all the combinations examined in this study was mainly dependent on the clinch strength of the joint. The yield strength and bearing resistance of the sheet material also had an effect on the shear strength. In addition, the surface condition of the sheet material had an influence on the shear strength of the joints. The failure mechanism during the shear test was by pull-out of the rivet and was therefore dependent on the clinch strength. The clinch strength was related to the frictional force at the interface between the riveted sheets and the rivet shank as rivet pull-out was taking place. The high strength of the sheet material was accompanied with a high yield strength and bearing resistance and led to a high shear strength of the joints. Paint-baking reduced the shear strength of the joints by reducing the strength of the riveted 5754 sheet via recovery. Pre-straining increased the strength of the sheet material leading to an increase in the shear strength of the joints. A thinner sheet material and a shorter overlap length led to a reduction in the bearing resistance of the sheet material and this resulted in a reduction in the shear strength of the fastenings. The use of a shorter rivet was accompanied with a smaller contact area between the rivet shank and the riveted sheets and therefore at an identical contact pressure the frictional force at the interface was reduced leading to a decrease in the shear strength of the joints.

The peel strength of the riveted joints with a (2mm+2mm) thickness combination was dominated by the clinch strength. Therefore any factors that affected the clinch strength such as coefficient of friction, had an influence on the peel strength. For the joints with a (1mm+2mm)/(0.9mm+2mm) thickness combination, the peel strength was dependent on the strength of the thinner sheet rather than the clinch strength since the maximum bending stress was inversely proportional to the square of the sheet thickness in this case.

The pull-out test was developed specially for measuring the clinch strength of the joints and therefore the clinch strength governed the pull-out strength of the joints of all combinations examined in this study.

The fatigue strength of the joints of a (2mm+2mm) thickness combination was dominated by both the fatigue performance of the rivet and that of the sheet material adjacent to the rivet depending on the magnitude of the applied load. At high applied loads, the fatigue strength of the joints was mainly dependent on the performance of the rivet since fracture of the rivet dominated the failure mode. At low applied loads, the sheet material governed the fatigue strength of the joints since fatigue cracks of the riveted sheet led to failure of the joints. For the joints with a (1mm+2mm)/(0.9mm+2mm) combination, failure of the joints was due to fracture of the thinner sheet indicating that the behaviour of the thinner sheet dominated the fatigue strength of the joints. The fatigue strength of the joints was also affected by the interfacial condition between the two riveted sheets since any change to the interfacial conditions altered the load transfer mechanism. The lower frictional force at the interface between the two riveted sheets the greater the load sustained by the rivet leading to a reduction in the fatigue strength of the fastenings due to fracture of the rivet.

7.3 Failure Mechanisms

The failure mechanisms of the riveted joints during static and fatigue testing were examined. Three failure modes, designated as *rivet pull-out, rivet fracture* and *sheet material failure* were observed to occur in both types of test.

It was evident that pull-out of the rivet was the only failure system that occurred during the shear tests. The effect of secondary bending and tilting of the rivet were believed to contribute to the failure system, whilst yielding and bearing of the sheet material facilitated the pull-out of the rivet. During peel testing, the joints with a (2mm+2mm) combination failed by rivet pull-out since the 2mm pierced sheet was strong enough to sustain the peel load and therefore the peel load concentrated on the clinch leading to pull-out of the rivet. For the joints with a (1mm+2mm)/(0.9mm+2mm) combination, the 1mm/0.9mm pierced sheet peeled off around the rivet head and this was because the thinner sheet failed to

sustain the peel load due to a high stress concentration. The pull-out test was specially designed to measure the clinch strength of the joints and therefore pull-out of the rivet was the only failure system for all samples tested by this means.

The fatigue failure mechanisms were more complicated than those observed in the static tests. Fretting was observed to occur mainly at the interface between the two riveted sheets and at the interface between the rivet shank and the riveted sheet and played an important role in the fatigue failure mechanisms. Both *rivet fracture* and *sheet material failure* occurred in fatigue tests depending on the magnitude of the applied load as well as the fretting behaviour. For the joints with a (1mm+2mm)/(0.9mm+2mm) combination, fracture of the thinner sheet was the only failure system. This was attributed to the combined effect of the axial applied load and secondary bending, which superimposed an additional stress on the sheet material leading to fracture of the thinner sheet material. Fretting at the interface between the two riveted sheets led to initiation and early propagation of cracks and therefore facilitated the fracture of the thinner sheet. At high applied loads, the joints with a (2mm+2mm) thickness combination failed by fracture of the rivet shank with some deformation of both the riveted sheets taking place. At low applied loads, sheet material fracture dominated the failure system. At high applied loads, major slip was most likely to take place. As a result, the rivet sustained high shear and bearing stresses. At the same time, a high tensile stress also acted on the net-section of the riveted sheets. These factors contributed to the fracture of both the rivet and the riveted sheets. By contrast, at low applied loads, major slip was less likely to occur. Therefore, the applied load was mainly sustained by the frictional force at the interface between the two riveted sheets. Hence the load sustained by the rivet was lower and the sheet material became more critical. Fretting at the interface between the two riveted sheets and at the interface between the rivet shank and the riveted sheets contributed to the initiation and propagation of fatigue cracks within the riveted sheets. In addition, the deformation that occurred during the riveting process produced weak points around the buttonhole of the locked sheet. Fracture of the locked sheet at these points therefore occurred leading to eventual failure of the joints. This study also examined ways to prevent fretting by inserting a PTFE tape at the interface between the two riveted sheets. It was observed that the PTFE tape could reduce the fretting damage at the interface between the two riveted sheets. However, more fretting damage and fatigue damage occurred at the rivet leading to rivet fracture. This was attributed to the very low

coefficient of friction at the interface between the two riveted sheets, which led to a change in the load transfer mechanism of the riveted lap joint. In this case the rivet had to sustain a greater load and therefore failed. It was therefore concluded that reducing the frictional force at the interface between the two riveted sheets was not an effective way to improve the fatigue performance of self-piercing riveted joints.

7.4 Examination and Analysis of Secondary Bending

Secondary bending as an inherent feature of single lap joints has been examined and analysed in this study. The distribution of secondary bending for the riveted joints was determined by means of strain measurement. Based on the experimental results and analysis, the following conclusions can be drawn:

1. A self-piercing riveted single lap joint has a very high secondary bending ratio.
2. The thickness of the riveted sheet had a significant effect on the distribution of secondary bending. This was probably due to the fact that the bending stress was inversely proportional to the square of the thickness.
3. Rivet-bonding can prevent secondary bending because the adhesive bond eliminated the effect of secondary bending by sustaining the bending moment and part of the external load.
4. Secondary bending had a significant influence on the mechanical behaviour and in particular on the fatigue strength of self-piercing riveted single lap joints by introducing an additional axial stress on the riveted sheet and an additional tensile component on the rivet.

CHAPTER EIGHT

8. RECOMMENDATIONS FOR FURTHER WORK

Based on the knowledge gained during the project, the following five principal areas of work could be further explored in order to extend the current understanding of the mechanical behaviour of self-piercing riveted joints:

1. Further analysis of the fretting behaviour. The effect of fretting on the crash behaviour will certainly be of interest. The fretting behaviour of the fastenings that join sheets of different hardness values should also be considered.
2. Simulation of the behaviour of self-piercing riveted joints by means of finite element analysis.
3. Investigation of the behaviour of multi-riveted samples. Of particular interest would be the examination of the effect of rivet-pitch on the mechanical properties of joints.
4. Further examination of secondary bending in order to enable an accurate prediction of its magnitude and its effect on the fatigue strength of self-piercing riveted joints.
5. Investigation of the behaviour of rivet-bonding joints.

8.1 Further Analysis of Fretting Behaviour

During the current study, fretting has been observed to play an important role during fatigue failure. According to Waterhouse [53], the effect of fretting on the initiation and

propagation of fatigue cracks leads to a reduction of fatigue strength. The current project has shown that the presence of a wax-based solid lubricant at the interface between the two riveted sheets can delay the onset of fretting and extend the fatigue life. However, it was also evident that the reduction of fretting at the interface between the two riveted sheets by inserting a PTFE layer led to a reduction of the fatigue strength of the joints. The reason was because the inserted PTFE tape led to a change in the load transfer mechanism. Therefore the effect of fretting needs to be investigated further. The study has shown that reducing the coefficient of friction at the interface between the two riveted sheets will not necessarily improve the fatigue performance. Further work is required to establish the effect of the coefficient of friction and of different coatings on the fretting behaviour. In addition, the current project has also shown that fretting led to an increase in the hardness of the riveted sheets and to crack initiation. It is therefore important to examine the effect of these factors on the crashworthiness of joints and in turn on car passenger safety.

Results from the current project have indicated that fretting leads to work hardening which in turn changes the hardness of the riveted sheets. Both work hardening and the hardness of the riveted sheets can affect the fretting behaviour of the joints. Further examination on the effect of hardness on the fretting behaviour of the joints and in particular, of joints between sheets of different hardness values, is recommended.

8.2 Simulation of the Behaviour of Self-piercing Riveted Joints

During the current study, it was attempted to simulate the deformation behaviour of a self-piercing riveted lap joint under shear loading by using ANSYS, a finite element analysis software package. Fig.8.1 shows the deformation results. The effect of secondary bending on the deformation behaviour is clearly shown in the figure. Although this part of the work was not one of the objectives of the current project, the preliminary results have shown the potential of simulating the behaviour of self-piercing riveted joints using the finite element method. In the case of joints, the main features to be modelled are the amount of load transferred by the fastener and the amount of secondary bending of the joint. There is currently very little data available on these values in real-life structures and in particular on self-piercing riveted joints. Therefore a definite scope exists for further research in

developing a valid finite element method to simulate the behaviour of self-piercing riveted joints for commercial use. However, due to the unusual configuration of the fastener, the modelling process will not be easy. In addition, the contact between two components of the joints needs to be taken into account in order to simulate the fretting behaviour and this will make the simulation even more difficult. Coupled with the consideration of the effect of secondary bending, the simulation process will certainly be a challenge.

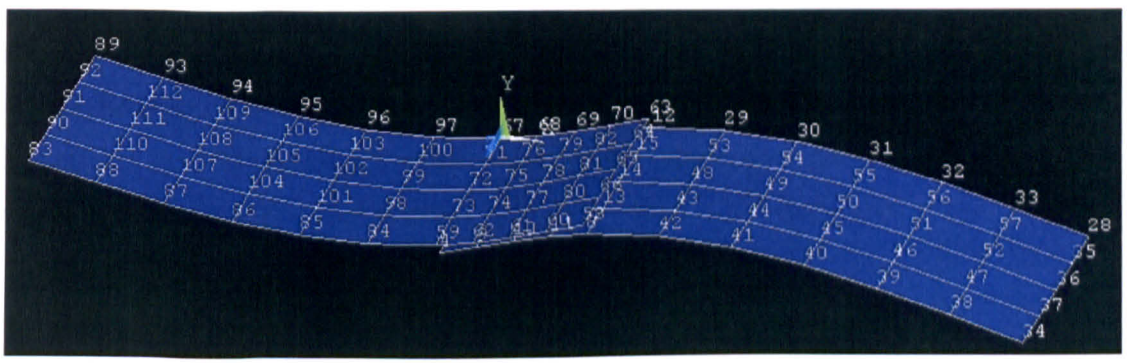

Figure 8.1: Simulation of the deformation behaviour of a self-piercing riveted joint

8.3 Investigation of Multi-riveted Joint Behaviour

This study has focussed on the behaviour of self-piercing riveted single lap joints. It is necessary to extend this to multiple-joint samples to gain a better understanding of the performance of self-piercing riveted structures. One of the primary influences of the behaviour of multiple-joint samples is the rivet-pitch and this therefore needs to be examined. In addition, secondary bending varies with specimen configuration and will probably be affected by the rivet-pitch.

8.4 Further Examination on Secondary Bending

Secondary bending has been examined and analysed for single riveted lap joints during this study. Since secondary bending is affected by many factors such as overlap length and sheet thickness, it is important to have a good understanding of the effect of these influential factors. In addition, a method to predict the fatigue strength by taking

consideration of the effect of secondary bending has been introduced. However, there are no experimental results to support this prediction. Therefore further experimental work is necessary to obtain data in order to understand the behaviour of secondary bending and its effect on the fatigue strength of self-piercing riveted joints.

8.5 Investigation of Rivet-bonding Joints Behaviour

During the current project, rivet-bonding samples were used in the examination of secondary bending. It was observed that rivet-bonding can eliminate secondary bending and its effects. As rivet-bonding joints are used by the automotive industry, it is therefore important to investigate their behaviour.

As a relatively new joining method, self-piercing riveting is still being developed. There are certainly many areas that can be developed further in the near future. One important area is to develop aluminium alloy rivets. This will eliminate galvanic corrosion that may occur between the steel rivet and the aluminium sheet and will also be beneficial to recycling. Another important area is the development of Non-Destructive Test (NDT). This can be coupled with the process monitoring system that has already been developed to make self-piercing riveting more reliable, more practical and more attractive.

CHAPTER NINE

9. REFERENCES

1. Polmear. I. J, "*Light alloys*", Third edition, Edward Arnold, 1995.
2. Patrick. E. P, Auhl. J. R and Sun. T. S, "*Understanding the process mechanisms is key to reliable resistance spot welding aluminium auto body components*", SAE Technical Paper, 840291, 1984.
3. Auhl. J. R and Patrick. E. P, "*A fresh look at resistance spot welding of aluminium automotive components*", SAE Technical Paper, 940160, 1994.
4. Gingell. A. B. D and Gooch. T. G, "*Review of factors influencing porosity in aluminium arc welds*", TWI Report, 625/1997.
5. Barnes. T. A and Pashby. I. R, "*Joining techniques for aluminium spaceframes used in automobiles, Part I – solid and liquid phase welding*", Journal of Materials Processing Technology, 99, p62-71, 2000.
6. Jones. L, "*Laser make advances in welding of automotive aluminium alloys*", TWI Bulletin 2 March, 1995.
7. Jones. I. A and Yoon. S. T and Wallach. E. R, "*laser welding of aluminium alloys*", TWI, Ref. 7241.01/95/848.3, 1995.
8. Kallee. S. W and Nicholas. E. D, "*Application of friction stir welding to lightweight vehicles*", SEA Technical Paper, 982362, 1998.
9. Waldron. D. J, Roberts. R. W, Dawes. C. J, Tubby. P. J, "*Friction stir welding-A revolutionary new joining method*", SAE Technical Paper, 982149, 1998.
10. Kallee. S. W, Thomas. W. M and Nicholas. E. D, "*Friction stir welding of lightweight materials*", International conference on magnesium alloys and their applications, 26-28 September, 2000, Munich.

11. Powell. H. J and Wiemer. K, "*Joining technology for high volume manufacturing of lightweight vehicle structures*", TWI, 1999.
http://stella.grantpark.com/joints_044/restricted/band_8/sphjpjune96.html
12. Tavakoli. S. M, "*Durability of structural adhesives and adhesively bonded joints and mechanisms of environmental attack - A review*", TWI, 1993.
13. Barnes. T. A and Pashby. I. R, "*Joining techniques for aluminium spaceframes used in automobiles, Part II – adhesive bonding and mechanical fasteners*", Journal of Materials Processing Technology, 99, p72-79, 2000.
14. Riches. S. T, Westgate. S. A, Nicholas. E. D and Powell. H. J, "*Advanced joining technologies for lightweight vehicle manufacture*", Materials for low weight vehicles, 24-25 November, 1995, UK.
15. Westgate. S. A, Doo. R, Liebrecht. F, Braeunling. S, Mattssin. T and Stromberg. K-O, "*The development of lightweight self-piercing riveting equipment*", SAE World Congress Detroit, March 5-8, 2001, Michigan.
16. Howard. R. M and Sunday. S. P, "*The corrosion performance of steel self-piercing rivets when used with aluminium components*", SAE Technical Paper, 831816, 1983.
17. Sunday. S. P, "*Self-piercing rivets for aluminium components*", SAE Technical Paper, 830526, 1983.
18. Patrick. E. P and Sharp. M. L, "*Joining aluminium auto body structure*", SAE Technical Paper, 920282, 1992.
19. Martukanitz. R. P, Smith. D. J, Baldantonl. A, and Plckering. E. R, "*Laser beam welding of aluminium alloys for automotive applications*", SAE Technical Paper, 940158, 1994.
20. Matsumoto. T and Lzuchi. S, "*Laser welding of aluminium alloy plate extrusion and casting*", SAE Technical Paper, 960160, 1996.
21. Larsson. J. K and Hanicke. L, "*Multi-materials application with integrated joining technologies in the new Volvo S80*", SAE Technical Paper, 1999-01-3147, 1999.
22. King. R. P, "*Analysis and quality monitoring self-pierce riveting process*", PhD dissertation, University of Hertfordshire, 1997.
23. Lapensee. M, "*No hole riveting*", Business News Publishing Company, May 2000.

24. Razmjoo. G. R and S Westgate. A, "*Fatigue properties of clinched, self-piercing riveted and spot welded joints in steel and aluminium alloy sheet*", TWI Report, 680/1999.

25. Olivier. C. A, "*Comparison of static properties of point and hybrid joints in steel sheets*", TWI Report, 695/2000.

26. Westgate. S. A and Razmjoo. G. R, "*Static and fatigue performance of mechanically fastened and hybrid joints in sheet metals*", TWI Report, 691/1999.

27. Krause. A. R and Chernenkoff. R. A, "*A comparative study of the fatigue behaviour of spot welded and mechanically fastened aluminium joints*", SEA Technical Paper, 950710, 1995.

28. Booth. G. S, Olivier. C. A and Westgate. S. A, Liebrecht. F and Braunling. S, "*Self-piercing riveted joints and resistance spot welded joints in steel and aluminium*", SAE Technical Paper, 2000-01-2681, 2000.

29. Fu. M and Mallick. P. K, "*Effect of process variables on the static and fatigue properties of self-piercing riveted joints in aluminium alloy 5754*" SAE paper, No. 0825 2001:117, 2001.

30. Fu. M and Mallick. P. K, "Fatigue of self-piercing riveted joints in aluminium alloy 6111", International Journal of Fatigue, 25, p183-189, 2002.

31. Mackenzie. A, "Charge of the light brigade", AI Online, May 2000.

32. Sibley. M, "*Quick-fix solutions*", Professional Engineering, October, 1997.

33. Bonde. N and Grange-Jansson. S, "*Self-piercing riveting in high strength steel – A way to increase fatigue life*", Advanced Technologies & Process, IBEC conference 25, p16-20, 1996.

34. Kulak. G. L, Fisher. J. W and Struik. J. H. A, "*Guide to design criteria for bolted and riveted joints*", Second Edition, John Wiley & Sons, Inc., ISBN 0-471-83791-1, 1987.

35. Hartman. A and Schijve. J, "*The effect of secondary bending on the fatigue strength of 2024-T3 Alclad riveted joints*", National Aerospace Lab. NLR, Report TR69116, Amsterdam, 1969.

36. Schűtz. D and Lowak. H, "The effect of secondary bending on the fatigue strength of joints", Royal Aircraft Establishment, Library translation 1858, 1974.

37. Carr. R, Keyte. R, Browne. D and Ricksm. R. A, "*An assessment of the "H" test specimen as a possible screening geometry for different joining methods, such as adhesive bonding*", Advanced Technologies and Processes, IBEC, 1997.

38. Iyer. K, "*Contribution of fretting to the fatigue and corrosive deterioration of a riveted lap joint*", Structural integrity in ageing aircraft, ASME AD-Vol. p47-60, 1995.

39. Szolwinski. M. P, "*Linking riveting process parameters to the fatigue performance of riveted aircraft structures*", Aircraft, 37jve, 2000.

40. Schijve. J, "*Multiple-site-damage fatigue of riveted joints*" Atlanta Technology Publications ISBN 0-9613474-6-5, 1992.

41. Draft International Standards, Resistance spot welding – "*Destructive tests of welds – method for the fatigue testing of spot welded joints*".

42. Bowden. F. P and Tabor. D, "*The friction and lubrication of solids*", Oxford University Press, Oxford, 1954.

43. Waterhouse. R. B, "*Fretting wear*" ASM Metals handbook No.18, p242-255, 1992.

44. Hogmark. S, Vingsbo. O and Fridstrom. S, "Mechanism of dry wear of some martensitic steel, wear, 31, p39-48, 1975.

45. Iyer. K, Rubin. C. A and Hahn. G. T, "*Three-Dimensional analysis of single rivet-row lap joints – part 1: Elastic response*", Recent Advances in Solids and Structures, ASME PVP-Vol. p398-501, 1999.

46. O'Connor. J. J, "*The role of elastic stress analysis in the interpretation of fretting fatigue failures*" Fretting Fatigue, Waterhouse R. B editor, Applied Science, London, ISBN 0-85334-932-0, p23-40, 1981.

47. Endo. K and Goto. H, "*Initiation and propagation of fretting fatigue cracks*", Wear, 38, p311-322, 1976.

48. Endo. K, "*Practical observations of initiation and propagation of fretting fatigue cracks*", Fretting Fatigue RB Waterhouse editor, Applied Science, London, ISBN 0-85334-932-0, p127-135, 1981.

49. Hurricks. P. L, "*The mechanism of fretting – A review*", Wear, 15, p389-409, 1970.

50. Godet. M, "*The third-body approach: A mechanical view of wear*", Wear, 100 p437-452, 1984.

51. Mindlin. R. D, "Compliance of elastic bodies in contact", J. Appl. Mech. (Trans. ASTM, Series E), 16, p259-278, 1949.

52. Forsyth. P. J. E, "*Occurrence of fretting fatigue in practice*", *In* Waterhouse. R.B, ed. *Fretting Fatigue*, Applied Science, London, ISBN 0-85334-932-0, p99-111, 1981.

53. Waterhouse. R. B, "*Theories of fretting processes*", In Waterhouse. R.B, ed. *Fretting Fatigue*, Applied Science, London, ISBN 0-85334-932-0, p203-219, 1981.

54. Alaham. D and Warburton. J, "The unlubricated fretting wear of mild steel in air", Wear, 106, p177-201, 1985.

LIST OF PUBLICATIONS

1. **L. Han, J. M. O'Sullivan, Y. K. Chen, A. Chrysanthou,** *"Failure in self-piercing riveted joints under dynamic loading"*, 18th National Conference on Manufacturing Research, September 2002, ISBN1860583784, pp527-531.
2. **L. Han, Y. K. Chen, A. Chrysanthou, J. M. O'Sullivan,** *"Self-pierce riveting – A new way for joining structures"*, ASME 2002, PVP-Vol. 446-2, pp123-127.
3. **L. Han, Y. K. Chen, A. Chrysanthou, J. M. O'Sullivan,** *"The influence of paint-bake cycle on the mechanical behaviour of self-piercing riveted aluminium alloy joints"*, The 10th International Conference on Sheet Metal 2003, Belfast, 14-16 April, pp412-419, ISBN 1859231713.
4. **Y. K. Chen, L. Han, A. Chrysanthou, J. M. O'Sullivan,** *"Fretting in self-piercing riveted aluminium alloy sheets"*, Wear 255(2003) 1463-1470.
5. **L. Han, Y. K. Chen, A. Chrysanthou, J. M. O'Sullivan,** *"Fretting behaviour of self-piercing riveted aluminum alloy joints under different interface conditions"*, Accepted by the STLE/ASME International Tribology Conference, Florida, 27-29 October. 2003.
6. **L. Han, Y. K. Chen, A. Chrysanthou, J. M. O'Sullivan,** *"Fretting behaviour of self-piercing riveted aluminum alloy joints under different interface conditions"*, Submitted to Transactions of the ASME, Journal of Tribology.

APPENDIX

List of Tables

List of Figures

APPENDIX A: DATA TABLE

Table A- 1: Shear test results for the FSN5 series of fastenings **Units: kN**

Code \ Test number	1	2	3	4	5	6	7	8
FSN51	5.6	5.6	5.7	5.5	5.7	5.7	5.6	5.9
FSN51*	4.5	4.6	4.7	4.6				
FSN52	3.4	3.7	3.6	3.5				
FSN53	2.7	2.8	2.7	2.8				
FSN53*	2.6	2.5	2.7	2.5				
FSN55	1	0.9	0.8	1				
FSN56	5.2	5.4	5.5	5.1				
Rivet-bonding	21	20.6	20	21.5				

Table A- 2: Peel test results for the FSN5 series of fastenings **Units: kN**

Code \ Test number	1	2	3	4	5	6	7	8
FSN51	2	1.9	2	2.2	2.2	2.1	2.1	2
FSN52	1.3	1.2	1.4	1.2				
FSN53	0.7	0.6	0.7	0.7				
FSN53*	0.5	0.6	0.6	0.6				
FSN55	0.1	0.1	0.1	0.1				

Table A- 3: Pull-out test results for the FSN5 series of fastenings **Units: kN**

Test number / Code	1	2	3	4
FSN51	3.6	3.5	3.9	3.7
FSN52	2.3	2.3	2.2	2.2
FSN53	2	2	2	1.9
FSN53*	2	2	1.9	2

Table A- 4: Fatigue test results for the FSN5 series of fastenings (Number of cycles)

Applied Load (kN)	Number of Cycles				
FSN51 Fastening					
4.5 - 0.5	139200	173200	107300	133800	135800
4.0 - 0.5	412050	489140	402540		
3.6 - 0.5	489300	636700	570300	411500	920870
3.0 - 0.5	4140310	9940420	2634340		
2.7 - 0.5	6983250	6663470	8325100	10552000	10098200

	FSN51* Fastening		FSN52 Fastening
4.5 - 0.5	138650	136790	
3.6 - 0.5	478900	467660	
3.2 - 0.5			927850
3.0 - 0.5	5671720	3360970	1087740
2.7 - 0.5			1654660
2.5 - 0.5			5322680
2.2 - 0.5			16234100

	FSN53 Fastening	FSN53* Fastening
2.6 - 0.5	95170	93870
2.4 - 0.5	307460	
2.2 - 0.5	970440	376030
2.0 - 0.5	1127110	920350
1.7 - 0.5	3820170	3296250

FSN56 Fastening					
4.5 - 0.5	36690	41600	35180	39400	35940
4.0 - 0.5	83440	100660			
3.6 - 0.5	102590	152180	151930	220882	184720
3.0 - 0.5	482750	472120			
2.7 - 0.5	853630	766110	570580	783420	670490

Table A- 5: Shear test results for the FSH5 series of fastenings **Units: kN**

Test number / Code	1	2	3	4
FSH51	6.1	6.2	6.4	6.6
FSH52	5.3	5.0	5.2	5.3

Table A- 6: Fatigue test results for the FSH5 series of fastenings (Number of cycles)

Applied Load (kN)	Number of Cycles					
	FSH51 Fastening	FSH52 Fastening				
5.0 – 0.5	58860					
4.5 - 0.5	101140	123890	97890	98550	112180	101560
4.0 - 0.5	215060	118640	187060			
3.6 - 0.5	573660	257550	320190	323270	272850	251600
3.0 - 0.5	1208920	1148210	664430			
2.7 - 0.5	3751210	1532930	1736180	1765630	2479100	3292360

Table A- 7: Shear test results for the FSA6 series of fastenings **Units: kN**

Test number / Code	1	2	3	4
FSA61*	6	6.2	6.4	
FSA62	6.2	6.2	6.1	6.1
FSA62*	5.8	5.9	5.8	5.8
FSA63*	6	5.8	6.1	6.4
FSA64*	2.6	2.8	2.9	
FSA65*	2.5	2.6	2.5	2.5
FSA66*	2.4	2.5	2.4	2.4

Table A- 8: Peel test results for the FSA6 series of fastenings **Units: kN**

Test number / Code	1	2	3	4
FSA61*	1.5	1.5	1.6	
FSA62	2.1	1.9	2	
FSA62*	1.7	1.8	1.7	
FSA63*	1.5	1.4	1.4	1.4
FSA64*	0.5	0.5	0.6	0.6
FSA65*	0.6	0.6	0.6	0.6
FSA66*	0.6	0.6	0.5	0.6

Table A- 9: Pull-out test results for the FSA6 series of fastenings **Units: kN**

Test number / Code	1	2	3	4
FSA61*	2.8	3.3	2.9	3.0
FSA62	3.61	3.48	3.68	3.48
FSA62*	2.96	3.03	3.15	3.2
FSA63*	3.5	3.1	3.5	3.5
FSA64*	2.2	2.1	2	2.2
FSA65*	2.32	2.24	1.94	2.72
FSA66*	2.49	2.18	2	2

Table A- 10: Fatigue test results for the FSA6 series of fastenings (Number of cycles)

Applied Load (kN)	Number of Cycles		
FSA61* Fastening			
4.5 - 0.5	464280	183870	
3.6 - 0.5	1596550	1872160	
3.2 - 0.5	3853570	3151960	
	FSA62 Fastening	**FSA62* Fastening**	**FSA63* Fastening**
5.0 - 0.5	92760	134740	81210
4.5 - 0.5	168560	230570	138200
4.0 - 0.5	421200	346130	
3.6 - 0.5	995690	969300	616240
3.2 - 0.5	1813990	3032580	3660010
	FSA64* Fastening	**FSA65* Fastening**	**FSA66* Fastening**
2.4 - 0.5	231630	202720	305290
2.3 - 0.5		425300	
2.1 - 0.5	959680	575740	693300
1.9 - 0.5	1651540	1052840	1306270
1.7 - 0.5	2851920	2165110	2764520

Table A- 11: Shear test results for the FSP5 series of fastenings **Units: kN**

Test number / Code	1	2	3
FSP50	5.4	5.7	5.8
FSP53	5.4	5.7	5.9
FSP55	5.7	5.7	5.8
FSP510	5.7	5.7	6.1
FSP50*	4.5	4.6	4.7
FSP53*	4.5	4.9	5.2
FSP55*	4.7	5.1	5.1
FSP510*	5.1	5.1	5.2

Table A- 12: Fatigue test results for the FSP5 series of fastenings (Number of cycles)

Applied Load (kN)	Number of Cycles					
	FSP53 Fastening		**FSP55 Fastening**		**FSP510 Fastening**	
4.5 - 0.5	224770	334220	330510	342800	344130	321210
3.6 - 0.5	1525860	1502330	2080450	1987970	3059430	3122140
3.2 - 0.5	3289390		5484330			
3.0 - 0.5	8691810		10600000		7139030	11022480
	FSP53* Fastening		**FSP55* Fastening**		**FSP510* Fastening**	
4.5 - 0.5	154800	148280	139510	178140	316590	235370
3.6 - 0.5	1005830	955660	1059456	1401050	1112860	1052200
3.0 - 0.5	1815350	2528380	1770170	2312500	2176160	1629420

APPENDIX

B: WEIBULL ANALYSIS OF FATIGUE DATA

B.1 Aims of the statistical analysis

In view of the large scatter in fatigue data, a single observed value is not reliable and therefore, repeating the fatigue test a number of times under identical conditions is required. However, this is usually difficult not only because fatigue tests are expensive and time consuming, but also because the data will differ from test to test even under uniform test conditions. Therefore a single set of co-ordinates has to be defined by means of its reliability distribution. Statistical analysis estimating the properties of the joints has thus to be introduced in the analysis of fatigue data.

There are a number of statistical methods that may be used to describe a scattered data distribution measured in a set of experiments. The results obtained from different methods might vary depending on the focus of the method. As a feature of statistical analysis, the accuracy of the results that strongly depend on the number of samples might also alter from one method to another. The Weibull distribution is one of the statistical methods in reliability engineering. It was originally designed to analyse the yield strength of steel alloys [1] and therefore it is most widely used in this kind of analysis. Weibull analysis can also be used to analyse the fatigue behaviour in various conditions [2, 3], but it requires considerable use of engineering judgment for meaningful application.

The purpose of using statistical analysis is to determine the reliability of fatigue life measurement and failure mechanisms and therefore provide a basis for comparing different designs and choosing the best design from the reliability point of view. The principal aims of the statistical analysis are as follows:

1. To determine the number of cycles that the joints can perform their required functions without failure.
2. To predict the number of cycles to failure.
3. To create P-S-N (Probability-Stress-Cycle) curves to predict the probability of failure at any number of cycles.
4. To determine failure patterns of the joint behaviour.

It must be emphasised that the results obtained here are not accurate enough due to pool sampling.

B.2 Procedure of the Statistical Analysis

The three fastening conditions, FSN51, FSN56 and FSH52 shown in Table 2.6, were tested and the resulting data were used for the statistical analysis. Each fastening condition was tested at 5 different load levels. The maximum applied load levels were 4.5kN, 4.0kN, 3.6kN, 3.0kN and 2.7kN. The statistical analysis for the three fastenings was performed at three load levels having a maximum load of 4.5kN, 3.6kN and 2.7kN. From the statistical point of view, the more the number of samples the more accurate the results. Ideally, at least 5 samples of each fastening condition have to be tested at the five load levels in order to perform the statistical analysis and obtain accurate results. However, due to cost and time limitations, only five of each fastening condition were tested at three load levels of 4.5kN, 3.6kN and 2.7kN.

B.2.1 Weibull Distribution

There are three principal parameters that are derived from the Weibull distribution each having an important effect on reliability. These parameters are designated β, η and γ. β is the shape parameter and describes the type of distribution. The effect of the shape parameter on a distribution is reflected in the shape of the probability density function, the reliability function and the failure rate function. For values of $0<\beta<1.0$, the failure rate decreases as the time increases beyond the value of γ. For values of $\beta>1.0$, the failure rate increases as the time increases. γ is the location parameter and represents the time that must elapse before failure can begin to occur. In the majority of cases, such as in the analysis of the yield stress of steel alloys, γ is usually zero which represents a two-parameter Weibull distribution, implying that failure starts at the origin. A positive location parameter indicates that failure cannot occur unless the value of γ is exceeded. Apparently the location parameter has a positive value since most materials and mechanical components have a failure-free period during fatigue testing. It is also possible for the location parameter to have a negative value which indicates that failure can occur before the component is used, e.g. items with shelf-lives. η is known as the characteristic life parameter or scale parameter and defines where the bulk of the distribution lies or how stretched out the distribution is. In the case of the normal distribution, the scale parameter is the standard deviation. For Weibull distribution, it is defined as the time taken for the reliability to fall to 36.8%.

Using the three parameters, the cumulative failure rate in a Weibull manner is defined by the following format:

$$F(t) = 1 - e^{-(\frac{t-\gamma}{\eta-\gamma})^{\beta}} \qquad \textbf{Equation B - 1}$$

where t is the time at failure. The term of $e^{-(\frac{t-\gamma}{\eta-\gamma})^{\beta}}$ represents reliability R(t).
Inverting each side,

$$\left(\frac{1}{1-F(t)}\right)=\exp\left(\frac{t-\gamma}{\eta-\gamma}\right)^{\beta} \qquad \textbf{Equation B - 2}$$

Taking the natural logarithm of both sides of the equation yields,

$$\ln\left(\frac{1}{1-F(t)}\right)=\left(\frac{t-\gamma}{\eta-\gamma}\right)^{\beta} \qquad \textbf{Equation B - 3}$$

Taking the natural logarithm of both sides again,

$$\ln\ln\left(\frac{1}{1-F(t)}\right)=\left[\beta\ln(t-\gamma)\right]-\left[\beta\ln(\eta-\gamma)\right] \qquad \textbf{Equation B - 4}$$

Equation B - 4 is linear of the form Y=bx+a, where x is a variable. Therefore the Weibull distribution should be in the form of a straight line.

Using the above formula it is possible to calculate the reliability of an item. However in its basic function, this can be extremely difficult unless all the three parameters are known. Therefore, the estimate of the three parameters is the first step to perform the Weibull analysis.

B.2.2 Estimation of the Weibull parameters

The three parameters can be estimated graphically using probability plotting paper. Weibull probability graph paper is based on the proof of the distribution and takes the form of a *lnln* scale. The time to failure is plotted on the X-axis, while on the Y-axis the cumulative percentage of failure rate is plotted. The latter is normally divided into groups of 10% to reflect the sample size. Median rank positions are used instead of other ranking methods because median ranks are at a specific confidence level of 50%. The Median rank can be found tabulated in many reliability books and can also be estimated using the following equation,

$$MR\% = \frac{i-0.3}{n+0.4} \times 100\% \qquad \textbf{Equation B - 5}$$

where i is the failure order number and n is the total sample size.

Plotting the data of the time-to-failure and their corresponding ranks on Weibull probability paper, a straight line can be obtained as shown in Fig.B-1. This implies that failure starts at the origin which means that the location parameter $\gamma = 0$. Then by drawing a line through the slope indicator, parallel to the one just obtained, the value of the shape parameter β can be estimated. In this case $\beta = 1.4$. At the $F(t) = 63.2\%$ ordinate point, a straight horizontal line is drawn until it intersects the fitted straight line. A vertical line is then drawn through this intersection until it crosses the abscissa. The value at the intersection of the abscissa represents the characteristic life parameter η. In this case η is equal to 76 hours (this is always at 63.2% since $F(t) = 1 - e^{-(\frac{\eta}{\eta})^{\beta}} = 1 - e^{-1} = 0.632 = 63.2\%$.)

Any reliability value for any mission time t can therefore be obtained. For example, the reliability for a mission of 15 hours, or any other time, can be obtained either from the plot or analytically. In order to do this, a vertical line is drawn from the abscissa, at $t = 15$ hours, to the fitted line. A horizontal line is then drawn from this intersection to the ordinate and $F(t)$ is read. In this case $F(t) = 9.8\%$. Thus, $R(t) = 1 - F(t) = 90.2\%$. This can also be obtained analytically, from the Weibull reliability function equation (1), since the three parameters are known.

$$R(t=15) = \lambda^{-\left(\frac{t-\gamma}{\eta-\gamma}\right)^{\beta}} = \lambda^{-\left(\frac{15-0}{76-0}\right)^{1.4}} = \frac{1}{\lambda\left(\frac{15}{76}\right)^{1.4}} = 90.2\%$$

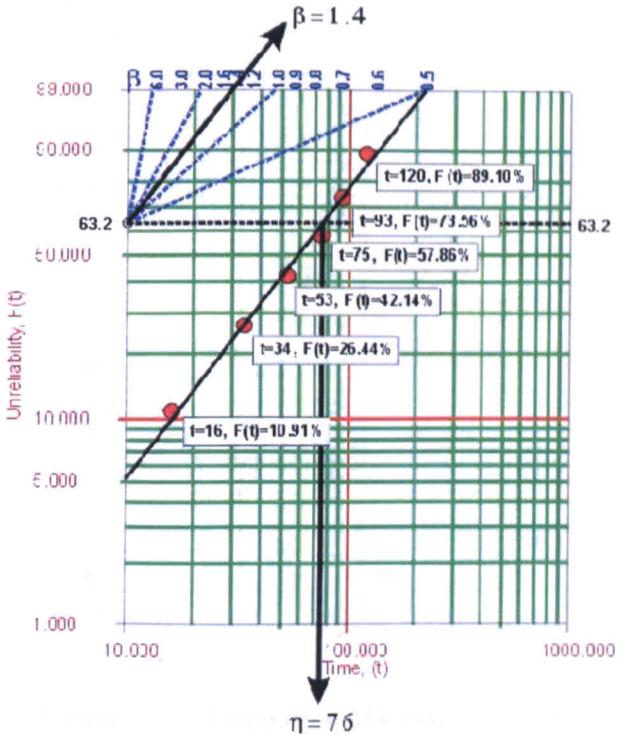

Figure B - 1: Estimation of shape parameter β and characteristic life η

However, for fatigue data, the location parameter γ is not zero. On the Weibull probability paper, the X-axis represents the number of cycles-to-failure (t_i). The median rank MR plotted against the t_i points does not fall on a satisfactory straight line originally. These points fall on a curve as shown in Fig.B-2. The curve normally appears as a convex shape for fatigue data. In order to obtain a straight line, the location parameter γ has to be known. An estimate of the location parameter can be obtained by plotting three equally spaced points on the Y-axis, as shown in Fig.B-2. The corresponding values, t_1, t_2 and t_3 on the X-axis are placed into the following equation:

$$\gamma = t_2 - \frac{(t_3 - t_2)(t_2 - t_1)}{(t_3 - t_2) - (t_2 - t_1)} \qquad \textbf{Equation B - 6}$$

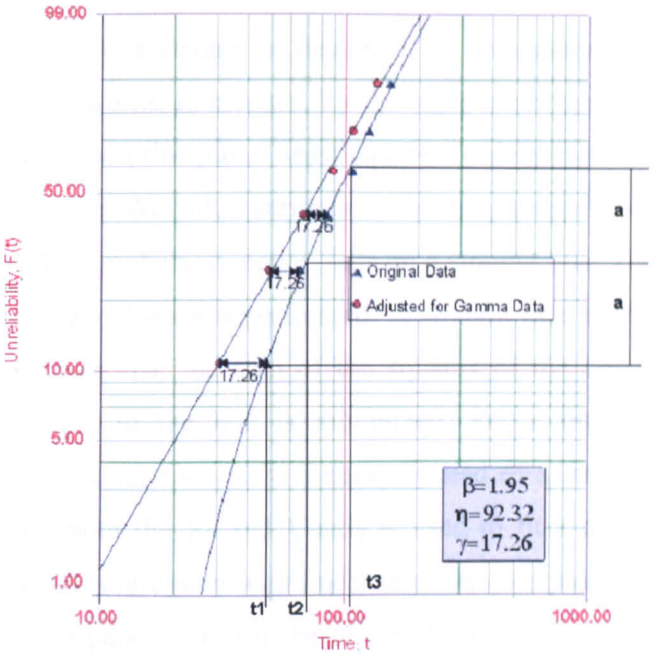

Figure B - 2: Estimation of location parameter γ

The location parameter γ can then be obtained from equation B -6. By subtracting the value of γ from t_i, new data can be obtained and re-plotted on the paper to produce a straight line, as shown in Fig.B-2. It is important to note that the x-axis scale for the straight line becomes $(t_i - \gamma)$ since the term t_i has been used to subtract a positive value of γ. The straight line can then be used to estimate the other two Weibull parameters β and η. The reliability at any time to failure can then be obtained graphically, as described above. Alternatively, the reliability at any time to failure can also be obtained from the Weibull reliability function $R(t) = e^{-(\frac{t-\gamma}{\eta-\gamma})^{\beta}}$ since the three parameters are known.

The three parameters can be estimated graphically as described above. The reliability at any time to failure can also be obtained from the estimated parameters. However, the accuracy of the estimation and the drudgery of hand calculations and plotting are not desirable. As a result, ReliaSoft's Weibull ++ 5.0 software was used in this study making the application much easier.

B.2.3 ReliaSoft's Weibull++ 5.0

ReliaSoft's Weibull ++ 5.0 software is designed to accurately determine the three parameters analytically. It works, in essence, by the same methodology as the probability plotting method and uses the principle of least squares to determine the line through the points. For a two-parameter Weibull distribution, the median-rank MR versus time-to-failure plotted on a Weibull probability paper, falls on a straight line. Therefore linear rank regression on both the X and Y-axis is performed. A straight line is fitted mathematically to a set of data points such that the sum of the squares of the horizontal and vertical deviations from the points to the line is minimized. For a three-parameter Weibull distribution, the plot of MR versus time is a curve instead of a straight line. Therefore, non-linear regression on both the X- and Y-axis is used to fit a curve through the data points. Based on non-linear regression with linear terms and employing the ordinary least squares method, the three parameters can be obtained analytically. The accuracy of the estimation can be characterised by a coefficient of determination, also known as the R-squared value that ranges from 0 to 1.0. This value reveals how closely the calculated values correspond to actual data. As this value approaches 1.0, the more accurate the values become. Since Weibull ++5.0 performs the non-linear and linear regression analytically, it is able to determine the values of the three parameters in such a way that the coefficient of determination is as close to 1.0 as possible.

B.2.4 P-S-N Curves (Probability-Stress-Cycle curve)

Basic fatigue data can be conveniently displayed on a plot of cyclic stress level versus the logarithm of number of cycles, as presented in Chapter Three. These plots, called S-N curves, constitute design information of fundamental importance to materials, machine parts and components subjected to repeated loading. From the reliability point of view, this S-N curve has a 50% reliability meaning that 50% of the samples are expected to fail above this S-N curve and the other 50% below it. Because of the scatter of fatigue life data at any given load level, it is important not only to have a normal S-N curve for a given material or component, but also to have S-N curves showing the probability of failure at a given set of conditions. These curves are called P-S-N curves or curves of constant probability of failure on a stress versus lifetime plot.

To develop a P-S-N curve, the probability of failure P obtained from the Weibull analysis has to be introduced to interconnect with the two other main quantities S and N to form the *P-S-N* curve. For instance, if the number of cycles with a 10% probability of failure at 4.5kN, 3.6kN and 2.7kN were known, the number of cycles versus the three load levels could be plotted and connected as a curve. This procedure gives the S-N curve with a 10% probability of failure or 10% unreliability.

B.3 Results and Discussion

B.3.1 Probability of Failure

B.3.1.1 FSN51 Fastening

The probability of failure versus the number of cycles for the FSN51 fastening at the three load levels were plotted by ReliaSoft's Weibull++ 5.0 software and are shown in Figs.B-3 - B-5. The original fatigue data fall on a curve with a convex shape. After adjusting for γ, a straight line was plotted. The R-squared value represented by ρ was also shown in the figures indicating the accuracy of the estimation. Figs.B-3 - B-5 also present the three Weibull parameters. The location parameter had a positive value at all three load levels providing an estimate of the earliest time-to-failure for such a fastening. At a maximum load of 4.5kN, failure of the fastening would start to occur after a value of γ of 6.4×10^4 cycles. The location parameter γ increased as the applied load decreased indicating that the lower the applied load the longer the failure-free time. The characteristic life parameter η representing the time taken for the probability of failure to reach 63.2% also increased as the load level decreased. At a maximum load of 4.5kN, a 63.2% probability of failure was reached after 6.3×10^4 cycles, whilst at a maximum load of 2.7kN, the same probability was reached after 3.7×10^6 cycles. The shape parameter β had a value greater than 1.0 at all load levels and this meant that the failure rate increased as the number of cycles increased. The fatigue behaviour of this fastening was therefore reliable at all load levels.

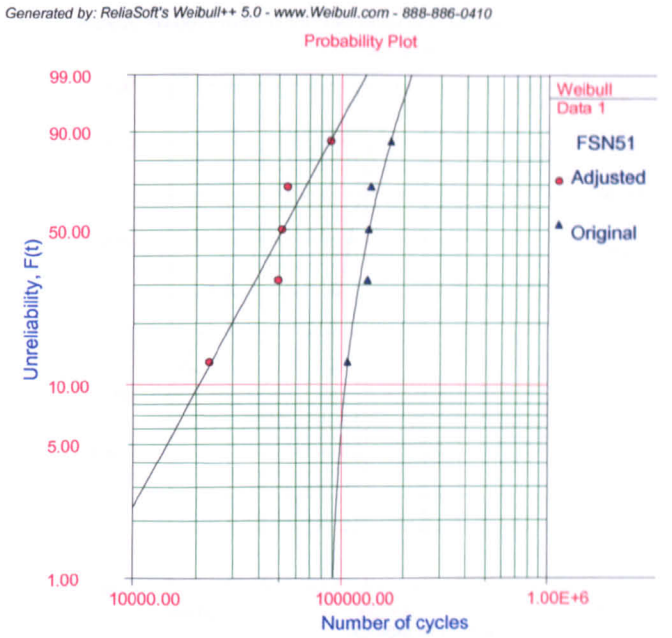

β=2.04, η=62705.83, γ=84157.50, ρ=0.95

Figure B - 3: Probability plot for the FSN51 at 4.5kN

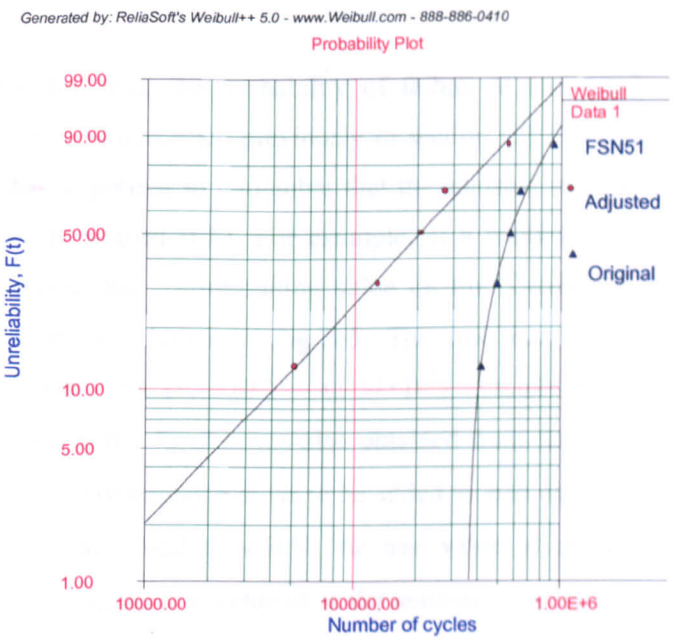

β=1.16, η=2.83E+5, γ=3.60E+5, ρ=1.00

Figure B - 4: Probability plot for the FSN51 at 3.6kN

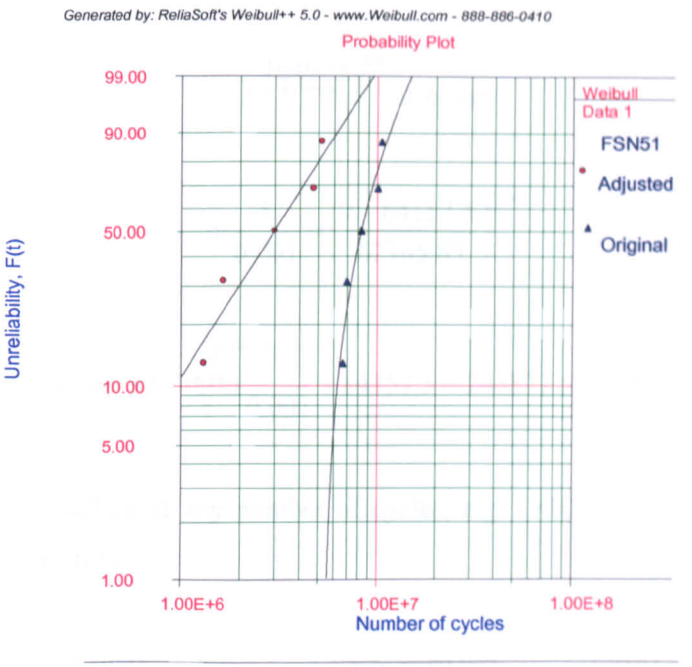

Figure B - 5: Probability plot for the FSN51 at 2.7Kn

From the probability plot, the probability of failure at any number of cycles can be obtained graphically as described previously in section 6.2.2 or mathematically by using equation B-1. It is important to remember that the adjusted straight line was obtained by plotting a reliability against (t-γ). For example, at a maximum load of 2.7kN, at 30% probability of failure, the corresponding value on the X-axis indicating the number of cycles was 1.1×10^6, as shown in Fig.B-5. The true number of cycles having 30% probability of failure was $(1.1\times10^6) + (5.34\times10^6) = 6.44\times10^6$. The characteristic life parameter η shown in the figures was also obtained from the adjusted straight line, and therefore the location parameter γ needs to be added to η to obtain the true value of η. For instance, at a maximum load of 4.5kN, the true value of η was $(6.27\times10^4+8.42\times10^4)$ $=1.47\times10^5$ cycles. Using the true value of η, the number of cycles t with a given probability of failure, e.g. 99.9%, can be calculated as follows:

$$99.9\% = 1 - \ell^{-\left[\frac{t-84157.5}{(62705.83+84157.5)-84157.5}\right]^{2.04}} = 1 - \ell^{-\left(\frac{t-84157.5}{62705.83}\right)^{2.04}}$$

$$\ell^{-\left(\frac{t-84157.5}{62705.83}\right)^{2.04}} = 0.001$$

$$\ln\frac{1}{0.001} = \left(\frac{t-84157.5}{62705.83}\right)^{2.04}$$

$$t = 62705.83 \times \sqrt[2.04]{\ln\frac{1}{0.001}} + 84157.5 = 245871.5 \approx 2.46\times10^{5}$$

The probability of failure at any number of cycles, e.g. 1×10^{5}, can also be obtained by using the above equation.

$$F(t) = 1-\ell^{-\left[\frac{100000-84157.5}{(62705.83+84157.5)-84157.5}\right]^{2.04}} = 1-\ell^{-\left(\frac{100000-84157.5}{62705.83}\right)^{2.04}} = 1-\ell^{-\left(\frac{15842.5}{62705.83}\right)^{2.04}} = 1-\ell^{-0.06}$$

$$F(t) = 1-\frac{1}{\ell^{0.06}} = 0.059 = 5.9\%$$

Table B-1 shows the number of cycles with 0% and 99.9% probability of failure for the FSN51 fastening at three load levels. The observed fatigue data of the FSN51 fastening from the fatigue test at five load levels, representing 50% reliability are also listed in the table.

Table B- 1: Number of Cycles with Different Probabilities of Failure for the FSN51

Load (kN)	Number of cycles with 0% failure probability	Number of cycles with 99.9% failure probability	Observed Data with 50% failure probability
4.5-0.5	8.42×10^{4}	2.46×10^{5}	137860
4.0-0.5			434570
3.6-0.5	3.6×10^{5}	1.86×10^{6}	605730
3.0-0.5			5571690
2.7-0.5	5.34×10^{6}	1.76×10^{7}	8524400

B.3.1.2 FSH52 Fastening

Figs.B-6 – B-8 show the probability plot for the FSH52 fastening conditions at different load levels. The three Weibull parameters and the R-squared value are also presented in the figures. A positive location parameter γ representing the 0% failure probability existed at all three load levels and increased as the load level decreased. At a maximum load of 4.5kN, failure would not occur below 9.77×10^4 cycles, whilst at a maximum load of 2.7kN, the fastening would not be expected to fail below 1.49×10^6 cycles. The characteristic life parameter η varied with the load level. The probability of failure reached 63.2% after 7.67×10^3 cycles at a maximum load of 4.5kN and after 7.01×10^5 cycles at a maximum load of 2.7kN. The shape parameter β was less than 1.0 at all three-load levels meaning that the failure rate decreased as the number of cycles increased. This suggested that the fatigue performance of this fastening was not reliable.

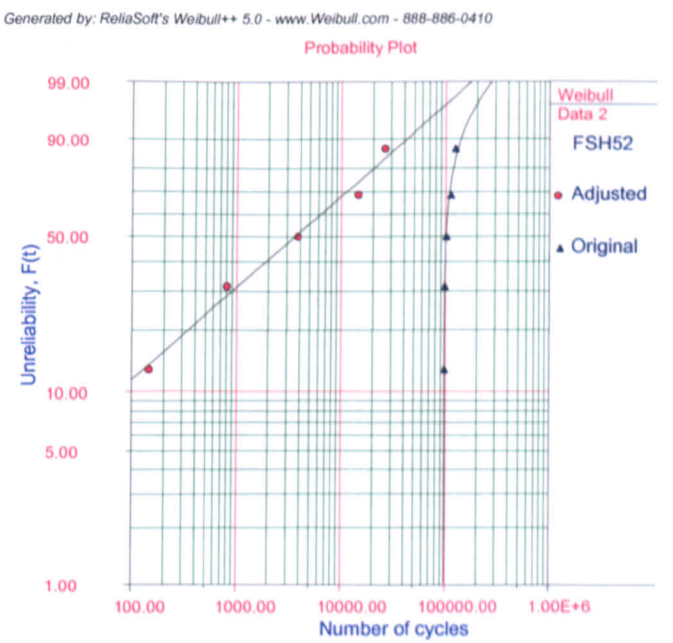

Figure B - 6: Probability plot for the FSH52 at 4.5kN

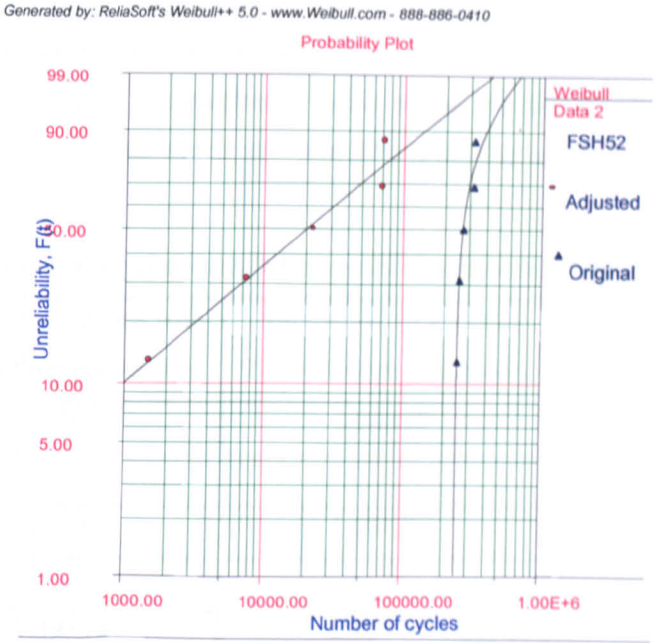

β=0.62, η=36881.78, γ=2.50E+5, ρ=0.98

Figure B - 7: Probability plot for the FSH52 at 3.6kN

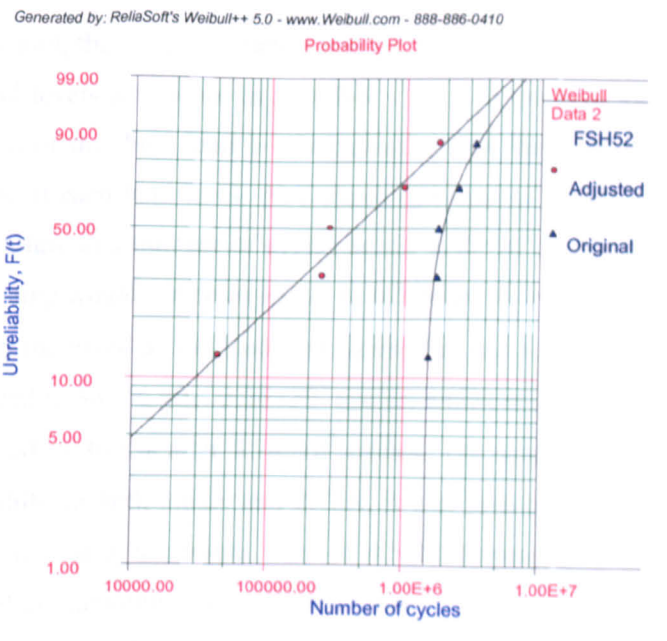

β=0.71, η=7.01E+5, γ=1.49E+6, ρ=0.98

Figure B - 8: Probability plot for the FSH52 at 2.7kN

By performing the same calculations as for the FSN51 fastening, the reliability at any number of cycles or the number of cycles at any probability of failure for the FSN51 fastening can be obtained. The number of cycles at two critical probabilities of failure and the experimental fatigue data which represent 50% reliability are listed in Table B-2.

Table B- 2: Number of Cycles with Different Probabilities of Failure for the FSH52

Load (kN)	Number of cycles with 0% failure probability	Number of cycles with 99.9% failure probability	Observed Data 50% failure probability
4.5-0.5	9.77×10^{4}	4.94×10^{5}	106810
4.0-0.5			152850
3.6-0.5	2.5×10^{5}	1.08×10^{6}	285090
3.0-0.5			906320
2.7-0.5	1.49×10^{6}	1.22×10^{7}	2161240

B.3.1.3 FSN56 Fastening

The probability plot, the three parameters and the R-squared value for the FSN56 fastening at the three load levels are shown in Figs.B-9 – B-11. A positive location parameter was obtained at each of the three load levels indicating that the FSN56 fastening also had a failure-free time at each load level. At a maximum load of 4.5kN, the FSN56 had a 0% probability of failure at a number of cycles below 3.48×10^{4}, while at a maximum load of 2.7kN, the fastening would not be expected to fail below 4.1×10^{5} cycles. The characteristic life parameter η increased as the load level decreased. At a maximum load of 4.5kN, the reliability dropped to 36.8% after 3.24×10^{3} cycles, whilst at a maximum load of 2.7kN the reliability dropped to 36.8% after 3.78×10^{5} cycles. The shape parameter β was less than 1.0 at 4.5kN, whilst at both 3.6kN and 2.7kN, it was greater than 1.0. The results meant that the failure rate at a maximum load of 4.5kN decreased as the number of cycles increased, whilst at maximum loads of 3.6kN and 2.7kN, the failure rate increased as the number of cycles increased. It was therefore suggested that at a maximum load of 4.5kN, the fatigue behaviour of this fastening was not reliable, whilst at maximum loads of 3.6kN and 2.7kN, the fatigue performance of this fastening became reliable.

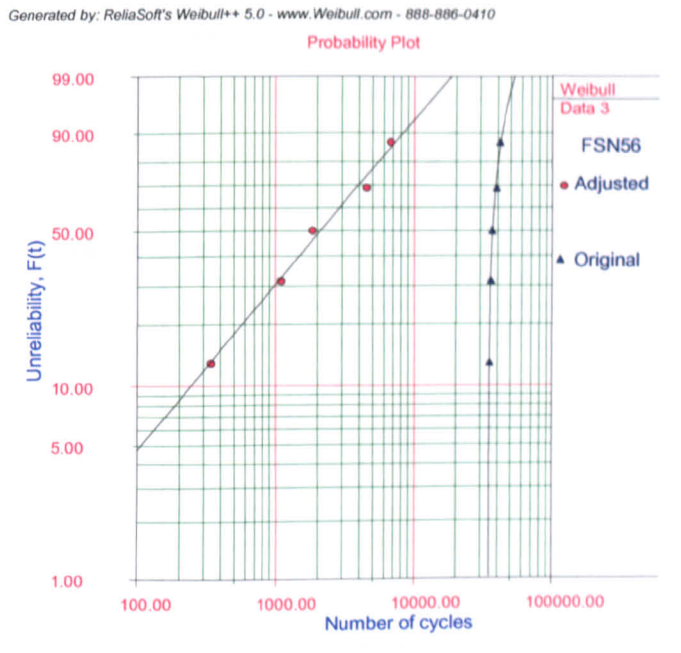

β=0.87, η=3240.89, γ=34840.25, ρ=0.99

Figure B - 9: Probability plot for the FSN56 at 4.5Kn

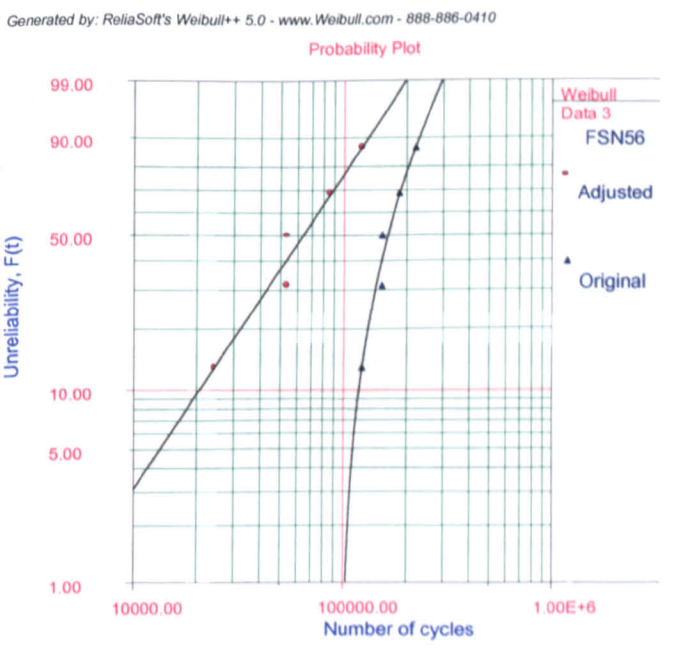

β=1.66, η=79643.69, γ=98459.05, ρ=0.98

Figure B - 10: Probability plot for the FSN56 at 3.6kN

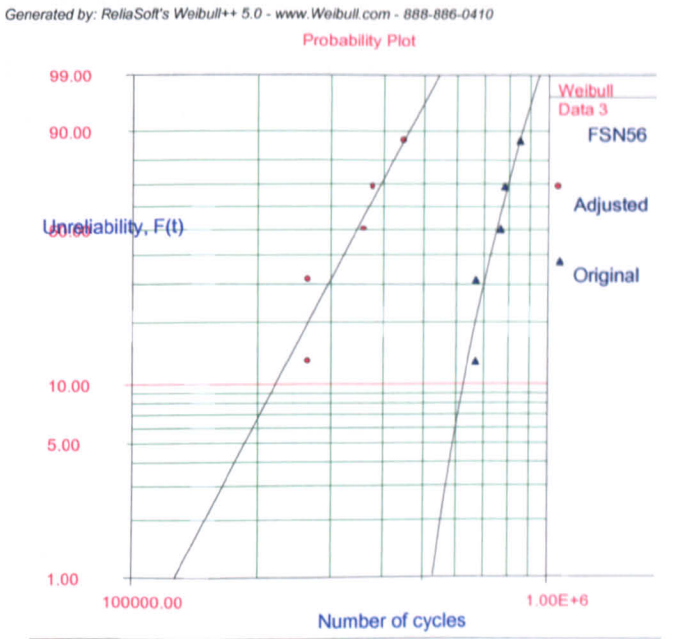

β=4.20, η=3.78E+5, γ=4.05E+5, ρ=0.93

Figure B - 11: Probability plot for the FSN56 at 2.7kN

The same calculations as for the FSN51 and the FSH52 fastenings were performed to obtain the number of cycles with a 99.9% probability of failure. The location parameters representing the number of cycles with 0% probability of failure, the number of cycles having a 99.9% probability of failure and experimental data are shown in Table B-3.

Table B- 3: Number of Cycles with Different Probabilities of Failure for the FSN56

Load (kN)	Number of cycles with 0% failure probability	Number of cycles with 99.9% failure probability	Observed Data (Number of cycles at failure)
4.5-0.5	3.48×10^4	6.47×10^4	37762
4.0-0.5			92050
3.6-0.5	9.85×10^4	3.54×10^5	162460
3.0-0.5			477435
2.7-0.5	4.05×10^5	1.0×10^6	728846

B.3.1.4 Probability Density Function

The probability of failure for the three fastenings can also be described by a probability density plot, as shown in Figs.B-12 – B-14.

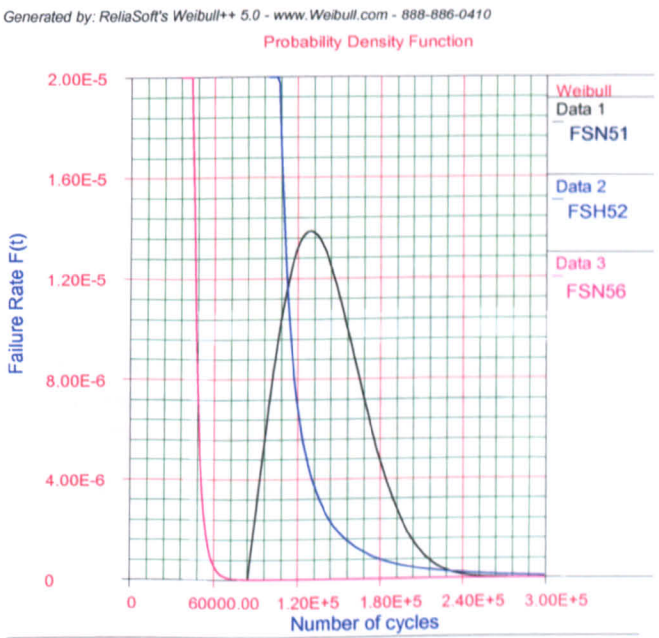

β2=0.49, η2=7667.61, γ2=97745.27, ρ=0.99
β1=2.04, η1=62705.83, γ1=84157.50, ρ=0.95
β3=0.87, η3=3240.89, γ3=34840.25, ρ=0.99

Figure B - 12: Probability density plot at 4.5kN

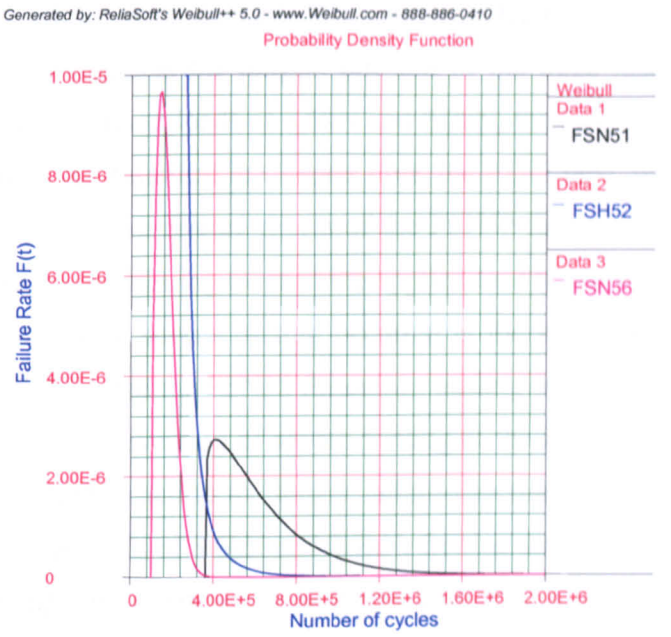

β1=1.16, η1=2.83E+5, γ1=3.60E+5, ρ=1.00
β2=0.62, η2=36881.78, γ2=2.50E+5, ρ=0.98
β3=1.66, η3=79643.69, γ3=98459.05, ρ=0.98

Figure B - 13: Probability density plot at 3.6kN

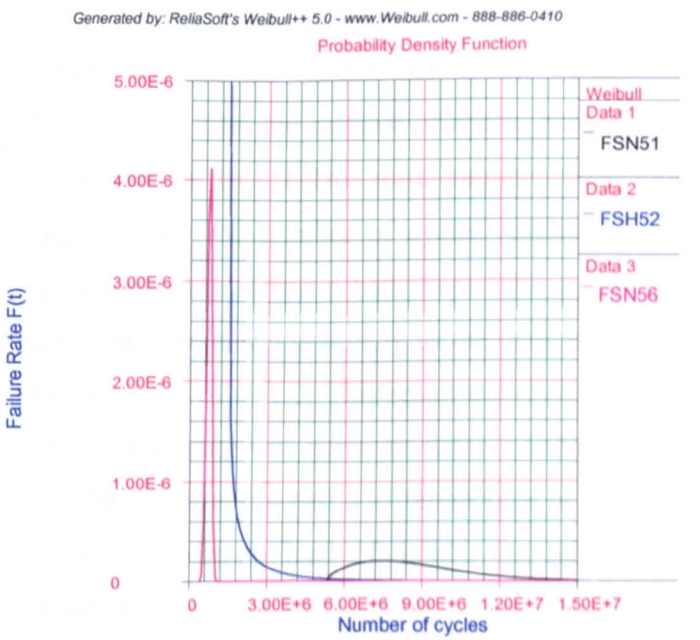

β1=1.63, η1=3.74E+6, γ1=5.34E+6, ρ=0.96
β2=0.71, η2=7.01E+5, γ2=1.49E+6, ρ=0.98
β3=4.20, η3=3.78E+5, γ3=4.05E+5, ρ=0.93

Figure B - 14: Probability density plot at 2.7kN

From the probability density plot, the failure-free time, whose value is indicated by the start point of the plot, can be easily derived. At a maximum load of 4.5kN, the failure-free time of the FSH52 fastening was the longest one out of the three fastenings that were examined. However, at maximum loads of 3.6kN and 2.7kN, the FSN51 fastening had the longest failure-free time. As described in Chapter Five, the PTFE tape, which was inserted at the interface between the two riveted sheets of the FSH52 fastening, prevented severe fretting at the interface by transferring most of the applied load to the rivet. By contrast, at the same load level of 4.5kN, severe fretting occurred at the interface between the two riveted sheets for the FSN51 and the FSN56 fastenings leading to fracture of both the rivet and the sheet material. The prevention of severe fretting at the interface between the two riveted sheets probably contributed to the longer failure-free time of the FSH52 fastening at this load level. At lower loads of 3.6kN and 2.7kN, fretting that occurred for the FSN51 and the FSN56 fastening conditions was less severe leading to a longer failure-free time than at a maximum load of 4.5kN. The FSN51 fastening had a higher load capacity than the FSN56 fastening due to the effect of geometry of the joints. Therefore the FSN51 fastening had the longest failure-free time of the three fastenings at lower load levels.

In addition to the failure-free time, the probability density plot also presents the failure rate. As shown in these figures, the failure rate of the FSH52 fastening decreased monotonically at all load levels after the number of cycles exceeded the value of γ. This was also reflected by the value of $\beta<1.0$. This result suggested that most of the fastenings failed almost immediately once the number of cycles reached the value of γ. For the FSN51 fastening, the failure rate plot had a bell shape with a right tail at all load levels indicating that the failure rate increased gradually as the number of cycles increased. This was also suggested by the value of $\beta>1.0$. This result therefore suggested that the fatigue performance of the FSN51 fastening was more predictable and reliable compared with the FSH52 fastening. The FSN56 fastening had a different type of probability density plot at different load levels. At a maximum load of 4.5kN, the failure rate of the fastening decreased as the number of cycles increased leading to the value of $\beta<1.0$. This indicated that the applied load of 4.5kN was too high for the FSN56 fastening. The failure rate plot for the FSN56 fastening had a convex shape as for the FSH52 fastening, indicating that most of the fastenings failed within a very short time. It was therefore suggested that at this load level, the fatigue behaviour of this fastening was not reliable. At maximum loads of

3.6kN and 2.7kN, the failure rate plot for the FSN56 fastening appeared as a bell shape as for the FSN51 fastening, leading to a gradual increase in the failure rate as the number of cycles increased. This is also indicated by the value of ß, which became greater than 1.0. It was therefore suggested that at a lower applied load, the FSN56 fastening could perform with a predicable probability of fatigue failure and the fatigue behaviour of this fastening was reliable.

Besides the failure-free time and the failure rate, the probability density plot also indicates the spread of the fatigue data. The area under the bell shape represents 100% failure, whilst the width indicates the spread of the fatigue data. At a maximum load of 3.6kN and 2.7kN the width of the bell shape for the FSN56 fastening was narrower than that for the FSN51 fastening. This meant that at these loads the fatigue data from 0% to 100% failure for the FSN51 joints exhibited a wider scatter than for the FSN56 joints. This indicated that the probability of failure for the FSN56 fastening was more predicable than that for the FSN51 fastening at low load levels. A possible cause of this was the fact that the FSN51 fastening was larger than the FSN56 fastening and probably contained a greater number of material defects which might be involved in the crack initiation and propagation process.

B.3.2 P-S-N Curve

Fig.b-15 shows the P-S-N curve of the FSN51 fastening plotted by using the data shown in Table b-1. In addition to the normal S-N curve having a 50% reliability, a S-N curve with a 0% probability of failure and another S-N curve with a 99.9% failure probability were also plotted in the figure. The S-N curve having a 0% probability of failure indicated that all samples would perform their desired function without failure below this curve. Moving to the right of this curve, the probability of failure gradually increased. The S-N curve with a 99.9% probability of failure meant that failure of all samples would have occurred at all values indicated by this curve. Between the two curves, failure could occur at any time with different probabilities. It must be mentioned here that some data slightly deviated from the curves with different failure probabilities, as shown in Fig.B–15. This is because the curves were plotted by performing power regression, in which inaccuracy always depends on the number of tested samples. In addition, Fig.B–15 does not include the

observed average fatigue life (marked in red colour in Table B-1) at maximum loads of 4.0kN and 3.0kN since those values were not used in the Weibull analysis. Although the data at 4.0kN and 3.0kN are located between 0% and 99.9% probability curves, as shown in Fig.B–16, the inclusion of these data could result in changes to the curve leading to inaccuracy of the results.

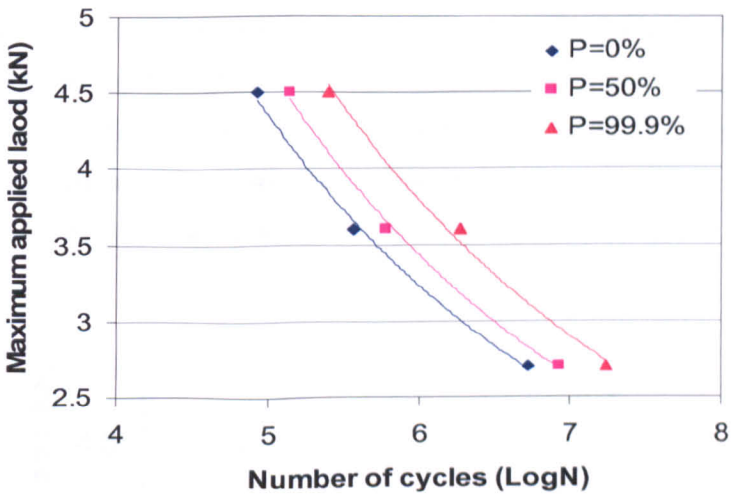

Figure B - 15: P-S-N curve for the FSN51 fastening

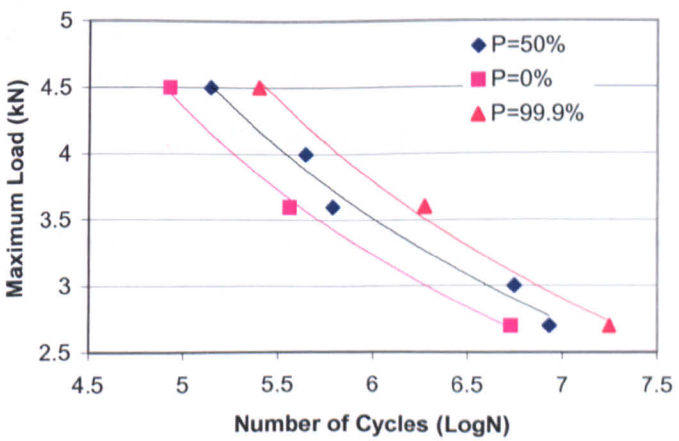

Figure B - 16: P-S-N curve for the FSN51 fastening including data at 4.0kN and 3.0kN

The P-S-N curve with three probabilities of failure for the FSH52 fastening condition is shown in Fig.B-17. The S-N curve having a 0% failure probability was very close to the S-N curve with a 50% reliability. At a maximum load of 4.5kN, the 0% and the 50% P-S-N curves are almost touching. By contrast, the S-N curve with a 99.9% probability of failure was far away from the S-N curve with a 50% failure probability. The failure probability increased sharply from 0% to 50%, whilst the rate of increase from 50% to 99.9% was much slower. It was therefore suggested that 50% of the fastenings failed within a very short time. Same as for the FSN51 fastening, the application of regression led to deviation of some data and the fatigue life at maximum loads of 4.0kN and 3.0kN were not included in Fig.B-17. Inclusion of these data would have resulted in changes to the 50% failure probability curve which is shown in Fig.B-18 leading to unreliable results.

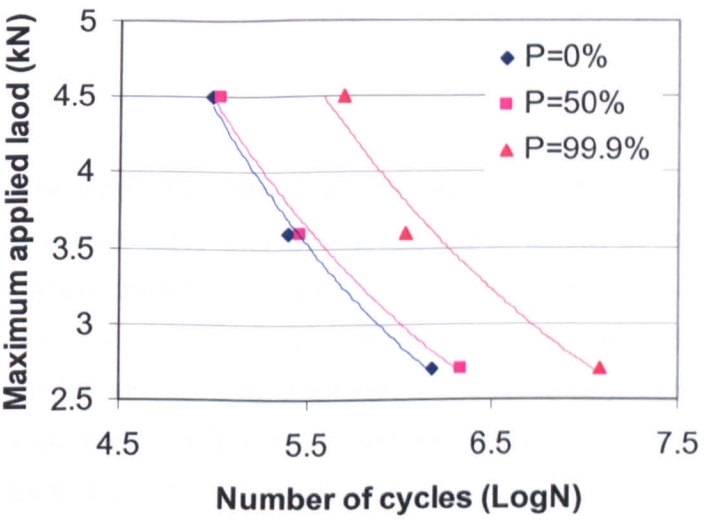

Figure B - 17: P-S-N curve for the FSH52 fastening

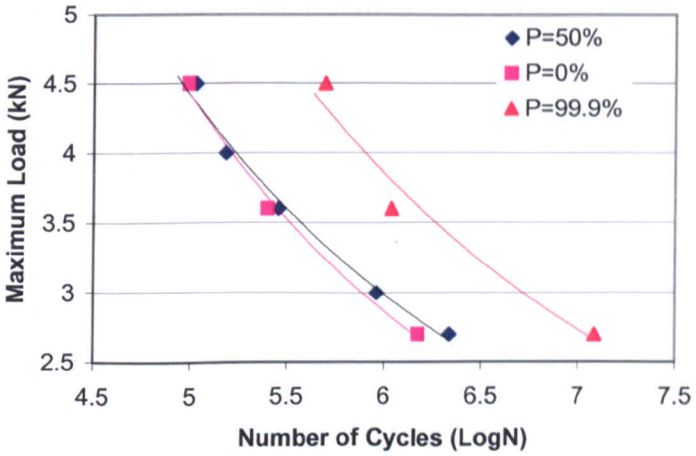

Figure B - 18: P-S-N curve for the FSH52 fastening including data at 4.0kN and 3.0kN

The P-S-N curve showing three probabilities of failure for the FSN56 fastening is shown in Fig.B-19. Below the S-N curve with a 0% probability of failure, no fastenings would be expected to fail. Above the S-N curve with a 99.9% failure probability, failure would have occurred. Between these two S-N curves with the two critical probabilities of failure, the fastening would fail at any time with a different failure probability. The figure also shows that at a maximum load of 4.5kN, the failure-free number of cycles was close to the number of cycles with a 50% failure probability. This indicated that 50% of the joints failed at an early period of the test at this load level. The analysis also suggested that the probability of failure from 0% to 50% occurred over a narrow range of fatigue cycles at this load level, whilst at lower load levels, this range widened. Same as for the FSN51 and FSH52 fastenings, the problems due to the application of regression have arisen again and some samples survived beyond the predicted 99.9% failure probability.

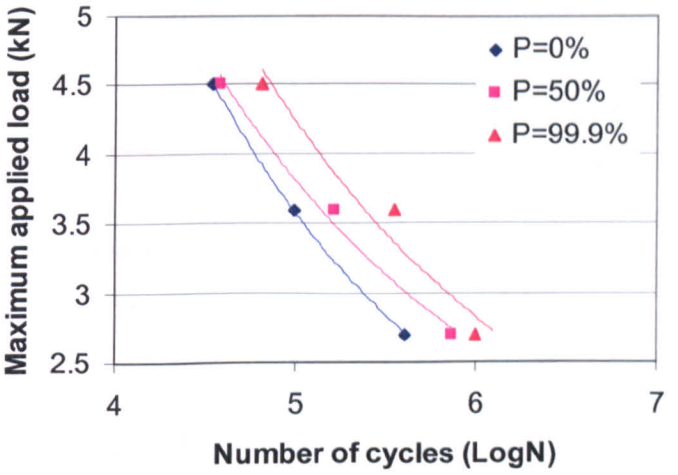

Figure B - 19: P-S-N curve of FSN56 fastening

B.3.3 Failure Patterns

According to Abernethy [4], there are three different types of failure patterns for continuous probability distributions used in reliability studies. The three most common ones are: early failure or infant mortality, chance failure or random failure and wear-out failure. These three patterns can be expressed by the failure rate, which is important in describing the life-history of a product. For early failure, the product begins its life at a high failure rate and exhibits a decreasing failure rate. For chance failure, the failure rate is constant. For wear-out failure, the failure rate increases as time increases. In a Weibull distribution, all the three patterns might occur depending on the appearance of the failure rate which is determined by the value of the shape parameter β.

The value of the shape parameter β has a marked effect on the failure rate of the Weibull distribution since the Weibull instantaneous failure rate, $f(t)$, is given by:

$$f(t) = \frac{F(t)}{R(t)} = \frac{\beta}{\eta}\left(\frac{t-\gamma}{\eta}\right)^{\beta-1} \qquad \textbf{Equation B - 7}$$

Inferences can be drawn about a population's failure characteristics just by considering whether the value of β is less than or greater than one.

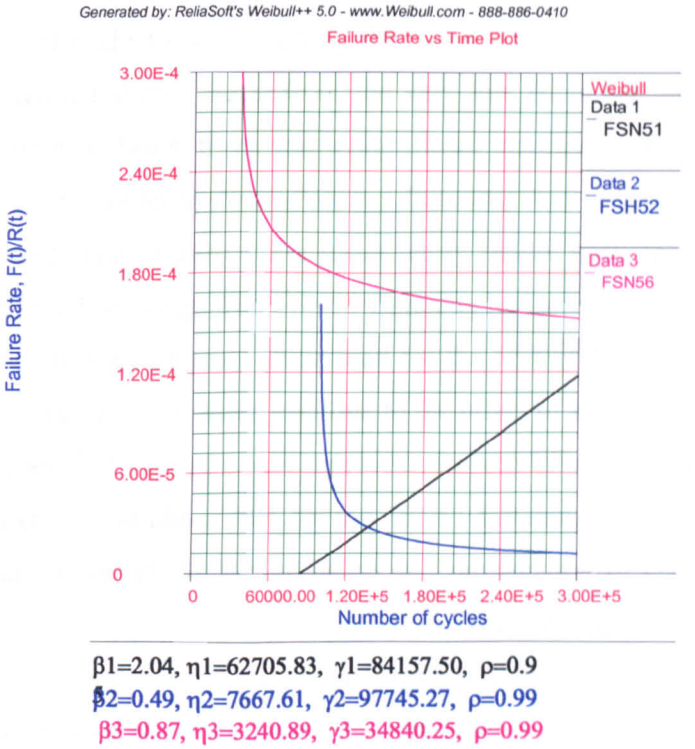

Figure B - 20: Failure rate versus time plot at 4.5kN

Fig.B-20 shows the failure rate versus time plot at a maximum load of 4.5kN for the three fastenings. The value of β for the FSN51 fastenings is greater than 1.0 but close to 2.0. This meant that at this load level the failure rate for the FSN51 fastening increased as the number of cycles increased. The failure rate exhibited a straight line relationship between $f(t)$ and t, starting at a value of $f(t) = 0$ at $t = \gamma$. Thereafter the failure rate increased at a constant rate as t increased. This suggested that the FSN51 fastening exhibited wear-out failure indicating that the fatigue behaviour of this fastening was reliable.

Both the FSH52 and the FSN56 fastenings had a value of β less than 1.0. This indicated that at this load level the failure rate decreased as the number of cycles increased. The Weibull failure rate plots were convex. At $t=\gamma$ the failure rate was infinity and decreased thereafter monotonically, approaching the value of zero as $t\rightarrow\infty$ and $f(\infty)=0$. This indicated that at this load level, an early failure (infant mortality) occurred for both the FSH52 and

the FSN56 fastenings and therefore the fatigue performance of the two fastenings was not reliable. From the reliability point of view, such behaviour is not desirable. For the FSH52 fastening, this was thought to be caused by the insert of the PTFE tape at the interface between the two riveted sheets. Because of the very low frictional force at the interface between the two riveted sheets, there was a significant increase in the load transferred to the fastener. The load transfer system of such a fastening was unbalanced and this is not desirable for a clamp-type of joint. As a result, early failure occurred by fracture of the rivet for all the FSH52 fastenings. The FSN56 fastening had an average ultimate shear load of 5.3kN, while the average ultimate shear load for the FSN51 fastening was 5.7kN. The former failed at a lower ultimate shear load due to the effect of sample size, as described in Chapter Four. The applied load of 4.5kN represented about 85% of the ultimate shear load for the FSN56 fastening and about 78% for the FSN51 fastening. Fatigue, as a progressive failure phenomenon, proceeds by the initiation and propagation of cracks to an unstable size. The relatively high applied-load for the FSN56 fastening led to relatively easy crack initiation. Once crack initiation occurred, propagation followed reaching to an unstable size and leading to fracture of the narrower sheet material of the FSN56 fastening within a very short period of time. The applied load was too high for the FSN56 fastening to allow the failure probability to increase gradually. This contributed to the early failure for the FSN56 fastening at this load level.

The failure rate versus time plot at a maximum load of 3.6kN for the three fastenings is shown in Fig.B-21. At this load level, both the FSN51 fastening and the FSN56 fastening had a value of β greater than 1.0, but less than 2.0 meaning that the failure rate increased as t increased. This suggested that at this load level, wear-out failure occurred for both the FSN51 and the FSN56 fastenings and therefore the fatigue behaviour of the two fastenings was reliable. However, the value of β for the FSH52 fastening was still less than 1.0 indicating that at this load level, the fatigue behaviour was still not reliable. The failure rate remained infinity at a number of cycles equal to γ and thereafter decreased as t increased. This suggested that early failure still occurred for the FSH52 fastening at this load level. The imbalance of the loading transfer system caused by the inserted PTFE tape dominated the fatigue failure mechanisms of these joints.

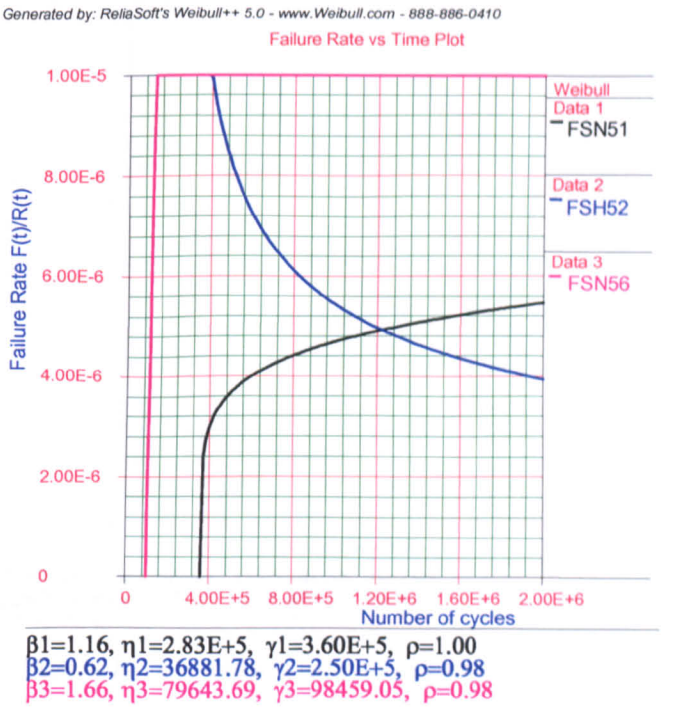

Figure B - 21: Failure rate versus time plot at 3.6kN

Fig.B-22 shows the failure rate versus time plot at 2.7kN for the three fastenings. The failure rate plot for the FSH52 fastening at this load level still indicated that early failure occurred for this fastening and the fatigue behaviour of this fastening was still not reliable. In the case of the FSN51 and the FSN56 fastenings, wear-out type of failure occurred at this load level indicating that the fatigue performance for the two fastenings was reliable. The value of β for the FSN51 fastening was between 1.0 and 2.0 leading to a convex-shaped plot as shown in Fig.6.20. The value of β for the FSN56 fastening was 4.20, that is, it was greater than 2.0 and therefore led to a concave curve as shown in Fig.B-23. The failure rate for both the FSN51 and the FSN56 fastenings increased as the number of cycles increased. However, compared with the FSN51 fastening, the failure rate for the FSN56 fastening increased rapidly as the number of cycles increased indicating that for the FSN56 fastening wear-out failure would occur within a relatively shorter period of time.

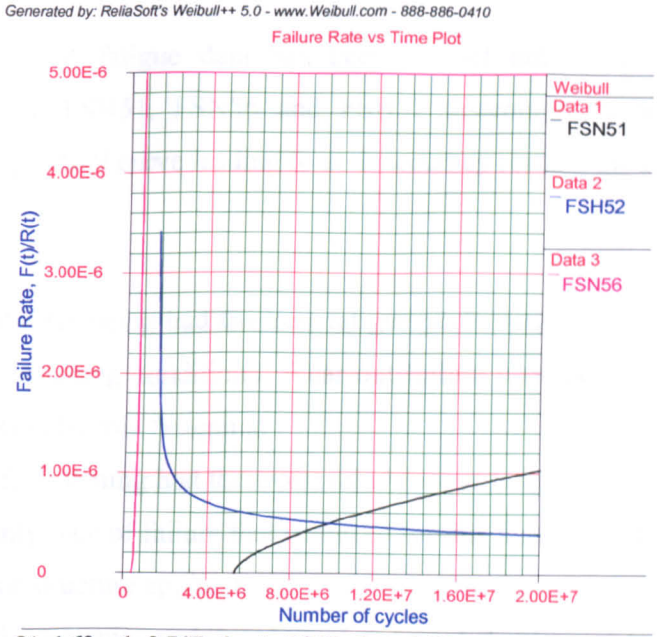

β1=1.63, η1=3.74E+6, γ1=5.34E+6, ρ=0.96
β2=0.71, η2=7.01E+5, γ2=1.49E+6, ρ=0.98
β3=4.20, η3=3.78E+5, γ3=4.05E+5, ρ=0.93

Figure B - 22: Failure rate versus time plot at 2.7kN

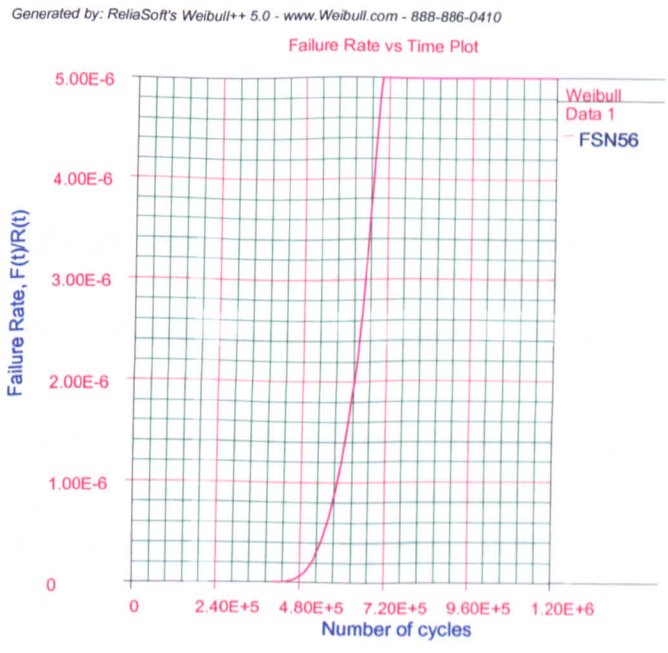

β=4.20, η=3.78E+5, γ=4.05E+5, ρ=0.93

Figure B - 23: Failure rate versus time plot of FSN56 fastening at 2.7kN

B.4 Conclusions

Statistical analysis of fatigue data has been carried out by means of the Weibull distribution for the FSN51, FSN56 and FSH52 fastenings. Although limitations are involved in crating P-S-N curve leading to an inaccuracy results, the following conclusions still can be drawn:

1. The FSN51 fastening had the best fatigue performance at all tested load levels in the three fastening conditions. Wear-out failure was the only type of failure that was expected by this fastening.
2. The FSH52 fastening had the worst reliability of fatigue performance. Early failure was the only type of failure that occurred for this fastening and therefore it was not suitable for structure application.
3. The FSN56 fastening exhibited good fatigue behaviour at low load levels. Early failure occurred at high load levels, and wear-out failure occurred at lower load levels.

B.5 References

1. Weibull. W, "*Fatigue testing and analysis of results*", Pergamon Press, 1961.
2. Ang AHS. "*A comprehensive basis for reliability analysis, design*", Japan–USA Joint Seminar on Reliability Approach in Structural Engineering, Marzuen, Co. Ltd., Tokyo, 1974. p. 29–47.
3. Ang AHS, Cheung MC, Shugar TA, Fernie J. "*Reliability-based fatigue analysis and design of floating structures*". Third International Workshop on Very Large Floating Structures, Honolulu, 22–24, September 1999.
4. Abernethy.R.B, "*The new Weibull handbook*", Third edition, ISBN 0-9653062-0-8, 1996.